ISBN 978-82-326-1614-5 (printed version)
ISBN 978-82-326-1615-2 (electronic version)
ISSN 1503-8181

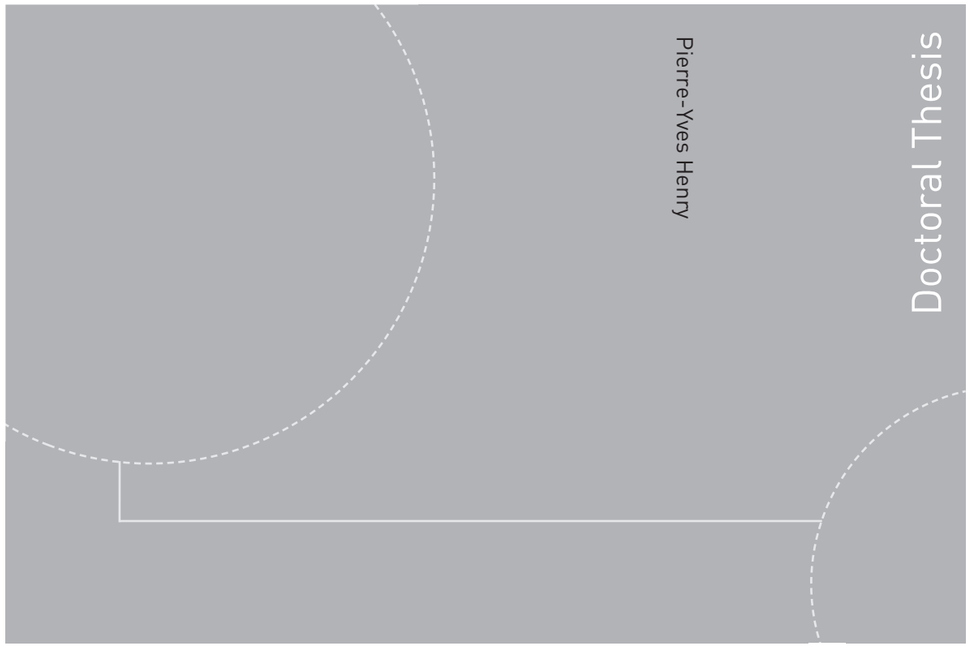

Doctoral theses at NTNU, 2016:138

Pierre-Yves Henry

Parametrisation of aquatic vegetation in hydraulic and coastal research: The importance of plant biomechanics in the hydrodynamics of vegetated flows

NTNU
Norwegian University of
Science and Technology
Faculty of Engineering
Science and Technology
Department of MarineTechnology

NTNU
Norwegian University of
Science and Technology

Doctoral theses at NTNU, 2016:138

NTNU

NTNU
Norwegian University of
Science and Technology

Pierre-Yves Henry

Parametrisation of aquatic vegetation in hydraulic and coastal research: The importance of plant biomechanics in the hydrodynamics of vegetated flows

Thesis for the degree of Philosophiae Doctor

Trondheim, May 2016

Norwegian University of Science and Technology
Faculty of Engineering
Science and Technology
Department of MarineTechnology

NTNU
Norwegian University of
Science and Technology

NTNU
Norwegian University of Science and Technology

Thesis for the degree of Philosophiae Doctor

Faculty of Engineering
Science and Technology
Department of MarineTechnology

ISBN 978-82-326-1614-5 (printed version)
ISBN 978-82-326-1615-2 (electronic version)
ISSN 1503-8181

Doctoral theses at NTNU, 2016:138

Printed by Skipnes Kommunikasjon as

Abstract

Understanding the complexity of the interactions between aquatic biological systems and their physical environment is a critical condition for the sustainable management of aquatic environments. In such ecosystems, aquatic vegetation holds a central place by influencing flow and turbulent processes, thus playing a major role both from an engineering and ecological point of view. However, the characterisation of the hydrodynamics of vegetated flows is facing several issues due to the complexity of the plant-flow interactions. In such a complex system, the plant's biomechanical properties are a key parameter governing the interplay between the living organism and its physical environment: a variation of the plant's mechanics in time or space will generally imply changes in these regulation processes, which in turn can lead to major changes in the physical/ecological environment. The consideration of mechanical interactions, however, is fairly new to engineers, biologists and ecologists, as it defines an interface between engineering and ecology. As a consequence, this area of research has remained mostly unexplored and a lot of processes are to be discovered at the edge of the different disciplines.

This thesis deepened the level of the understanding of plant-flow mechanical interactions and of the plant structural properties, in order to improve the parametrisation of aquatic vegetation in hydraulic and coastal research. Measurement techniques and experimental protocols were developed to collect plant biomechanical properties and a methodology for the collection of such data was provided based on the flexibility of the plant elements. New methods to design plant surrogates for hydraulic experimentation were further investigated based on mechanical similarity. In parallel, this thesis reviewed the measurement techniques commonly used to measure drag forces on submerged plants, and developed a theoretical framework to estimate random wave and random wave-plus-current induced drag forces on submerged plants. This framework is based on the definition of a drag coefficient for a given type of plant. Moreover, the common drag coefficient formulations were discussed, identifying possibilities for a standardisation of the formulations for oscillatory and steady flows. Finally, in order to understand the effects of the development of a biological community at an interface fluid/solid, the example of marine biofouling was investigated through flow visualisation. The methodologies developed in this thesis are to be used in on-going projects and will trigger new research activities at NTNU and elsewhere.

Preface

This doctoral work was carried out at the Department of Marine Technology, located in the Faculty of Engineering Science and Technology at the Norwegian University of Science and Technology (NTNU). Three years of the project were supported by NTNU, and one year was supported by the European Community's 7th Framework Programme through the grant to the budget of the Joint Research Activity 'PISCES', part of the Integrated Infrastructure Initiative HYDRALAB-IV, Contract No. 261520. This thesis has been submitted for partial fulfilment of the requirements for the degree of 'philosophiae doctor' at NTNU, Trondheim, Norway.

The work has been supervised by Professor Dag Myrhaug (NTNU), Professor Bjørnar Pettersen (NTNU) and later Professor Jochen Aberle (NTNU). The project started in August 2011 and was completed for submission in January 2016.

The author, Pierre-Yves Henry, declares that this thesis and the work presented herein is the result of original research that has not previously been submitted for a degree at any university or other institution.

The author is indebted to Professors Dag Myrhaug, Jochen Aberle and Bjørnar Pettersen for the quality of their supervision and support at every stage of the project, as well as to all the PISCES project members for having being able to learn at their sides. The author also thanks all colleagues, friends and family that have been involved in this long journey.

Pierre-Yves Henry

Trondheim, 05 February 2016

Contributions

PAPER I *Henry and Myrhaug* [2013]

Henry, P.-Y. and Myrhaug, D., [**2013**]. Wave-induced drag force on vegetation under shoaling random waves. *Coastal Engineering*, 78(0): 13-20.

PAPER II *Henry et al.* [2015]

Henry, P.-Y., D. Myrhaug, and J. Aberle [**2015**], Drag forces on aquatic plants in nonlinear random waves plus current, *Estuarine, Coastal and Shelf Science*, 165, 10-24.

PAPER III *Paul et al.* [2014]

Paul, M., **Henry, P.Y.T.** and Thomas, R.E., [**2014**]. Geometrical and mechanical properties of four species of northern European brown macroalgae. *Coastal Engineering*, 84: 73-80.

PAPER IV *Paul and Henry* [2014]

Paul, M, **Henry, P-Y T.** [**2014**], Evaluation of the Use of Surrogate Laminaria digitata in eco-hydraulic Laboratory Experiments, *Journal of Hydrodynamics*, Ser. B, 26(3), 374–383.

PAPER V *Henry* [2014]

Henry, P.-Y.T., [**2014**]. Bending properties of a macroalga: Adaptation of peirce's cantilever test for in situ measurements of laminaria digitata (laminariaceae). *American Journal of Botany*, 101(6): 1050-1055.

PAPER VI *Henry et al.* [2016a]

Henry, P.-Y.T., Nedrebø, E. L., Myrhaug, D., [**2016**]. Visualisation of the effect of different types of marine growth on cylinders' wake structure in low Re steady flows. *Ocean Engineering*, In Press.

PAPER VII *Detert et al.* [2015]

Detert, M., Weitbrecht, V., Aberle, J., Rowinski, P., **Henry, P.Y.** [**2015]**. 6.5 Auxiliary hydrodynamic variables, in "Experimental hydraulics: Methods, Instrumentation, Data processing & Management" by Muste et al. *IAHR Monograph* under publication process, Taylor & Francis.

Additional contributions (Appendixes)

APPENDIX I *Thomas et al.* [2014]

Thomas, R.E. Johnson, M., Frostick, L., Parsons, D., Bouma, T.J., Dijkstra, J., Eiff, O., Gobert, S., **Henry, P.Y. T.**, Kemp, P., McLelland, S., Moulin, F.Y., Myrhaug, D., Neyts, A., Paul, M., Penning, E., Puijalon, S., Rice, S., Stanica, A., Tagliapietra, D., Tal, M., Tørum, A., Vousdoukas, M., [**2014**]. Physical modelling of water, fauna and flora: Knowledge gaps, avenues for future research and infrastructural needs. *Journal of Hydraulic Research*, 52(3): 311-325.

APPENDIX II *Thomas et al.* [2015]

Thomas, R.E., McLelland, S., **Henry, P.Y.,** Paul, M., Eiff, O., Evertsen, A.J., Aberle, J., Teacă, A. [**2015**]. Not all Laminaria digitata are the same! Phenotypic plasticity and the selection of appropriate surrogate macroalgae for ecohydraulic experimentation. *EGU General Assembly*; 2015 Vienna.

APPENDIX III *Henry et al.* [2016b]

Henry, P.Y., Aberle, J., Dijkstra, J., Myrhaug, D., [**2016**]. An integrated, multi-sensing approach to describe the dynamic relations between turbulence, fluid-forces, and reconfiguration of a submerged plant model in steady flows. *EGU General Assembly*; 2016 Vienna.

Contents

List of abbreviations

ADV – Acoustic Doppler velocimeter

ANOVA – Analysis of variance

cdf – Cumulative distribution function

DOC – Dissolved organic carbon

JRA – Joint research activity

pdf – Probability density function

PISCES – Protocols and instrumentation for combined hydraulic and ecological models one of the JRAs of the former Hydralab IV research program.

RECIPE - Representing climate change in physical experiments: one of the JRAs of the ongoing Hydralab+ research program.

Rms – Root-mean-squared

SNR – Signal-to-noise ratio

TKE – Turbulent Kinetic Energy

VIV – Vortex Induced Vibrations

List of symbols

A	[m]	Wave amplitude
a	[-]	Gradient (slope) of the initial straight-line portion of a load deflection curve
A_{Ref}	[m^2]	Reference area of an object experiencing drag forces
b	[m]	Width of the plant/sample
C	[m]	Bending length
Ca	[-]	Cauchy-number
C_D	[-]	Drag coefficient
C_L	[-]	Lift coefficient
C_w	[ms^{-1}]	Speed of sound in water
D	[m]	Characteristic length of an object subject to drag forces
d	[m]	Distance from the bed to the point where the resultant fluid force acts
df	[-]	Degree of freedom (ANOVA)
E	[Nm^{-2}]	Young modulus. Often reported in MPa [MNm^{-2}]
E_b	[Nm^{-2}]	Young modulus under bending loads, or 'Bending modulus'. Often reported in MPa [MNm^{-2}]
EI	[Nm^2]	Flexural rigidity.
e	[-]	Engineers' strain
e_f	[-]	Flexural strain
e_t	[-]	True strain
F	[N]	Force applied on a biomaterial sample
f	[s^{-1}]	Wave frequency
F_B	[N]	Buoyancy force
F_b	[N]	Bending (reaction) force
F_D	[N]	Drag force
$f_{Doppler}$	[s^{-1}]	Change in received frequency (Doppler shift)
F_G	[N]	Gravity force
F_L	[N]	Lift force
F_R	[N]	Restoring force due to plant's rigidity
f_{Source}	[s^{-1}]	Transmitted acoustic pulses along the ADV beams
F_T	[N]	Tensile (reaction) force
F_v	[-]	F value (ANOVA)
G	[Nm^{-2}]	Torsion modulus. Often reported in MPa [MNm^{-2}]
g	[m^2s^2]	Gravity acceleration
G_{sh}	[Nm^{-2}]	Shear modulus. Often reported in MPa [MNm^{-2}]
G_o	[-]	Centre of gravity of the reference cross-section S_o of a beam
G_1	[-]	Centre of gravity of the reference cross-section S_1 of a beam
H	[m]	Wave height
H_{mo}	[m]	Significant wave height
h	[m]	Water depth
I	[m^4]	Second moment area of a beam cross section
J	[Nm]	Flexural rigidity per unit width
k	[m^{-1}]	Wave number associated with a given wave period
L	[m]	Plant height
l	[m]	Cantilever length
M	[Nm]	Bending moment
m_0, m_2	[m^2, m^2s^{-2}]	0^{th} and 2^{nd} spectral moment of the wave spectrum
N	[-]	Number of independent multiple comparisons

P	[-]	Statistical significance (ANOVA)
R	[m]	Radius of a circular beam/sample
r	[m]	Radius of curvature of a deflected beam
Re	[-]	Reynolds number
q	[Nm^{-1}]	Load distributed over a beam
s	[m]	Distance from the top of a deflected beam (curvilinear coordinate), or from the hanging edge of a sample for the case of a cantilever bending test.
s_p	[m]	Span between the two support points in a 3-point bending test
S	[-]	Wave steepness
S(f)	[m^2s]	Wave spectrum
S_o	[m^2]	Particular cross-sectional area perpendicular to the direction of the force applied on a sample (tension/compression), or parallel to the force applied on a sample (shear). Before deformation.
S_1	[m^2]	Particular cross-sectional area perpendicular to the direction of the force applied on a sample (tension/compression), or parallel to the force applied on a sample (shear). After deformation.
T	[s]	Wave period
T_{02}	[s]	Mean wave period
t	[m]	Thickness of a plant/sample
U	[m/s]	Flow velocity
U_R	[-]	Ursell number
u	[ms^{-1}]	Velocity vector, with the velocity components u_x u_y and u_z in the Cartesian reference system
$\overline{\mathbf{u}}$	[ms^{-1}]	Time averaged velocity vector
u'	[ms^{-1}]	Turbulent velocity vector
w	[m]	Ordinate describing the deflection of a beam
w_g	[N/m^2]	Weight per unit area of a sample subject to a cantilever bending test
x	[m]	First coordinate of the Cartesian reference system
x_o	[m]	Initial reference length of a sample (width in Fig.6)
x_1	[m]	Reference length (width in Fig.6) of a sample after deformation
Δx	[m]	Variation of the reference length after a mechanical test
y	[m]	Second coordinate of the Cartesian reference system
z	[m]	Third coordinate of the Cartesian reference system
z_1	[m]	Longitudinal length of the sample, linked to x in Fig. 6
α	[-]	Significance level (ANOVA)
γ	[-]	Shear strain
κ	[m^{-1}]	Curvature of a deflected beam
λ	[m]	Wave length
λ_e	[-]	Extension ratio of a deformed sample
ν	[m^2s^{-1}]	Water kinematic viscosity
Φ	[m^2s^{-1}]	Velocity potential
φ	[rad]	Deflection angle between the beam central axis and the vertical coordinate.
ρ	[kg/m^3]	Density of the fluid considered
ρ_p	[kg/m^3]	Density of the plant
σ	[N/m^2]	Mechanical stress (tension/compression)
σ_f	[N/m^2]	Flexural stress
τ	[N/m^2]	Mechanical shear stress
θ	[rad]	Angle between the inclined plane of reference for the cantilever bending test, and the horizontal plane.
ϑ	[-]	Vogel exponent.

1. Introduction

Understanding the complexity of the interactions between aquatic biological systems and their physical environment is a critical condition for the sustainable management of aquatic environments and their ecosystems [*Marion et al.*, 2014]. The recent increase of the research efforts in different fields related to eco-oriented disciplines highlights the urgent need of understanding this multiscale/multidisciplinary problem in the context of our current climate and of the coming environmental changes [*Nikora*, 2010; *Rice et al.*, 2010]. Sea-level rise, temperature changes, increased storm intensity and frequency, and related flooding and erosion events are processes expected to trigger shifts in the dynamic interactions between ecology and hydraulics [*Parry et al.*, 2007; *Solomon et al.*, 2007; *Thorne et al.*, 2007]. Many aspects of these interactions are still to be investigated and many answers will most probably be found at the different discipline interfaces, which are least studied and understood [*Nikora*, 2010; *Marion et al.*, 2014]. Due to this complexity, physical modelling and other experimental works stand as an essential link between field observations and theoretical/numerical models when characterising the impact of environmental changes on aquatic ecosystems [*Thomas et al.*, 2014].

In such ecosystems, aquatic vegetation plays a central role. Benthic assemblages of marine macroalgae and seagrasses are good examples, as they can be a net source of dissolved organic carbon (DOC) that is vital for the microbial food web in the nearshore water column [*Barrón et al.*, 2004; *Wada and Hama*, 2013]. Kelp forests are among the most productive of all marine macrophyte communities [*Reed and Brzezinski*, 2009]. Plant canopies regulate turbulent processes, playing a major role in aquatic environments, from an engineering point of view (e.g. wave dampening, *Möller et al.* [2014]) or from an ecological point of view (e.g. productive kelp forests, *Smale et al.* [2013]). A variation of the plants' mechanics in time or space will imply changes in these regulation processes, which in turn can lead to major changes in the physical/ecological environment.

The hydrodynamics of vegetated flows is a young topic, at the interface between fluid mechanics and plant ecology. Fig. 1 illustrates this fact by reporting the evolution of the number of publications per year registered in the scientific library Scopus®, Elsevier B.V., depending on three different associations of the keywords 'vegetation', 'hydrodynamics', biomechanics', 'plant' and 'plant ecology'. The research activity focussing on 'vegetation' and 'hydrodynamics' started slowly in the 90s while in 2014, about 15 new papers were

published every month on the topic. Similarly, research on plant biomechanics started its development in the 80s, and in 2014, about 13 new publications can be found every month. In the context of climate change and the development of sustainable societies, there is a clear need of understanding and better prediction of the hydrodynamics of vegetated flows. As this scientific area is mostly unexplored, many research groups refocus their activities towards these areas at the interface of major established field of research, leading to a very high dynamism of these new eco-oriented areas of research. However, when it comes to combining more than two fields, such as 'biomechanics', 'plant ecology' and 'hydrodynamics' only four papers could be found, three being reference foresight papers [*Ennos*, 1999; *Nikora*, 2010; *Rice et al.*, 2010], and only one being a research paper [*Puijalon et al.*, 2005]. Although these results come only from one scientific library, thus depending on the keyword research tool implemented, it suggests that the hydrodynamics of vegetated flows remain mostly unexplored as it is a combination of at least three main different fields (hydrodynamics, organism biomechanics and ecology, see *Nikora* [2010]).

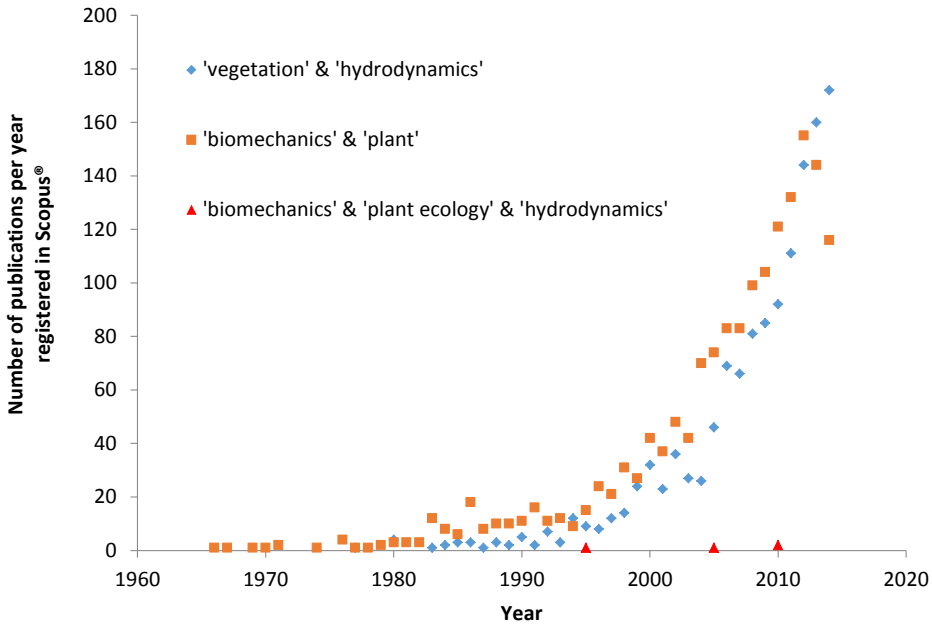

Figure 1- Evolution of the number of publications per year registered in the scientific library Scopus®, Elsevier B.V., depending on three different keywords associations within the period 1966-2014,

Thomas et al. [2014] identified the main issues that research on aquatic biological systems and their physical environment is currently facing (for more details see Appendix I). These issues include the adaptation processes due to spatio-temporal changes of environmental factors, the complexity of the interaction and feedback processes between organisms, the natural variability among organisms and both the possibility and need to scale down these processes for a proper representation of aquatic ecosystems. These processes are mostly regulated at the interfaces between the different elements defining an aquatic biological system (water, sediment, biota and atmosphere, see *Marion et al.* [2014]).

When it comes to the hydrodynamics of vegetated flows, two main types of interactions can be identified: chemical/biological, and mechanical. Chemical and biological interactions between aquatic vegetation and its environment are already well documented as they are at the heart of aquatic biology and ecology [*O'Hare*, 2015]. The consideration of mechanical interactions, however, is fairly new to engineers, biologists and ecologists, as it defines an interface between engineering and ecological thematic. In this context, this thesis investigated the role of aquatic vegetation biomechanics in the hydrodynamics of vegetated flows and aimed at including plant biomechanical considerations in hydraulic and coastal research.

1.1. Objectives and research questions

The main objective of this thesis work was to create a solid base of knowledge on aquatic plant biomechanics for future hydraulic experimentations, and trigger new research at NTNU and elsewhere. The main issues addressed were:

- Identification of the key processes of plant-flow mechanical interactions through literature surveys and critical reviews.
- Improvement of the understanding of plant structural properties and their variability.
- Development of new methods to design plant surrogates for hydraulic experimentation, based on mechanical similarity.

This thesis being linked to the PISCES project (part of the EU-funded HYDRALAB-IV research program), it also shared some of its approaches. Thus, measurement techniques and experimental methodologies were developed and improved to better incorporate plants and in hydraulic modelling; and assess some of the major limitations of using surrogates in flumes to evaluate effects of organisms on flow characteristics.

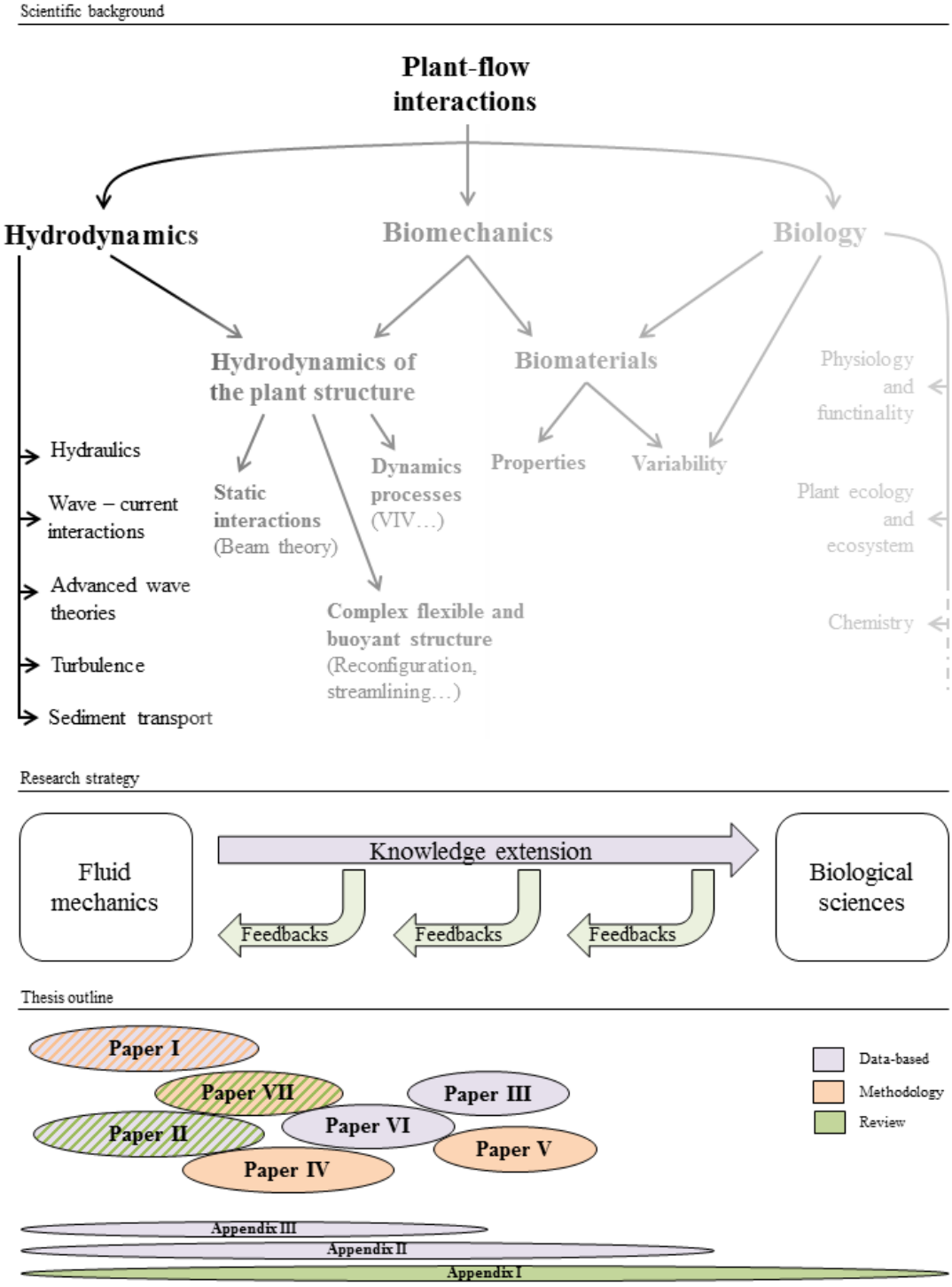

Figure 2 - Overview of the of the thesis' scope and outline

1.2. Research strategy and thesis outline

Strategy **–** Fig. 2 provides a graphical overview of the scientific background, the adopted strategy, and the thesis outline related to the different areas of plant-flow interactions. The amount of knowledge in the different areas is represented by the different grey tones in the 'Scientific background' diagram. Thus it is clear that the main scientific background at the beginning of this thesis work focused on general fluid mechanics. As the hydrodynamics of vegetated flows is an interplay of three different main fields of research, the strategy adopted has been to extend the current knowledge towards the biological sciences, via plant biomechanics, in order to better capture the complexity of plant-flow interactions. However, as clearly stated by *Denny* [1988], "*we approach the topic* [of plant-flow interactions] *from the viewpoint of a team of engineers assigned to the task of designing a new, improved plant* […]. *A potential difficulty with this mechanistic view is that it works exactly backwards from the process of evolution*". To compensate for the bias of this engineering approach, discussions of reviews and new scientific results were focussed on the 'feedbacks' of this new knowledge on the original main scientific background; e.g. how do plant properties and the variations of plant characteristics affect plant hydrodynamics (see Fig. 2).

Outline **–** As a result, this thesis is organised around six journal papers, one book chapter, and completed by three appendices. These contributions are data-based or methodology oriented papers, some of them including reviews of the topic, and are organised along a 'gradient' from fluid mechanics to biological sciences (see Fig. 2). Some of the papers can be grouped in sets, papers I and II looking at wave and wave-plus-current induced drag forces on submerged plants, and papers III and IV focusing on some of the advances made within the PISCES project. The various scientific notions underlying these contributions are developed in the following sections.

2. Scientific background

2.1. Plants and macroalgae as complex biological systems

Plants, algae, seaweeds, seagrasses… a short explanation **–** There is the need to clarify the use of the term "plants", as this is a seed for long passionate discussions between scientists. The different types of algae were once considered to share a common ancestor with land plants (monophyletic), and were therefore grouped in the same Plant kingdom. However, it is now known that red, green and brown algae have different ancestors (polyphyletic), and are

therefore placed in different divisions within the Plant kingdom [*Bhattacharya and Medlin*, 1998]. The first land plants probably evolved from shallow freshwater green algae, and fossils of isolated land plant spores suggest land plants may have been around as long as 475 million years, prior to the Silurian geological age [*Wellman et al.*, 2003]. Macroalgae is a term used to group multicellular macro organism of the red, brown and green algae; while seaweed describes marine macroalgae living near the seabed (benthic). Finally, seagrass describes aquatic submerged vegetation that evolved from land plants, and that are fully adapted to underwater saline environment (Fig. 3 - *Atwell et al.* [1999]). Despite these clear differences, the word 'plants' is in use as a catch-all term to design vegetation type organisms.

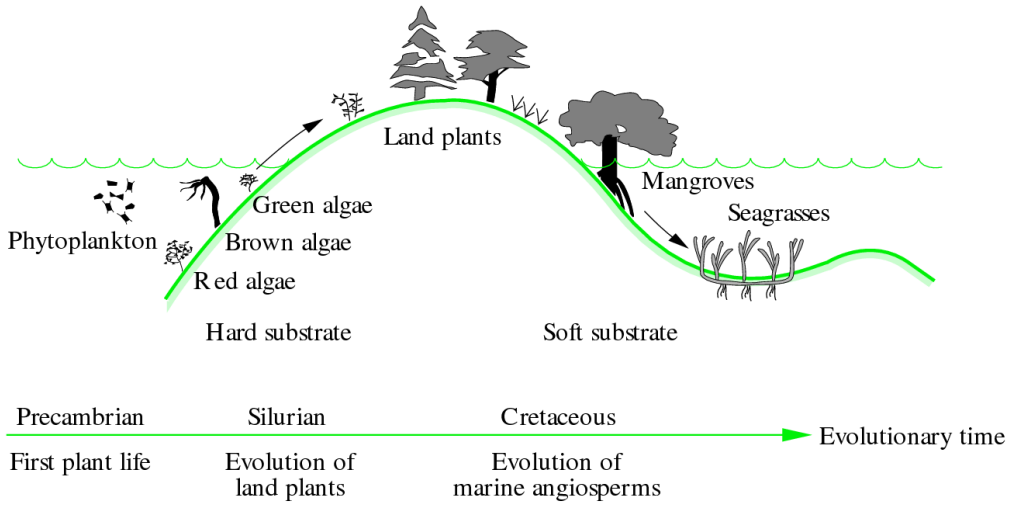

Figure 3 – "Evolution of seagrasses from algae. Algal evolution in the Silurian was followed by appearance of the first land plants which diversified by developing higher plant characteristics such as woodiness and sexual reproduction. During the Cretaceous, marine angiosperms evolved, characterised by mangroves and salt-marsh plants in intertidal zones and seagrasses as the dominant submerged macrophytes". Taken from *Atwell et al.* [1999].

Plant's functions as design criteria – 'Plants' are organisms designed and optimised, like animals, to survive in their environment. For doing so, they must perform simultaneously a set of functions which are defined by underlying physical laws. As each function comes with a set of requirements that the plant must meet, combining all requirements at once mostly leads to design incompatibilities [*Niklas*, 1992]. Therefore, compromises are found on the basis that the plant must perform in its environment and meet some minimum specifications. In some cases, the problem of conflicting design specifications is solved by some

evolutionary innovation, i.e. a small change in the plant structure/metabolism that leads to a net improvement of the performance for several functions simultaneously. An example of the main functions that a terrestrial plant must perform is illustrated in Fig. 4. Such a set of functions is also found for aquatic vegetation with exception of the evaporation process. The source of energy is the most critical criterion in an organism's design. Plants and algae are autotroph, meaning they manufacture food from inorganic compound using an external source of energy. Most of the plants and algae use the sunlight as an external source and are therefore classified as 'photoautotroph'. In an aquatic environment, this implies a certain range of depth below the water surface were life is possible at a reasonable cost. Although organisms performing photosynthesis have been found at more than 100m water depth, most of the macroalgae are found in less than 30m where the light levels are high enough to result in a net carbon gain [*Denny*, 1988]. As a consequence, benthic macroalgae are most abundant in open shallow waters, were the wave action is the strongest.

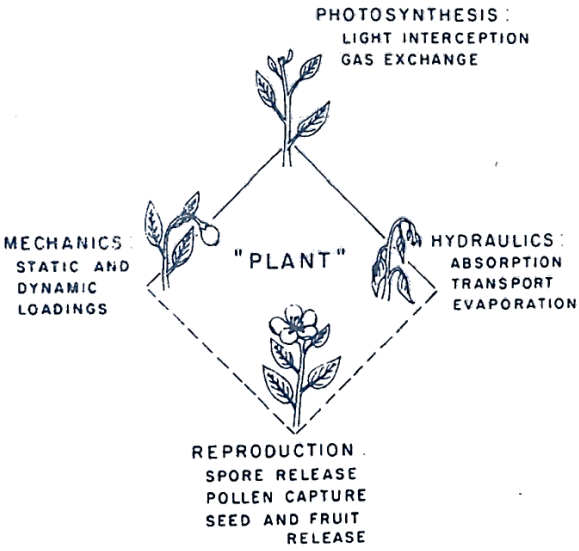

Figure 4 – Principal vegetative and reproductive functions that must be performed by all plants (photoautotrophs). Taken from *Niklas* [1992].

The rigidity of the plant structure and the plant morphology form the second set of criterion defining the mechanical performance of an organism in its environment. Plants and macroalgae can clearly be divided into two categories, those that opted for high flexibility and those that opted for a higher rigidity. In general, aquatic plants, and especially organisms living in a wave-swept environment, are considerably more flexible than land plants (see

Table 1, p15), as a rigid structure will experience larger hydrodynamic loads compared to a flexible structure of the same size in the same environment. An increased flexibility allows the organism to bend and reduce its frontal area (i.e. area of the plant projected in the flow), and adopt a more streamlined disposition, which is crucial in energetic aquatic environments (developed in details in the coming sections). As plants and macroalgae have several advantages in growing tall (improving photosynthesis and reproduction), the modulation of the plant's rigidity appears to be a key criterion in maintaining a good overall performance in environments with higher hydrodynamic stresses.

Mechanics also influences the plants' reproduction, this function being often based on diffusion and dispersion processes of seeds from flowers (seagrasses) or spores (macroalgae). However, the constrain of the physical environment also pushed some species of macroalgae to develop alternative strategies, such as vegetative propagation (*Endocldia*, *Rhodymenia* , see *Denny* [1988]). Finally, the plant relying on nutrient and carbon exchanges, flux control and internal hydraulics are major functions that must be performed efficiently by the plant. These exchanges depend highly on plant motion, which in turn is influenced by plant mechanics [*Huang et al.*, 2011; *Rominger and Nepf*, 2014].

Convergence and adaptation – In order to carry on with the different functions necessary to life, the plants differentiate their tissues (organisation of groups of similar cells), which then gives shape to different organs, adapted to perform specific functions in a given environment [*Atwell et al.*, 1999]. The heterogeneity of the different physical environments will certainly lead to different shapes and strategies characterising the plant biological system, and *a contrario*, plants distantly related, but living in a similar environment, will evince morphological and physiological convergence [*Niklas et al.*, 2006]. This convergence phenomenon is one of the consequences of the adaptive natural selection process. Adaptations are changes in a biological system that enhances the survival or reproduction of an organism compared to previous generations [*Futuyma*, 2009]. As natural selection is a mechanism constantly in action, organisms are constantly adapting to their environment, providing an example of feedback between a plant and its physical environment (Fig. 5). However, convergence and adaptation are processes occurring at relatively large time scales, typically over hundreds of generations to give significant changes to the morphology and physiology of an organism.

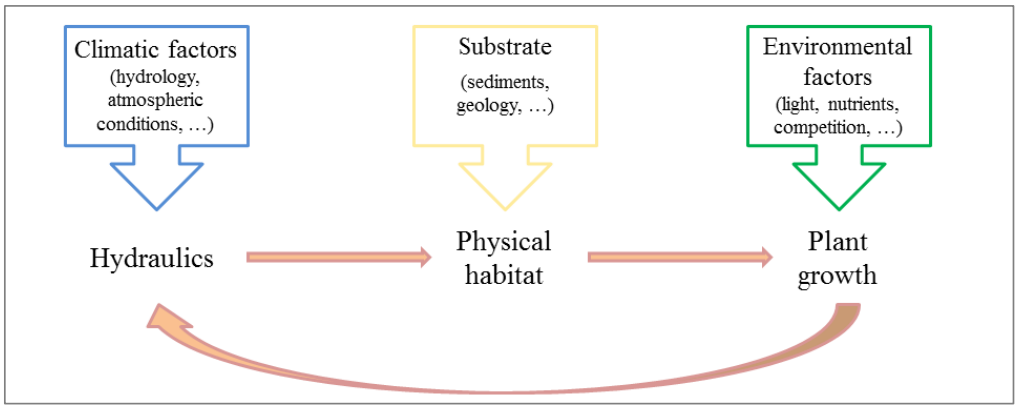

Figure 5 – Simplification of the dynamic feedbacks between aquatic vegetation and hydraulics over time, with inputs from the local environment. Adapted from *O'Hare* [2015].

Seasonality, succession and spatial heterogeneity – Due to their dependency on light availability, most of the plants base their growing activity on the yearly cycle of day-length, with a growth-rate peaking in spring to reach its maximum in summer. This is also the case for all aquatic vegetation such as freshwater macrophytes and riparian vegetation [*O'Hare*, 2015], or marine macroalgae [*Schaffelke and Lüning*, 1994]. Growth phases can also be synchronised with seasonal hydraulic events (in tropical regions: floods, seasonal rain), or nutrient availability (in darker polar regions, e.g. *Davison et al.* [1984]). After the growing season, some plants completely die off, or simply lose their leafs/blades, and regenerate the coming year from seeds or propagule for annual plants, or roots/stems for perennial plants. This implies a dramatic change of the vegetation morphology from summer to winter, which in turn will affect the local hydraulics and sediment trapping properties of the canopy, which is another example of the dynamic feedbacks between aquatic vegetation and hydraulics (Fig. 5). Colonisation and succession are also time dependent processes. When a new environment is available, opportunistic species establish a first colony and locally modify the substrate and/or the hydraulic conditions [*Gurnell*, 2014]. These local modifications will consequently generate new favourable conditions for other species. Then, the competition for the same resources will induce the retreat of the less performant species in favour of some newcomers. This process, known as succession, a cornerstone concept in plant ecology first described by *Clément* [1916], implies significant changes in the vegetation characteristic, and occurs over time scales varying from one season to hundreds of years. During this process, habitat-scale

and large scale distributions are linked to the ability that the species have to disperse and settle, and tolerate different environmental conditions and disturbances [*O'Hare*, 2015]. Predation by a grazing fauna has also a strong impact on these temporal and spatial variations, with some cases of canopy disappearing in a few years-time (see the example of kelp-sea urchin interaction, *Steneck et al.* [2002]).

2.2. The mechanics of biomaterials

Basic properties of biomaterials – In mechanics, stress is a physical quantity that characterises the internal forces that neighbouring particles of a continuous material exert on each other, while strain is the measure of the deformation of the material under a given stress.

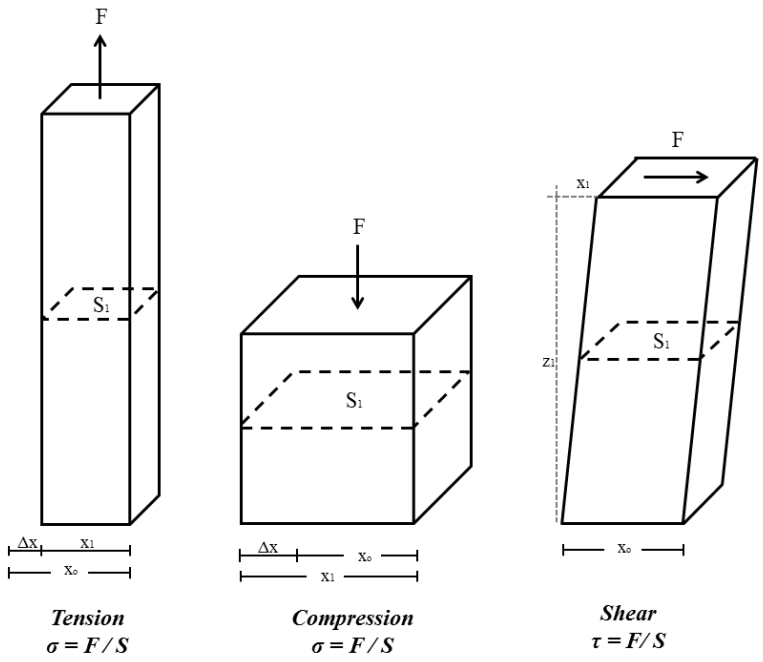

Figure 6 – Simplified definition of stress and normalized deformation for tension, compression and shear of a discrete biomaterial sample. Adapted from *Denny* [1988]

As illustrated in Fig. 6, stresses are generated by external forces (noted F in Fig. 6) and the stress under a given load is the force divided by the particular cross-sectional area S_1 resisting the force. This cross-section is perpendicular to the axis along which the force is applied for tension/compression loads and the normal stress σ is defined as $\sigma = F/S_1$. If forces are applied

in shear, the cross-section S_1 is assumed to lie in a plane parallel to the force F and the reaction force $-F$. The shear stress τ is expressed as $\tau = F/S_1$. The amount of deformation of a biomaterial under a given load is a function of its size, and therefore the strain is defined as a normalised deformation. In order to quantify these deformations, a reference length x_o is defined prior to the test and measured after deformation (x_1), allowing the quantification of variation in terms of Δx ($= x_0 - x_1$) of the reference length after a mechanical test. Based on this parametrisation, four common definitions of the strain are typically in use (see e.g. *Niklas et al.* [2006]; see Fig.6 for the notation): **1.** The extension ratio λ_e is defined as the ratio of the deformed length to the initial length $\lambda_e = x_1/x_o$. **2.** In engineering, the strain is characterised by the change in length and is expressed as $e = \lambda_e - 1 = \Delta x/x_o$. This definition is most common and, like the previous definition, valid for deformations under tension and compression. **3.** The 'true' strain is defined as $e_t = ln\ \lambda_e$. **4.** The shear strain γ, which is the gradient of the deformation under a shear load is defined as $\gamma = dx/dz$, where x and z are the coordinates of the Cartesian reference system The stiffness properties of a material, i.e. how much a material deforms under a given stress, can be estimated from the ratio of stress to strain, called the Young modulus $E = \sigma/e$ (relation known as Hook's law). Young's modulus is a material constant and can vary with the type of load (e.g. compression or tension), or if the material has non-linear properties (developed in the next paragraph and in Fig. 8). Similarly, it is possible to characterise a shear modulus $G_{sh} = \tau/\gamma$ and a torsion modulus G based on the ratio torque to angular deformation recorded during a torsion test (see *Harder et al.* [2006]). All mentioned moduli are expressed in the S.I. unit Pascal (*Pa*).

Due to the heterogeneity of the tissues forming the structure of a plant or macroalgae, these biomechanical properties are anisotropic, and can vary considerably depending on the type of load applied and the orientation of the plant's tissues. As an example, *Ochroma pyramidale*, known as balsa tree, is characterised by a Young modulus of the order 3-4 GPa along its wood fibres, and 0.1 GPa across the fibres. In addition, water is an important part of plant composition (for example up to 15 % in the macroalgae *Laminaria japonica*). Thus internal water variation and water fluxes can have a major impact on plant physiology and the mechanics of the plant's tissues. Water fluxes in a plant organism are driven by the osmosis process, which is a net movement of solvent molecules through a semi-permeable membrane (cell walls) into a region of higher solute concentration in the direction that tends to equalize the solute concentrations on each side of the membrane [*Niklas*, 1992]. The osmotic flow will adjust the water content of a cell depending on the hydration of its neighbouring cells,

affecting the internal pressure in the cell itself – the turgor pressure (Fig. 7). The turgor pressure is vital for plant tissue biomechanics because it influences directly the tensile stresses generated within the cell walls, especially for thin-walled cells and tissues. For thicker walled-tissues, a loss of water induces an increase of the elastic modulus of the tissue, as a result of dehydration of the cellulosic components in the cell wall as well as the densification of the cell wall material in the tissue [*Niklas*, 1992]. As water content in a plant is known to vary with the climate, the growing phase of the plant, the water temperature and water turbidity for the case of macroalgae; the biomechanical properties of a plant's tissue will by definition vary constantly with time.

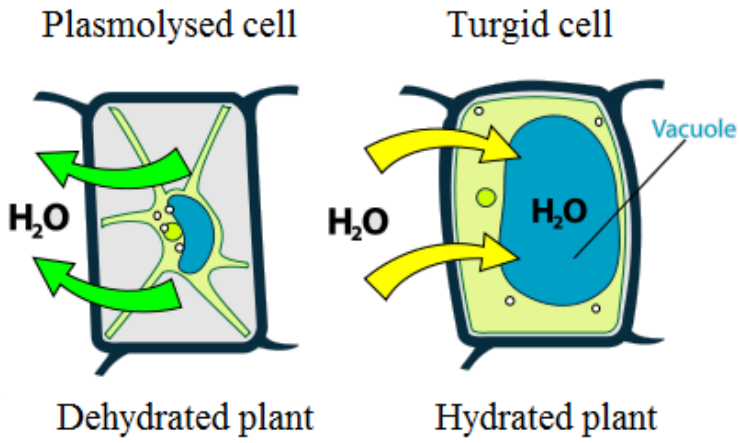

Figure 7 – Sketch of the effects, at a cell level, of the variation of the turgor pressure driven by osmotic flows. Adapted from the "Turgor pressure on plant cells diagram" released in the public domain (https://commons.wikimedia.org) by Mariana Ruiz Villarreal.

Elasticity, plasticity, viscoelasticity, creeping **–** A purely elastic material is a material in which stresses are linearly related to strains via Hook's law (curve (a) in Fig. 8A). Some materials are non-linear elastic, meaning that Hook's law does not apply for the full deformation of the material (typically for low strains). Such materials are still considered elastic as the loading and unloading curves superimpose each other (curve (b) in Fig. 8A). Plasticity is characterised by non-recoverable deformations, meaning that the loading and unloading curves will mismatch, and the amount of plastic deformation will be characterised by the remaining strain after unloading (curve (b) in Fig. 8A). Figs. $8C_1$ to $8C_3$ depict the difference between the three different types of non-elastic behaviour: plasticity (Fig. $8C_1$), elastoplasticity (Fig. $8C_2$, similar to curve (c) in Fig. 8A), and viscoelasticity (Fig. $8C_3$). For a

plastic material, deformations are not recoverable leading to a vertical unloading curve in a stress-strain diagram, while for an elastoplastic material some of the deformations are recovered. Viscoelasticity, however, is different from elasticity and plasticity: a viscoelastic material will return to its original shape after the sample has been unloaded, even though it may take some time. This is due to the viscous properties of the material generating a resistance to the strain rate (variation of the deformation in time) when a stress is applied.

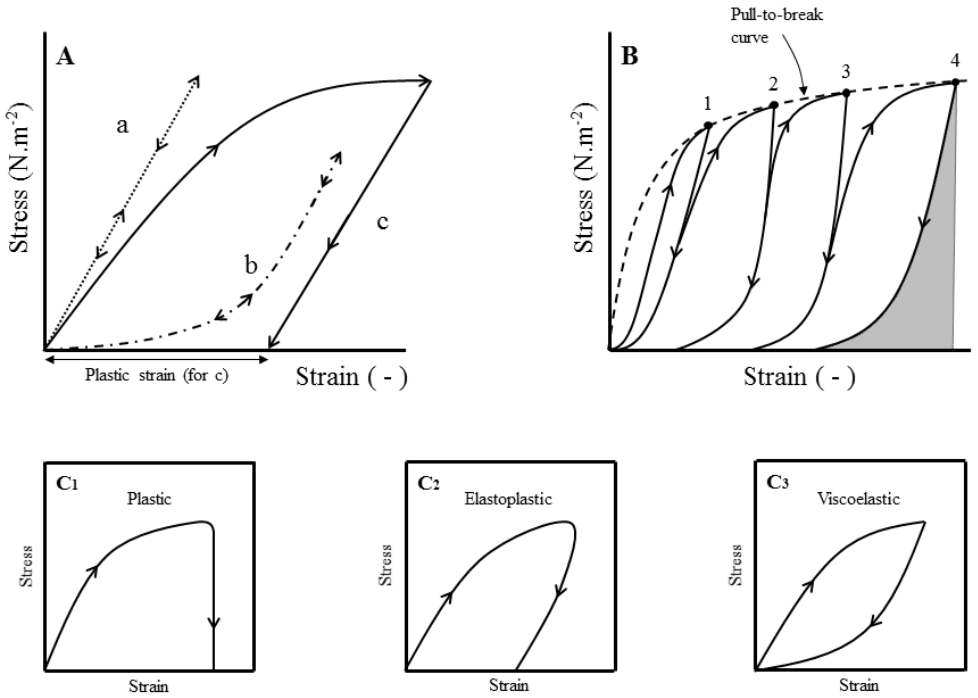

*Figure 8 – Examples of complex stress-strain behavior. (**A**) Typical curves for a linear elastic material (a), a non-linear elastic material (b), and an elastoplastic material with the unloading phase revealing the final plastic deformation (c). (**B**) Typical stress-strain behavior of a macroalgae material subject to cyclic loads with increasingly larger strains. Each cycle is composed of a nonlinear-elastic then elastoplastic extension followed by a nonlinear retraction. Each cycle induce plastic deformations. The tips of the extension-retraction cycles follow the curve of an elastoplastic pull-to-break test. The grey area represents the recoverable strain energy density after the last cycle. Adapted from Mach et al. [2007a] and Mach et al. [2007b]. (**C**) Stress-strain curves for purely plastic (C_1), elastoplastic (C_2), and purely viscoelastic materials (C_3).*

For biological materials it is possible to define regimes of pure elasticity, plasticity or a combination of both, depending of the way the stresses are applied. However, most

biomaterials, if not all, are viscoelastic to a greater or lesser extent. Creeping is another time dependent process characterising biomaterials, and relates to the tendency of the material to deform more or less permanently under a given load. Creeping may be related to viscoelasticy for polymers, but in the case of biomaterials it is rather due to the fibre rearrangements and tissue structural modification. Creep is characterised by a time dependent strain rate and occurs typically over larger time scales.

Mechanical testing **–** Mechanical properties of biomaterial are usually determined via standardised mechanical tests (tensile, compressive, bending, and tension tests, or dynamic and transient tests). Customised test benches coexist with commercial solutions, and their domain of applicability depends on the properties of the examined tissue [*Henry*, 2014]. As most of the biomaterials show behaviours caused by a combination of the three main types of deformation (linear/nonlinear elastic, plastic, and viscoelastic), it can be challenging to identify a zone of linear elasticity in order to define Young's modulus. For biomaterials, Young's modulus is typically defined as the slope of the first linear part of a stress–strain curve [*Vincent*, 1992]. Fig. 8B gives a typical example of the complex behaviour of a macroalgae material under cyclic loadings with increasing strain (adapted from *Mach et al.* [2007b]). The first cycle describes a pure non-linear viscoelastic deformation, as there is no remaining strain at the end of the cycle. With increasing the strain, each cycle is characterised by a nonlinear-elastic then elastoplastic extension followed by a nonlinear retraction. Thus, each cycle induces plastic deformations in addition to viscoelasticity as highlighted by *Mach et al.* [2007b] for a macroalgae material. The tips of the extension-retraction cycles follow the typical curve of an elastoplastic pull-to-break test, which refers to a standard test where the sample is pulled at a constant strain rate until failure.

The wide range of biological materials **–** Table 1 gives an example of the wide variety of biomechanical properties found in nature, ranging from viscous slimes to strong fibre structures (e.g. cellulose). In general, the average density of aquatic vegetation is slightly higher than the density of water. However, the presence of gas pockets or light mucilage may lead to positive buoyancy for some macroalgae or parts of macroalgae [*Stewart*, 2006b; *Luhar and Nepf*, 2011]. Mechanical properties, such as Young's modulus are directly affected by processes occurring at the cell scale. Variations in water content, salinity, or seasonal growth are thus modulating these ‘mean’ mechanical properties based on the variation of external environmental variables (e.g., seasons, rainfalls, wave climate, etc.; see also *Pratt and Johnson* [2002]).

Table 1 – Mechanical properties of typical of biological materials and man-made materials. Adapted from Denny [1988].

	Tensile strength (MPa)	Breaking Strain (-)	Young modulus E (MPa)	Density, x10^3 (kg/m^3)
Slimes				
Seawater	-	-	-	1.02
Pedal mucus[a]	0.1 – 0.3	-	-	1.0 - 1.1
Barnacle cement[a]	0.1 - 0.3	-	-	1.2
Rubbers				
Resilin	4 - 6	2 - 3	2	1.2
Abductin	8 – 12	2 - 3	4	1.2
Elastin	4 – 6	2 - 3	2	1.2
Fibers				
Silks	500 – 1 000	0.2 – 0.35	5 000 – 10 000	1.2
Collagen	50 – 100	0.08 – 0.1	2 000	1.2
Cellulose	500 – 1 000	0.02 – 0.1	20 000 – 80 000	1.2
Plant tissues				
(Freshwater algae)[b]	2 – 25	0.1 – 0.2	10 – 550	-
(Kelp stipes)[c]	1 – 3	0.2 – 0.6	3 – 30	-
Oak – *Q. Alba* (Wood)[d]	121	-	14 180	0.79
Crystalline Composites				
Coral skeleton[e]	40	< 0.001	60 000	2
Mussel shell[f]	56	0.002	31 000	2.7
Bone	190	0.01	18 000	2
Man-made materials				
Steel	3 000	0.015	200 000	7.9
Glass	100	< 0.001	100 000	2.5
Cement	4	< 0.001	4 000	2.8
Fiberglass	300 - 1 000	0.01	30 000 – 100 000	1.5 - 2

[a] *Denny et al.* [1985] [c] *Harder et al.* [2006] [e] *Vosburgh* [1982] All other data from
[b] *Miler et al.* [2014] [d] *Niklas* [1992] [f] *Currey* [1980] *Wainwright et al.* [1982]

2.3. Plant/macroalgae as a structure opposing the flow

Plants and macroalgae in natural flows are exposed to flow forces in the same way as any other body. Due to their rigidity and internal structure, they offer an obstruction to the main flow and the drag in flow direction represents a major part of the fluid forces. These organisms are typically located in the boundary layer which is a zone where turbulence is generated due to increasing shear as the mean flow velocity decreases towards the bed. Turbulence contributes to drag fluctuations and increases the intensity of the maximum forces experienced by the plant [*Nikora*, 2010]. In order to reduce the impact of these forces, aquatic plants have developed strategies based on their flexibility to reduce the force intensity by streamlining and thus by reconfiguring their geometry [*Koehl et al.*, 2008; *Nikora*, 2010]. Drag forces are driving reconfiguration processes and these processes are modulated by the plant's structural properties [*Gosselin et al.*, 2010b; *de Langre et al.*, 2012; *Albayrak et al.*,

2013]. In order to investigate the plant-flow mechanical interaction, there is the need to detail the following key concepts.

Static beam theory **–** Simple loading regimes are rare in nature (e.g., pure tension, pure compression) due to varying loadings and the complexity of the vegetation structures. In order to capture the main processes of plant-flow interactions, plants and algae have been commonly modelled in a simplified way as beams [*Dijkstra and Uittenbogaard*, 2010; *Luhar and Nepf*, 2011; *Maza et al.*, 2013]. The mechanics of beam structures is the core of many engineering applications and its simplest formulation, the Euler-Bernoulli beam theory, represents the basis for the determination of static beam deformations [*Gere and Goodno*, 2012]. This theory is based on the "Bernoulli-Euler Hypothesis" and was derived around 1750. This hypothesis lead to the formulation of the 1-D Euler-Bernoulli static beam equation, relating a beam's deflection to the applied load [*Gere and Goodno*, 2012]:

$$\frac{d^2}{dz^2}\left(EI \frac{d^2 w}{dz^2} \right) = q \tag{1}$$

where $w(z)$ is the ordinate describing the beam deflection and q is a distributed load (in Nm^{-1}). The quantity EI, known as flexural rigidity, is the product of the elastic modulus E (or E_b in the case of bending an anisotropic material) and the second moment area of the beam's cross section I [*Gere and Goodno*, 2012]. For a given cross section, I is calculated for the "neutral" axis of the cross section, i.e. the axis passing through the centroid of the cross-section and which is perpendicular to the applied load. For a beam oriented along the vertical z with a horizontally applied load in x-direction (Fig. 9), the second moment area is defined as [*Young et al.*, 2011]

$$I = \iint x^2 \, dy \, dx \tag{2}$$

for a centroid (centre of the cross-section) with the coordinates $y = x = 0$. For real plants, E and I will mostly vary with z. Ignoring this fact, EI may be considered as being constant leading to the relation

$$EI \frac{d^4 w}{dz^4} = q \tag{3}$$

Furthermore, assuming a linear-elastic material behaviour, integration of the bending stresses over the beam's cross section can be used to determine the resulting deflection through the relation

$$1/r = M/EI \tag{4}$$

where r is the radius of curvature of the deflected beam, M is the bending moment at a given section, and EI is the bending rigidity or flexural rigidity of the beam. The curvature κ of the beam is given as $\kappa = 1/r$ [*Gere and Goodno*, 2012], resulting in

$$M = EI\kappa \tag{5}$$

Considering a point P at a distance s from the top of the beam, φ is the angle between the tangent in P and the vertical plane (see Fig. 9) and is defined as $\varphi = dw/dz$. The curvature κ is equal to $d\varphi/ds$ and the bending moment $M = EI\, d\varphi/ds$. The relation between s and w can be found by solving Eq. 3.

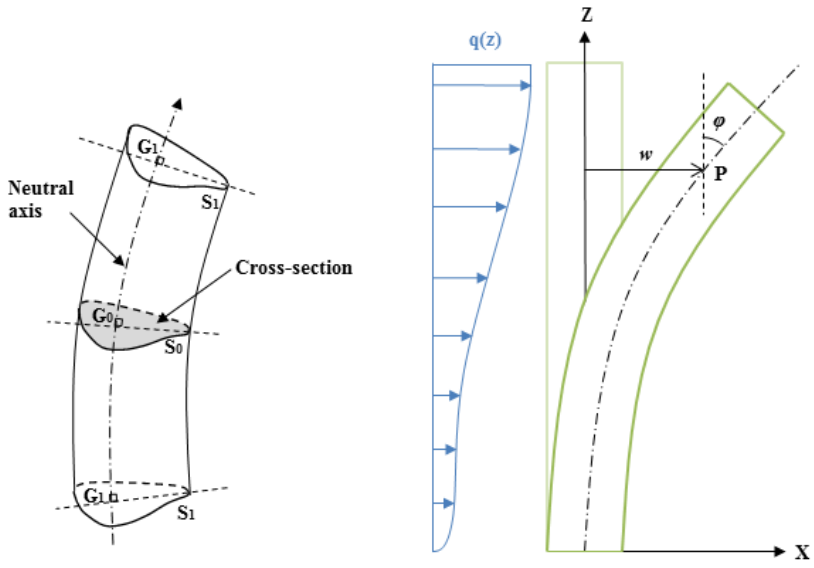

Figure 9 – Static bending: illustration of the parametrization of Euler-Bernoulli cantilever bending under the (hydrodynamic) load q(z). Illustration from P-Y Henry.

The simplest and most common type of deformation found in nature (in aerial or aquatic environments) is the cantilever bending. This form of bending, represented in Fig. 9, occurs when a beam is held fixed in one end and remaining free in the other end with the load being applied along its length. This type of loading induces shear forces in the beam which are compensated by the rigidity of a beam section [*Denny*, 1988; *Dijkstra and Uittenbogaard*, 2010; *Luhar and Nepf*, 2011]. For a cantilever bending, the bending moment will be maximum at the fixed end and null at the free end for any kind of load. Provided that EI is

constant, most of the bending moment will therefore occur close to the fixed end (deduced directly from Eq. 5).

Drag and flexibility– The characterisation of the interaction of a plant/macroalgae with its environment requires a better understanding of the relevant physical processes and hence, an appropriate parameterisation of the of fluid forces main component, the drag force. This drag force is commonly parameterized as $F_D = 0.5\rho C_D A_{Ref} U^2$, where ρ = fluid density, C_D = drag coefficient, A_{Ref} = reference area, and U = flow velocity. For a submerged rigid bluff body (A_{Ref} constant), the drag force F_D is proportional to the square of the flow velocity for sufficiently high Reynolds-numbers Re, i.e. where the drag coefficient C_D is constant, with $Re = UD/\nu$, ν is the water kinematic viscosity, and D is a characteristic length of the object. The drag coefficient C_D depends not only on Re but also on the shape of the object. As developed in previous sections, the mechanical action of the drag forces on the plant structure will be compensated by a reaction force depending on the rigidity of the plant and buoyancy forces. This reaction force is commonly called restoring force and noted F_R. At an initial stage prior to deformation, if $F_{Do} \leq F_{Ro}$, an object behaves as a rigid body, whereas it will be deformed if $F_{Do} > F_{Ro}$, leading to an increase of the magnitude of F_R (increasing bending moment). This defines the onset of reconfiguration via two different mechanisms: first, the reconfiguration process leads to the reduction of the frontal area of the vegetation element, and second, the reconfigured shape tends to be more streamlined [*de Langre*, 2008], which in turn will lead to a decrease of C_D. Streamlining can thus result in a substantial drag reduction reflecting the effort of the object to minimize pressure drag [*Vogel*, 1994; *Nikora*, 2010].

Many studies with plants and artificial objects have shown that the drag growth with velocity is lower for flexible elements than the usual rigid-body proportionality [*Gosselin et al.*, 2010b]. This has been parameterised by considering the scaling of drag force with velocity according to $F_D \sim U^{2+\vartheta}$, where ϑ denotes the Vogel exponent [*de Langre*, 2008]. This parameter, consolidating the effects of changes in A_{Ref} and C_D on F_D, describes the drag force response in regions of large deformations that may even be used if the local bending behaviour is non-linear [*de Langre et al.*, 2012]. Theoretically derived values for ϑ, which have also been confirmed experimentally, have been summarized recently by *de Langre et al.* [2012] for flexible plates (ϑ = -4/3), beams (ϑ = -2/3), and packing of beams under axial flow (ϑ = -2/3). For natural plants and leaves ϑ has been found to vary between -0.2 and -1.2 [*Albayrak et al.*, 2012; *Aberle and Järvelä*, 2013].

Dynamic effects – Besides the general framework related to considerations in a time-averaged domain, the dynamic reconfiguration of aquatic plants in response to turbulence is gaining more interest. Significant correlations between drag fluctuations, plant movements, and upstream turbulence were found recently by *Siniscalchi and Nikora* [2013], highlighting the importance of the dynamic reconfiguration for aquatic flexible plants. Drag force fluctuations are likely to be related to large-scale eddies interacting with the object (such as 1 and 2 in Fig. 10), but it has also been suggested that shear layer turbulence at the object-surface contributes to the dynamic behaviour (indicated by 3 and 4 in Fig. 10, see *Siniscalchi et al.* [2012]; *Cameron et al.* [2013]): force fluctuations are generated by well-known fluid-structure interaction processes, such as Vortex-Induced-Vibrations (VIV, 5 in Fig. 10), fluttering (flag in the wind) and galloping, which is a lock-in effect between VIV/fluttering and the natural frequency of a structure (leading to the famous collapse of the Tacoma bridge – for more details on these processes, see *Blevins* [2001]). *Rominger and Nepf* [2014] characterised these processes in the context of marine macroalgae and showed that this dynamic behaviour can increase the mean and peak drag significantly below a certain threshold for the flexural rigidity, as well as the mass exchange rates, vital for the reproduction of a plant and chemical exchanges with its environment.

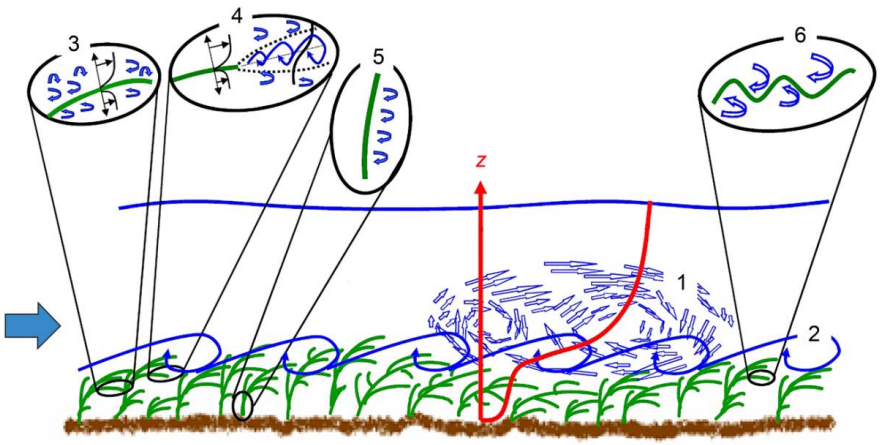

Figure 10 – Overview of the different scales of turbulence and identification of the corresponding flow-structure interaction processes for a dense canopy. 1- Large scale turbulence inherent to the flow, forcing the exchanges within the canopy. 2- Eddies generated by the shear layer at the top of the canopy (S-shape of the velocity profile), leading to Monami waves propagating at the top of the canopy. 3- Blade boundary layer, generating skin friction. 4- Blade wake instabilities, fluttering. 5- Stem wake turbulence generating Vortex Induced Vibrations. 6- Interactions between blade scale turbulence and blade ruffles. The red line indicate the evolution of the mean velocity profile, as a function of the elevation z over the river bed. Adapted from Nikora [2010].

However, these unstable processes can lead to a mechanical fatigue of the plant structure, which in turn generate crack initiation in the plant/macroalgae's tissues, and subsequently fatigue failure [*Mach et al.*, 2007b; *Mach et al.*, 2007a; *Mach*, 2009]. For this reason, the streamlining mechanism observed in plants or aquatic vegetation, is vital as it is known to reduce these instabilities, such as VIV [*Miller et al.*, 2012]. These dynamic effects are more important in oscillatory flows such as in waves, as a third time scale – the wave period - enters in interaction with the natural frequency of the plant structure (a function of the plant's mechanical properties) and the characteristic period of large eddies. Although an understanding of the coupling between flexural stiffness buoyancy and wave period has emerged [*Stewart*, 2006a], the effect of such flow conditions on drag forces and/or reconfiguration is barely known within applications in environmental hydraulics and coastal sciences, although it represents an important issue related to drag reduction with regard to habitat [*Denny*, 2006].

Dimensionless framework – In order to characterise plant-flow interactions in terms of non-dimensional numbers, we must first consider the set of basic forces acting in the system [*Nikora*, 2010]:

Flow-induced forces

$$F_D = 0.5\rho C_D A_{Ref} U^2 \quad \text{- Drag force} \tag{6}$$

$$F_L = 0.5\rho C_L A_{Ref} U^2 \quad \text{- Lift force} \tag{7}$$

Body forces

$$F_B = \rho g V_p \quad \text{- Buoyancy force} \tag{8}$$

$$F_G = \rho_p g V_p \quad \text{- Gravity force} \tag{9}$$

Structural forces

$$F_T = EeS_o \quad \text{- Tensile (reaction) force} \tag{10}$$

$$F_b = E_b I / rd \quad \text{- Bending (reaction) force} \tag{11}$$

where ρ and ρ_p are fluid and plant densities, g is the gravity acceleration, C_L is the lift coefficient characterising the plant, V_p is the plant volume; S_o is the plant cross-sectional area;

e is the strain defined previously (i.e. plant elongation under the fluid forces), r is the radius of curvature at a point where bending force is defined, and d is the distance from the bed to the point where the resultant fluid force acts.

Non-dimensional similarity numbers can be derived from the ratios between these different forces in order to characterise and model the vegetation-flow interactions, and have been discussed in detail by [*Nikora*, 2010]. The knowledge of how drag scales with velocity does not allow for the parameterization of F_D based on the use of the Vogel exponent, as the incorporation of ϑ as an exponent in the drag equation results in an expression that is not dimensionally homogeneous. The parameterization of a dimensionally homogeneous F_D-U relationship for flexible vegetation can be achieved within a general dimensionless framework by considering various dimensionless parameters in addition to the Reynolds-number Re and the drag coefficient C_D:

- The Cauchy-number Ca describing the deformation of an elastic solid under the effect of flow, which can directly be derived as the ratio of Eqs. (6) and (11) [*Alben et al.*, 2002]. L and b being the plant height and width, respectively, *Luhar and Nepf* [2011] defined this number as:

$$Ca = \frac{1}{2}\frac{C_D b U^2 L^3}{EI} \tag{12}$$

- The slenderness ratio S_l; ratio of the larger plant scale to the smallest plant scale (typically the plant height L over the plant diameter b). The Cauchy number mentioned above includes the effect of slenderness [*Nikora*, 2010; *Whittaker et al.*, 2013].
- The buoyancy parameter B, defining the ratio of the restoring forces due to buoyancy and the restoring forces due to stiffness (based on Eqs. 8, 9 and 11). With t as a reference thickness for the plant, *Luhar and Nepf* [2011] defined B as:

$$B = \frac{\left(\rho - \rho_p\right) g b t L^3}{EI} \tag{13}$$

The analysis of plant-flow interactions within a dimensionless context is to some extent hampered by the definitions of characteristic length scales, hydrodynamic variables, and plant properties required to form the dimensionless parameters. *Statzner et al.* [2006] demonstrated that the use of differently defined variables for the assessments of C_D or Re can produce opposite trends in the relationship between C_D and Re and that, for a given plant and flow, C_D

values can differ by about two orders of magnitude. This shows that conventions about the use of variables are required for experiments on drag and reconfiguration [*Statzner et al.*, 2006], which should be based on physical reasoning. This reflects also the statement by *Alben et al.* [2002] that experimental studies on fluid-structure interactions generally lack a theoretical interpretation that unifies the body and flow mechanics.

2.4. Vegetation parametrization in hydraulic experiments

Due to the complexity of (aquatic) vegetation, experimental and numerical models of vegetated flows often need to adopt a simplified description of aquatic plants. From an experimental point of view, there are three approaches to consider plants or macroalgae: 1) the use of artificial surrogates, 2) the use of scaled (living) plants, or 3) the use of natural plants. Living plants are rarely used in flume-studies as this imposes strong constraints on flume size (minimum size to avoid blockage and side wall effects – see *Frostick et al.* [2011]), on conditions needed to maintain the plants alive [*Johnson et al.*, 2014a], and on the need to monitor the plants' adaptation to flume conditions (phenotype plasticity – see *Johnson et al.* [2014a]; *Johnson et al.* [2014b]). However, the use of full-scale plants avoids the issue of replicating plant properties, and can provide a good insight on the effect of the complex plant structure on the flow [*Siniscalchi and Nikora*, 2013; *Whittaker et al.*, 2013]. To overcome the size issue, 'scaled' plants can be used experimentally by taking parts of a plant [*Yagci et al.*, 2010; *Västilä et al.*, 2013], or smaller plants (such as alfalfa in river morphodynamic studies, e.g. *Tal and Paola* [2010]). However, the scaling laws applying to the dynamic interaction plant-flow have barely been tested [*Wilson et al.*, 2003] limiting the use of scaled living plants in hydrodynamic experiments (see *Johnson et al.* [2014b] for a review of this issue). The use of unscaled artificial surrogates is therefore the method mainly used, as surrogates solve the problem of biological and chemical interactions within the laboratory environment. In addition, the shapes and mechanical properties of surrogates are almost unlimited as the range of artificial material available and manufacturing technique is very wide. Despite this large amount of possible designs, the most common and still-in-use plant surrogate, is the rigid cylinder [*Aberle and Järvelä*, 2013]. Although this representation of plant canopies allows for the characterisation of the main hydrodynamic processes occurring in vegetated canopies [*Nepf*, 1999; *Kothyari et al.*, 2009], the structural properties and hydrodynamics of rigid cylinders are far from representing vegetated flows accurately [*Aberle and Järvelä*, 2013]. Therefore, more advanced flexible surrogates are being designed to better reflect natural properties and variability found in plants and macroalgae, based on

their morphological characteristics and special distribution [*Frostick et al.*, 2011], biomass [*Neumeier*, 2005; *Neumeier*, 2007], Leaf Area Index [*Jalonen et al.*, 2013], and biomechanical properties [*Paul and Henry*, 2013]. The variation of these different parameters is fairly well understood for terrestrial and marine ecosystem, but to a lesser extent understood for freshwater ecosystems [*Nikora*, 2010]. However, their incorporation into hydraulic experiments is still rare. This is also the reason why the use of plant flow-similarity numbers based on plant stiffness and buoyancy (such as the Cauchy number and buoyancy parameter) have never been used in testing the analytical laws to scale down vegetation in flume experiments [*Johnson et al.*, 2014b], although possible scale effects in modelling the different processes in vegetated flows may be identified with a physical model at different scales up to near full-scale [*Frostick et al.*, 2011].

3. Material and methods

3.1. Experimental methods

As explicitly stated by *Nikora* [2010], "*a wide expansion of the biomechanical approaches in aquatic studies* […] *is slowed down by very limited information on plant material parameters and their variability across species, scales and environments.*" Therefore, in order to improve the knowledge of the plant/macroalgae parametrisation in hydraulic research and coastal sciences, "*the collection of such information should be among the top priorities of Hydrodynamics of Aquatic Ecosystems.*" This has been the main motivation of the experimental work carried out within this thesis, leading to the development of different mechanical testing procedures for collecting data sets on marine macroalgae.

The acquired data sets allowed for the development of different surrogates, whose hydrodynamic performances were partly tested. This section reviews the main methods developed and used within this thesis, leaving some of the detailed descriptions to the relevant papers included in the thesis.

3.1.1. Mechanical tests *(Papers III-IV-V)*

As mentioned previously, due to the heterogeneity of the plant material, plant tissues will behave differently if they are loaded in tension, bending or torsion. As plants and macroalgae are mostly bending under hydrodynamic loads, the characterisation of the Kelp bending

moduli has been in the focus of papers III, IV, and V. The description of these mechanical properties was done in parallel to a characterisation of the macroalgae-morphology.

Three-point bending test – This test allows for the determination of the Young modulus E in bending by measuring the deflection of beam-like samples under a central load. The anisotropic properties of biomaterials often impose the renaming of the "Young modulus in bending" as bending modulus (or alternatively flexural modulus), commonly denoted as B. More precisely, the three-point bending test consists of laying a stripe of material on two supports (two points) and applying a force in the centre of the sample (third point). The applied force F is recorded and plotted against the amount of displacement of the centre point w, allowing the bending modulus to be determined via the calculation of the flexural stress σ_f for a recangular or circular cross section [*Niklas et al.*, 2006; *Young et al.*, 2011]:

$$\sigma_f = {3F s_p}/{2bt^2} \quad \text{- rectangular cross section} \tag{14}$$

$$\sigma_f = {F s_p}/{\pi R^3} \quad \text{- circular cross section} \tag{15}$$

and the calculation of the flexural strain e_f:

$$e_f = {6wt}/{s_p{}^2} \quad \text{- rectangular cross section} \tag{16}$$

$$e_f = {12wR}/{s_p{}^2} \quad \text{- circular cross section} \tag{17}$$

In these equations, the symbol s_p denotes the span between the two support points, b the width of the sample, w the maximum deflection of the centre of the beam, and R the radius of the beam. Denotes the gradient (i.e., slope) of the initial straight-line portion of the load deflection curve as $a = F/w$, the flexural or bending modulus E_b can be derived as:

$$E_b = {\sigma_f}/{e_f} = {s_p{}^3 a}/{4bt^3} \quad \text{- rectangular cross section} \tag{18}$$

$$E_b = {\sigma_f}/{e_f} = {s_p{}^3 a}/{12bR^4} \quad \text{- circular cross section} \tag{19}$$

The main constraint of this test is that the tested length of the sample (the distance sp between the two support points) should be maximum 16 times the thickness of the sample; otherwise

the test deviates from a pure bending case (refer to the standard ISO 178:2010 [ISO, 2010] for further information). The test-bench used and presented in Fig. 11 was custom-made based on drill columns, and equipped with force and displacement sensors to log the force-displacement curves (see Paper III; *Paul et al.* [2014] for more details).

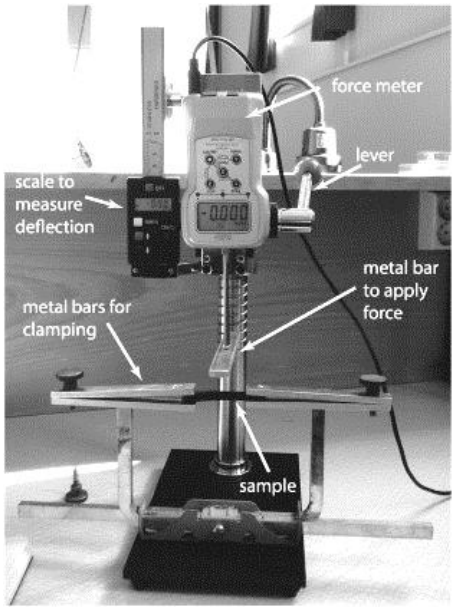

Figure 11 – Test bench developed for the characterization of the mechanical properties of marine macroalgae. Set-up designed by M. Paul for bending tests only, data used in Papers, III and IV.

Cantilever bending test – As macroalgae blades are generally thinner than the stem, the condition on the span/thickness ratio for the use of a three-point bending test could not be met. Therefore an alternative method to determine bending moduli had to be developed for thin flexible biomaterial [*Henry*, 2014]. Based on the bending theory described earlier and on the work of *Peirce* [1930], the bending behaviour of a thin beam (strip) can be derived. The use of Eqs. 4 and 5 leads to the definition of the bending moment $M = -EI\, d\varphi /ds$, where s is the distance from the hanging edge of the strip (see the parametrisation in Fig. 12). For an infinitesimal change in the distance Δs, the variation of the bending moment $\Delta(-EI \cdot d\varphi/ds)$ is equal to the change of the overhanging weight, $w_g s \cos\varphi \Delta s$ where w_g is the weight per unit area of the strip [*Peirce*, 1930]. Thus, the flexural rigidity EI is related to the deflection characteristics (s and φ) through the nonlinear second order differential equation along the strip:

$$d^2\varphi/ds^2 = -w_g s \cos\varphi / EI \qquad (20)$$

This problem was analysed numerically by *Szablewski and Kobza* [2003], but at the time when this problem was derived, only an approximation of the exact solution could be proposed. *Peirce* [1930] described a simple test for characterizing the flexural rigidity of strips. Based on a cantilever test (a strip fixed on one edge and bending under its own weight), the sample was first slowly moved forward until the tip of the specimen touched a plane at an angle of $\theta = 43$ ° with the horizontal plane.

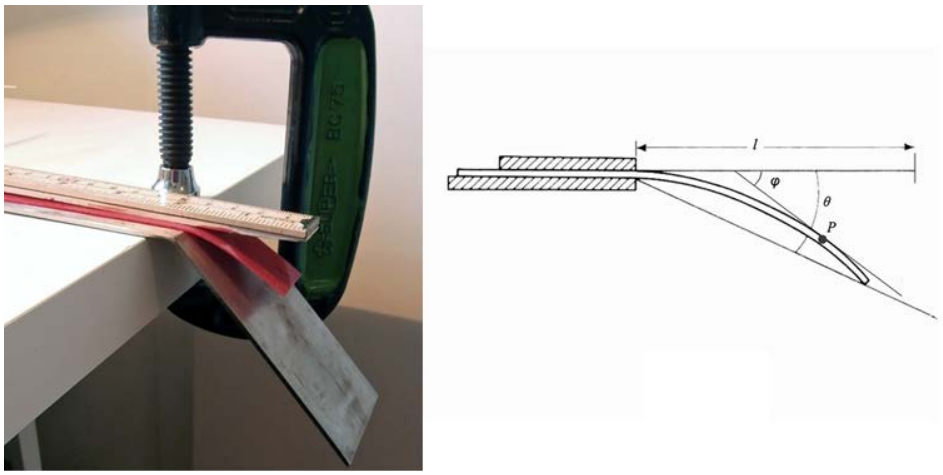

Figure 12 – Field cantilever bending test bench and parametrization of the problem. Adapted from *Booth* [1969] and *Henry* [2014].

The projection of the sample length on the horizontal plane, known as the cantilever length l (see Fig. 12), could then be measured. *Peirce* [1930] introduced the notion of bending length C defined as:

$$C = lf(\theta) \tag{21}$$

where the function $f(\theta)$ is expressed by:

$$f(\theta) = 0.5\left(\frac{\cos\theta/2}{\tan\theta}\right)^{1/3} \tag{22}$$

The flexural rigidity J (per unit width) of the sample is related to these quantities by $J = C^3 w_g$, where w_g is the weight per unit area of the strip (in N/m^2). This yields the relationship

between the length of the overhanging strip l, the angle θ of the inclined plane and the flexural rigidity per unit width J, also known as Peirce's formula:

$$J = w_g l^3 \left(\frac{\cos \theta / 2}{8 \tan \theta} \right) \tag{23}$$

The bending modulus of the sample can finally be deduced from:

$$E_b = Jb / I = \frac{12 w_g l^3}{t^3} \left(\frac{\cos \theta / 2}{8 \tan \theta} \right) \tag{24}$$

where I is the second moment area of the sample considering a rectangular cross section, given by $I = bt^3/12$, where b is the width and t the thickness of the sample [*Young et al.*, 2011]. *Peirce* [1930] designed this test with θ = 43° for practical purposes as $\cos(43/2)/\tan(43) \approx 1$. However, this relation is also valid for different values of θ, and angles of θ = 41.5° and θ = 45° can also be used. *Szablewski and Kobza* [2003] conducted a sensitivity analysis of Peirce's formula and found that a test conducted with an angle of θ=53° gives the best accuracy for the definition of the flexural rigidity. Although the variation of this accuracy is relatively small for angles between 40° and 50°, they recommended to keep the angle of the inclined plane in this range (θ > 40°) to reduce the uncertainties introduced during the measurements.

3.1.2. Force sensing on benthic vegetation *(Papers IV-VI-VII)*

Important insights of plant-flow interaction processes have been gained using drag measurements [*Vogel*, 1989; *Gosselin et al.*, 2010a; *Luhar and Nepf*, 2011; *Albayrak et al.*, 2012; *Albayrak et al.*, 2013; *Siniscalchi and Nikora*, 2013]. For example, *Albayrak et al.* [2013] conducted a systematic study of plant-flow interaction at different scales by analyzing statistics and cross-correlations of velocity and drag force measurements. Detailed drag measurements underlined the scale-specific reconfiguration processes that allow the plant to control the drag forces effectively. Because of non-linear interactions between the different scales, this type of study is an example of the need for further investigations of the plant-fluid interaction via the collection and analysis of fluid (drag) force measurements. The present section reviews the techniques used to document drag forces in vegetated flows and identifies some of the involved challenges.

Review of the common drag measurement techniques - The measurement of fluid forces experienced by plants requires the use of force sensing technologies. In modern sensors, the most commonly used method is measuring the strain produced on a reference body. Optical and electromagnetic methods are also used, but are rather dedicated to smaller scale applications (nanosensing). Force sensors (transducers) are often basic mechanical components converting strain into an electric signal [*Cutkosky et al.*, 2008]. Such transducers can be made of piezoelectric crystals or strain gages. Due to their simplicity and stability, strain gages have, until today, been predominantly used in ecohydraulic experiments. When implementing drag sensors, two categories of set-ups are generally used: attaching the plant to a friction free trolley and measuring the force with a load cell [*Callaghan et al.*, 2007; *Tinoco and Cowen*, 2013], or by directly measuring the strain on a beam structure, directly attached to the plant element [*Schoneboom*, 2011; *Albayrak et al.*, 2013]. Some alternatives have also been implemented, for example determining the drag force by measuring the strain on a plate [*Ishikawa et al.*, 2003; *Dwivedi et al.*, 2010] and hence determining the forces in several dimensions, or by balancing the mean force with a spring/balance system [*Marshall*, 1971; *Sand-Jensen*, 2008]. What distinguishes the different techniques is the way the sensors are implemented, either above the (water) surface [*Sand-Jensen*, 2008; *Albayrak et al.*, 2013; *Whittaker et al.*, 2013] to keep them dry, or submerged in water in a double bottom [*Callaghan et al.*, 2007; *Dwivedi et al.*, 2010; *Schoneboom*, 2011; *Siniscalchi et al.*, 2012]. The reasons for the development of these different techniques and implementations have been mainly due to the simplicity, reliability and the cost of sensing technology.

Figure 13 – Implementation of a drag force sensor in the field for testing the hydrodynamic performance of a *L. digitata* surrogate (right), and comparison with its natural counterpart (unpublished data – PISCES project).

Strain on a single beam, the low-cost solution – In many studies, the force experienced by a plant has been measured by attaching the plant to a beam and by measuring the strain (deformations) of the beam [*Luhar and Nepf*, 2011; *Schoneboom*, 2011; *Siniscalchi et al.*,

2012; *Albayrak et al.*, 2013]. As the beam is deformed, the gages are deformed causing their electrical resistance to change. This change, usually measured using a Wheatstone bridge, is related to the strain and thus the force experienced by the beam. Although this is a rather simple and easily available technology that has been implemented in many laboratories, it can be shown, based on standard strain gage specifications, that this technique needs a long beam in order to be able to measure very small forces (<1N). As aquatic plants often experience very low drag, the investigation of plant-fluid interactions therefore calls for sensors big enough to measure small forces in order to investigate smaller scale processes. Thus "small force measurements" in confined space is one of the main limitations of this traditional "low-cost" approach.

General implementation issues - Considering aspects of plant-fluid interaction, it is sometime possible to work with force sensors which are located above the water surface [*Sand-Jensen*, 2008; *Albayrak et al.*, 2013; *Whittaker et al.*, 2013]. However in nature, aquatic plants are embedded in multiple-scale turbulent boundary layers generated by the bed, the (restricted) water depth and the organisms themselves. In addition, considering vegetation canopies, the turbulence generated at the canopy-scale (mixing layer analogy) and scale dependent wake flow characteristics (e.g., leaf, stem, and plant scale), have a significant effect on the flow field and drag forces on the plants. In order to investigate these issues, sensors should best be implemented in-situ (in the bed or in a double-bottom). Thus, another main limitation is the space available for the implementation of a sensor, especially in flume experiments, as well as the ability to operate the sensor in submersed conditions.

Challenges with other solutions - As presented earlier, there are other ways to measure drag force on a plant in boundary layer flows. *Callaghan et al.* [2007] designed a sensor catching the drag force on a plant using a trolley set-up. Even though this set-up allows the use of a sensor with a fine resolution and high sampling rate ($5x10^{-4}$N at 10Hz), *Plew et al.* [2008] reported some issues to accurately measure mean drag forces due to the weight of the trolley itself. On the other hand, *Dwivedi et al.* [2010] successfully designed a small sensitive sensor (10^{-3}N at 1000Hz) measuring in 6 degrees of freedom in boundary layer flows. However, such sensors require careful calibration which is not always easily achieved.

Alternative solutions - Many of the force sensors used in the studies mentioned have been custom built, in order to better fit the requirements of a given experimental set-up. However, the compromises made in a home-made solution can easily lead to calibration issues, low

signal-to-noise ratio, or a limited measuring range. On the opposite, commercial sensors tend to rely on more stable technologies, and are calibrated for a wider range of applications. This is possible due to the use of more advanced technologies such as piezoelectric crystals, or improving the quality and the manufacturing of the used materials. Fields like biomechanical research, robotics or robotic surgery are massively relying on small sensors measuring in confined environment, therefore off-the-shelf sensors are a promising and alternative way to improve force sensing in ecohydraulic experiments. These sensors can measure down to 10 mN in 6 degrees of freedom (forces and torques).

3.1.3. Basics on Acoustic Doppler Velocimetry *(Paper IV)*

Principle of operation **–** An Acoustic Doppler Velocimeter (ADV) is a sensor measuring the three components of the quasi-instantaneous velocity of particles in the flow, based on the Doppler shift effect. It consists of a transmitter and three or four receivers (Fig. 14). The probe is submerged in the flow and the receivers are slanted at an angle from the axis of the transmit transducer, focusing on a common sample volume that is located some centimetres away from the probe (depending on the manufacturer). The system operates by transmitting short acoustic pulses along the transmitted beam at a frequency f_{Source}. As the pulses propagate through the water column, a fraction of the acoustic energy is scattered back by small particles suspended in the water. If the emitter and the receiver would be one and the particles move in a straight line towards or away from the emitter/receiver, particle movement would modify the frequency of the signal scattered back to the receiver, and this shift in frequency can be calculated using the equation:

$$f_{Doppler} = -f_{Source} \, U / C_w \tag{25}$$

where $f_{Doppler}$ is the change in received frequency (Doppler shift), U is the particle velocity and C_w is the speed of sound in water. Due to the geometry of the probe and the turbulent nature of the flow, the derivation of the particle velocity is slightly more complex, and more details are given by, for example, *Voulgaris and Trowbridge* [1998]. ADV measurements consist of time-series of velocity vectors $\mathbf{u} = \overline{\mathbf{u}} + \mathbf{u}'$, which is decomposed into mean (time-averaged) $\overline{\mathbf{u}}$, and fluctuating $\mathbf{u}'$ components, respectively.

Figure 14 – Principle of operation of a three-branch ADV probe. Acoustic waves are generated by the central emitter, reflected by particles moving in the sampling volume and propagating back to one of the three receivers.

Characteristics of the turbulent flow can be derived from these measurements, such as the turbulent kinetic energy (TKE), which is the root-mean-square (rms) of the velocity fluctuation, expressed as:

$$\mathrm{TKE} = \frac{1}{2}\left(\overline{u_x^{'2}} + \overline{u_y^{'2}} + \overline{u_z^{'2}}\right) \tag{27}$$

where $u_x^{'}$, $u_y^{'}$ and $u_z^{'}$ are the three components of $\mathbf{u}^{'}$. Physically, TKE characterises the mean kinetic energy per unit mass contained in the eddies of the turbulent flow. Mean velocity and TKE profiles have been obtained in Paper IV using ADV probes.

ADV post-processing – Although few ADV measurements are included in this thesis, it is important to mention that velocity data recorded from an ADV probe must always be post-processed, even when considering mean-values only. As ADVs are relying on a pulse-pair algorithm [*Lhermitte and Serafin*, 1984], Doppler velocities must first be phase unwrapped, or dealiased [*Franca and Lemmin*, 2006]. The mean value of the Doppler frequency $f_{Doppler}$, from which the particle velocity is deduced, corresponds to the phase angle of the autocorrelation function of the complex echo signal which is estimated for a sample of consecutive pulse-pairs [*Lemmin and Rolland*, 1997]. In order to deduce the velocity magnitude, the Doppler frequency has to be in the range $-\pi$ to π, otherwise phase wrapping or aliasing will occur [*Franca and Lemmin*, 2006]. Moreover, velocity time series must be despiked and filtered for noise, and several advanced filtering techniques are well-documented [*Goring and Nikora*, 2002; *Wahl*, 2003]. A summary of common post-

processing techniques can be found in *Thomas and McLelland* [2015]. Note that simple threshold filtering can also be applied, such as setting a minimum for the Signal-to-Noise Ratio or signal correlation values to ensure a minimum quality of the ADV data [*McLelland and Nicholas*, 2000]. Paper IV implemented such a threshold criterion, keeping correlation values above 80 and SNR above 20. Despiking was done according to the algorithm developed by *Mori et al.* [2007].

3.2. Notions on statistics.

3.2.1. Statistical analysis of discrete populations *(Papers III)*

In this thesis, statistical analyses have been conducted in order to characterise the variation of the mechanical properties of different macroalgae species (Papers III). This section aims to provide the main concepts of statistical analysis based on *Motulsky* [2013]. Since no advanced statistical tools were used nor developed, the detailed derivation of the method used is not included in the thesis work.

P values, statistical significance, hypothesis testing – A statistical analysis is entirely based on the test of an initial assumption, called the null hypothesis. Probabilities P are calculated based on this null hypothesis, answering the following question: If the null hypothesis is true, what is the chance that random sampling would lead to a difference equal to or larger than that observed in this study? Thus, a P value cannot be understood without knowing the null hypothesis. A P value is a result of a statistical test, often designed to draw a clear conclusion about potential effects of a factor on a population. Therefore, a threshold P value is usually defined for declaring whether a result is "statistically significant" or not. This threshold is called the significance level α and usually set to 0.05. If $P < \alpha$, the conclusion is that the difference is statistically significant, and the null hypothesis is rejected. It is important to stress that when it comes to hypothesis testing, the adjective 'significant' has a meaning completely different to what most people understand. In addition, statistical hypothesis testing reduces all findings to only two conclusions –"statistically significant", or "not statistically significant". Thus, care must be taken as a conclusion of statistical significance does not mean that the difference is large enough to be of interest, or does not mean that the finding is scientifically significant. A common method to compare the means of two groups is the unpaired t-test. In this test, the null hypothesis is that both sets of data are sampled randomly from (Gaussian) populations with identical mean values and variances. The P value

is then calculated from a *t-ratio*, which is computed from the difference between the two sample mean values and standard deviations, and the sample size of each group [*Motulsky*, 2013].

Multiple comparison concepts – Realising a series of independent comparisons poses the problem of increasing the chance to make a statistically significant observation just by chance. If two comparisons are made on a dataset, assuming that both null hypotheses (no difference between the groups) are true, the probability for each test that the test will not give a significant result is 95%. As a consequence, the chance that both comparisons are not significant is 0.95 x 0.95 = 0.9025%. Generalising this issue to multiple comparisons, with N being the number of independent multiple comparisons, the chance that none of the comparison is statistically different is 0.95^N. Thus the increase of the number of comparisons being made increases the probability that at least one of the comparisons will be significant by chance. In order to compensate for this bias, some methods exist to correct for multiple comparison [*Motulsky*, 2013]. As these methods have not been directly used during this thesis work, the simplest and most common will be mentioned: the Bonferroni correction, which consists in dividing the value of significance (α) by the number of comparisons made. For more details, see e.g. *Motulsky* [2013].

Analysis of variance – The analysis of variance, commonly called ANOVA, is a type of methods analyzing the variation between the mean values of several groups, assuming that all values are sampled from a Gaussian population. Comparing the mean values of, for example, four groups with classic t-tests would imply that 4! = 24 different tests need to be carried out, inducing an increased risk of finding a false-positive (multiple comparison issue described above). ANOVA methods test two hypothesis: 1) The null hypothesis (all populations share the same mean) and 2) The alternative hypothesis (at least one population has a mean different from the rest). To define which hypothesis is more likely to be true, the quality of the fitting of each of the tests is quantified by the sum-of-squares of the difference between each value of the groups and the mean of all the groups (for further details see *Motulsky* [2013]). ANOVA tests also compute P values from a F_v value which can be considered as the ratio of the variances from the two hypothesis and the degree of freedom df of the test which is equal to the number of values in the dataset minus the number of parameters estimated from the dataset (general mean, group means…). The work done within this thesis did not go deeper into the derivation of these statistical tests, but as df, F_v, and P values must be reported after each ANOVA test, it is necessary to understand its main concepts. ANOVA tests are

based on the same assumptions as the unpaired t-test. One-way and ANOVA tests were carried out in paper III. 'One-way' refers to the fact that the dataset is categorized in only one way, looking at only one factor (for example the species of kelp sampled). The null hypothesis would then be 'the population means are equal for each category of the second factor'.

Multiple comparison tests after ANOVA - ANOVA tests are designed to detect an overall difference between the mean values of the different groups, without specifying which group is different from an other group. Thus, an ANOVA test revealing a significant effect is usually followed up by one or several additional tests to identify more precisely where the difference comes from. Follow-up tests are often distinguished in terms of whether they are planned (a priori) or post hoc. Planned tests are determined before looking at the data and post hoc tests are performed after looking at the data. Many different types of tests exists for a post hoc analysis (see e.g. *Motulsky* [2013]), representing different adaptations/improvements of the classic t-test. However, the use of such tests was not needed in Paper III as only two groups were compared (Bending moduli blades/stems).

3.2.2. Wave statistics *(Papers I-II)*

Wave theories and statistical tools to describe irregular waves are well known and developed in several reference books [*Dean and Dalrymple*, 1991; *Mei et al.*, 2005]. Therefore, the following sections only introduce the main concepts used in papers I and II.

Wave theories – Gravity waves are perturbations propagating at the surface of a homogeneous fluid layer. Considering the velocity potential Φ, where the flow velocity vector is $\boldsymbol{u} = \nabla\Phi$ for an incompressible and irrotational fluid, Φ must satisfy the following sets of equations (see e.g. *Dean and Dalrymple* [1991] for the detailed equations and their derivation):

- The continuity equation,
- The kinematic boundary condition at the seabed,
- The kinematic boundary condition at the free surface,
- The Bernoulli equation at the free surface (dynamic free-surface boundary condition).

The simplest description of water waves was derived by *Airy* [1841] based on a linearization of the aforementioned set of equations, valid for small-amplitude gravity waves (small wave

amplitude A compared to the wave length λ, i.e. $A/\lambda << 1$). Linear (Airy) waves are first-order waves with a sinusoidal shape. The initial nonlinear set of equations was solved by *Stokes* [1847] by expressing the velocity potential in Taylor series around the still water level, expanding the linear solution with non-linear terms. The degree of non-linearity of the waves is usually characterised by the steepness parameter S and the Ursell number U_R [*Dean and Dalrymple*, 1991; *Mei et al.*, 2005]. These parameters are expressed as:

$$S = \frac{2\pi}{g}\frac{H}{T^2} \tag{28}$$

$$U_R = \frac{H}{k^2 h^3} \tag{29}$$

where H is the wave height ($H = 2A$) , T is the wave period, k is the wave number corresponding to T via the dispersion relation, h the water depth. Stokes waves can also be described as the modification of the surface elevation of the fundamental wave component (the linear wave), by several of its harmonics. The order of the Stokes wave corresponds then to the number of harmonics plus the fundamental needed to form the non-linear wave. Stokes wave theory have been derived for a limited amount of orders (most commonly from 2nd to 5th order), and is valid for the description of wave non-linearities in intermediate and deep waters (i.e. $\lambda < 2h$). More precisely, in shallow water, theories based on Stokes expansions break down when the wave parameters approach the ratio $H\lambda^2 / h^3 = 26$ (i.e. when the wave length and the depth reach a similar order of magnitude, see *Le Méhauté* [1976]). Beyond this limit, i.e. when the wavelength becomes larger than the water depth, other theories become more appropriate – such as the Boussinesq approximation and the Korteweg–de Vries equation – leading to the description of nonlinear dispersive long waves, such as cnoidal waves [*Mei et al.*, 2005]. The range of validity of these different theories is given in Fig. 15 as a function of the normalised wave height and water depth. This thesis only considered linear and Stokes 2nd order waves in papers I and II, respectively. For the case of second order random Stokes waves, the second order component is actually composed of two terms, a sum-frequency term and a difference-frequency term obtained from the derivation of the wave velocity potential [*Sharma and Dean*, 1981]. The second order effect increases with decreasing water depth. The difference-frequency term has no effect in deep water, but as the water depth decreases, this term becomes more significant and is almost of the same magnitude as the sum-frequency term. Since the difference-frequency term is negative, it will give a reduction of the second order component (set-down effect).

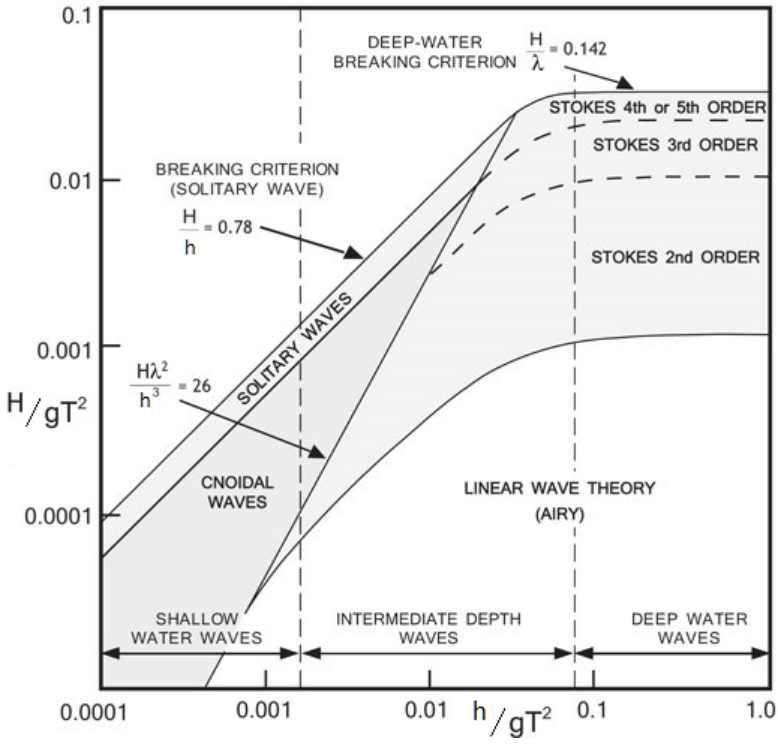

Figure 15 – Domain of validity of different wave theories as a function of the 'depth parameter' $\left(h/_{gT^2}\right)$ *and the steepness parameter* $\left(H/_{gT^2}\right)$ *. Courtesy of Flow Science, developers of FLOW-3D ®, www.flow3d.com. Adapted after Le Méhauté, 1976, Sorensen, 2005 and USACE, 2008*

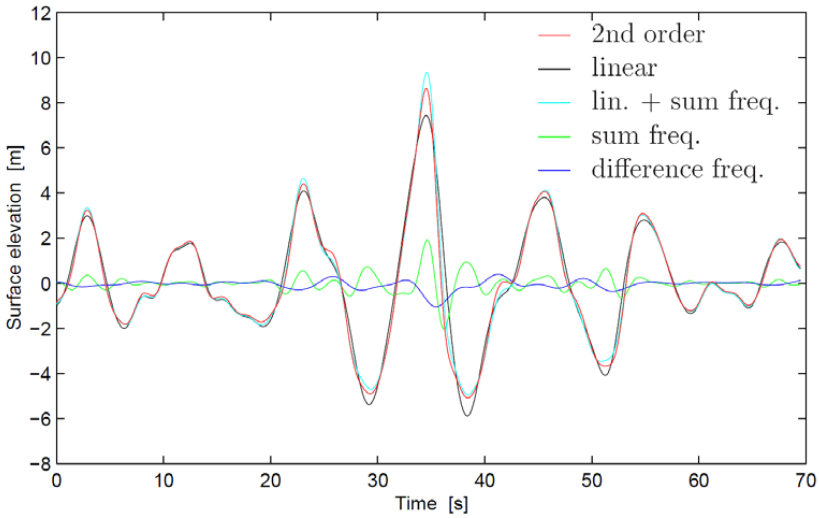

Figure 16 – Different components of the surface elevation in a simulated time series of long-crested (2D) random waves in finite water depth. Taken from *Wist* [2003].

To illustrate the influence of the second order terms, *Wist* [2003] provided an example of decomposition of a simulated time series of long crested (2D) random 2nd order Stokes waves into the linear part, the sum-frequency part and the difference-frequency part (Fig. 16). These simulations are based on typical field data conditions of random water waves in finite water depth.

Long- and short- crested random waves – When waves are propagating in the same direction, the waves are referred to as 'long-crested' (2D), while when the wave components are multi-directional, waves are referred to as 'short-crested' (3D). In deep water, the sum-frequency effects are larger for 2D waves than for 3D waves yielding higher wave crests for 2D waves than for 3D waves (see Fig. 17). In finite water depths, as mentioned in the previous section, both second order sum-frequency and second order difference-frequency effects are present. The second order negative difference-frequency effects are smaller for 3D waves than for 2D waves, leading to smaller wave set-down effects for 3D waves than for 2D waves. This is the dominating effect for finite water depths yielding higher wave crests for 3D waves than for 2D waves, i.e. contrary to the deep water case (Fig. 17).

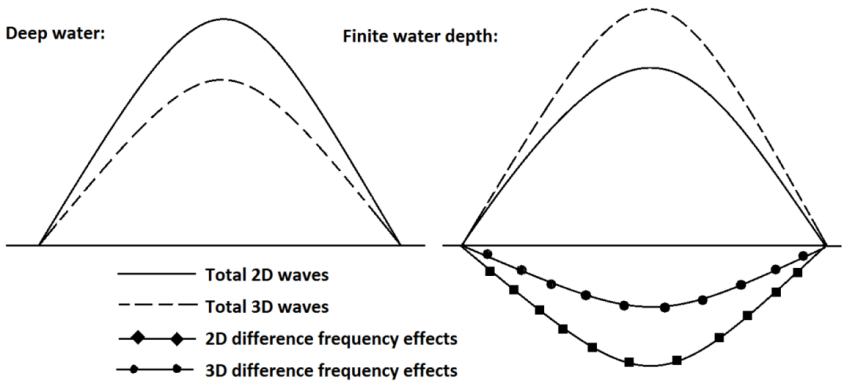

Figure 17 – Principal sketch of the 2D and 3D waves in deep and finite water, with the influence of the difference frequency effects. Taken from *Hesten* [2011].

Wave spectrum and statistics – Ocean waves and waves along coastlines can almost always be described as irregular, i.e. a superposition of several regular waves with different frequencies, amplitudes and phases. Irregular waves are described with stochastic tools and characterised by the wave spectrum $S(f)$, where f is the wave frequency in Hertz (s^{-1}). When the waves are propagating in different directions (3D), the directional spectrum $S(f)D(\theta, f)$

must be used to describe the sea state condition, where $D(\theta, f)$ is the directional distribution. The k^{th} spectral moments m_k is defined as:

$$m_k = \int f^k S(f)\, df \quad ; \quad k = 0,1,2,\ldots \tag{30}$$

and the characteristic sea state parameters such as the significant wave height H_{mo} and the mean zero-crossing wave period T_{02} are derived from different combinations of these spectral moments according to $H_{mo} = 4\sqrt{m_0}$ and $T_{02} = \sqrt{m_0/m_2}$ (see e.g. *Dean and Dalrymple* [1991]). The irregular wave height distribution is described by a probability density function (pdf), which is the function that describes the probability for the wave height to take a given value. The integration of this function gives the cumulative distribution function (cdf). In the case of a stationary Gaussian narrow-banded wave process, the cdf satisfies the well-known Rayleigh distribution. Wave spectra and distributions are affected by different coastal processes such as shoaling, radiation stress and dissipation processes at the seabed. In the context of aquatic vegetation, submerged plants will interact with irregular waves at different levels, and the plant response will depend on both wave frequency and amplitude [*Jadhav et al.*, 2013; *Möller et al.*, 2014].

4. Presentation of the publications

Papers I and II: Wave induced drag forces on submerged vegetation under transformed random waves (shoaling, non-linear or combined wave-current).

These papers develop a practical method for estimating the drag force on vegetation elements under transformed random waves, i.e. shoaling and breaking random waves (Paper I), and nonlinear random waves plus current (Paper II). Reviewing the different plant drag coefficients C_D valid in oscillatory flows (Paper II) and comparing different formulations (Papers I and II), these papers first highlight the lack of normalisation of the different existing C_D-formulations and identify possibilities for a standardisation of the formulations for oscillatory and steady flows. A stochastic method to compute the expected wave induced forces is developed considering the wave height distribution for a given sea state condition (or wave crest height distribution for non-linear waves) based on appropriate C_D formulations developed by *Méndez et al.* [1999]; *Mendez and Losada* [2004] or *Ozeren et al.* [2014] for waves alone, and *Hu et al.* [2014] for waves-plus current (see Fig. 18). The waves are assumed to be a stationary narrow-band random process and propagating in shallow waters.

The effects of shoaling and breaking waves are included in Paper I by adopting the *Mendez et al.* [2004] wave height distribution, and nonlinear wave effects (long- and short-crested) are included and discussed in Paper II considering the *Forristall* [2000] wave crest height distribution. This method improves the characterisation of the stochastic plant–flow interactions by allowing the calculation of expected values under different random waves plus current conditions. Results are compared to a classic deterministic approach in both papers and some differences are identified, calling for further investigations against experimental datasets.

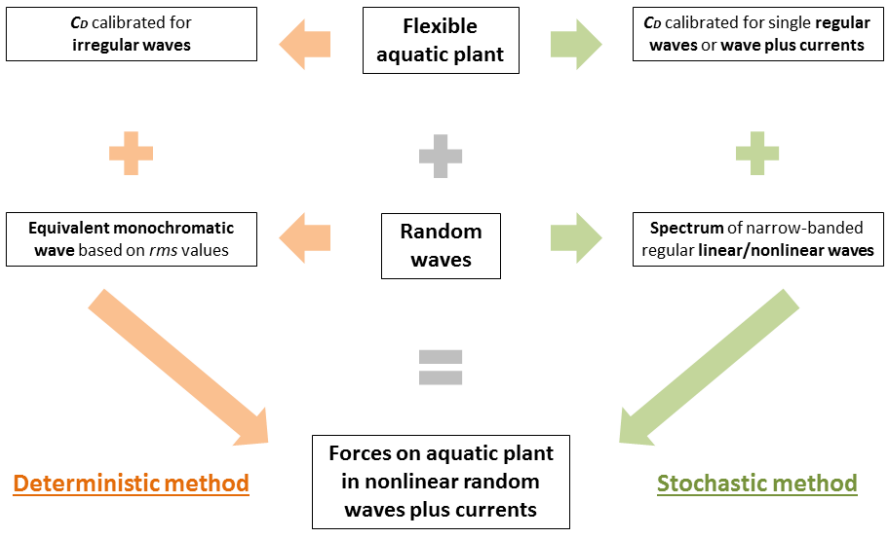

Figure 18 – Sketch of the description of the deterministic and stochastic approaches to compute forces on aquatic plants in nonlinear random waves plus current developed in Paper II (adapted from Henry et al. [2015]).

These differences also raise the question of the validity of representing a random sea state by an equivalent monochromatic wave. Based on the used C_D formulations, Paper II finally reveals that wave nonlinearities have a significant effect on expected wave forces for a higher wave activity, and that in presence of an increasing current, the effect of wave nonlinearities decreases while the expected wave forces increase.

Papers III and IV: Morphological and mechanical characterisation of brown macroalgae for surrogate production prior to eco-hydraulic experiments – the PISCES project.

As developed in the introduction section, parts of this thesis work were affiliated with the PISCES project, supported by the European Community's 7th Framework Programme through the grant to the budget of the Integrated Infrastructure Initiative HYDRALAB-IV.

The PISCES project aimed at developing and improving measurement technologies and experimental methodologies in order to better incorporate plants and animals in hydraulic modelling. The set formed by Papers III and IV addresses the question of characterising and representing the complexity of aquatic vegetation by plant-surrogates based on a number of simplifications of plant/macroalgae properties. The information on macroalgae biomechanics is often insufficient to model this type of vegetation correctly. Thus, Paper III extends the existing knowledge by providing data for four northern European brown macroalgae, and provides a comparison between the mechanical properties of stem and blade tissue for these species. Specimens of Alaria esculenta, Laminaria digitata, *Fucus serratus* and *Fucus vesiculosus* were collected from the small tidal inlet of the Hopavågen bay at the entrance of Trondheimsfjord, Sør-Trøndelag, Norway. Buoyancy and bending moduli were characterised for different parts of the macroalgae. More precisely, the dimensions of the sample tested led to the characterisation of the bending moduli for algae's stems and tangent moduli for the blade parts (see *Henry* [2014] and *Paul and Henry* [2014] for further details and discussions). All stems showed bending moduli in agreement with previous studies with respect to their order of magnitude. In Paper IV, algae's shape, stiffness and buoyancy of *L. digitata* were further evaluated and compared to the properties of inert materials. Different surrogate materials and shapes were exposed to unidirectional flow to evaluate each of the surrogate performance, and to characterise the effect of the variation of the mechanical properties on the mean velocities and TKE measured at three fixed stations. These results confirmed that buoyancy is an important factor in low flow conditions and that a basic shape might be sufficient to model complex shaped plants resulting in the same streamlined shape.

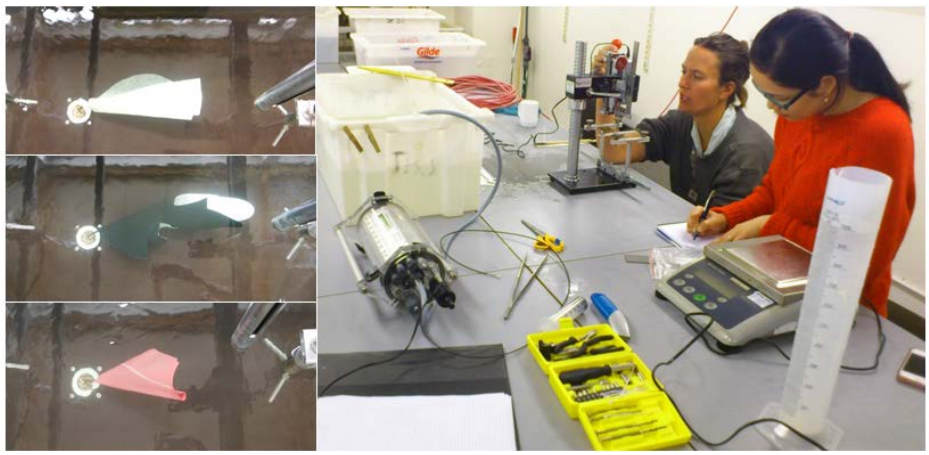

Figure 19 – Surrogate testing (papers IV) and bending tests (paper III) realised during the PISCES project.

Paper V: Bending properties of a macroalga: Adaptation of Peirce's cantilever test for in situ measurements of *Laminaria digitata*.

In parallel of the PISCES field work, Paper V aimed at improving and refining the methodology used to collect biomechanical data on kelp. The motivation for this work was to provide a comprehensive dataset for future representation of kelp plants to be included in experimental or numerical models. As the different adaptations of the classical 3-point bending test can affect the interpretation of the flexural rigidity of an element, Paper V developed a simple and robust method which was applied to a biomaterial and validated as an alternative to measure flexural rigidity of thin, flexible plant elements. Based on a bending test procedure developed for the textile industry, an apparatus for in-situ measurements was developed and compared with other normalized methods. It was subsequently used in a field test on the blade of a marine macroalga (*Laminaria digitata*) to assess its suitability to measure the bending modulus of a biomaterial. Results of the presented method on selected surrogate materials agreed with a normalized cantilever method (ISO 9073-7:1998) and a 3-point bending test (ISO 178:2010). Values determined for the bending moduli for blades of *L. digitaria* were in the typical range for algal material. The range of validity of the different methods was discussed further in Paper V.

Paper VI: Effect of rough and soft marine fouling on cylinders' hydrodynamics: a visualisation of the interaction of a poroelastic system with the ambient flow

This paper aimed at exemplifying the effect of different roughness types on boundary layers using the cylinder example via a simple visualisation study. To some extent, similarities can be seen between a soft fouling community waving at the surface of a cylinder in a steady current and the behaviour of a vegetated canopy on a flat ground or seabed. This paper first presented a short review of the marine growth issue from a multidisciplinary point of view. Following this review, changes on cylinder hydrodynamics induced by a developing fouling community were highlighted by flow visualisations for surfaces ranging from smooth, small hard roughness to fully developed soft fouling. Qualitative results from wake visualisations and simple drag force measurements confirmed that soft and hard roughness have completely different effects on the cylinder hydrodynamics for the transitional subcritical regime, as soft fouling act as a passive flow separation control. The visualisations were made for low steady flows with low *Re*-numbers ($2.16 \times 10^3 < Re < 1.94 \times 10^4$).

Paper VII: Review of the main "auxiliary" variables encountered in experimental hydraulics

This book chapter is a contribution to the book "Experimental Hydraulics: Methods, Instrumentation, Data Processing and Management" by Muste et al., to be published by CRC Press in autumn 2016. It summarizes the instrumentation and experimental methods for the determination of auxiliary hydraulic variables such as water depth, bed and water surface slopes, pressure, bed shear stress, and drag forces. Corresponding instruments are described and discussed with regard to the spatial and temporal resolution as well as error sources. Such variables are not necessarily the main focus of scientific publications, but they are certainly part of the first sets of variables to be monitored when setting-up a flume experiment, prior to data collection. Based on the presentation by *Henry et al.* [2014] given at the 10th International Symposium on Ecohydraulics, the main contribution has been done on the drag-force sub-chapter, generalising the force-sensing techniques based on the experience gained from measuring fluid forces on vegetation elements.

5. Conclusions and outlook

One of the main outcomes of this thesis is the development of methodologies to improve the representation of aquatic vegetation in waves and/or currents. This has been achieved from a theoretical point of view in waves and waves-plus current conditions, and from an experimental point of view with the development of kelp surrogates. As the proper understanding of plant's mechanics is vital in order to describe the interactions between living organisms and their physical environment, the developed approaches contribute to an innovative framework for future representation of aquatic vegetation in experimental and numerical models. More importantly, this thesis provides a clarification on the methodology to adopt to collect bending properties of flexible plant elements. The available information on biomechanical properties of aquatic plants is still rather scarce although, as reviewed in this thesis, the forces experienced by the plants and their reconfiguration in different flows depend on their biomechanical properties. Therefore the collection of such data is the first important step towards a proper plant parametrisation.

However, the plant parametrisation investigations raised a new set of questions, which, at this stage, could only be partially addressed within the PISCES project (Appendices I and II). One of the concerns when designing plant surrogates is to know to what extent the complexity and

variability of the natural system modelled must be replicated in order to adequately reproduce the hydraulics of such a "ecological" system in a flume and hence laboratory environment. The following questions highlights this issue: Does the spatial organisation of organisms need to be replicated? What would be the differences between the flow effects of some commonly used surrogates and their living counterparts? Preliminary results were presented by *Thomas et al.* [2015] (see in Appendix II), highlighting the importance of selecting surrogates that adequately represent the mean characteristics of the species of interest. These results will trigger new research activities within the on-going RECIPE project; part of Hydralab+ (successor of Hydralab IV). In this project, the interrelations between the plant's 'health used in hydraulic experiments, the relevant biomechanical properties, and the hydraulic performance of the plants are to be investigated. The method developed in Paper V by *Henry* [2014] will be a corner stone in monitoring plants' biomechanical properties.

The methods and knowledge developed during this thesis work will also allow for the improved design of plant surrogates. In this context, techniques based on casted silicone are currently being developed and will be implemented in future works. The production of inert silicone surrogates will allow the investigation of dynamic relations between turbulence, fluid-forces, and reconfiguration of submerged plant models. Preliminary results are presented in Appendix III by *Henry et al.* [2016b]. These approaches will open the possibilities of further investigating the detailed effects of flexibility/buoyancy and blade characteristics on plant performance.

6. References

ABERLE, J., AND J. JÄRVELÄ. 2013. Flow resistance of emergent rigid and flexible floodplain vegetation. *Journal of Hydraulic Research* 51: 33-45.

AIRY, G. B. 1841. Tides and Waves. *In* H. J. Rose [ed.], *Encyclopaedia Metropolitana*, vol. 3, *Mixed Science* Also *Trigonometry, On the Figure of the Earth, Tides and Waves.*, pp 396 + plates.

ALBAYRAK, I., V. NIKORA, O. MILER, AND M. O'HARE. 2012. Flow-plant interactions at a leaf scale: effects of leaf shape, serration, roughness and flexural rigidity. *Aquatic Sciences* 74: 267-286.

ALBAYRAK, I., V. NIKORA, O. MILER, AND M. O'HARE. 2013. Flow–plant interactions at leaf, stem and shoot scales: drag, turbulence, and biomechanics. *Aquatic Sciences*: 1-26.

ALBEN, S., M. SHELLEY, AND J. ZHANG. 2002. Drag reduction through self-similar bending of a flexible body. *Nature* 420: 479-481.

ATWELL, B. J., P. E. KRIEDEMANN, AND C. G. N. TURNBULL. 1999. Plants in Action: Adaptation in Nature, Performance in Cultivation. Macmillan Education Australia, Melbourne, Australia.

BARRÓN, C., N. MARBÉ, J. TERRADOS, H. KENNEDY, AND C. M. DUARTE. 2004. Community metabolism and carbon budget along a gradient of seagrass (Cymodocea nodosa) colonization. *Limnology and Oceanography* 49: 1642-1651.

BHATTACHARYA, D., AND A. L. MEDLIN. 1998. Algal Phylogeny and the Origin of Land Plants. *Plant Physiology* 116: 9-15.

BLEVINS, R. D. 2001. Flow-induced Vibration. 2 ed., pp 477. Krieger Publishing Company.

BOOTH, J. E. 1969. Principles of textile testing: an introduction to physical methods of testing textile fibres, yarns, and fabrics. 3 ed. Chemical Publishing Company, Inc., New York, NY.

CALLAGHAN, F. M., G. G. COOPER, V. I. NIKORA, N. LAMOUROUX, B. STATZNER, P. SAGNES, J. RADFORD, et al. 2007. A submersible device for measuring drag forces on aquatic plants and other organisms. *New Zealand Journal of Marine and Freshwater Research* 41: 119-127.

CAMERON, S. M., V. I. NIKORA, I. ALBAYRAK, O. MILER, M. STEWART, AND F. SINISCALCHI. 2013. Interactions between aquatic plants and turbulent flow: a field study using stereoscopic PIV. *Journal of Fluid Mechanics* 732: 345-372.

CLÉMENT, F. E. 1916. Plant succession. Carnegie Institute Publication 242, Washington DC, USA.

CURREY, J. D. 1980. Mechanical properties of mollusc shell. *Symp Soc Exp Biol* 34: 75-97.

CUTKOSKY, M., R. HOWE, AND W. PROVANCHER. 2008. Force and Tactile Sensors. *In* B. Siciliano AND O. Khatib [eds.], Springer Handbook of Robotics, 455-476. Springer Berlin Heidelberg.

DAVISON, I. R., M. ANDREWS, AND W. D. P. STEWART. 1984. Regulation of growth in Laminaria digitata: use of in-vivo nitrate reductase activities as an indicator of nitrogen limitation in field populations of Laminaria spp. *Marine Biology* 84: 207-217.

DE LANGRE, E. 2008. Effects of wind on plants. *Annual Review of Fluid Mechanics* 40: 141-168.

DE LANGRE, E., A. GUTIERREZ, AND J. COSSE. 2012. On the scaling of drag reduction by reconfiguration in plants. *Comptes Rendus Mécanique* 340: 35-40.

DEAN, R. G., AND R. A. DALRYMPLE. 1991. Water Wave Mechanics for Engineers & Scientists. World Scientific.

DENNY, M. 2006. Ocean waves, nearshore ecology, and natural selection. *Aquatic Ecology* 40: 439-461.

DENNY, M. W. 1988. Biology and the Mechanics of the Wave-Swept Environment. Princeton University Press.

DENNY, M. W., T. L. DANIEL, AND M. A. R. KOEHL. 1985. Mechanical Limits to Size in Wave-Swept Organisms. *Ecological Monographs* 55: 69-102.

DETERT, M., V. WEITBRECHT, J. ABERLE, P. ROWINSKI, AND P. Y. HENRY. 2015. 6.5 Auxiliary hydrodynamic variables. *In* M. Muste, et al. [eds.], Experimental hydraulics: Methods, Instrumentation, Data processing & Management, Book Series IAHR Monograph, pp 450. Taylor & Francis.

DIJKSTRA, J. T., AND R. E. UITTENBOGAARD. 2010. Modeling the interaction between flow and highly flexible aquatic vegetation. *Water Resour. Res.* 46: W12547.

DWIVEDI, A., B. W. MELVILLE, A. Y. SHAMSELDIN, AND T. K. GUHA. 2010. Drag force on a sediment particle from point velocity measurements: A spectral approach. *Water Resources Research* 46: W10529.

ENNOS, A. R. 1999. The aerodynamics and hydrodynamics of plants. *Journal of Experimental Biology* 202: 3281-3284.

FORRISTALL, G. Z. 2000. Wave Crest Distributions: Observations and Second-Order Theory. *Journal of Physical Oceanography* 30: 1931-1943.
FRANCA, M. J., AND U. LEMMIN. 2006. Eliminating velocity aliasing in acoustic Doppler velocity profiler data. *Measurement Science and Technology* 17: 313.
FROSTICK, L. E., S. J. MCLELLAND, AND T. MERCER. 2011. Ecological experiments, Users Guide to Physical Modelling and Experimentation, IAHR Design Manual, 127-170. CRC Press.
FUTUYMA, D. J. 2009. 11- Natural Selection and Adaptation. *In* D. J. Futuyma [ed.], Evolution, 279-301. Sinauer Associates.
GERE, J., AND B. GOODNO. 2012. Mechanics of Materials. 8 ed., pp 1056. Cengage Learning.
GORING, D. G., AND V. I. NIKORA. 2002. Despiking acoustic doppler velocimeter data. *Journal of Hydraulic Engineering* 128: 117-126.
GOSSELIN, F., E. DE LANGRE, AND B. A. MACHADO-ALMEIDA. 2010a. Drag reduction of flexible plates by reconfiguration. *Journal of Fluid Mechanics* 650: 319-341.
GOSSELIN, F., E. DE LANGRE, AND B. MACHADO-ALMEIDA. 2010b. Drag reduction of flexible plates by reconfiguration. *J. Fluid Mech.* 650: 319.
GURNELL, A. 2014. Plants as river system engineers. *Earth Surface Processes and Landforms* 39: 4-25.
HARDER, D. L., C. L. HURD, AND T. SPECK. 2006. Comparison of mechanical properties of four large, wave-exposed seaweeds. *American Journal of Botany* 93: 1426-1432.
HENRY, P.-Y. 2014. Bending properties of a macroalga: Adaptation of Peirce's cantilever test for in situ measurements of Laminaria digitata (Laminariaceae). *American Journal of Botany* 101: 1050-1055.
HENRY, P.-Y., AND D. MYRHAUG. 2013. Wave-induced drag force on vegetation under shoaling random waves. *Coastal Engineering* 78: 13-20.
HENRY, P.-Y., D. MYRHAUG, AND J. ABERLE. 2015. Drag forces on aquatic plants in nonlinear random waves plus current. *Estuarine, Coastal and Shelf Sci.* 165: 10-24.
HENRY, P. Y., E. L. NEDREBØ, AND D. MYRHAUG. 2016a. Visualisation of the effect of different types of marine growth on cylinders' wake structure in low *Re* flows. *Ocean Eng.* In Press.
HENRY, P. Y., J. ABERLE, D. MYRHAUG, AND B. PETTERSEN. 2014. Force measurement techniques in the benthic boundary layer: Application to the plant-flow interactions, 10th International Symposium on Ecohydraulics, Trondheim, Norway.
HENRY, P. Y., J. ABERLE, J. DIJKSTRA, AND D. MYRHAUG. 2016b. An integrated, multi-sensing approach to describe the dynamic relations between turbulence, fluid-forces, and reconfiguration of a submerged plant model in steady flows., EGU General Assembly 2016, Vienna.
HESTEN, P. 2011. Scour around wind turbine foundations, marine pipelines and short cylinders due to long-crested and short-crested non-linear random waves plus currents. MSc's thesis, NTNU, Trondheim.
HU, Z., T. SUZUKI, T. ZITMAN, W. UITTEWAAL, AND M. STIVE. 2014. Laboratory study on wave dissipation by vegetation in combined current–wave flow. *Coastal Engineering* 88: 131-142.
HUANG, I., J. ROMINGER, AND H. NEPF. 2011. The motion of kelp blades and the surface renewal model. *Limnology and Oceanography* 56: 1453-1462.
ISHIKAWA, Y., T. SAKAMOTO, AND K. MIZUHARA. 2003. Effect of density of riparian vegetation on effective tractive force. *Journal of Forest Research* 8: 235-246.
JADHAV, R. S., Q. CHEN, AND J. M. SMITH. 2013. Spectral distribution of wave energy dissipation by salt marsh vegetation. *Coastal Engineering* 77: 99-107.

JALONEN, J., J. JÄRVELÄ, AND J. ABERLE. 2013. Leaf Area Index as Vegetation Density Measure for Hydraulic Analyses. *Journal of Hydraulic Engineering* 139: 461-469.

JOHNSON, M. F., S. P. RICE, W. E. PENNING, AND J. T. DIJKSTRA. 2014a. Maintaining the health and behavioural integrity of plants and animals in experimental facilities, Users Guide to Ecohydraulic Modelling and Experimentation, IAHR Design Manual, 11-21. CRC Press.

JOHNSON, M. F., R. E. THOMAS, J. T. DIJKSTRA, M. PAUL, W. E. PENNING, AND S. P. RICE. 2014b. Using surrogates, including scaling issues, in laboratory flumes and basins, Users Guide to Ecohydraulic Modelling and Experimentation, IAHR Design Manual, 23-41. CRC Press.

KOEHL, M. A. R., W. K. SILK, H. LIANG, AND L. MAHADEVAN. 2008. How kelp produce blade shapes suited to different flow regimes: A new wrinkle. *Integrative and Comparative Biology* 48: 834-851.

KOTHYARI, U. C., K. HAYASHI, AND H. HASHIMOTO. 2009. Drag coefficient of unsubmerged rigid vegetation stems in open channel flows. *J. of Hydraulic Research* 47: 691-699.

LE MÉHAUTÉ, B. 1976. An introduction to hydrodynamics and water waves, 315. Springer-Verlag, University of Michigan.

LEMMIN, U., AND T. ROLLAND. 1997. Acoustic Velocity Profiler for Laboratory and Field Studies. *Journal of Hydraulic Engineering* 123: 1089-1098.

LHERMITTE, R., AND R. SERAFIN. 1984. Pulse-to-Pulse Coherent Doppler Sonar Signal Processing Techniques. *Journal of Atmospheric and Oceanic Technology* 1: 293-308.

LUHAR, M., AND H. M. NEPF. 2011. Flow-induced reconfiguration of buoyant and flexible aquatic vegetation. *Limnology and Oceanography* 56: 2003-2017.

MACH, K. J. 2009. Mechanical and biological consequences of repetitive loading: crack initiation and fatigue failure in the red macroalga Mazzaella. *Journal of Experimental Biology* 212: 961-976.

MACH, K. J., D. V. NELSON, AND M. W. DENNY. 2007a. Techniques for predicting the lifetimes of wave-swept macroalgae: a primer on fracture mechanics and crack growth. *Journal of Experimental Biology* 210: 2213-2230.

MACH, K. J., B. B. HALE, M. W. DENNY, AND D. V. NELSON. 2007b. Death by small forces: a fracture and fatigue analysis of wave-swept macroalgae. *Journal of Experimental Biology* 210: 2231-2243.

MARION, A., V. NIKORA, S. PUIJALON, T. BOUMA, K. KOLL, F. BALLIO, S. TAIT, et al. 2014. Aquatic interfaces: a hydrodynamic and ecological perspective. *Journal of Hydraulic Research* 52: 744-758.

MARSHALL, J. K. 1971. Drag measurements in roughness arrays of varying density and distribution. *Agricultural Meteorology* 8: 269-292.

MAZA, M., J. L. LARA, AND I. J. LOSADA. 2013. A coupled model of submerged vegetation under oscillatory flow using Navier–Stokes equations. *Coastal Engineering* 80: 16-34.

MCLELLAND, S. J., AND A. P. NICHOLAS. 2000. A new method for evaluating errors in high-frequency ADV measurements. *Hydrological Processes* 14: 351-366.

MEI, C. C., M. STIASSNIE, AND D. K. P. YUE. 2005. Theory and Applications of Ocean Surface Waves: Nonlinear aspects. World Scientific.

MENDEZ, F. J., AND I. J. LOSADA. 2004. An empirical model to estimate the propagation of random breaking and nonbreaking waves over vegetation fields. *Coastal Engineering* 51: 103-118.

MENDEZ, F. J., I. J. LOSADA, AND R. MEDINA. 2004. Transformation model of wave height distribution on planar beaches. *Coastal Engineering* 50: 97-115.

MÉNDEZ, F. J., I. J. LOSADA, AND M. A. LOSADA. 1999. Hydrodynamics induced by wind waves in a vegetation field. *J. Geophys. Res.* 104: 18383-18396.
MILER, O., I. ALBAYRAK, V. NIKORA, AND M. O'HARE. 2014. Biomechanical properties and morphological characteristics of lake and river plants: implications for adaptations to flow conditions. *Aquatic Sciences* 76: 465-481.
MILLER, L. A., A. SANTHANAKRISHNAN, S. JONES, C. HAMLET, K. MERTENS, AND L. ZHU. 2012. Reconfiguration and the reduction of vortex-induced vibrations in broad leaves. *J Exp Biol* 215: 2716-2727.
MORI, N., T. SUZUKI, AND S. KAKUNO. 2007. Experimental study of air bubbles and turbulence characteristics in the surf zone. *Journal of Geophysical Research: Oceans* 112: C05014.
MOTULSKY, H. 2013. Intuitive Biostatistics: A Nonmathematical Guide to Statistical Thinking. Oxford University Press.
MÖLLER, I., M. KUDELLA, F. RUPPRECHT, T. SPENCER, M. PAUL, B. K. VAN WESENBEECK, G. WOLTERS, et al. 2014. Wave attenuation over coastal salt marshes under storm surge conditions. *Nature Geosci* 7: 727-731.
NEPF, H. 1999. Drag, turbulence, and diffusion in flow through emergent vegetation. *Water Resour. Res.* 35: 479.
NEUMEIER, U. 2005. Quantification of vertical density variations of salt-marsh vegetation. *Estuarine, Coastal and Shelf Science* 63: 489-496.
NEUMEIER, U. 2007. Velocity and turbulence variations at the edge of saltmarshes. *Continental Shelf Research* 27: 1046-1059.
NIKLAS, K. J. 1992. Plant Biomechanics: An Engineering Approach to Plant Form and Function. University of Chicago Press.
NIKLAS, K. J., H. C. SPATZ, AND J. VINCENT. 2006. Plant biomechanics: an overview and prospectus. *American Journal of Botany* 93: 1369-1378.
NIKORA, V. 2010. Hydrodynamics of aquatic ecosystems: An interface between ecology, biomechanics and environmental fluid mechanics. *River Research and Applications* 26: 367-384.
O'HARE, M. T. 2015. Aquatic vegetation – a primer for hydrodynamic specialists. *Journal of Hydraulic Research* 10.1080/00221686.2015.1090493 10.1080/00221686.2015.1090493: 1-12.
OZEREN, Y., D. WREN, AND W. WU. 2014. Experimental Investigation of Wave Attenuation through Model and Live Vegetation. *Journal of Waterway, Port, Coastal, and Ocean Engineering* 140: 04014019.
PARRY, M. L., O. F. CANZIANI, J. P. PALUTIKOF, P. J. VAN DER LINDEN, AND C. E. HANSON. 2007. Climate change 2007: Impacts, adaptation and vulnerability.
PAUL, M., AND P.-Y. HENRY. 2013. Evaluation of the Use of Surrogate Laminaria Digitata in Eco-Hydraulic Experiments 35th IAHR W. Congress, Chengdu, China: 2043-2054.
PAUL, M., AND P.-Y. T. HENRY. 2014. Evaluation of the use of surrogate Laminaria digitata in eco-hydraulic laboratory experiments. *Journal of Hydrodynamics* 26: 374-383.
PAUL, M., P.-Y. HENRY, AND R. E. THOMAS. 2014. Geometrical and mechanical properties of four species of northern European brown macroalgae. *Coastal Eng.* 84: 73-80.
PEIRCE, F. T. 1930. The "handle" of cloth as a measurable quantity. *Journal of the Textile Institute Transactions* 21: T377-T416.
PLEW, D. R., G. G. COOPER, AND F. M. CALLAGHAN. 2008. Turbulence-induced forces in a freshwater macrophyte canopy. *Water Resources Research* 44: W02414.
PRATT, M. C., AND A. S. JOHNSON. 2002. Strength, drag, and dislodgment of two competing intertidal algae from two wave exposures and four seasons. *Journal of Experimental Marine Biology and Ecology* 272: 71-101.

PUIJALON, S., G. BORNETTE, AND P. SAGNES. 2005. Adaptations to increasing hydraulic stress: morphology, hydrodynamics and fitness of two higher aquatic plant species. *J Exp Bot* 56: 777-786.

REED, D. C., AND M. A. BRZEZINSKI. 2009. Kelp forests. *In* D. L. a. G. Grimsditch [ed.], The management of natural coastal carbon sinks, p. 30–38. International Union for Conservation of Nature (IUCN).

RICE, S. P., S. LITTLE, P. J. WOOD, H. J. MOIR, AND D. VERICAT. 2010. The relative contributions of ecology and hydraulics to ecohydraulics. *River Research and Applications* 26: 363-366.

ROMINGER, J. T., AND H. M. NEPF. 2014. Effects of blade flexural rigidity on drag force and mass transfer rates in model blades. *Limnology and Oceanography* 59: 2028-2041.

SAND-JENSEN, K. 2008. Drag forces on common plant species in temperate streams: consequences of morphology, velocity and biomass. *Hydrobiologia* 610: 307-319.

SCHAFFELKE, B., AND K. LÜNING. 1994. A circannual rhythm controls seasonal growth in the kelps Laminaria hyperborea and L. digitata from Helgoland (North Sea). *European Journal of Phycology* 29: 49-56.

SCHONEBOOM, T. 2011. Widerstand flexibler Vegetation und Sohlenwiderstand in durchströmten Bewuchsfeldern. Leichtweiss-Inst. für Wasserbau der Techn. Univ. Braunschweig.

SHARMA, J. N., AND R. G. DEAN. 1981. Second-Order Directional Seas and Associated Wave Forces. *Society of Petroleum Engineers Journal* 21: 129-140.

SINISCALCHI, F., AND V. NIKORA. 2013. Dynamic reconfiguration of aquatic plants and its interrelations with upstream turbulence and drag forces. *J. Hydraulic Res.* 51: 46-55.

SINISCALCHI, F., V. I. NIKORA, AND J. ABERLE. 2012. Plant patch hydrodynamics in streams: Mean flow, turbulence, and drag forces. *Water Resour. Res.* 48: W01513.

SMALE, D. A., M. T. BURROWS, P. MOORE, N. O'CONNOR, AND S. J. HAWKINS. 2013. Threats and knowledge gaps for ecosystem services provided by kelp forests: a northeast Atlantic perspective. *Ecology and Evolution* 3: 4016-4038.

SOLOMON, S., D. QIN, M. MANNING, Z. CHEN, M. MARQUIS, K. B. AVERYT, M. TIGNOR, AND H. L. MILLER. 2007. Climate change 2007: The physical science basis. Contribution of Working Group I to the Fourth Assessment Report of the IPCC, Cambridge, UK.

STATZNER, B., N. LAMOUROUX, V. NIKORA, AND P. SAGNES. 2006. The debate about drag and reconfiguration of freshwater macrophytes: comparing results obtained by three recently discussed approaches. *Freshwater Biology* 51: 2173-2183.

STENECK, R. S., M. H. GRAHAM, B. J. BOURQUE, D. CORBETT, J. M. ERLANDSON, J. A. ESTES, AND M. J. TEGNER. 2002. Kelp forest ecosystems: biodiversity, stability, resilience and future. *Environmental Conservation* 29: 436-459.

STEWART, H. L. 2006a. Hydrodynamic consequences of flexural stiffness and buoyancy for seaweeds: a study using physical models. *Journal of Exp. Biology* 209: 2170-2181.

STEWART, H. L. 2006b. Ontogenetic changes in buoyancy, breaking strength, extensibility, and reproductive investment in a drifting macroalga Turbinaria ornata (Phaeophyta). *Journal of Phycology* 42: 43-50.

STOKES, G. G. 1847. On the Theory of Oscillatory Waves, Transactions of the Cambridge Philosophical Society, vol. VIII, 441–455.

SZABLEWSKI, P., AND W. KOBZA. 2003. Numerical analysis of Peirce's cantilever test for the bending rigidity of textiles. *Fibres and Textiles in Eastern Europe October/December 2003* 11: 54-57.

TAL, M., AND C. PAOLA. 2010. Effects of vegetation on channel morphodynamics: results and insights from laboratory experiments. *Earth Surface Processes and Landforms* 35: 1014-1028.

THOMAS, R. E., AND S. J. MCLELLAND. 2015. The impact of macroalgae on mean and turbulent flow fields. *Journal of Hydrodynamics, Ser. B* 27: 427-435.

THOMAS, R. E., S. J. MCLELLAND, P. Y. HENRY, M. PAUL, O. EIFF, A.-J. EVERSTSEN, J. ABERLE, AND A. TEACA. 2015. Not all Laminaria digitata are the same! Phenotypic plasticity and the selection of appropriate surrogate macroalgae for ecohydraulic experimentation, EGU General Assembly 2015, Vienna.

THOMAS, R. E., M. F. JOHNSON, L. E. FROSTICK, D. R. PARSONS, T. J. BOUMA, J. T. DIJKSTRA, O. EIFF, et al. 2014. Physical modelling of water, fauna and flora: knowledge gaps, avenues for future research and infrastructural needs. *Journal of Hydraulic Research* 52: 311-325.

THORNE, C. R., E. P. EVANS, AND E. C. PENNING-ROWSELL. 2007. Future flooding and coastal erosion risks.

TINOCO, R., AND E. COWEN. 2013. The direct and indirect measurement of boundary stress and drag on individual and complex arrays of elements. *Exp. in Fluids* 54: 1-16.

VINCENT, J. F. V. 1992. Biomechanics--materials: A Practical Approach. IRL Press at Oxford University Press.

VOGEL, S. 1989. Drag and reconfiguration of broad leaves in high winds. *Journal of Experimental Botany* 40: 941-948.

VOGEL, S. 1994. Life in Moving Fluid: The Physical Biology of Flow. 2 ed. Princeton University Press.

VOSBURGH, F. 1982. Acropora reticulata: Structure, Mechanics and Ecology of a Reef Coral. *Proceedings of the Royal Society of London B: Biological Sciences* 214: 481-499.

VOULGARIS, G., AND J. H. TROWBRIDGE. 1998. Evaluation of the Acoustic Doppler Velocimeter (ADV) for Turbulence Measurements*. *Journal of Atmospheric and Oceanic Technology* 15: 272-289.

VÄSTILÄ, K., J. JÄRVELÄ, AND J. ABERLE. 2013. Characteristic reference areas for estimating flow resistance of natural foliated vegetation. *Journal of Hydrology* 492: 49-60.

WADA, S., AND T. HAMA. 2013. The contribution of macroalgae to the coastal dissolved organic matter pool. *Estuarine, Coastal and Shelf Science* 129: 77-85.

WAHL, T. L. 2003. Discussion of "Despiking Acoustic Doppler Velocimeter Data" by Derek G. Goring and Vladimir I. Nikora. *Journal of Hydraulic Engineering* 129: 484-487.

WAINWRIGHT, S. A., W. D. BIGGS, J. D. CURREY, AND J. M. GOSLINE. 1982. Mechanical Design in Organisms. Princeton University Press.

WELLMAN, C. H., P. L. OSTERLOFF, AND U. MOHIUDDIN. 2003. Fragments of the earliest land plants. *Nature* 425: 282-285.

WHITTAKER, P., C. WILSON, J. ABERLE, H. P. RAUCH, AND P. XAVIER. 2013. A drag force model to incorporate the reconfiguration of full-scale riparian trees under hydrodynamic loading. *Journal of Hydraulic Research* 51: 569-580.

WILSON, C. A. M. E., T. STOESSER, P. D. BATES, AND A. BATEMANN PINZEN. 2003. Open Channel Flow through Different Forms of Submerged Flexible Vegetation. *Journal of Hydraulic Engineering* 129: 847-853.

WIST, H. T. 2003. Statistical properties of successive ocean wave parameters. Dr. ing., NTNU, Trondheim.

YAGCI, O., U. TSCHIESCHE, AND M. S. KABDASLI. 2010. The role of different forms of natural riparian vegetation on turbulence and kinetic energy characteristics. *Advances in Water Resources* 33: 601-614.

YOUNG, W., R. BUDYNAS, AND A. SADEGH. 2011. Roark's Formulas for Stress and Strain, 8th Edition. McGraw-Hill Education.

PAPER I

Henry, P.-Y. and Myrhaug, D., [**2013**]. Wave-induced drag force on vegetation under shoaling random waves. *Coastal Engineering*, 78(0): 13-20.

Coastal Engineering 78 (2013) 13–20

Contents lists available at SciVerse ScienceDirect

Coastal Engineering

journal homepage: www.elsevier.com/locate/coastaleng

Wave-induced drag force on vegetation under shoaling random waves

Pierre-Yves Henry *, Dag Myrhaug

Department of Marine Technology, Norwegian University of Science and Technology, NO-7491 Trondheim, Norway

ARTICLE INFO

Article history:
Received 19 December 2012
Received in revised form 11 March 2013
Accepted 18 March 2013
Available online 13 April 2013

Keywords:
Vegetation field
Drag forces
Shoaling random waves
Stochastic method

ABSTRACT

This paper provides a practical method for estimating the drag force on a vegetation field in shoaling conditions beneath non-breaking and breaking random waves. This is achieved by using a simple drag formula based on two empirical drag coefficients given by Méndez et al. (1999) and Méndez and Losada (2004), respectively, in conjunction with a stochastic approach. Here the waves are assumed to be a stationary narrow-band random process and propagating in shallow waters. The effects of shoaling and breaking waves are included by adopting the Méndez et al. (2004) wave height distribution. Results are presented and discussed for different slopes, and an example of calculation is also provided to demonstrate the application of the method.

1. Introduction

Benthic vegetation fields occur frequently in coastal regions. Due to the light intensity, underwater vegetation grows particularly well in coastal waters and organizes itself in patches of different sizes. However, shallow waters are often exposed to strong flow conditions due to waves and currents. Therefore, during their evolution, marine plants (i.e. macroalgae, seagrasses and wetlands) adapted their structure in order to interact with their environment and being able to survive. Over the three last decades experimental, theoretical and numerical works have been devoted to try to understand the interaction between the flow and vegetation. It is fairly well accepted that vegetation patches will reduce the wave activity. This is the case for seagrass fields (Infantes et al., 2012; Paul et al., 2012; Sánchez-González et al., 2011), wetlands (Feagin et al., 2011), and seaweeds (Dubi, 1995; Løvås, 2000). The hydrodynamics inside the canopy is quite complex and may vary significantly according to the species involved. In general, the wave-induced turbulent kinetic energy is damped by the plants (Pujol et al., 2012), but can increase towards the bed due to stem-wake-turbulence (Pujol and Nepf, 2012). By changing the hydrodynamic conditions, vegetation patches control sediment transport and transport processes at different levels (Coulombier et al., 2012; Gacia and Duarte, 2001; Luhar and Nepf, 2008), and ecological processes such as nutrient uptake and larval dispersal and recruitment (Koch et al., 2006). In the end, these interactions control the biogeomorphic evolution of many landscapes (Vandenbruwaene et al., 2011). The basis of the interaction plant-flow is the relation between the flow-induced drag on the plant and the mechanical response of the plant (Denny and Gaylord, 2002, 2010). Experimental and theoretical works have been carried out to study the wave damping induced by vegetation fields as well as the wave-induced drag force on plants, e.g. Dalrymple et al. (1984), Asano et al. (1993), Kobayashi et al. (1993), Dubi (1995), Dubi and Tørum (1995, 1997), Méndez et al. (1999), Massel (1999), Løvås (2000), Løvås and Tørum (2000), Løvås and Tørum (2001), Méndez and Losada (2004), Li and Yan (2007), Vo-Luong and Massel (2008), Myrhaug et al. (2009), Dijkstra and Uittenbogaard (2010), and Myrhaug and Holmedal (2011). Among these works, Massel et al. (1999), Méndez and Losada (2004), as well as Vo-Luong and Massel (2008) considered the effect of wave breaking. Méndez and Losada (2004) have taken into account the effect of wave breaking and vegetation damping by including two dissipation terms. Vo-Luong and Massel (2008) considered the effect of wave breaking and wave–trunk interactions in mangrove forests by applying a mild-slope equation modified with a dissipation term. A more fundamental discussion of the variation of the full frequency spectrum under wave breaking and interaction with vegetation element was made by Massel et al. (1999).

The purpose of this study is to provide a practical method for estimating the drag force on a vegetation field in shoaling conditions beneath non-breaking and breaking random waves. This is achieved by using the Méndez et al. (1999) and Méndez and Losada (2004) drag coefficients for regular waves, combined with the Méndez et al. (2004) wave height distribution including shoaling and breaking, and assuming the waves to be a stationary narrow-band random process. It should be noted that the influence of wave breaking in the Méndez et al. (2004) wave height distribution adopted here, is generic as long as the assumptions it is based upon are fulfilled. This model is derived by considering a bore approach for modelling the energy dissipation in the surf zone. Results for different slopes are presented and discussed, and an example of calculation is given to demonstrate the application of the method.

* Corresponding author. Tel.: +47 735 50 445.
E-mail address: pierre-yves.henry@ntnu.no (P.-Y. Henry).

0378-3839/$ – see front matter © 2013 Elsevier B.V. All rights reserved.
http://dx.doi.org/10.1016/j.coastaleng.2013.03.004

2. Drag force for regular waves

2.1. The Morison-type approach

In order to derive the wave-induced force on the plant, its motion is neglected and the wave-induced forces acting on the vegetation field are expressed in terms of a Morison-type equation which neglects the swaying motion and inertial forces. This approach is commonly used and is, for example, the basis of the wave-propagation model over vegetation fields derived by Méndez and Losada (2004). It can be argued that the dissipation term proportional to the vertical force times the vertical velocity component is negligible in comparison with the dissipation term proportional to the horizontal force times the horizontal velocity component (Méndez and Losada, 2004), so only the horizontal force is considered. Thus the horizontal time-varying force per unit volume is derived as:

$$F(t) = \frac{1}{2}\rho C_D b N u(t)|u(t)| \tag{1}$$

where $u(t)$ is the undisturbed horizontal wave-induced velocity in the vegetation region, t is the time, ρ is the density of water, b is the plant area per unit height of each vegetation stand normal to $u(t)$, i.e. the plant width (see Fig. 1), N is the number of vegetation stands per unit horizontal area, and C_D is a depth-averaged drag coefficient. It should be noted that the correct calculation of $F(t)$ requires that the relative velocity between the fluid and the plant is used instead of $u(t)$.

However, by using another expression for the drag coefficient C_D than for rigid plants, Eq. (1) is also taken to be valid for flexible plants (this is discussed in the following subsection). The maximum horizontal drag force within a wave cycle is given by

$$F_{max} = \frac{1}{2}\rho C_D b N U_{max}^2 \tag{2}$$

where U_{max} is the maximum horizontal velocity within the wave cycle.

2.2. Different drag models

The definition of the wave force exerted on the plant is based on the definition of a proper bulk drag coefficient C_D. In theory, the value of this parameter depends on the flow condition around the plant as well as its biomechanical properties. But it is far from obvious to sum up those properties in a generic formula for C_D. There have been several attempts regarding oscillatory flows (Asano et al., 1993; Dubi, 1995; Méndez et al., 1999). Méndez et al. (1999) proposed the following drag coefficient, obtained as best fit to the experimental data by Asano et al. (1993):

$$C_D = \hat{\alpha} + \left(\frac{\hat{\beta}}{R}\right)^{\gamma}. \tag{3}$$

Here $R = bu_r / \nu$ is the Reynolds number based on the plant width b and the velocity u_r is a characteristic velocity acting on the plant and defined as the maximum horizontal velocity at the top of the vegetation, i.e. at $z = -h + \Delta h$, where h is the water depth, Δ is the relative plant height (see Fig. 1), and ν is the kinematic viscosity of water. The following coefficients $\hat{\alpha}$, $\hat{\beta}$ and γ were obtained as best fit to the data. For rigid plants:

$$\left(\hat{\alpha}, \hat{\beta}, \gamma\right) = (0.08, 2200, 2.2); \quad 200<R<15500 \tag{4}$$

and for swaying plants

$$\left(\hat{\alpha}, \hat{\beta}, \gamma\right) = (0.40, 4600, 2.9); \quad 2300<R<20000\,. \tag{5}$$

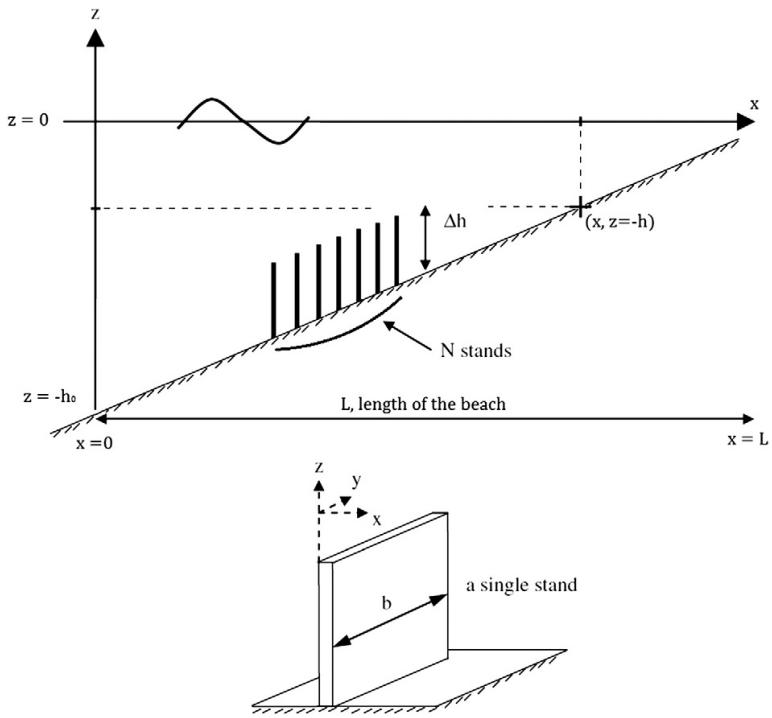

Fig. 1. Definition sketch of a vegetation field.

It should be noted that for high Reynolds numbers these drag coefficients approach the values 0.08 and 0.40, respectively (see also Méndez et al. (1999) Fig. 3). Thus, Eqs. (1) and (2) can be used for both rigid and swaying plants by using Eq. (3) with the coefficients in Eqs. (4) and (5), respectively.

This previous model needs a calibration of the drag coefficient through physical experiments. In addition, the plant is assumed to behave in the same way at a given Reynolds number R for different wave conditions. Several studies showed that the drag coefficient can be reduced under increased wave activity, through some reconfiguration processes (Boller and Carrington, 2006; Luhar and Nepf, 2011; Martone et al., 2012). In order to improve those formulas, Méndez and Losada (2004) derived another expression for C_D focussing mainly on the hydrodynamic processes and based on a Keulegan–Carpenter number; defining $\tilde{C}_D$ as:

$$\tilde{C}_D = \frac{\exp(-0.0138Q)}{Q^{0.3}}; 7<Q<172 \tag{6}$$

where $Q = K / \Delta^{0.76}$ is a modified Keulegan–Carpenter number, K is the Keulegan–Carpenter number defined as, $K = u_r T_p / b$. The velocity u_r defined above is obtained using H_{rms} (=root-mean-square (rms) value of the wave height H) and T_p (=spectral peak period) as the wave height and the wave period corresponding to an equivalent monochromatic wave. Méndez and Losada (2004) validated this model empirically by showing that the data of Løvås (2000) collapsed into a single curve when plotting the drag coefficient versus K. Following the definition of K, Q and R, the modified Keulegan–Carpenter number in Eq. (6) is a linear function of R. Thus, a direct comparison of those models can be done, provided that b, Δ and T_p are known. An example is given in Fig. 2a showing the drag coefficients versus R. For this particular case, it is observed that the drag coefficients are similar for R in the range 6×10^3 to 4×10^4. However, by closer inspection (not shown here) it appears that Eqs. (3), (5) and (6) give the same drag coefficient at $R \sim 7 \times 10^3$ and $R \sim 2.6 \times 10^4$. Moreover, for $7 \times 10^3 < R < 2.6 \times 10^4$, Eq. (6) gives higher values of $\tilde{C}_D$. By extending the definition of Eq. (6) to higher values of R, for $R > 2.6 \times 10^4$, Eq. (6) predicts much lower values of $\tilde{C}_D$ than the Méndez et al. (1999) model for swaying plants (Eqs. (3) and (5)). At $R \sim 3 \times 10^5$, $\tilde{C}_D$ is one order of magnitude smaller than C_D defined by Méndez et al. (1999) for swaying plants. This is contradicting the assumption commonly made that the Méndez et al. (1999) model for swaying plants can be extended beyond its range of validity by using its asymptotic behaviour (i.e. C_D approaching 0.4 for high R). Thus, for the models being calibrated against experimental data, it appears important to restrict their use to their defined domains. Fig. 2b shows the drag coefficients versus K for $R = 2.6 \times 10^4$. It is seen that the Méndez and Losada (2004) $\tilde{C}_D$ model decreases as K increases, while the two C_D models are constant due to R being constant.

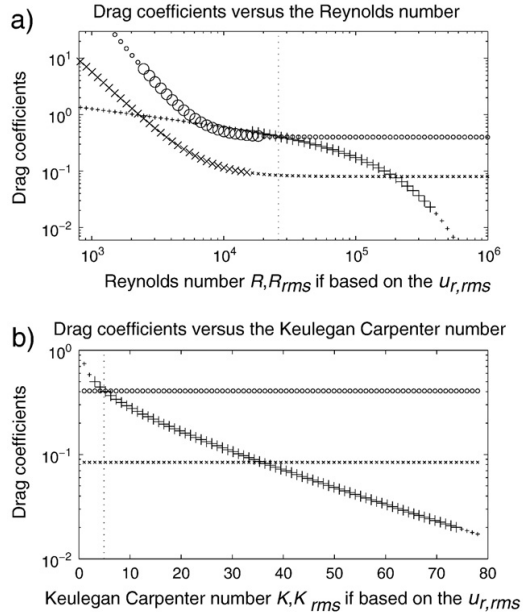

Fig. 2. Comparison of different drag coefficient models versus R (a) and K for $R = 2.6 \times 10^4$ (b). The oblique crosses (x) represent the Méndez et al. (1999) model for rigid plants (Eqs. (3) and (4)), the circles (○) represent the Méndez et al. (1999) model for swaying plants (Eqs. (3) and (5)), the straight crosses (+) describe the Méndez and Losada (2004) model (Eq. (6)). The big symbols represent the definition domain of each formula, while the smaller symbols illustrate the behaviour of these models outside their definition domain. Example for $b = 0.1$ m, $\Delta = 0.33$ and $T_p = 1.91$ s (a) or $R = 2.6 \times 10^4$ (b). The vertical lines show when the two graphs define the same conditions ($K = 4.9$ and $R = 2.6 \times 10^4$).

3. Drag force in shoaling conditions for random waves

The maximum drag force is taken according to Eq. (2) with U_{max} evaluated using linear wave theory, which then is given by the maximum horizontal orbital velocity under the wave height, H. At a fixed point in a sea state with stationary narrow-band random waves consistent with linear regular waves in finite water depth, the non-dimensional maximum horizontal particle velocity evaluated at an elevation z between the mean free surface and the sea bottom, $\hat{U}_{max} = U_{max}/U_{rms}$, is (Dean and Dalrymple, 1991)

$$\hat{U}_{max} = \hat{H}\frac{\cosh k_p(z+h)}{\cosh k_p h} \tag{7}$$

$$U_{rms} = \frac{H_{rms}}{2}\frac{\omega_p \cosh k_p h}{\sinh k_p h}. \tag{8}$$

Here $\hat{H} = H/H_{rms}$ is the non-dimensional wave height. By combining Eqs. (7) and (8) the maximum horizontal orbital velocity at an elevation z in dimensional form is given as:

$$U_{max} = \frac{H}{2}\frac{\omega_p \cosh k_p(z+h)}{\sinh k_p h}. \tag{9}$$

Now the drag force formula for regular waves in Eq. (2) can be re-arranged to a formula valid for individual random waves in the following way: By taking U_{max} from Eq. (9), and substitution of this in Eq. (2), Eq. (2) can be re-arranged to give the non-dimensional maximum drag force f_{max} for individual narrow-band random waves as

$$f_{max} \equiv \frac{F_{max}}{\frac{1}{2}\rho C_D b N U_{rms}^2} = \hat{H}^2 \frac{\cosh^2 k_p(z+h)}{\cosh^2 k_p h}. \tag{10}$$

The total non-dimensional drag force per unit horizontal area is obtained by integration over the height Δh of the plants, i.e.

$$\overline{f}_{max} \equiv \frac{\overline{F}_{max}}{\frac{1}{2}\rho C_D b N U_{rms}^2} = \int_{-h}^{-h+\Delta h} f_{max}\,dz. \tag{11}$$

This integration requires evaluation of an integral, giving

$$\int_{-h}^{-h+\Delta h} \cosh^2 k_p(z+h)\,dz = \frac{1}{2}\left(\frac{1}{2k_p}\sinh 2k_p\Delta h + \Delta h\right). \tag{12}$$

By combining Eqs. (10) to (12), $\overline{f}_{max}$ can be expressed as

$$\overline{f}_{max} = r\hat{H}^2 \tag{13}$$

where r is given as

$$r = \frac{1}{2\cosh^2 k_p h}\left(\frac{1}{2k_p}\sinh 2k_p\Delta h + \Delta h\right). \tag{14}$$

Moreover, C_D in Eq. (3) can be re-arranged to give the drag coefficient for individual narrow-band random waves as

$$C_D = \hat{\alpha} + \left(\frac{\hat{\beta}}{R_{rms}}\right)^{\gamma}\hat{H}^{-\gamma} \tag{15}$$

where

$$R_{rms} = \frac{H_{rms}b}{2\nu}\frac{\omega_p\cosh k_p\Delta h}{\sinh k_p h}. \tag{16}$$

By taking R_{rms} as a characteristic statistical value of R for random waves (i.e. the characteristic of an equivalent sinusoidal wave), the same threshold values as for R are used, i.e. $200 < R_{rms} < 15{,}500$ for rigid plants and $2300 < R_{rms} < 20{,}000$ for swaying plants, with the corresponding coefficients given in Eqs. (4) and (5), respectively. Here the reference velocity at the top of the plants, i.e. at $z = -h + \Delta h$, is taken as the maximum horizontal particle velocity given from Eq. (9) as $u_r = H\,\omega_p\cosh k_p\Delta h / 2\sinh k_p h$.

By combining the definition of $\overline{f}_{max}$ in Eq. (11) with Eqs. (13) and (15), it follows that the non-dimensional maximum drag force $\hat{F}$ for individual random waves is given as

$$\hat{F} \equiv \frac{\overline{F}_{max}}{\frac{1}{2}\rho bNU_{rms}^2} = C_D\overline{f}_{max} = r\left[\hat{\alpha}\hat{H}^2 + \left(\frac{\hat{\beta}}{R_{rms}}\right)^{\gamma}\hat{H}^{2-\gamma}\right]. \tag{17}$$

Similarly, $\tilde{C}_D$ in Eq. (6) can be re-arranged to give the drag coefficient based on the Keulegan–Carpenter number for individual narrow-band random waves as

$$\tilde{C}_D = \frac{\exp\left(-0.0138Q_{rms}\hat{H}\right)}{Q_{rms}^{0.3}\ \hat{H}^{0.3}};\ 7<Q_{rms}<172 \tag{18}$$

where

$$Q_{rms} = K_{rms}/\Delta^{0.76} \tag{19}$$

$$K_{rms} = \frac{\pi H_{rms}\cosh k_p\Delta h}{b\sinh k_p h}. \tag{20}$$

By combining the definition of $\overline{f}_{max}$ in Eq. (11) with Eqs. (13), (18), (19) and (20), the non-dimensional drag force $\hat{F}$ for individual random waves taking into account the reconfiguration process of the plants is given by:

$$\hat{F} \equiv \frac{\overline{F}_{max}}{\frac{1}{2}\rho bNU_{rms}^2} = \tilde{C}_D\overline{f}_{max} = r\frac{\exp\left(-0.0138Q_{rms}\ \hat{H}\right)}{Q_{rms}^{0.3}}\hat{H}^{1.7} \tag{21}$$

where r is given in Eq. (14).

A quantity of interest is the expected value of the non-dimensional force $\hat{F}$ caused by the $(1/n)$th highest waves in a sea state, given by

$$E\left[\hat{F}\left(\hat{H}\right)|\hat{H} > \hat{H}_{1/n}\right] = n\int_{\hat{H}_{1/n}}^{\infty}\hat{F}\left(\hat{H}\right)p\left(\hat{H}\right)\mathrm{d}\hat{H} \tag{22}$$

where $\hat{H}_{1/n}$ is the value of $\hat{H}$ which is exceeded by the probability $1/n$, and $p\left(\hat{H}\right)$ is the probability density function (pdf) of $\hat{H}$.

Moreover, another quantity of interest is the rms value of $\hat{F}$ given by

$$\hat{F}_{rms} = \left(E\left[\hat{F}^2\right]\right)^{1/2} = \left(\int_0^{\infty}\hat{F}^2\left(\hat{H}\right)p\left(\hat{H}\right)\mathrm{d}\hat{H}\right)^{1/2}. \tag{23}$$

Here the wave height distribution including shoaling and breaking on planar beaches given by Méndez et al. (2004) is adopted. This model is derived by considering a bore approach for modelling the energy dissipation in the surf zone. The distribution of the wave height is then given by the cumulative distribution function (cdf)

$$P\left(\hat{H}\right) = 1 - \exp\left[-\left(\frac{\phi(\kappa)\hat{H}}{1-\kappa\hat{H}}\right)^2\right];\quad 0\le\hat{H}\le\frac{1}{\kappa} \tag{24}$$

where $\kappa = H_{rms}/H_{max}$ is a shape parameter, and H_{max} is the maximum wave height, and

$$\phi(\kappa) = \left(1-\kappa^{0.944}\right)^{1.187};\quad 0\le\kappa\le 1. \tag{25}$$

It should be noted that $\kappa = 0$ corresponds to the seaward conditions, i.e. before shoaling, where Eq. (24) reduces to the Rayleigh distribution. The waves are assumed to be narrow-banded in frequency at the seaward boundary, which is consistent with the Rayleigh pdf for the wave height distribution. The shallow water theory is also assumed to be valid at this location. For the asymptotic case of $\kappa = 1$, Eq. (24) reduces to the Dirac delta distribution. More details are given in Méndez et al. (2004). H_{rms} represents a local value which in the Méndez et al. (2004) distribution is given by the following relationship with the seaward value $H_{rms,0}$:

$$H_{rms} = \left(\frac{h_0}{h}\right)^{1/4}\phi(\kappa)H_{rms,0} \tag{26}$$

where $(h_0/h)^{1/4}$ is the shoaling coefficient for shallow water waves, h_0 is the water depth at the seaward location, $h = h_0 - mx$, m is the bed slope, and x is the horizontal coordinate with $x = 0$ at the seaward location and positive towards the shoreline, with $x = L$ at the shoreline (see Fig. 1). Thus, Eq. (26) shows clearly that the transformation of H_{rms} is induced by shoaling ($(h_0/h)^{1/4}$) and breaking ($\phi(\kappa)$); κ being a measure of the degree of the wave saturation and the characteristics of the breaking process (Méndez et al. (2004); Section 4.1). It should be noted that it is possible to set up a relationship between κ and the wave parameters, based on experimental data (Méndez et al., 2004).

Now the expected value of the maximum force induced by the $(1/n)$th highest waves follows from Eq. (24), and $\hat{H}_{1/n}$ is given in Méndez et al. (2004) as

$$\hat{H}_{1/n} = \frac{\sqrt{\ln n}}{\phi(\kappa) + \kappa\sqrt{\ln n}}. \tag{27}$$

4. Results and discussion

Several experiments have been carried out in wave flumes to characterise the wave–vegetation interaction (Asano et al., 1993; Augustin et al., 2009; Dubi, 1995; Løvås, 2000). However, none of these studies focused on the wave induced forces on plants under shoaling conditions for random breaking waves. Consequently, the results in this section should be taken as tentative, and data for comparisons are required before any conclusion can be made regarding the validity of the method. However, the results should be useful as an engineering approach to estimate forces on plants under shoaling conditions. An example is given to illustrate the use of the method.

4.1. Stochastic method

As presented previously, the wave height distribution including shoaling and breaking on planar beaches by Méndez et al. (2004) is used to describe the wave transformation towards the shore. In this example the conditions at the seaward location are taken similar to those used by Méndez et al. (2004): the wave height $H_{rms0} = 0.1$ m, the water depth $h_0 = 1$ m, and the peak wave period $T_p = 1.91$ s. Three different slopes are considered: 1/10, 1/20 and 1/50. In order to present these data for the different slopes, the results are plotted against the non-dimensional horizontal coordinate, $\hat{x} = x/L$, from the seaward location ($\hat{x} = 0$) to the shoreline ($\hat{x} = 1$) (see Fig. 1).

First, Fig. 3 shows some results of implementing the Méndez et al. (2004) model for the different slopes. Fig. 3a shows κ versus $\hat{x}$ for the three slopes. It appears that for all the slopes κ increases as $\hat{x}$ increases; $\kappa = 0$ at $\hat{x} = 0$ for all the slopes corresponding to the waves to be Rayleigh distributed; $\kappa \to 1$ as $\hat{x} \to 1$ corresponding to the waves to be described by one single frequency (Dirac distributed). Moreover, at a given location $\hat{x}$ it appears that κ increases as the slopes take the values 1/20, 1/50 and 1/10; except that for $\hat{x} > 0.9$ it appears that κ increases as the slope increases. It should be noted that according to Méndez et al. (2004), the amount of breaking waves is directly related to κ by the empirical expression:

$$N_{br} \simeq \kappa^{1.033+0.297\kappa-3.816\kappa^2+2.517\kappa^3} \tag{28}$$

where N_{br} is the ratio of breaking waves varying between 0 (no wave breaking) and 1 (all the waves break). It also follows that the higher κ is, the higher the percentage of breaking waves. Thus the results in Fig. 3a suggest that the slope 1/20 induces less energy dissipation due to less wave breaking along the beach, and that most of the breaking process is concentrated towards the shore.

Then H_{rms} can be obtained from κ by considering the breaking process as a source of energy dissipation (Méndez et al. (2004); Model I).

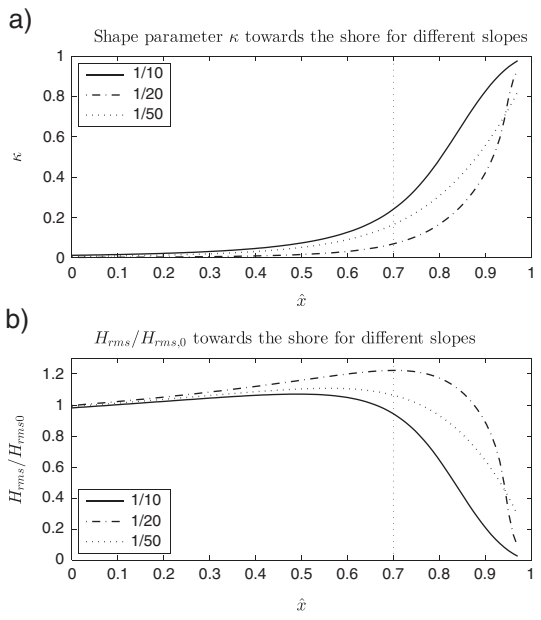

Fig. 3. Results of the wave transformation over planar beaches for different slopes. a) Shape parameter κ used in Eqs. (25) and (26) versus $\hat{x}$. b) H_{rms} / $H_{rms,0}$ versus $\hat{x}$. The vertical lines represent the example given in Table 1 for $\hat{x} = 0.7$.

Fig. 3b shows H_{rms} / $H_{rms,0}$ versus $\hat{x}$. First, it is observed that for all slopes, H_{rms} increases slightly during the propagation over the first half of the beach, while H_{rms} decreases afterwards. This is due to the shoaling process being dominant in the lower part of the beach ($(h_0 / h)^{1/4}$ in Eq. (26)), while the breaking process is dominant in the upper part of the beach ($\phi(\kappa)$ in Eq. (26)). Thus, as H_{rms} is directly related to κ, the previous results for κ in Fig. 3a imply that H_{rms} is largest for $m = 1/20$ for $0<\hat{x}<0.95$, while for $0.95<\hat{x}<1$, H_{rms} is largest for $m = 1/50$.

Fig. 4 shows the statistical values of $\hat{F}$ versus $\hat{x}$ for the slope 1/50 based on C_D (the Méndez et al. (1999) model for swaying plants in Eqs. (3) and (5)) and $\tilde{C}_D$ (the Méndez and Losada (2004) model in Eq. (6)). The statistical values considered are $\hat{F}_{rms}$, and $E\left[\hat{F}\left(\hat{H}\right)|\hat{H} > \hat{H}_{1/n}\right]$ for $n = 3{,}10$ denoted as $\hat{F}_{1/3}$ and $\hat{F}_{1/10}$, respectively. It should be noted that here $\hat{F}$ represents the maximum wave-induced drag force on a plant with height Δh, i.e. that the height of the plant depends on the position $\hat{x}$ on the slope, given by $\Delta h = \Delta h_0(1-\hat{x})$. From Fig. 4 it appears that the results based on C_D and $\tilde{C}_D$ show different behaviour: $\hat{F}$ based on C_D increases as $\hat{x}$ increases from the seaward location up to about 0.2, then $\hat{F}$ decreases as $\hat{x}$ increases towards the shore; $\hat{F}$ based on $\tilde{C}_D$ decreases as $\hat{x}$ increases from the seaward location to the shore. Moreover, $\hat{F}$ based on C_D is larger than $\hat{F}$ based on $\tilde{C}_D$ for $\hat{x} > 0.05-0.15$, reflecting that $\tilde{C}_D < C_D$ for $R \gtrsim 2.6 \times 10^4$ as shown in Fig. 2a. For $\hat{x}<0.05-0.15$, the opposite trend is observed. It should be noted that the drag coefficients vary along the slope due to variation of κ and R, as the depth reduces and the wave height changes towards the shore (Fig. 3b) ($R \sim 1.3 \times 10^4$ for all the slopes at $\hat{x} = 0$ and increases as $\hat{x}$ increases). Finally, it appears that the differences between the statistical values of $\hat{F}$ and the two models decrease as $\hat{x} \to 1$, as the wave height distribution approaches the Dirac distribution.

Fig. 5 shows $\hat{F}_{rms}$ (Fig. 5a), $\hat{F}_{1/3}$ (Fig. 5b) and $\hat{F}_{1/10}$ (Fig. 5c) versus $\hat{x}$ for the C_D and $\tilde{C}_D$ models and the three slopes. It should be noted that the results for the slope 1/50 are the same as those given in Fig. 4 representing the same quantities. Thus it appears that the results in Fig. 5 have the same features as those discussed in Fig. 4. Moreover, for each model the differences between the results for the three slopes are small for $\hat{F}_{rms}$, $\hat{F}_{1/3}$ and $\hat{F}_{1/10}$.

4.2. Alternative derivation of the wave-induced force. Approximate method

An alternative pragmatic way of deriving the wave-induced force on plants under random waves is to represent the random wave by a

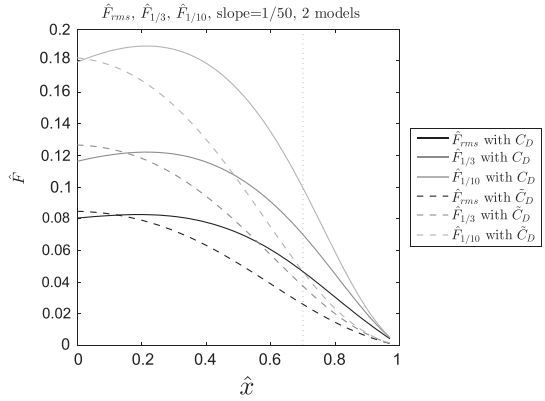

Fig. 4. $\hat{F}_{rms}$, $\hat{F}_{1/3}$, and $\hat{F}_{1/10}$ versus $\hat{x}$ for $m = 1/50$; C_D (Méndez et al. (1999), Eqs. (3) and (5)); $\tilde{C}_D$ (Méndez and Losada (2004)) Eq. (6)). The vertical line represents the example given in Table 1 for $\hat{x} = 0.7$.

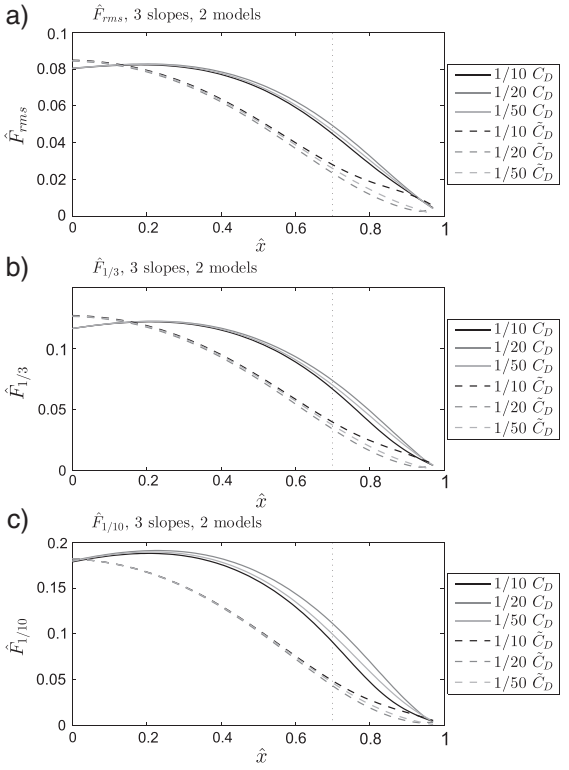

Fig. 5. $\hat{F}_{rms}$ (a), $\hat{F}_{1/3}$ (b), and $\hat{F}_{1/10}$ (c) versus $\hat{x}$ for the C_D and $\tilde{C}_D$ models and the three slopes. The vertical lines represent the example given in Table 1 for $\hat{x} = 0.7$.

characteristic regular wave, for example the rms or significant wave height and a characteristic wave period. This approach, commonly used for engineering applications, will be considered by comparing the results with the present stochastic method. One question is how well the mean value of the non-dimensional maximum force induced on vegetation by the (1/n)th highest waves, $E\left[\hat{F}\left(\hat{H}\right)|\hat{H} > \hat{H}_{1/n}\right]$, can be represented by using the mean value of the (1/n)th highest waves in the maximum force formulas for regular waves, i.e. corresponding to that $\hat{H}$ is replaced with $E\left[\hat{H}_{1/n}\right]$ in Eqs. (17) and (21). Mendez et al. (2004, Table 1) give the following polynomial functions for $E\left[\hat{H}_{1/n}\right]$ for $n = (3, 10)$:

$$E\left(\hat{H}_{1/n}\right) = \begin{pmatrix} \hat{H}_{1/3} \\ \hat{H}_{1/10} \end{pmatrix} = \begin{pmatrix} 1.416 \\ 1.800 \end{pmatrix} - \begin{pmatrix} 0.140 \\ 0.830 \end{pmatrix}\kappa - \begin{pmatrix} 0.749 \\ 0.477 \end{pmatrix}\kappa^2 + \begin{pmatrix} 0.887 \\ 0.985 \end{pmatrix}\kappa^3 - \begin{pmatrix} 0.413 \\ 0.478 \end{pmatrix}\kappa^4; n = \begin{pmatrix} 3 \\ 10 \end{pmatrix}. \quad (29)$$

Another question is how well the rms value of the non-dimensional maximum force can be represented by using the rms wave height in the maximum force formulas for regular waves, i.e. corresponding to that $\hat{H} = H_{rms}/H_{rms} = 1$ in Eqs. (17) and (21).

It is of interest to compare the stochastic and the approximate method. Fig. 6 shows the ratio between the stochastic and approximate method results for $\hat{F}_{rms}$ (Ra_{rms}, Fig. 6a), $\hat{F}_{1/3}$ ($Ra_{1/3}$, Fig. 6b) and $\hat{F}_{1/10}$ ($Ra_{1/10}$, Fig. 6c) versus $\hat{x}$ for the two models and the three slopes. Overall, the results for the three ratios show the same features; the ratios for the C_D model are larger than one, while the ratios for the $\tilde{C}_D$ model are about one, and the ratios approach 1 at the shore for both models. More specifically: for the C_D model (Ra_{rms}, $Ra_{1/3}$, $Ra_{1/10}$) are approximately (1.4, 2.1, 3.3) for $\hat{x}$ up to about (0.5, 0.5, 0.4) depending on the slope, and for larger $\hat{x}$ the ratios approach 1. For the $\tilde{C}_D$ model Ra_{rms} is about 1.2 at $\hat{x} = 0$ and decreases towards 1 as $\hat{x} \to 1$, while $Ra_{1/3}$ and $Ra_{1/10}$ are close to 1 for all $\hat{x}$; this is the case for all slopes. Overall it appears that the stochastic method cannot be replaced by the approximate method when using the Méndez et al. (1999) model (C_D,

Table 1
Example of calculation.

$H_{rms,0}$,h_0,T_p,Δ,b	0.1 m, 1 m, 1.91 s, 0.33, 0.1 m
$\hat{x}$, h, Δh	0.7, 0.3 m, 0.1 m
x (m), L (m), $\left[\frac{1}{10};\frac{1}{20};\frac{1}{50}\right]$	[7;14; 35], [10; 20; 50]
H_{rms}, $\left[\frac{1}{10};\frac{1}{20};\frac{1}{50}\right]$, (m)	[0.09; 0.12; 0.11]
κ, $\left[\frac{1}{10};\frac{1}{20};\frac{1}{50}\right]$	[0.24; 0.07; 0.17]
$R_{rms}\times 10^{-4}$, $\left[\frac{1}{10};\frac{1}{20};\frac{1}{50}\right]$,	[4.85; 6.28; 5.46]
$\hat{F}\times 10^2$	using C_D, using $\tilde{C}_D$
$\hat{F}_{rms}\times 10^2$, $\left[\frac{1}{10};\frac{1}{20};\frac{1}{50}\right]$	[4.50; 4.95; 4.68], [2.82; 2.36; 2.61]
$\hat{F}_{1/3}\times 10^2$, $\left[\frac{1}{10};\frac{1}{20};\frac{1}{50}\right]$	[6.73; 7.42; 7.04], [4.01; 3.44; 3.77]
$\hat{F}_{1/10}\times 10^2$, $\left[\frac{1}{10};\frac{1}{20};\frac{1}{50}\right]$	[9.16; 11.19; 10.01], [4.92; 4.37; 4.70]
Ratio,	using C_D, using $\tilde{C}_D$
Ra_{rms}, $\left[\frac{1}{10};\frac{1}{20};\frac{1}{50}\right]$	[1.24; 1.37; 1.29], [1.05; 1.04; 1.05]
$Ra_{1/3}$, $\left[\frac{1}{10};\frac{1}{20};\frac{1}{50}\right]$	[1.86; 2.05; 1.94], [1.00; 0.99; 1.00]
$Ra_{1/10}$, $\left[\frac{1}{10};\frac{1}{20};\frac{1}{50}\right]$	[2.53; 3.09; 2.76], [1.00; 1.00; 1.00]

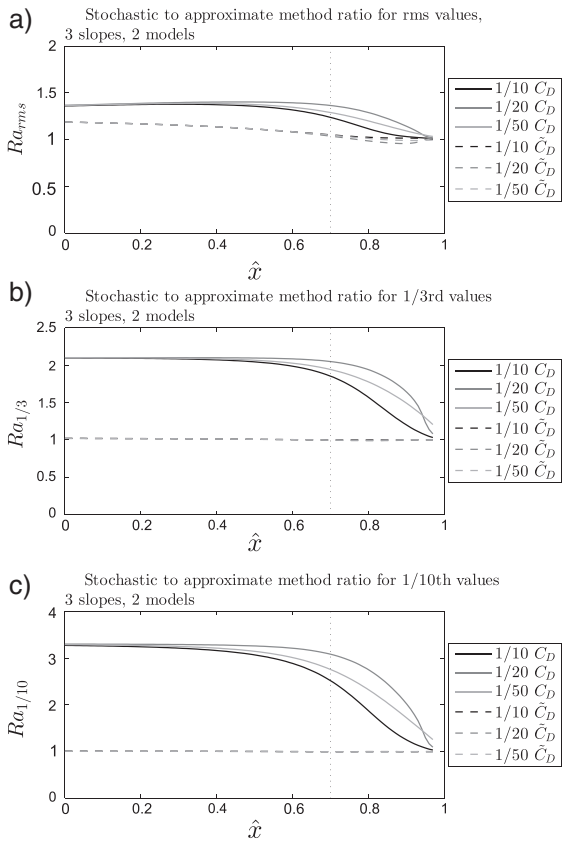

Fig. 6. Stochastic to approximate method ratios for $\hat{F}_{rms}$ (Ra_{rms}, a), $\hat{F}_{1/3}$ ($Ra_{1/3}$, b), $\hat{F}_{1/10}$ ($Ra_{1/10}$, c) versus $\hat{x}$ for the two models and the three slopes. The vertical lines represent the example given in Table 1 for $\hat{x} = 0.7$.

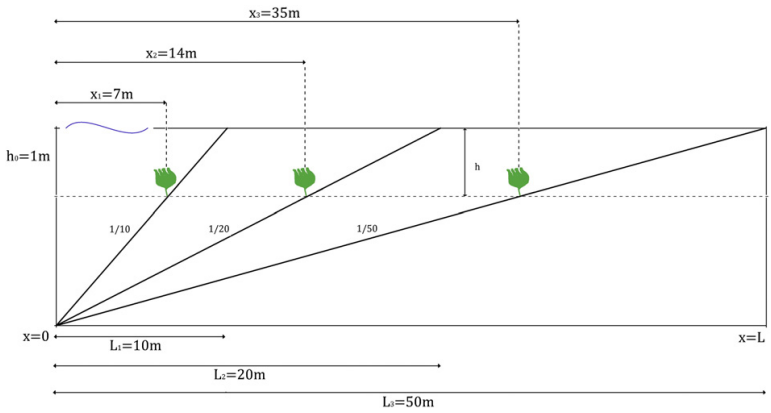

Fig. 7. Illustration of the example of calculation, see also Table 1.

Eqs. (3) and (5)). However, this approximation holds if the Méndez and Losada (2004) is used for $\hat{F}_{1/3}$ and $\hat{F}_{1/10}$, while for $\hat{F}_{rms}$ it is only the case when $\hat{x}$ approaches 1. It should be noted that these results are valid for this example, i.e. for $b = 0.1$, $\Delta = 0.33$ and $T_p = 1.91$ s. More discussion of the results will be given in the Example of calculation.

4.3. Example of calculation

An example is given to illustrate the use of the graphs presented in Figs. 3–6. As already mentioned, the conditions at the seaward location are taken similar to those used by Méndez et al. (2004): $H_{rms,0} = 0.1$ m, $h_0 = 1$ m and $T_p = 1.91$ s. Table 1 gives the results calculated at the horizontal location $\hat{x} = 0.7$. At this location the water depth is $h = h_0 - (h_0/L)x = h_0 - h_0\hat{x} = h_0 - h_0 \times 0.7 = 0.3$m, the dimensions of the plant are $\Delta h = 0.33 \times 0.3$ m $= 0.1$ m and $b = 0.1$ m. For the three slopes it corresponds to that the calculations are made at the locations $x = 7$ m, 14 m, 35 m; Fig. 7 shows a sketch of these three situations.

From Table 1 it is seen that the slope 1/20 leads to the highest H_{rms} and the lowest κ, suggesting a lower breaking activity at this location. Moreover, R_{rms} varies between 4.85×10^4 and 6.28×10^4, which is within the definition domain of $\tilde{C}_D$, but outside of the definition domain of C_D (see Section 2.2 and Fig. 2a). As mentioned in Section 2.2, the definition of C_D by Eqs. (3) and (5) is extended to higher values of R to serve the purpose of demonstrating the use of the methods. At $\hat{x} = 0.7$ it is also seen that for the $\tilde{C}_D$ model the stochastic method can be replaced by the approximate method, while this is not the case for the C_D model; for the $\tilde{C}_D$ model the ratios are in the range 0.99 to 1.05 depending on the statistical values considered; for the C_D model the ratios are in the range 1.24 to 3.09 depending on the statistical values considered.

The presented figures and Table 1 give non-dimensional parameters. As seen from Eqs. (1), (2), (11) and (17), the total wave-induced drag force on a vegetation patch is taken to be equal to the sum of the individual drag forces on each plant. Recently Siniscalchi et al. (2012) performed some flume experiments with a vegetation patch in steady flow. They found that the mean drag force experienced by each individual plant is fairly constant, with only a weak reduction of the forces along the patch axis. But there is no evidence that this is the case in oscillatory flow. The dimensional force is obtained by multiplying the non-dimensional force with the factor $\frac{1}{2}\rho bNU_{rms}^2$. Thus it is possible to limit the results to one plant ($N = 1$), or to assume that the drag force on a vegetation patch is the sum of the forces on each plant (with $N > 1$). In that case the wave related quantities used in the formulas (i.e. H_{rms}, u_{rms}) should be evaluated at the horizontal position in the middle of the vegetation field. This approach should be sufficiently accurate for engineering applications.

5. Summary

A practical stochastic method for estimating the drag force on vegetation exposed to shoaling non-breaking and breaking random waves is provided. An example of calculation has illustrated the effect of energy dissipation due to wave breaking on the wave-induced maximum drag force on a plant at different positions on a planar beach with three different slopes. Two different drag models are considered: C_D (Méndez et al., 1999) and $\tilde{C}_D$ (Méndez and Losada, 2004), and the stochastic method has been compared to a deterministic approach. The stochastic method is represented by using the rms value of the maximum wave-induced drag force and the expected value of the maximum wave-induced drag force caused by the $(1/n)$ th highest wave.

For the flow conditions exemplified here, the present results suggest that the drag force formula based on $\tilde{C}_D$ for regular waves can be applied for random waves if the random waves are represented by the mean of the $(1/n)$th highest waves for $n = 3$ and $n = 10$, and by the rms wave height, but only close to the shore. However, this is not the case for the drag force formula based on C_D; the stochastic method is required. It should be noted that for other flow conditions, the results may be different.

Although the stochastic method is simple, it should be useful for having first estimates for engineering applications of the drag force on a vegetation field in shoaling conditions beneath non-breaking and breaking random waves on a planar beach.

References

Asano, T., Deguchi, H., Kobayashi, N., 1993. Interaction between water waves and vegetation. Proceedings of the 23rd International Conference on Coastal Engineering, vol. 3. ASCE, Venice, Italy, pp. 2710–2723.

Augustin, L.N., Irish, J.L., Lynett, P., 2009. Laboratory and numerical studies of wave damping by emergent and near-emergent wetland vegetation. Coastal Engineering 56 (3), 332–340.

Boller, M.L., Carrington, E., 2006. The hydrodynamic effects of shape and size change during reconfiguration of a flexible macroalga. Journal of Experimental Biology 209 (10), 1894–1903.

Coulombier, T., Neumeier, U., Bernatchez, P., 2012. Sediment transport in a cold climate salt marsh (St. Lawrence Estuary, Canada), the importance of vegetation and waves. Estuarine, Coastal and Shelf Science 101, 64–75.

Dalrymple, R.A., Kirby, J.T., Hwang, P.A., 1984. Wave diffraction due to areas of energy dissipation. Journal of Waterway, Port, Coastal & Ocean Engineering, ASCE 110 (1), 67–79.

Dean, R., Dalrymple, R., 1991. Water Wave Mechanics for Engineers & Scientists. World Scientific.

Denny, M., Gaylord, B., 2002. The mechanics of wave-swept algae. Journal of Experimental Biology 205 (10), 1355–1362.
Denny, M.W., Gaylord, B., 2010. Marine ecomechanics. Annual Review of Marine Science 2 (1), 89–114.
Dijkstra, J., Uittenbogaard, R., 2010. Modeling the interaction between flow and highly flexible aquatic vegetation. Water Resources Research 46 W12547.
Dubi, A., 1995. Damping of water waves by submerged vegetation: a case of study on *Laminaria hyperborea*. PhD thesis, University of Trondhiem.
Dubi, A., Tørum, A., 1995. Wave damping by kelp vegetation. Proceedings of the 24th International Conference on Coastal Engineering, vol. 1. ASCE, Kobe, Japan, pp. 142–156 (Part 1 (of 3)).
Dubi, A., Tørum, A., 1997. Wave energy dissipation in kelp vegetation. Proceedings of the 1996 25th International Conference on Coastal Engineering, vol. 3. ASCE, Orlando, FL, USA, pp. 2626–2639 (Part 1 (of 4)).
Feagin, R.A., Irish, J.L., Möller, I., Williams, A.M., Colón-Rivera, R.J., Mousavi, M.E., 2011. Short communication: engineering properties of wetland plants with application to wave attenuation. Coastal Engineering 58 (3), 251–255.
Gacia, E., Duarte, C.M., 2001. Sediment retention by a Mediterranean *Posidonia oceanica* meadow: the balance between deposition and resuspension. Estuarine, Coastal and Shelf Science 52 (4), 505–514.
Infantes, E., Orfila, A., Simarro, G., Terrados, J., Luhar, M., Nepf, H., 2012. Effect of a seagrass (*Posidonia oceanica*) meadow on wave propagation. Marine Ecology Progress Series 456, 63–72.
Kobayashi, N., Raichle, A.W., Asano, T., 1993. Wave attenuation by vegetation. Journal of Waterway, Port, Coastal, & Ocean Engineering, ASCE 119 (1), 30–48.
Koch, E., Ackerman, J., Verduin, J., Keulen, M., 2006. Fluid dynamics in seagrass ecology—from molecules to ecosystems. Seagrasses: Biology, Ecology and Conservation. Springer, Netherlands, pp. 193–225.
Li, C.W., Yan, K., 2007. Numerical investigation of wave–current–vegetation interaction. Journal of Hydraulic Engineering 133 (7), 794–803.
Løvås, S.M., 2000. Hydro-physical conditions in kelp forests and the effect on wave damping and dune erosion: a case study on *Laminaria hyperborea*. PhD thesis, University of Trondheim.
Løvås, S.M., Tørum, A., 2000. Effect of submerged vegetation upon wave damping and run-up on beaches: a case study on *Laminaria hyperborea*. Coastal Engineering 2000—27th International Conference on Coastal Engineering, ICCE 2000, vol. 276. NSW, Sydney, pp. 851–864.
Løvås, S.M., Tørum, A., 2001. Effect of the kelp *Laminaria hyperborea* upon sand dune erosion and water particle velocities. Coastal Engineering 44 (1), 37–63.
Luhar, M.J.R., Nepf, H., 2008. Interaction between flow, transport and vegetation spatial structure. Environmental Fluid Mechanics 8, 423.
Luhar, M., Nepf, H.M., 2011. Flow-induced reconfiguration of buoyant and flexible aquatic vegetation. Limnology and Oceanography 56 (6), 2003–2017.
Martone, P.T., Kost, L., Boller, M., 2012. Drag reduction in wave-swept macroalgae: alternative strategies and new predictions. American Journal of Botany 99 (5), 806–815.
Massel, S., 1999. Fluid Mechanics for Marine Ecologists. Springer.
Massel, S., Furukawa, K., Brinkman, R., 1999. Surface wave propagation in mangrove forests. Fluid Dynamics Research 24 (4), 219–249.
Méndez, F.J., Losada, I.J., 2004. An empirical model to estimate the propagation of random breaking and nonbreaking waves over vegetation fields. Coastal Engineering 51 (2), 103–118.
Méndez, F.J., Losada, I.N.J., Losada, M.A., 1999. Hydrodynamics induced by wind waves in a vegetation field. Journal of Geophysical Research 104 (C8), 18383–18396.
Méndez, F.J., Losada, I.N.J., Medina, R., 2004. Transformation model of wave height distribution on planar beaches. Coastal Engineering 50 (3), 97–115.
Myrhaug, D., Holmedal, L.E., 2011. Drag force on a vegetation field due to long-crested and short-crested nonlinear random waves. Coastal Engineering 58 (6), 562–566.
Myrhaug, D., Holmedal, L.E., Ong, M.C., 2009. Nonlinear random wave-induced drag force on a vegetation field. Coastal Engineering 56 (3), 371–376.
Paul, M., Bouma, T.J., Amos, C.L., 2012. Wave attenuation by submerged vegetation: combining the effect of organism traits and tidal current. Marine Ecology Progress Series 444, 31–41.
Pujol, D., Colomer, J., Serra, T., Casamitjana, X., 2012. A model for the effect of submerged aquatic vegetation on turbulence induced by an oscillating grid. Estuarine, Coastal and Shelf Science 114, 23–30.
Pujol, D., Nepf, H., 2012. Breaker-generated turbulence in and above a seagrass meadow. Continental Shelf Research 49, 1–9.
Sánchez-González, J.F., Sánchez-Rojas, V., Memos, C.D., 2011. Wave attenuation due to *Posidonia oceanica* meadows. Journal of Hydraulic Research 49 (4), 503–514.
Siniscalchi, F., Nikora, V.I., Aberle, J., 2012. Plant patch hydrodynamics in streams: mean flow, turbulence, and drag forces. Water Resources Research 48 (1), W01513.
Vandenbruwaene, W., Temmerman, S., Bouma, T.J., Klaassen, P.C., de Vries, M.B., Callaghan, D.P., van Steeg, P., Dekker, F., van Duren, L.A., Martini, E., Balke, T., Biermans, G., Schoelynck, J., Meire, P., 2011. Flow interaction with dynamic vegetation patches: implications for biogeomorphic evolution of a tidal landscape. Journal of Geophysical Research 116 (F1) F01008.
Vo-Luong, P., Massel, S., 2008. Energy dissipation in non-uniform mangrove forests of arbitrary depth. Journal of Marine Systems 74 (1–2), 603–622.

PAPER II

Henry, P.-Y., D. Myrhaug, and J. Aberle [**2015**], Drag forces on aquatic plants in nonlinear random waves plus current, *Estuarine, Coastal and Shelf Science*, 165, 10-24.

Estuarine, Coastal and Shelf Science 165 (2015) 10–24

Contents lists available at ScienceDirect

Estuarine, Coastal and Shelf Science

journal homepage: www.elsevier.com/locate/ecss

Drag forces on aquatic plants in nonlinear random waves plus current

Pierre-Yves Henry [a, *], Dag Myrhaug [a], Jochen Aberle [b]

[a] Department of Marine Technology, Norwegian University of Science and Technology, NO-7491 Trondheim, Norway
[b] Department of Hydraulics and Environmental Engineering, Norwegian University of Science and Technology, NO-7491 Trondheim, Norway

ARTICLE INFO

Article history:
Received 7 March 2015
Received in revised form
22 August 2015
Accepted 26 August 2015
Available online 31 August 2015

Keywords:
Nonlinear random wave
Wave plus current
Drag force
Drag coefficient
Stochastic method
Salt marsh

ABSTRACT

Plant-flow interactions are characterised by an assemblage of processes acting at different temporal and spatial scales. In order to mathematically characterise these interactions, such processes have to be parameterised given some simplifications. Typically, drag coefficients are derived from experiments to characterise the plant reconfiguration and wave energy dissipation processes. By reviewing the different plant drag coefficients C_D valid in oscillatory flows, this study first highlights the lack of normalisation of the different existing C_D formulations and identifies possibilities for a standardisation of the formulations for oscillatory and steady flows. Then, by taking into account the wave crest height distribution of a sea state condition, this study further develops a stochastic method to compute the expected wave induced forces on a plant in linear/nonlinear random waves plus current based on two different C_D formulations for waves alone and waves plus current. This method improves the characterisation of the stochastic plant–flow interactions by allowing the calculation of expected values under different random wave plus currents conditions. Results are compared to a classic deterministic approach and some differences are identified, calling for further investigations against experimental datasets. Based on the appropriate C_D formulations, this study finally revealed that wave nonlinearities have a significant effect on expected wave forces for a higher wave activity, and that in presence of an increasing current, the effect of wave nonlinearities decreases while the expected wave forces increase.

1. Introduction

Vegetation is a ubiquitous feature in aquatic environments affecting many physical, chemical, and biological processes across a wide range of spatial and temporal scales (Nikora, 2010; Nepf, 2012; Nikora et al., 2012). The interaction between flow and vegetation has important implications for many ecological and engineering applications and has consequently been in the focus of research in the past decades. A large body of research has focused on the exerted drag forces by mimicking vegetation with stiff elements such as cylinders although most plants are flexible (e.g., Aberle and Järvelä, 2013). Both stiff elements and flexible plants offer resistance to the incoming flow, generating an energy transfer from the flow to the plant, which in turn affects turbulence and wave-patterns. Compared to stiff elements, flexible plants will, under energetic flow conditions (high currents or wave-induced velocities), adopt a streamlined shape and reduce their projected frontal area to reduce their exposure to the flow attack (de Langre et al., 2012; Miller et al., 2012; Siniscalchi et al., 2012; Albayrak et al., 2013). The reconfiguration depends on the plants' mechanical and structural properties and is the key to their survival in high energy flows.

Flexible plants such as salt marsh plants and seagrasses have, among others, been recognised as potential wave-dampers (Feagin et al., 2011; Paul and Amos, 2011; Möller et al., 2014). The adequate design of such natural engineering structures requires an enhanced understanding of the relevant processes and hence of fluid forces (and the corresponding main component, the drag force), energy dissipation (turbulence, wave damping), and plant ecology (plant mechanical and physiological stresses). One of the keys for the adequate description of drag forces can be seen in the parameterisation of a proper plant related drag coefficient C_D (Mendez and Losada, 2004; Möller et al., 2014; Ozeren et al., 2014; Zeller et al., 2014). This parameterisation is presently one of the major difficulties when describing plant–flow interactions not only in coastal but also in fresh water environments (Aberle and Järvelä, 2013, 2015). In general, many different approaches for the parameterisation of drag forces have been suggested for both environments

* Corresponding author.
E-mail address: pierre-yves.henry@ntnu.no (P.-Y. Henry).

http://dx.doi.org/10.1016/j.ecss.2015.08.021
0272-7714/

(Nepf, 2011). However, drag coefficients for flexible aquatic plants have always been derived from experimental datasets as information on plant reconfiguration and wave energy dissipation is required for their determination. Thus, the derived formulations are, in theory, limited to the conditions covered by the experiments.

Moreover, many experimental or numerical studies focused on drag force estimations under simplified boundary conditions (linear waves or current alone; e.g. (Suzuki et al., 2012; Anderson and Smith, 2014; Ozeren et al., 2014) although these estimations are generally more complex in field conditions (Massel et al., 1999; Paul and Amos, 2011; Jadhav et al., 2013). Deterministic approaches are commonly used to characterise random wave conditions, reducing for example the spectrum of wave-induced velocities to a single statistical value (typically the root-mean-square value). These approaches may lead to a misrepresentation of the stochastic plant–flow interactions (Bradley and Houser, 2009; Jadhav et al., 2013; Anderson and Smith, 2014).

After a critical review of the available C_D formulations under wave conditions, this study develops a stochastic method to compute characteristic statistical values of the wave-induced forces on a single plant in various random waves plus current conditions. C_D formulations derived for regular waves by Ozeren et al. (2014) (waves alone) and Hu et al. (2014) (waves plus current) are applied, within their domain of applicability, to each single wave of the narrow-banded irregular wave spectrum. Nonlinear wave effects (long- and short-crested) are included and discussed considering the Forristall (2000) wave crest height distribution. Finally, the method is applied to live salt marsh plants (*Juncus roemerianus*) using the Ozeren et al. (2014) C_D formulations, and discussed in the light of the conclusions of the critical review.

2. C_D formulations for an aquatic plant in waves

2.1. Drag forces for regular waves plus current

The simplest approach to derive an expression of the fluid forces experienced by plants is to consider only the main component, i.e. the drag force, and neglecting the plants' swaying motion and inertial force (Mendez and Losada, 2004) resulting in a so-called Morison-type equation. This approach is systematically used in coastal engineering descriptions of plant–flow interaction and the horizontal time-varying force on a plant community per unit volume is thus expressed as:

$$F(t) = \frac{1}{2}\rho C_D b_v N\, u(t)\ |u(t)| \tag{1}$$

where $u(t)$ is the undisturbed horizontal wave-induced velocity at a reference location along or in the vegetation region, t is the time, ρ is the density of water, b_v is the mean plant width (corresponding to the plant area per unit height of the vegetation stand normal to $u(t)$), N is the number of plants per unit area, and C_D is a bulk drag coefficient. It should be noted that the correct calculation of $F(t)$ requires the use of the relative velocity between the fluid and the plants instead of $u(t)$. In addition, there is normally no linear relation between the total force exerted on a plant patch and its number of stems. However, it is common practice to link $F(t)$ and N linearly as described in Eq. (1) so that potential shading effects and interactions with other stems are taken into account by C_D as done in river flows by Lindner (1982) or Li and Shen (1973). In order to provide general results, the dimensional forces computed in this section correspond to the force on one plant per unit area (N chosen equal to 1 by default in Eq. (1)). Eq. (1) is also valid for a flexible plant (Mendez and Losada, 2004; Henry and Myrhaug, 2013). Applying Eq. (1) to oscillatory flows, the maximum horizontal drag force per unit volume within a wave cycle is given by

$$F_{max} = \frac{1}{2}\rho C_D b_v U_w^2 \tag{2}$$

where U_w is the maximum horizontal velocity within the wave cycle. For the case of regular waves plus current $U_{max} = U_w + U$ may be used instead of U_w, where U is the bulk velocity of the steady current. The accuracy of this formulation depends not only on the plant width but also on the definition of the drag coefficient C_D.

2.2. Drag coefficient formulations for oscillatory flows

Formulations for the drag coefficient C_D have generally been derived by determining the ratio F_{max}/U_w^2 from experimental data for different flow conditions. Regarding oscillatory flows, C_D-values have mostly been determined from observations of the wave decay over a vegetation patch following the method first described by Dalrymple et al. (1984), although it is also possible to determine these values using direct measurements of F_{max} and U_w (Hu et al., 2014). In general, two different kind of formulations have been developed for the determination of C_D which are based on the Reynolds number Re and the Keulegan–Carpenter number K_C, respectively, with the corresponding approaches being summarized in Table 1.

Expressing C_D as a function of the Reynolds number Re is the classical expression used in fluid mechanics. For waves the corresponding relationship is mostly written as $C_D = \widehat{\alpha} + (\widehat{\beta}/Re)^{\gamma}$, where $(\widehat{\alpha}, \widehat{\beta}, \gamma)$ are non-dimensional parameters, and $Re = U_w b_v/\nu$, where ν is the kinematic viscosity of the fluid. As for steady flow cases, typical for fresh water environments, various parameters $(\widehat{\alpha}, \widehat{\beta}, \gamma)$ have been suggested for oscillatory flows (Table 1 and (Nepf, 2011)). On the other hand, C_D can also be expressed as a function of the Keulegan–Carpenter number K_C (defined as the ratio between the fluid particle excursion amplitude and the characteristic dimension of the plant) for oscillatory flows. The corresponding expressions can take different forms (Table 1), but the most common expression is $C_D = a\, K_C^b$, where (a,b) are non-dimensional parameters, and $K_C = U_w T/b_v$, where T is the wave period which can be replaced by the spectral peak wave period T_p in the case of random waves. Inertia forces cannot be neglected for relatively small values of K_C (Ozeren et al. (2014)) so that in a coastal environment, approaches based on Eq. (1) are only valid for larger values of K_C (or Re), i.e. when drag forces dominate over inertia forces due to the flow separation and vortex shedding processes in the wake of the plants. However, Bradley and Houser (2009) argued that under lower-energy conditions, wave energy dissipation is driven by relative blade motion, best described by K_C, and not in-canopy turbulent dissipation typical for high-energy conditions (and best described by Re). As a consequence, there exists a range between very low energy and high energy flows where a formulation of the bulk drag coefficient based on K_C seems to describe experimental data better than that based on a Reynolds number (Mendez and Losada, 2004; Lowe et al., 2007; Sánchez-González et al., 2011; Jadhav et al., 2013; Ozeren et al., 2014). This may explain why Möller et al. (2014) observed that the expression for C_D dependent on Re formulation led to over prediction of wave dissipation for low-energy conditions. It should be noted, however, that all of these different formulations neglect the relative velocity of the plant compared to the flow, and doesn't explicitly include reconfiguration processes (bending, pronation), which may lead to inaccuracies in wave forces and energy dissipation estimations (Zeller et al., 2014).

In the case of irregular waves, the bulk drag coefficient C_D varies for each individual wave, depending on the wave height and wave period. Bradley and Houser (2009) argued that plants (seagrasses)

Table 1
Review of the different bulk drag coefficients formulations for wave forces on different aquatic plants. Here, U_w is the characteristic velocity acting on the plants (defined as the maximum horizontal velocity within the wave cycle at the top of the vegetation), b_v is the plants average width and ν is the kinematic viscosity of the surrounding flow, T_p is the spectral peak wave period, H_s is the significant wave height, and U is the steady flow velocity component (current). Δ is the vegetation height divided by the water depth ($\Delta > 1$ for emergent vegetation and $\Delta < 1$ for submerged vegetation) and h is the water depth.

(Bulk) drag coefficient formulation	Author	Comments
1. $C_D = \widehat{\alpha} + \left(\frac{\widehat{\beta}}{Re}\right)^{\gamma}$ **or** $C_D = \widehat{\alpha} + \left(\frac{\widehat{\beta}}{Re_{rms}}\right)^{\gamma}$, **with** $Re = \frac{U_w b_v}{\nu}$ **and** $Re_{rms} = \frac{U_{rms} b_v}{\nu}$		
$(\widehat{\alpha}, \widehat{\beta}, \gamma) = (0.08,\ 2200,\ 2.4)$; $2200 < Re < 18000$	Kobayashi et al. (1993)	Best fit to flume data of Asano et al. (1988) – Regular waves over artificial seaweeds (polypropylene strips)
$(\widehat{\alpha}, \widehat{\beta}, \gamma) = (0.08,\ 2200,\ 2.2)$; rigid plants & $200 < Re < 15500$	Méndez et al. (1999)	Best fit to flume data of Asano et al. (1993) – Regular waves over artificial seaweeds (polypropylene strips)
$(\widehat{\alpha}, \widehat{\beta}, \gamma) = (0.40,\ 4600,\ 2.9)$; swaying plants & $2300 < Re < 20000$		
$(\widehat{\alpha}, \widehat{\beta}, \gamma) = (0.1,\ 925,\ 3.16)$ $200 < Re_{rms} < 800$	Bradley and Houser (2009)	Best fit to field records of irregular waves over live seagrass meadow (*Thalassia testudinum*) in fetch-limited conditions
$(\widehat{\alpha}, \widehat{\beta}, \gamma) = (0.06,\ 153,\ 1.45)$ $H_S \geq 0.1m$	Paul and Amos (2011)	Best fit to field records of irregular waves over live seagrass meadow (*Zostera noltii*) at four different stages during the growth cycle.
$(\widehat{\alpha}, \widehat{\beta}, \gamma) = (0,\ 2400,\ 0.77)$; $1000 < Re < 3200$	Koftis et al. (2013)	Best fit to flume data of Stratigaki et al. (2011) – Regular waves over artificial seaweeds (*P. oceanica*-PVC)
$(\widehat{\alpha}, \widehat{\beta}, \gamma) = (0.87,\ 2200,\ 0.88)$; $2800 < Re < 8500$	Maza et al. (2013)	Best fit to flume data of Stratigaki et al. (2011) – Regular waves over artificial seaweeds (*P. oceanica*-PVC)
$(\widehat{\alpha}, \widehat{\beta}, \gamma) = (-0.05,\ 306,\ 0.98)$; regular waves, $1000 < Re < 10500$	Möller et al. (2014)	Best fit to large-scale experiments for regular and irregular waves over salt marshes
$(\widehat{\alpha}, \widehat{\beta}, \gamma) = (0.16,\ 227,\ 1.62)$; irregular waves, $200 < Re < 12000$		
$(\widehat{\alpha}, \widehat{\beta}, \gamma) = (2.1,\ 793,\ 2.39)$; regular waves, $400 < Re < 4300$;	Ozeren et al. (2014)	Best fit to flume data of regular and irregular waves. $(\widehat{\alpha}, \widehat{\beta}, \gamma)$ estimated for rigid cylinders, valid for different densities/submergence ratios.
$(\widehat{\alpha}, \widehat{\beta}, \gamma) = (1.5,\ 1230,\ 0.95)$; irregular waves, $200 < Re < 1600$;		
2. Other *Re*-based C_D formulations		
$C_D = \widehat{\alpha} + \left(\frac{\widehat{\beta}}{Q_{Re}}\right)^{\gamma}$, with $Q_{Re} = \frac{Re_{rms}}{\Delta^{1.5}}$	Anderson and Smith (2014)	Spectral analysis of wave attenuation over salt marsh mimics (flume work) and definition of bulk C_D
$(\widehat{\alpha}, \widehat{\beta}, \gamma) = (0.11,\ 2067.7,\ 0.64)$		
$C_D = \widehat{\alpha} + \left(\frac{\widehat{\beta}}{Re}\right)^{\gamma}$, $Re = \frac{(U_w + U) b_v}{\nu}$	Hu et al. (2014)	Best fit to experiments for pure reg. waves and reg. waves plus current over staggered arrays of submerged stiff cylinders
$(\widehat{\alpha}, \widehat{\beta}, \gamma) = (1.04,\ 730,\ 1.37)$ for $300 < Re < 4700$		
3. $C_D = a K_C^b$ **or** $C_D = a K_{Crms}^b$, **with** $K_C = U_w T / b_v$ **and** $K_{Crms} = U_{rms} T_p / b_v$		
$(a,b) = (126.45,\ -2.76)$ for $1 < K_{Crms} < 6$	Bradley and Houser (2009)	(see above)
1) $(a,b) = (22.9,\ -1.09)$ 2) $(a,b) = (35.5,\ -1.12)$ 3) $(a,b) = (39.5,\ -1.08)$ for $15 < K_C < 425$	Sánchez-González et al. (2011)	1) flume tests of reg. and irreg. waves over artificial seagrass 2) derived from Asano et al. (1993); 3) derived from Mendez and Losada (2004)
$(a,b) = (70,\ -0.86)$	Jadhav et al. (2013)	Spectral average of the drag coefficient obtained on the field for salt marsh vegetation (Spartina alterniflora) under a tropical storm (random waves).
4. Other K_C–based C_D formulations		
$C_D = \frac{\exp(-0.0138\ Q)}{Q^{0.3}}$; $7 < Q < 172$, with $Q = K_{C\,rms}/\Delta^{0.76}$, and $K_{C\,rms} = U_{rms} T_p / b_v$	Mendez and Losada (2004)	Best fit to flume data of Dubi and Torum (1995) – Irregular waves (JONSWAP spectrum) over a bed of artificial kelp (*L. digitata*)
$C_D = \widehat{\alpha} + \left(\frac{\widehat{\beta}}{Q_{Kc}}\right)^{\gamma}$, with $Q_{Kc} = \frac{K_{Crms}}{\Delta^{1.5}}$	Anderson and Smith (2014)	(see above)
$(\widehat{\alpha}, \widehat{\beta}, \gamma) = (0.97,\ 33.5,\ 1.69)$		
$C_D = a[K_C \Delta^{-2}]^b$, with $K_C = \frac{U_w T_p}{b_v}$, $(a,b) = (55.2,\ -0.817)$; regular waves, $5 < K_C < 80$; $(a,b) = (58.5,\ -0.641)$; irregular waves, $3 < K_C < 40$;	Ozeren et al. (2014)	Best fit to flume data of regular and irregular waves over artificial and live seagrasses. *(a,b)* valid for different densities/submergence ratios

tend to move out of phase with waves at the (higher) peak frequency, while moving in phase with less energetic waves at a lower frequency. As a consequence higher frequency waves tend to be more attenuated than lower frequency waves, leading to a frequency dependent drag coefficient. Jadhav et al. (2013) discussed the dependency of C_D upon the wave frequency and concluded that a frequency-dependent drag coefficient predicts the spectral distribution of wave energy dissipation better than a drag coefficient averaged over the frequencies. Similarly, Anderson and Smith (2014) showed that for irregular waves propagating over a vegetation field with a double peaked spectrum, the attenuation of the different frequency ranges is not necessarily uniform, depending on the plant's submergence ratios and the stem density. However, the definition of a wave-frequency dependent drag coefficient depends on both wave conditions and the tested plants, and is impractical to determine a-priori. Thus for random waves, the plant drag coefficient is generally derived as a function of Re_{rms}, the root-mean-square value of Re (or K_{Crms} instead of K_C, as defined in Table 1), by replacing the maximum horizontal velocity U_w in periodic waves by its *rms* value in random waves (U_{rms}). The wide

range of available approaches for the determination of the drag coefficient and their different ranges of validity (see Table 1) shows that care must be taken when selecting a given drag coefficient formulation.

Among these different formulations, Hu et al. (2014) proposed an approach for the determination of the drag coefficient valid for waves alone and waves plus current:

$$C_D = 1.04 + \left(\frac{730}{Re}\right)^{1.37} \quad \text{with} \quad Re = \frac{(U_w + U)b_v}{\nu} \tag{3}$$

This formulation is the only one taking into account steady currents in Table 1. For waves alone, Ozeren et al. (2014) derived C_D-formulations for regular and irregular waves, valid for rigid cylinders:

$$C_D = 2.1 + \left(\frac{793}{Re}\right)^{2.39} \quad \text{with} \quad Re = \frac{(U_w + U)b_v}{\nu} \tag{4a}$$

$$C_D = 1.5 + \left(\frac{1230}{Re_{rms}}\right)^{0.95} \quad \text{with} \quad Re_{rms} = \frac{(U_{rms} + U)b_v}{\nu} \tag{4b}$$

and live salt marsh plants (see Table 1 for details on the range of validity):

$$C_D = 55.2\left[K_C\Delta^{-2}\right]^{-0.817} \quad with \quad K_C = \frac{U_w T_p}{b_v} \tag{4c}$$

$$C_D = 58.5\left[K_{Crms}\Delta^{-2}\right]^{-0.641} \quad with \quad K_{Crms} = \frac{U_{rms} T_p}{b_v} \tag{4d}$$

The comparison between the stochastic and deterministic methods developed in the following sections is made possible by the fact that these sets of equations (Eqs. (4a-b) and (4c-d)) are valid for similar conditions in regular and irregular waves. This range of validity also corresponds to the one of Eq. (3), allowing steady currents to be taken into account.

2.3. Links between the drag coefficient and Vogel exponent

The drag coefficient formulations given in Table 1 are functions of the inverse of Re or K_C, and thus C_D decreases as the flow velocity increases. As a consequence, the drag forces are no longer proportional to U_w^2 (Eq. (2)). For large enough Re, this drag reduction is mainly due to the reconfiguration processes (i.e. the plant modify its shape and position) of the plant under higher hydrodynamic loadings (Vogel, 1984; Gaylord et al., 1994; Gosselin and De Langre, 2011). In steady flows, this has been expressed by the Vogel exponent ψ:

$$F \sim U^{2+\psi} \tag{5}$$

with ψ between 0 and −2; the most commonly reported values being between −0.2 and −1.2 (de Langre et al., 2012), and U is the steady flow velocity component (current). The Vogel exponent was originally derived to investigate the drag force response of vegetation in regions of large deformation, i.e. above a certain threshold velocity. Although this approach is mostly adopted in steady flows, it might as well be derived for waves by combining the expression of C_D such as $C_D = a\,K_C^b$ in Eq. (2). Then it can be shown that:

$$F_{max} \sim U_w^{2+b} \tag{6}$$

which is the same as Eq. (5) in case $U = 0$. As a consequence, C_D formulations based on K_C define directly a Vogel exponent for different plants tested in oscillatory flows. For the formulations based on the $(\widehat{\alpha}, \widehat{\beta}, \gamma)$ coefficients (all the formulations based on Re and some based on K_C), the link is more complex as $F \sim \widehat{\alpha}U_w^2 + \widehat{\beta}^{\gamma}U_w^{2-\gamma}$. The deviation from the U^2-proportionality is therefore more difficult to assess and γ cannot be related to the Vogel exponent. However, recent works showed that C_D formulations based on K_C perform better in low-energy wave conditions (Mendez and Losada, 2004; Sánchez-González et al., 2011; Jadhav et al., 2013; Ozeren et al., 2014; Zeller et al., 2014) so that the calibration of a Vogel exponent in steady flow and a C_D based on K_C in oscillatory flows represents a possibility to consider the reconfiguration processes (or drag reduction) of flexible plants under different types of low-energy hydrodynamic loadings leading to large plant deformations (high flexibility). However, further investigations are needed for unifying the drag coefficient formulations for higher energy flows.

The multitude of the different C_D-coefficients is a major problem if the general processes involved in the plant–flow interactions are to be understood and modelled for further engineering purposes. In order to incorporate a physical meaning into these coefficients, Aberle and Järvelä (2013); Whittaker et al. (2013); Västilä and Järvelä (2014) and Whittaker et al. (2015) recently attempted to link the morphological and biomechanical properties of different types of aquatic vegetation to the force–velocity relationship. To the authors' knowledge, this type of parameterisation has not been used in the open literature for oscillatory flow. However such an approach, developed for both oscillatory and steady flows, is needed to both improve our understanding of the links between plant reconfiguration and flow energy dissipation, and allow for a better modelling of plant–flow interactions.

The above review clearly points out that there is currently no universal formulation for C_D available which is valid for different types of conditions (waves alone, current alone, or combined condition) and for different plant-types (live/surrogate, rigid/flexible). As a consequence more complex conditions have to be described with existing and simplified formulations which is associated with a narrower range of applicability. Based on this reasoning, the second part of this paper investigates drag forces on submerged salt marsh-like plants (surrogate/live) in nonlinear random waves based on the Hu et al. (2014) and Ozeren et al. (2014) drag coefficient formulations, allowing a direct comparison of the stochastic and deterministic methods derived, and considering the effect of steady currents on wave induced forces in combined random-waves plus currents.

3. Drag forces for nonlinear random waves plus current

3.1. Mathematical formulation

Based on a similar approach to the one applied by Myrhaug et al. (2009), Myrhaug and Holmedal (2011) and Henry and Myrhaug (2013), this section derives drag forces exerted on a plant for nonlinear random waves plus current. For these conditions, the maximum drag force is parameterized according to Eq. (2) and by replacing U_w with $U_{max} = U_c + U$, where U_c is evaluated using Stokes' second-order wave theory, given by the horizontal orbital velocity under the wave crest. At a fixed point in a sea state with stationary narrow-band random waves consistent with Stokes second-order regular waves in finite water depth, η_c is defined as the nonlinear crest height and a_{rms} the *rms* value of the wave amplitude. Then, the non-dimensional nonlinear crest height, $w_c = \eta_c/a_{rms}$, and the non-dimensional nonlinear maximum horizontal particle velocity under the wave crest, $\hat{u}_c = U_c/U_{rms}$, are (Dean and Dalrymple, 1991)

$$w_c = \hat{a} + O(k_p a_{rms})\hat{a}^2 \tag{7}$$

$$\hat{u}_c = \hat{a}\frac{\cosh k_p(z+h)}{\cosh k_p h} + O(k_p a_{rms})\hat{a}^2 \tag{8}$$

Here $\hat{u}_c$ is evaluated at any elevation z between the mean free surface and the sea bottom, and $\hat{a} = a/a_{rms}$ denotes the non-dimensional linear wave amplitude defined as the ratio of the linear wave amplitude a to the *rms*-value a_{rms}, with h the water depth, and

$$U_{rms} = a_{rms}\frac{\omega_{pr}\cosh k_p h}{\sinh k_p h} \tag{9}$$

Moreover, $O(k_p a_{rms})$ denotes the second-order (nonlinear) terms which are proportional to the characteristic wave steepness of the sea state, $k_p a_{rms}$, where k_p is the wave number corresponding to ω_p (=peak frequency of wave spectrum) given by the dispersion relationship for linear waves with a following current (which is also valid for Stokes second-order waves)

$$(\omega_p - k_p U)^2 = g k_p \tanh k_p h \tag{10}$$

where g is the acceleration due to gravity. Moreover, $\omega_{pr} = (g k_p tanh k_p h)^{1/2}$ is the frequency relative to a reference system moving with the current velocity U. Eq. (7) can be inverted to give $\hat{a} = w_c - O(k_p a_{rms})\hat{a}^2$, which substituted in Eq. (8) gives $\hat{u}_c$ as in Eq. (8) with $\hat{a}$ replaced by w_c (see details in Appendix). Neglecting the higher order terms, the maximum orbital velocity under the wave crest at an elevation z in dimensionless and dimensional forms can thus be expressed as:

$$\hat{u}_c = w_c\frac{\cosh k_p(z+h)}{\cosh k_p h} \tag{11}$$

$$U_c = \eta_c\frac{\omega_{pr}\cosh k_p(z+h)}{\sinh k_p h} \tag{12}$$

The drag force formula for regular waves in Eq. (2) can be rearranged to obtain a formula valid for random waves plus currents. To do so $U_{max} = U_c + U$ is used instead U_w, where $U_c = \hat{u}_c U_{rms}$ with $\hat{u}_c$ from Eq. (11). Normalising U_{max} by U_{rms}, and using the non-dimensional symbol ˆ gives:

$$\hat{U}_{max} = \frac{U_C + U}{U_{rms}} = \hat{u}_C + \frac{U}{U_{rms}} \tag{13}$$

Substituting Eq. (13) in Eq. (2), a dimensional formulation of the maximum drag force F_{max} is obtained for waves plus currents. Consequently, the non-dimensional maximum drag force f_{max} for individual narrow-band nonlinear random waves can be derived as

$$f_{max} \equiv \frac{F_{max}}{\frac{1}{2}\rho C_D b_v N U_{rms}^2} = \left[\hat{u}_C + \frac{U}{U_{rms}}\right]^2 \tag{14}$$

which finally gives:

$$f_{max} = w_c^2\frac{\cosh^2 k_p(z+h)}{\cosh^2 k_p h} + w_c\frac{2U\omega_{pr}\cosh k_p(z+h)}{a_{rms} g k_p \cosh k_p h} + \left(\frac{U\omega_{pr}}{a_{rms} g k_p}\right)^2 \tag{15}$$

The total non-dimensional drag force per unit horizontal area is obtained by integration over the height Δh of the plants, i.e.

$$\bar{f}_{max} \equiv \overline{\left(\frac{F_{max}}{\frac{1}{2}\rho C_D b_v N U_{rms}^2}\right)} = \int_{-h}^{-h+\Delta h} f_{max}\, dz \tag{16}$$

This integration requires the evaluation of the integrals:

$$\int_{-h}^{-h+\Delta h}\cosh^2 k_p(z+h)dz = \frac{1}{2}\left(\frac{1}{2k_p}\sinh 2k_p\Delta h + \Delta h\right) \tag{17}$$

$$\int_{-h}^{-h+\Delta h}\cosh k_p(z+h)dz = \frac{1}{k_p}\sinh k_p\Delta h \tag{18}$$

By combining Eqs. (15)–(18), $\bar{f}_{max}$ can be expressed as

$$\bar{f}_{max} = A w_c^2 + B w_c + C \quad \text{with}$$

$$\begin{cases} A = \dfrac{1}{2\cosh^2 k_p h}\left(\dfrac{1}{2k_p}\sinh 2k_p\Delta h + \Delta h\right) \\ B = \dfrac{2U\omega_{pr}}{a_{rms} g k_p^2}\sinh k_p\Delta h \\ C = \left(\dfrac{U\omega_{pr}}{a_{rms} g k_p}\right)^2\Delta h \end{cases} \tag{19}$$

Having derived a formulation for $\bar{f}_{max}$ based on w_c, the drag coefficient C_D also needs to be expressed as a function of w_c. In Section 2 we showed the benefit of using a C_D-formulation based on K_C for low-energy flows as such a formulation offers the possibility to link K_C to the Vogel exponent. This allows the consideration of both waves and currents. Hu et al. (2014) developed an alternative approach to derive C_D for these conditions by considering the combined velocities in the Reynolds number (Eq. (3)). Even though *Re*-based drag coefficients tend to be better suited for higher energy flows (Bradley and Houser, 2009), the Hu et al. (2014) approach is the only existing formulation allowing for the direct consideration of waves plus currents in the drag coefficient. Thus, in order to gain insight on the effect of wave nonlinearities on the drag force experienced by an aquatic plant for combined random waves plus currents, the Hu et al. (2014) C_D formulation is adopted (Eq. (3)). The Reynolds number in Eq. (3) has to be modified to be valid for nonlinear random waves so that $Re = (U_{c,rms} + U)b_v/\nu = \hat{u}_c Re_{rms} + Re_c$, where $Re_{rms} = U_{rms} b_v/\nu$ and $Re_c = U b_v/\nu$, with $\hat{u}_c = U_c/U_{rms}$ being the non-dimensional nonlinear maximum horizontal particle velocity under the wave crest evaluated at the top of the plants ($z = -h + \Delta h$). Eq. (3) can be rearranged to give the drag coefficient for individual narrow-band nonlinear random waves as

$$C_D = \hat{\alpha} + \left(\frac{\hat{\beta}}{w_c r Re_{rms} + Re_c}\right)^{\gamma} \tag{20}$$

with the parameters defined by Hu et al. (2014) in Eq. (3): $(\hat{\alpha}, \hat{\beta}, \gamma) = (1.04, 730, 1.37)$, and

$$r = \frac{\cosh k_p\Delta h}{\cosh k_p h} \tag{21}$$

Moreover, by taking $Re_{rms} + Re_c$ as a characteristic statistical value of *Re* for random waves plus currents (i.e. considering an equivalent sinusoidal wave), the same threshold values for *Re* can be used to define the range of validity of the C_D-formulation, i.e. $300 < Re_{rms} + Re_c < 4700$. By combining the definition of $\bar{f}_{max}$ in Eq. (19) with Eqs. (20) and (21), it follows that the non-dimensional drag force $\bar{F}$ for individual nonlinear random waves plus currents is given as

$$\widehat{F}\equiv\overline{\left(\frac{F_{max}}{\frac{1}{2}\rho b_v N U_{rms}^2}\right)}=C_D\overline{f}_{max}=\left[Aw_c^2+Bw_c+C\right]\left[\widehat{\alpha}+\frac{\widehat{\beta}}{w_c r R_{rms}+Re_c}\right]^{\gamma} \tag{22}$$

This equation is valid for random waves plus currents and for random waves alone when $U=0$. In order to compare the work of Hu et al. (2014) (leading to Eq. (22)) with the work by Ozeren et al. (2014), Eqs. (4a) and (4b) in Table 1 can be re-arranged as:

$$C_D=\widehat{\alpha}+\left(\frac{\widehat{\beta}}{w_c r R_{rms}}\right)^{\gamma} \tag{23}$$

with the associated $(\widehat{\alpha},\widehat{\beta},\gamma)$ coefficients, leading to the non-dimensional drag force $\widehat{F}$ for individual nonlinear random waves:

$$\widehat{F}\equiv\frac{\overline{F}_{max}}{\frac{1}{2}\rho b_v N U_{rms}^2}=C_D\overline{f}_{max}=Aw_c^2\left[\widehat{\alpha}+\left(\frac{\widehat{\beta}}{w_c r R_{rms}}\right)^{\gamma}\right] \tag{24}$$

Finally, considering the C_D formulations for live salt marsh plants (Eq. (4c) and (4d) last row of Table 1), the drag coefficient can be expressed as

$$C_D=\widehat{\alpha}+\left(\frac{\widehat{\beta}}{w_c r K_{Crms}\Delta^{-2}}\right)^{\gamma} \tag{25}$$

with $K_{Crms}=(U_{rms}\ T_p)/b_v$ as the Keulegan–Carpenter number for irregular waves. Thus, the non-dimensional drag force is given as:

$$\widehat{F}\equiv\overline{\left(\frac{F_{max}}{\frac{1}{2}\rho b_v N U_{rms}^2}\right)}=C_D\overline{f}_{max}=Aw_c^2\left[\widehat{\alpha}+\left(\frac{\widehat{\beta}}{w_c r K_{Crms}\Delta^{-2}}\right)^{\gamma}\right] \tag{26}$$

It should be noted that here $(\widehat{\alpha},\widehat{\beta},\gamma)=(0,\ a,\ -b)$ where a and b are given in Eqs. (4c) and (4d).

The waves are parameterised applying the Forristall (2000) crest height distribution based on second-order theory. This model includes both sum-frequency and difference-frequency effects and has been derived for 2D (long-crested) and 3D (short-crested) random waves using a two-parameter Weibull distribution with the cumulative distribution function (cdf) of the form

$$P(w_c)=1-\exp\left[-\left(\frac{w_c}{\sqrt{8}\alpha}\right)^{\beta}\right]\quad;\quad w_c\geq 0 \tag{27}$$

The Weibull parameters α and β based on the wave steepness S_1 and the Ursell parameter U_R defined by

$$S_1=\frac{2\pi}{g}\frac{H_S}{T_1^2} \tag{28}$$

and

$$U_R=\frac{H_S}{k_1^2 h^3} \tag{29}$$

Here H_S is the significant wave height, T_1 is the spectral mean wave period, and k_1 is the wave number corresponding to T_1. It should be noted that $H_S=2\sqrt{2}\ a_{rms}$ when the wave amplitude is Rayleigh distributed. For a narrow-band process T_1 and k_1 can be replaced by T_p and k_p, respectively, in Eqs. (28) and (29). Moreover, for random waves plus currents $T_p=2\pi/\omega_{pr}$. The wave steepness and the Ursell number characterize the degree of nonlinearity of the waves in finite water depth. At zero steepness and zero Ursell number (linear waves) Forristall (2000) forced the fits to match the Rayleigh distribution, i.e. $\alpha=1/\sqrt{8}\approx 0.3536$ and $\beta=2$. Note that this is the case for both 2D and 3D linear waves. The resulting parameters for the 2D-model (long-crested waves) are

$$\begin{aligned}\alpha_{2D}&=0.3536+0.2892\,S_1+0.1060\,U_R\\ \beta_{2D}&=2-2.1597\,S_1+0.0968\,U_R^2\end{aligned} \tag{30}$$

and for the 3D-model (short-crested waves)

$$\begin{aligned}\alpha_{3D}&=0.3536+0.2568\,S_1+0.0800\,U_R\\ \beta_{3D}&=2-1.7912\,S_1+0.5302\,U_R+0.284\,U_R^2\end{aligned} \tag{31}$$

Forristall (2000) demonstrated that wave setdown effects are smaller for short-crested than for long-crested waves, which is due to the second-order negative difference-frequency terms being smaller for 3D waves than for 2D waves. Consequently the wave crest heights are larger for 3D waves than for 2D waves.

For a better description of the stochastic process, the expected value of the (1/n)th largest values of the non-dimensional force $\widehat{F}$ caused by the (1/n)th highest wave crests in a sea state is a quantity of interest, and is given by

$$\widehat{F}_{1/n}\equiv E\left[\widehat{F}(w_c)\middle|w_c>w_{c\frac{1}{n}}\right]=n\int_{w_{c\frac{1}{n}}}^{\infty}\widehat{F}(w_c)p(w_c)dw_c \tag{32}$$

where $w_{c\frac{1}{n}}=\sqrt{8}\alpha(\ln n)^{1/\beta}$ and $p(w_c)$ is the probability density function (pdf) derived from Eq. (26) as $p(w_c)=dP(w_c)/dw_c$. This expected value is obtained by numerical integration. Similarly, the root-mean-square (rms) value of $\widehat{F}$ is given as

$$\widehat{F}_{rms}\equiv\left(E\left[\widehat{F}^2\right]\right)^{1/2}=\left(\int_0^{\infty}\widehat{F}^2(w_c)p(w_c)dw_c\right)^{1/2} \tag{33}$$

In the following sections, the subscripts *linear*, *2D* and *3D* are added to $\widehat{F}_{rms}$ and $\widehat{F}_{1/n}$ to refer to the non-dimensional forces under linear, long-crested (2D) or short-crested waves (3D), respectively.

3.2. Rationale

A practical way to characterise wave forces on an aquatic plant under random waves is to use a bulk C_D coefficient formulation directly calibrated against Re_{rms} or K_{Crms} and use the *rms* wave velocity of the corresponding sea state conditions. This approach, hereafter named deterministic method, is widely used to characterise wave attenuation and wave forces on plants (Mendez and Losada, 2004; Bradley and Houser, 2009; Paul and Amos, 2011; Sánchez-González et al., 2011; Möller et al., 2014). In this study, this deterministic method is used to calculate the non-dimensional force $\widehat{F}_{rms}$ per unit area on a plant, introducing the velocity of the equivalent rms monochromatic wave U_{rms} in Eq. (2) and C_D expressed as in Eq. (23) with $w_c=1$ (i.e. corresponding to linear waves) and the coefficients from Eq. (4b) (see Fig. 1). This bulk coefficient, which has been calibrated by Ozeren et al. (2014) against experimental data, characterises the plant's reconfiguration under the tested conditions. Thus calculating $\widehat{F}_{rms}$ with this deterministic method gives an averaged representation of the experiments conducted by Ozeren et al. (2014) in irregular waves. However, this approach is based only on a single statistical quantity describing the wave activity, typically the rms values of the wave height or wave induced velocities, and therefore any potential changes in the plant's behaviour due to the interaction with a stochastic process (irregular waves) are not taken into account (see

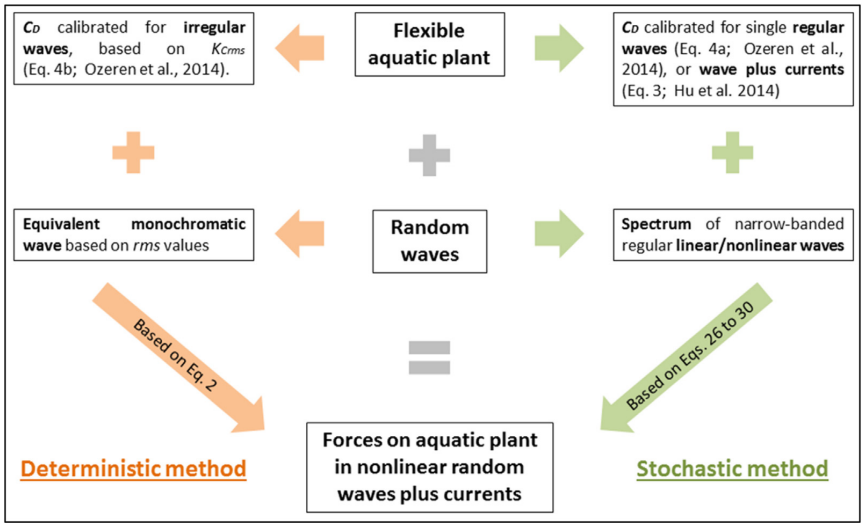

Fig. 1. Description of the deterministic and stochastic approaches to compute forces on aquatic plants in nonlinear random waves plus current.

Section 2). The previous section detailed the implementation of a stochastic method to compute different statistical values of $\widehat{F}_{linear}$, $\widehat{F}_{2D}$ and $\widehat{F}_{3D}$ using C_D as expressed by Eq. (4a) (Ozeren et al., 2014) and Eq. (3) (Hu et al., 2014), together with the wave spectrum parameterised in Eqs. (27) to (31) (Forristall, 2000) (see Fig. 1). Thus, this method allows for the characterisation of the wave action on the plant under each single wave height composing the irregular wave spectrum.

The stochastic approach based on Forristall (2000) wave crest height distribution can be used to address effects of wave non-linearities on the expected wave-induced forces for 2D and 3D crested irregular waves plus currents (with the corresponding coefficients from Eqs. (30) and (31), respectively). Using the appropriate (α, β) coefficients for linear, 2D and 3D waves, nonlinear results can be compared with the corresponding linear results for both 2D and 3D waves. For waves alone, the nonlinear to linear ratios for 2D and 3D waves are calculated based on Eq. (32):

$$R_{2D/linear} = \widehat{F}_{1/n,2D} \Big/ \widehat{F}_{1/n,linear} \tag{34}$$

$$R_{3D/linear} = \widehat{F}_{1/n,3D} \Big/ \widehat{F}_{1/n,linear} \tag{35}$$

Additionally, the ratio between the total non-dimensional wave forces on the models per unit volume for 3D and 2D nonlinear waves is given as:

$$R_{3D/2D} = \widehat{F}_{1/n,3D} \Big/ \widehat{F}_{1/n,2D} \tag{36}$$

The effects of currents in combined irregular waves plus current conditions are described using the Hu et al. (2014) drag coefficient formulation, as C_D is a function of $U_{rms} + U$ (derived from Eq. (3)). By taking Eq. (3) to be valid for regular waves, the non-dimensional drag force $\widehat{F}$ for individual nonlinear random waves in waves plus current conditions is deduced by implementing Eq. (22). The *rms* value and the expected value due to the 1/nth highest wave crest are given by Eqs. (33) and (32), respectively. Expected wave-induced forces are subsequently computed and examined against a current to wave velocity parameter defined as:

$$U_{cwrms} = U/(U + U_{rms}) \tag{37}$$

4. Results and discussion

Unless otherwise stated, the results presented in this section are computed for a water depth $h = 1$ m, a submergence ratio $\Delta = h_v/h = 0.8$, a plants width $b_v = 1$ cm, and a peak wave period $T_p = 2$ s. This set of input-parameters is an example of the conditions tested by Ozeren et al. (2014) and Hu et al. (2014), representing a common field condition over salt marshes (Jadhav et al., 2013). In addition, since K_{Crms} is directly related to Re_{rms} by the relation $K_{Crms} = Re_{rms}[\nu T_p/b_v^2]$, dimensional and non-dimensional forces are only plotted versus K_{Crms}. First, salt marsh mimics (rigid cylinders) are considered for waves alone (linear/nonlinear) and waves plus current conditions, and then an example for live salt marsh plants (*J. roemerianus*) is given and discussed to illustrate the use of the stochastic method.

4.1. Waves alone

4.1.1. Deterministic and stochastic methods

The results from the deterministic method applied to rigid cylinders are represented in Figs. 2 and 3 by the full lines. The grey shaded area represents a confidence interval based on the *rms* error defined during the fitting process (*rms* error of 0.99 for the calibration of Eq. (4b), see Ozeren et al. (2014)). In addition, Figs. 2 and 3 present the expected values (broken lines) of the total wave forces on the plants per unit area versus K_{Crms} depending on the C_D-formulation considered in the stochastic method. In these two figures, the left column (subfigures a, c and e) shows the non-dimensional forces, while the right column (subfigures b, d and f) shows the dimensional forces. Additionally, each row corresponds to the values under a given wave crest height. Rows 1, 2 and 3 correspond to $\widehat{F}_{rms}$, $\widehat{F}_{1/3}$ and $\widehat{F}_{1/10}$, respectively. $\widehat{F}_{1/3}$ and $\widehat{F}_{1/10}$ are computed using Eq. (32) for n = 3 and n = 10, respectively, while $\widehat{F}_{rms}$ is computed using Eq. (33). Fig. 2 shows the comparison between the deterministic method as derived in Section 3, and the

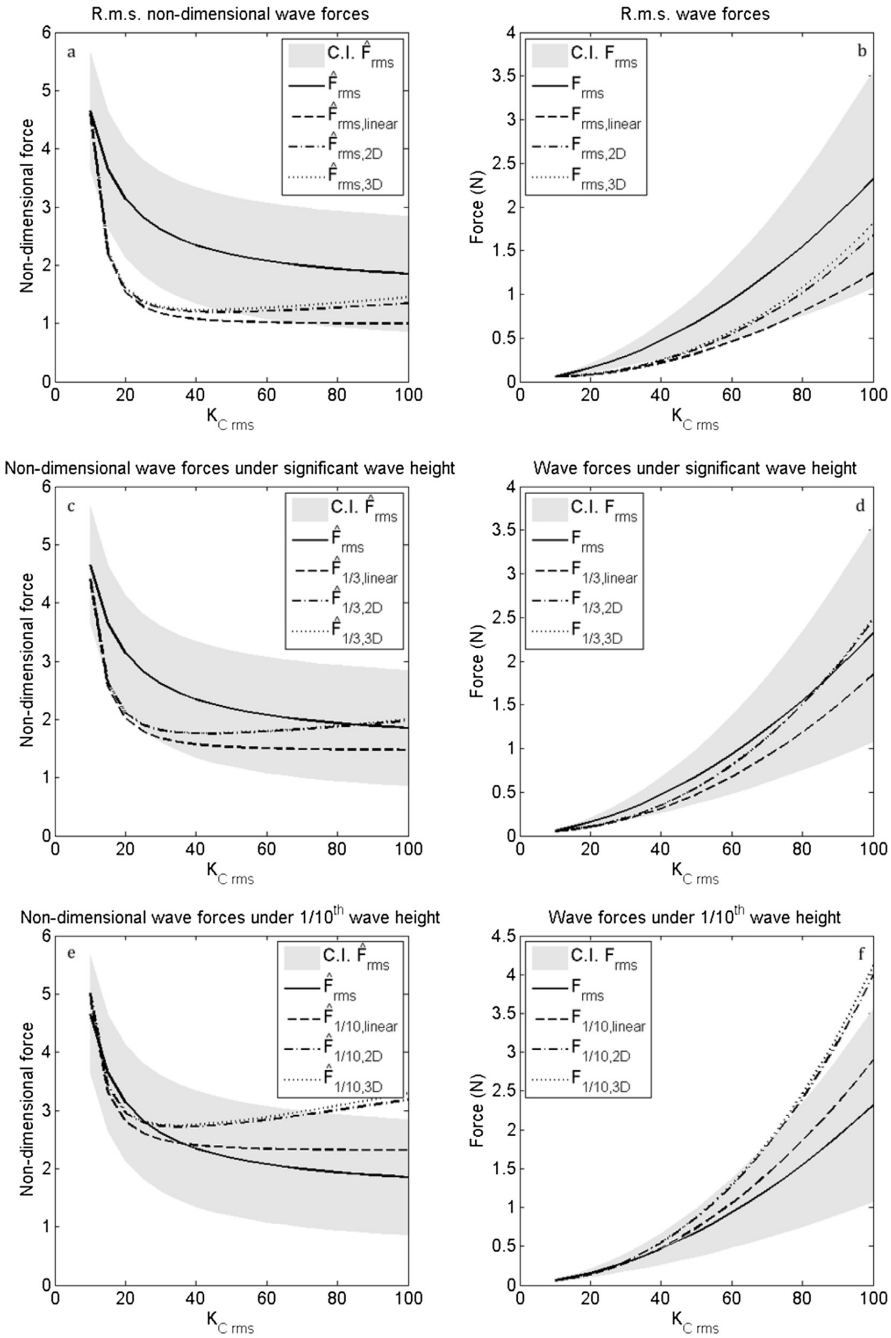

Fig. 2. Comparison of the deterministic method for linear waves (full line) and the stochastic approach to computed wave forces on a rigid cylinder using C_D for irregular and regular waves, respectively, from Ozeren et al. (2014). For the stochastic approach, linear waves are represented by the dashed line, long-crested waves (2D) are represented by the dash-dotted line, while the short-crested waves (3D) are represented by the dotted line. The rms force calculated with the deterministic method is represented in every sub-plot for comparison and the grey shaded area represents a confidence interval based on the rms error (Ozeren et al., 2014).

stochastic approach used to compute the expected wave forces using the C_D-formulation from Ozeren et al. (2014), derived for regular waves (Eq. (4a)). Fig. 3 shows a similar comparison, but the stochastic approach is using the C_D-formulation for regular waves plus current applied to waves-alone from Hu et al. (2014) (Eq. (3)). Thus, between Figs. 2 and 3, only the C_D-formulation used in the

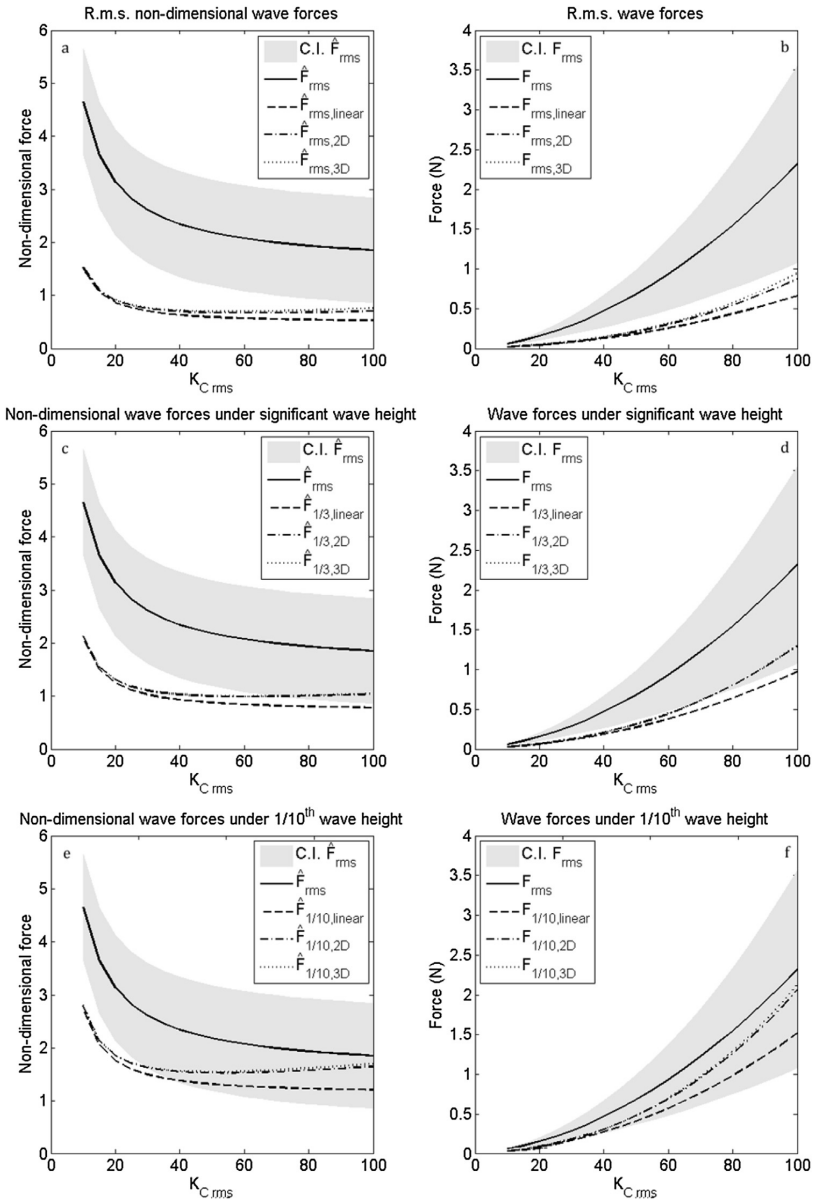

Fig. 3. Comparison of the deterministic method for linear waves using C_D for irregular waves from Ozeren et al. (2014) (full lines) and the stochastic approach to the computed wave forces on a rigid cylinder using C_D for regular waves plus current applied to waves-alone from Hu et al. (2014) (broken lines). For this stochastic approach, linear waves are represented by the dashed line; long-crested waves (2D) are represented by the dash-dotted line, while the short-crested waves (3D) are represented by the dotted line. The rms force calculated with the deterministic method is represented in every sub-plot for comparison and the grey shaded area represents a confidence interval based on the rms error (Ozeren et al., 2014).

stochastic methods (broken lines) is different, while the deterministic method results (full lines) are the same.

Figs. 2 and 3 show that $\widehat{F}_{rms,linear}$, $\widehat{F}_{rms,2D}$ and $\widehat{F}_{rms,3D}$ are lower compared to $\widehat{F}_{rms}$. A-priori, this result is contradictory to the findings of Henry and Myrhaug (2013), who first compared the stochastic and deterministic methods using the drag coefficient formulations of Mendez and Losada (2004), showing a good agreement between the methods, and then the Méndez et al. (1999) formulation for swaying plants, leading to a clear underestimation of the stochastic results by the deterministic method. This suggests that the agreement between the stochastic and deterministic methods depends on the input flow conditions as well as on the C_D-formulation used.

However the choice of different drag coefficients implemented

in the two approaches does not affect the results, as it can be shown that the use of the same C_D-formulation leads to similar deviations between the stochastic and deterministic approach.

$\widehat{F}_{rms,linear}$, $\widehat{F}_{1/3,linear}$, and $\widehat{F}_{1/10,linear}$ (in the rows 1,2 and 3, respectively, of Figs. 2 and 3) have been computed with the stochastic method in order to compare it with the deterministic method. It appears that $\widehat{F}_{rms}$ and F_{rms} (deterministic method, linear waves) agree better with the stochastic method using C_D from Eq. (4a) (Ozeren et al., 2014), i.e. $\widehat{F}_{1/3,linear}$ and $F_{1/3,linear}$ in Fig. 3c and d. Using C_D from Eq. (3) for waves alone (Hu et al., 2014), $\widehat{F}_{rms}$ and F_{rms} are better represented by $\widehat{F}_{1/10,linear}$ and $F_{1/10,linear}$ (Fig. 3e and f). This confirms that the choice of the C_D-formulation has an impact on the results, and is crucial when calculating wave induced forces.

4.1.2. Nonlinear effects

The non-dimensional forces (Figs. 2a, c, e and 3a, c, e) decrease rapidly as the wave activity increases for small K_{Crms}. For larger values of K_{Crms} the forces level off for linear waves while they increase for 2D and 3D nonlinear waves for higher wave activity. This trend is clearest in Fig. 2a, c and e using C_D from Ozeren et al. (2014) and is observed for approximately $K_{Crms} > (40, 35, 30)$ under the rms, 1/3rd (significant) and 1/10th wave crest height, respectively. According to Fig. 3a, c and e this increase starts around $K_{Crms} = (65, 60, 45)$ for the *rms*, 1/3rd and 1/10th wave crest height, respectively, using C_D from Hu et al. (2014). Considering the dimensional forces on a plant (right column), all estimated forces increase as K_{Crms} increases. From Figs. 2 and 3 it appears that nonlinear waves induce larger drag forces than linear waves, which is a direct effect of wave second-order non-linearities on the wave-induced forces. The deviation from the linear wave case increases as the wave activity increases, and the forces under nonlinear waves can be up to 1.3 times that for linear waves for higher wave activity ($K_{Crms} > 500$, Figs. 2 and 3). This is caused by the larger maximum velocity under the wave crest for second-order stokes waves compared to linear waves. Moreover, Figs. 2 and 3 show that 3D nonlinear waves give slightly larger forces than 2D nonlinear waves. This is caused by the smaller wave setdown effect for 3D waves than for 2D waves in finite water depth, which is due to the smaller second-order negative difference frequency effects for 3D waves (as discussed in Section 3.2). However, the effects of this difference on the wave-induced forces on the plant are small and only visible for higher values.

Fig. 4, shows the isocurves of the ratios $R_{2D/linear}$, $R_{3D/linear}$ and $R_{3D/2D}$ defined by Eqs. (34)–(36) versus the Ursell number U_R (Eq. (29)) and the wave steepness S_1 (Eq. (28)) for the same input parameters as for the results presented in Figs. 2 and 3. Based on the discussion of Figs. 2 and 3, the ratios are shown for the best agreement with the results from the deterministic method, i.e. for the 1/3rd value using the Ozeren et al. (2014) C_D-formulation (left column); for the 1/10th crest height using the Hu et al. (2014) C_D-formulation (right column). The corresponding wave conditions described by T_p, Re_{rms} and K_{Crms} are shown in the mid column. Overall, the results in the left and right columns of Fig. 4 show the same qualitative behaviour for both 2D (Fig. 4a,c) and 3D (Fig. 4d,f) waves: for a given value of U_R (i.e. for a given water depth), the nonlinear to linear ratio increases as S_1 increases; for a given value of S_1, the ratio increases as U_R increases (i.e. as the water depth decreases). As nonlinear effects on the wave-induced velocities increase with an increase in S_1 or U_R, these features appear to be physically sound. Moreover, the nonlinear to linear ratio ranges up to about 2.2 (Fig. 4a) and 2.4 (Fig. 4c) for 2D waves, and up to about 2.4 (Fig. 4d) and 2.6 (Fig. 4f) for 3D waves, indicating that the nonlinear to linear ratio is only slightly larger for 3D waves than for 2D waves, except for smaller values of S_1. This is confirmed by Fig. 4g and i, where the isocurves for the 3D results to the 2D results ratios are plotted against S_1 and U_R.

Except for the smaller values of S_1 (i.e., for S_1 smaller than 0.4 (Fig. 4i) to 0.6 (Fig. 4g)), it appears that the force is always larger beneath 3D waves than beneath 2D waves, which is due to the smaller wave setdown effect for 3D waves than for 2D waves. However, the differences in the results for 2D and 3D waves are small, i.e. in the ranges 0.96–1.06 (Fig. 4g) and 0.94–1.14 (Fig. 4i). The higher value in Fig. 4i compared with those in Fig. 4g are due to the larger nonlinear effects beneath 3D waves among the 1/10th highest waves rather than the 1/3rd highest waves compared to 2D waves. This highlights again the importance of the choice of an appropriate characteristic wave and a drag coefficient formulation in order to obtain a good description of the expected force per unit area.

It should be noted that the wave conditions tested by Hu et al. (2014) and Ozeren et al. (2014) are within the ranges of U_R and S_1 shown in Fig. 4. In the Hu et al. (2014) experiments, U_R and S_1 were in the ranges (0.02; 1.12) and (0.02; 0.04), respectively; while for Ozeren et al. (2014), U_R and S_1 were in the ranges (0.001; 0.82) and (0.005; 0.20), respectively, suggesting that these studies contained nonlinear waves. These conditions correspond to the parameter ranges $1.5s < T_p < 3\ s$; $0 < Re_{rms} < 8000$ and $0 < K_{Crms} < 250$.

4.2. Waves plus current

Hu et al. (2014) derived a C_D-formulation (Eq. (3), Table 1) valid for both waves alone and waves plus currents. Since this formulation is based on regular sinusoidal waves, the mean velocity U should correspond exactly to the current speed. However, for waves alone, Hu et al. (2014) observed a non-zero mean velocity in the opposite direction of the wave propagation suggesting a weak recirculation current due to the wave propagation in a flume (Hudspeth and Sulisz, 1991). Hu et al. (2014) calibrated their drag coefficient including this recirculation. In this study, the mean velocity U is considered to be the same as the current speed, so that waves alone correspond to $U = 0$.

By using the same input conditions as in Section 4.1, Fig. 5 shows the computed values of $\widehat{F}_{1/10}$ for linear (Fig. 5a), 2D (Fig. 5b) and 3D (Fig. 5c) nonlinear waves plus current, as well as the corresponding nonlinear to linear ratios for 2D (Fig. 5d) and 3D (Fig. 5e) waves, and the 3D to 2D ratio (Fig. 5f) defined by the Eqs. (34)–(36). These results are plotted against $U_{cwrms} = U/(U + U_{rms})$, corresponding to the validity range of the Hu et al. (2014) formula from 0 (waves alone) to 0.7 (for currents alone $U_{cwrms} = 1$).

U_R ranges from 0.01 to 0.71 and S_1 from 0.003 to 0.078. Fig. 5 shows that for a given Re_{rms} (i.e. for a given wave activity), the non-dimensional force ($\widehat{F}_{1/10}$) increases as U_{cwrms} increases (i.e. as the current increases) for linear waves (Fig. 5a), 2D (Fig. 5b) and 3D (Fig. 5c) nonlinear waves. For waves alone ($U_{cwrms} = 0$) the results in Fig. 5a, b and c correspond to the results in Fig. 3e, showing that $\widehat{F}_{1/10}$ decreases as Re_{rms} increases for small wave activity for linear waves, 2D and 3D nonlinear waves; then $\widehat{F}_{1/10}$ levels off for linear waves (Fig. 5a) and increases slightly for 2D (Fig. 5b) and 3D (Fig. 5c) nonlinear waves as Re_{rms} increases for larger wave activity. Overall, this is also the case as Re_{rms} increases for a given value of U_{cwrms} (Fig. 5a,b,c).

The effects of wave nonlinearity on $\widehat{F}_{1/10}$ are also explored in Fig. 5d–f: for a given value of U_{cwrms} (i.e. for a given relative magnitude between current and waves), the nonlinear to linear ratio increases as Re_{rms} increases (i.e. as the wave activity increases) for both 2D (Fig. 5d) and 3D (Fig. 5e) nonlinear waves. These results confirm that the effect of wave non-linearities on drag forces increases as the wave activity increases. As discussed in section 4.1.2, these ratios ranges up to 1.4 for higher wave activity in wave dominated conditions (U_{cwrms} close to 0). However, in Fig. 5d–f, for a given value of Re_{rms}, the nonlinear to linear ratio decreases as U_{cwrms} increases (i.e. as the current increases), indicating that the

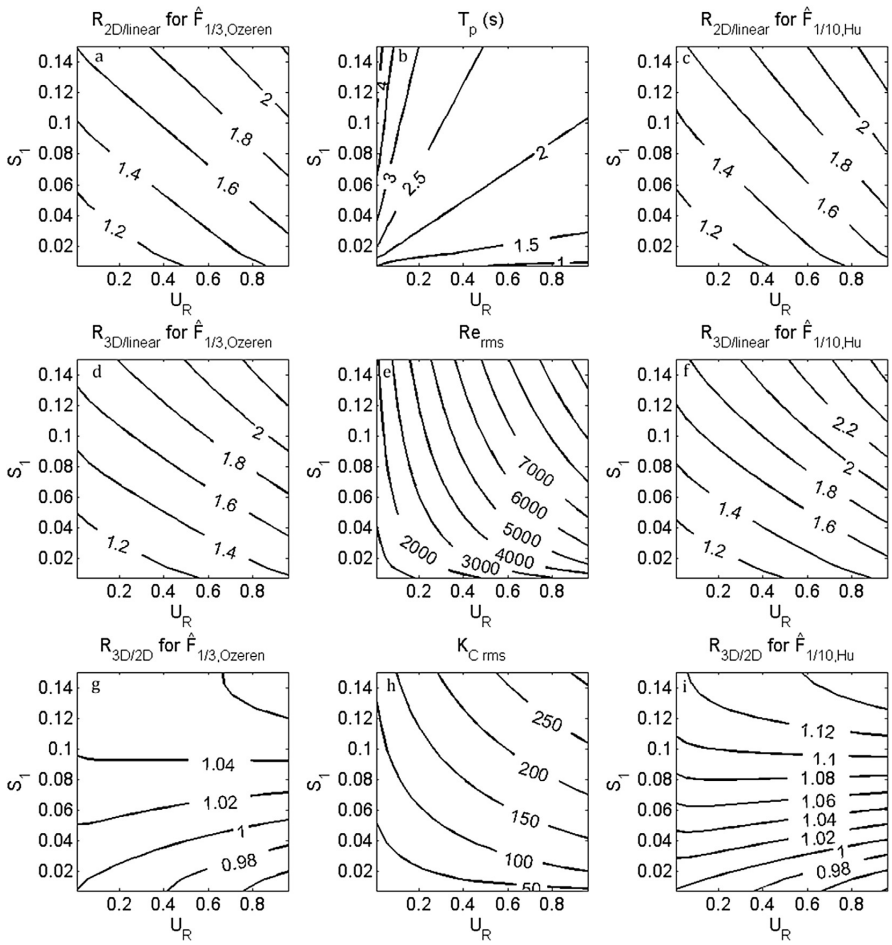

Fig. 4. Influence of the wave steepness and Ursell number on the nonlinear to linear ratio results for the expected 1/3rd (left column) and 1/10th (right column) wave heights on a rigid cylinder using C_D for regular waves from Ozeren et al. (2014) on the left column and from Hu et al. (2014) on the right column. The middle column details the wave conditions the parameter range corresponds to.

effect of wave nonlinearities on the forces decreases as the current increases. In current dominated conditions (U_{cwrms} closer to 1), the magnitude of wave-induced velocities is small compared to the current, and thus small nonlinear deviations from the linear wave-induced velocity will be attenuated in wave plus current conditions compared to that for waves alone. Furthermore, the nonlinear ratios are only slightly larger for 3D waves than for 2D waves, consistent with the slightly smaller wave setdown effects for 3D waves than for 2D waves. These features are demonstrated in Fig. 5f, showing that the 3D to 2D ratios range up to about 1.04 for high wave activity in wave dominated conditions ($Re_{rms} > 4000$, U_{cwrms} close to 0). However, as the current attenuates the nonlinear effects, these small differences between 3D and 2D nonlinearities become even smaller for current-dominated conditions ($R_{3D/2D} \rightarrow 1$ as $U_{cwrms} \rightarrow 1$).

4.3. Example of application

Although valid for cylinders, which is a simple representation of a salt marsh, the results presented above describe the effects of wave nonlinearities on the expected forces on plants for waves alone and waves plus current conditions. In their study on wave attenuation through model and live vegetation, Ozeren et al. (2014) also derived drag coefficients for a live salt marsh plant species (*J. roemerianus*) for different plant submergence (Eqs. (4c) and (4d)). Thus, the same approach as in Section 4.1 can be applied to the case of live plants using C_D as expressed in these two equations. Since Ozeren et al. (2014) derived C_D based on the wave energy decay, no observed experimental data of measured force on stems exist to validate these theoretical results. As in the previous sections, only the stochastic and the deterministic method are compared using the two empirically determined drag formulations derived from wave attenuation measured by Ozeren et al. (2014) for a specific case (2857 stems/m^2 for *J. roemerianus*). The results presented in Fig. 6 have been obtained for the same conditions as in Section 4.1, i.e. for a water depth $h = 1$ m, a submergence ratio $\Delta = h_v/h = 0.8$, a spectral peak period $T_p = 2$ s, but for a smaller stem diameter compared to the rigid cylinders, i.e. $b_v = 1.5$ mm. This stem diameter is typical for the plant characterized by Ozeren et al. (2014). Considering that the vegetation parameterisation using the

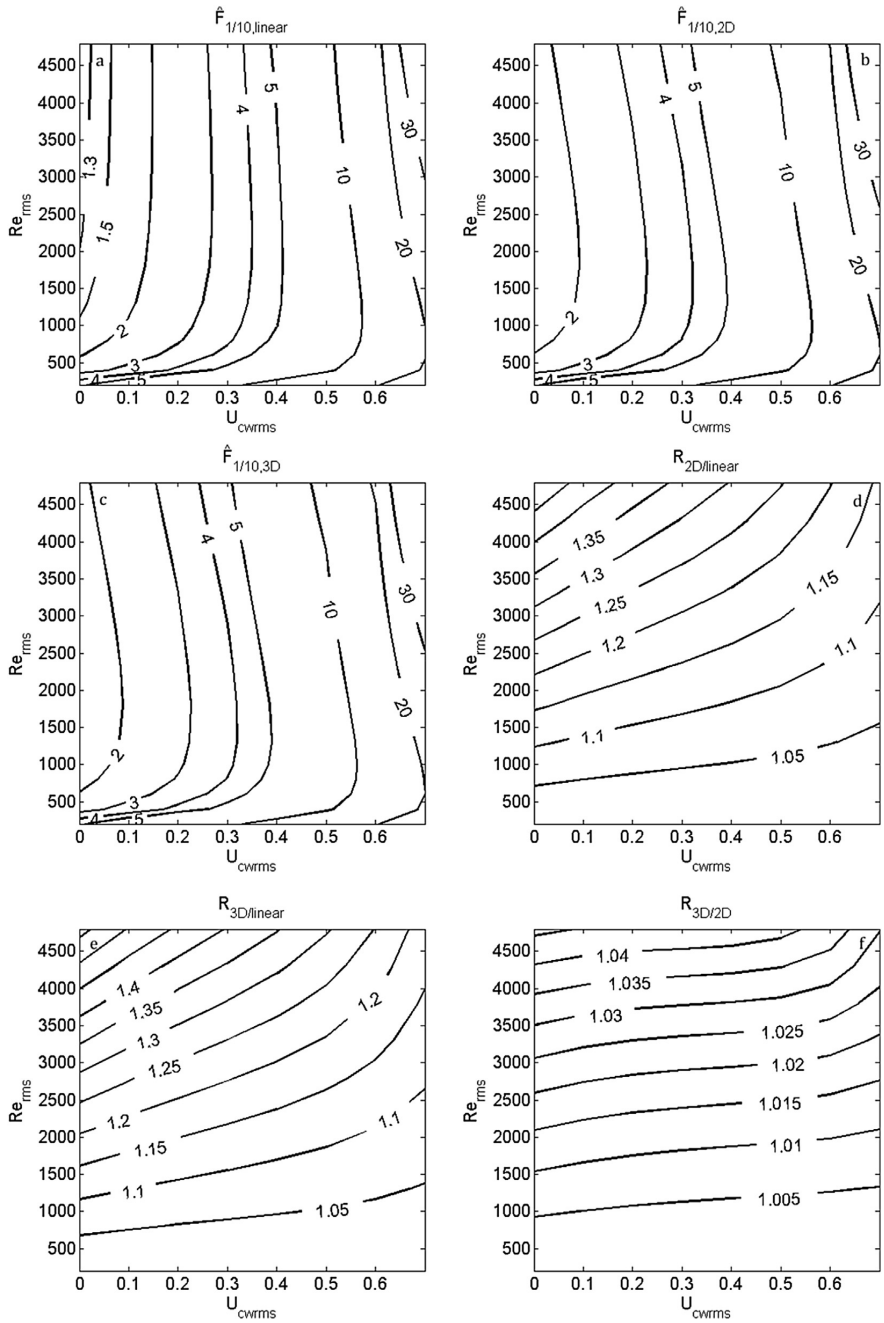

Fig. 5. Effect of wave nonlinearities on the expected wave forces under the 1/10th wave crest using the stochastic approach and the C_D for regular waves plus current from Hu et al. (2014).

different C_D coefficients is physically meaningful and that the flexibility of salt marsh vegetation is comparable to that of the vegetation used in Ozeren et al. (2014), the results in Fig. 6 are estimates of the expected forces on salt marsh plants in nonlinear random waves. Fig. 6 is organised as Figs. 2 and 3 (see detailed description in section 4.1) except that rows 1, 2 and 3 correspond to $\hat{F}_{rms}$, $\hat{F}_{1/10}$ and $\hat{F}_{1/100}$, respectively. U_R ranges from 0.02 to 0.23 and S_1 from 0.004 to 0.054.

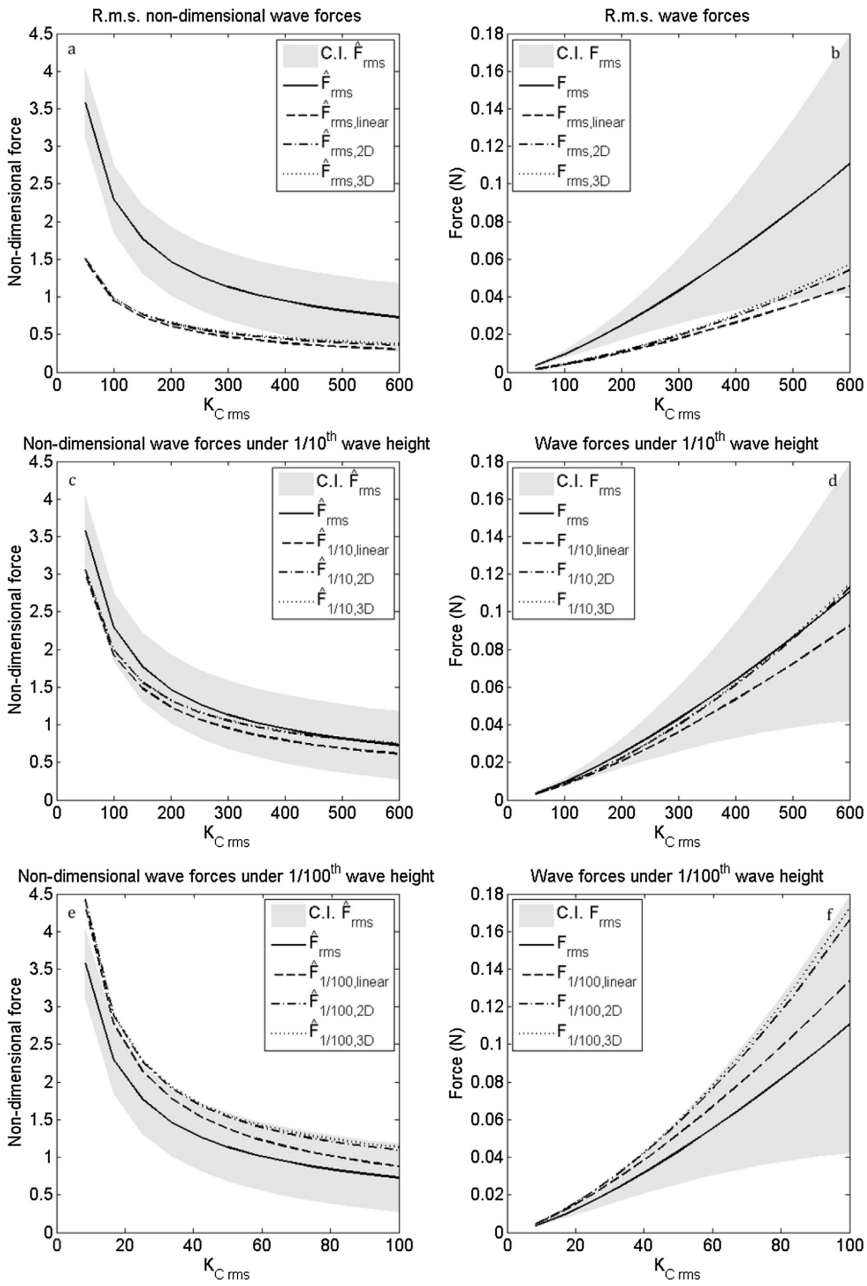

Fig. 6. Comparison of the deterministic method for linear waves (full line) and the stochastic approach to the computed wave forces (broken lines) on emergent *J. roemerianus* using C_D for irregular and regular waves, respectively, from Ozeren et al. (2014). For the stochastic approach, linear waves are represented by the dashed line; long-crested waves (2D) are represented by the dash-dotted line, while the short-crested waves (3D) are represented by the dotted line. The rms force calculated with the deterministic method is represented in every sub-plot for comparison and the grey shaded area represents a confidence interval based on the rms error (Ozeren et al., 2014).

Overall, Fig. 6 shows the same features as in Figs. 2 and 3 for the different forces (see the discussion of Figs. 2 and 3 in Section 4.1 for further details). The *rms* error originating from the drag coefficient calibration for irregular waves is smaller for the live plant (0.45) compared to the cylinders (0.99), but the *rms* error increases as the wave activity increases (i.e. as K_{Crms} increases), corresponding to the increased shaded area in the right column of Fig. 6. It can be seen that Re_{rms} remains low despite of large wave activity (i.e. Re_{rms} in

Fig. 6e, f is about 1/10th of Re_{rms} in Fig. 2e, f and 3e, 3f) which is associated with the small plant diameter. Moreover, Fig. 6 shows that $F_{1/10,linear}$ is about 3 times larger compared with $F_{rms,linear}$, while $F_{1/100,linear}$ is only about 1.5 times larger compared with $F_{1/10,linear}$. This smaller increase of the forces for higher wave characteristics is a direct consequence of the drag coefficient reduction for larger wave velocities, and depends on the coefficient formulation.

4.4. General comments

As there are no experimental data, to the authors' knowledge, available for irregular waves allowing for a validation of both methods, it is not possible to conclude if the deterministic or stochastic approach performs better. Thus further experimental investigations are needed. The use of a stochastic method appears, however, justified to describe forces under random waves, allowing for the consideration of different types of wave distributions. In addition, the stochastic aspect of plant–flow interactions can be better captured as the expected forces under different characteristic wave heights can be computed. This is an improvement compared to the averaged representation of the wave height condition by a single value (here the *rms* wave height) used in the common deterministic approach. In addition, it should be noted that the effects of wave nonlinearity due to 2D and 3D Stokes second-order waves are not possible to estimate by using the deterministic method since nonlinearities are not included in the regular wave formulae. Hence this stochastic approach is more mathematically sound than using H_{rms} and T_p in an otherwise deterministic method. Moreover, it also provides results which arise from 2D and 3D Stokes second-order wave nonlinearities inherent in the Forristall (2000) parametric wave crest distribution, and comparison with more data is required to confirm these results. In the meantime the approach should be of practical interest for estimating random wave-induced forces on a plant based on available wave statistics in waves plus current.

As for a classic deterministic method, the relevance of this stochastic method is bounded to the correct parameterisation of the vegetation and its reconfiguration in the drag coefficient C_D used. As highlighted in Section 2, the physical processes linking wave-induced drag forces and wave attenuation remains fundamentally unexplained and the different drag coefficient derived cannot be generalised to different type of aquatic vegetation because of their calibration against specific experiments. Aquatic vegetation is often characterised by complex geometries, varying mechanical properties and spatial distributions. Incorporating this type of complexity in the formulation of the drag force as exerted on the plants poses a challenge that has to be met before the physics of the interaction between vegetation and wave-induced as well as current forces is to be fully understood and mathematically captured over spatial scales of several metres distance. Thus, a unified C_D formulation based on the description of the physical processes is to be developed before any approach can be meaningfully compared to flume/field experiments.

5. Summary

By reviewing the different plant drag coefficients proposed for oscillatory flows, this study first pointed out the lack of normalisation of the different C_D formulations. Due to of their calibration against experimental datasets, there is a multitude of coefficients which are in theory strictly valid for the flow conditions tested, and the plant species or surrogate used. The generalisation of these coefficients to the characterisation of plant–flow interactions in waves and currents is thus not straight forward, although a direct link can be established between a C_D based on a K_C number (low-energy wave conditions) and a Vogel exponent (current). An alternative approach to link waves and currents in the C_D formulation is to consider the sum of the wave-induced and current bulk velocities in the Reynolds number. To this date, this approach has only be adopted by Hu et al. (2014). Overall, a meaningful parameterisation of the plant–flow interactions seem to depend on an expression of C_D based upon some key biomechanical and morphological properties, which are still to be formulated.

Based on existing C_D formulations (Hu et al., 2014; Ozeren et al., 2014), this study further develops a stochastic method to compute the wave-induced forces on a plant in various random waves plus current conditions. By taking into account the Forristall (2000) wave crest height distribution, this method allowed the calculation of characteristic statistical values of the forces for a range of flow conditions, which is an improvement compared to the commonly used procedure of substituting the wave-related quantities with their characteristic statistical values, such as the *rms* values, in an otherwise deterministic approach. The comparison between these two approaches revealed differences between the estimated values, depending on the flow conditions. However, experimental data for comparison are required before any conclusion can be made regarding the validity of the approach. This study includes 2D and 3D nonlinear wave effects on the forces, demonstrating an increase of 20–40% compared to linear waves for the conditions exemplified. However, 3D waves give only slightly larger forces than 2D waves. For combined waves plus current conditions, using the Hu et al. (2014)'s C_D formulation, the forces increase as the current increases, while the effect of wave nonlinearity on the wave-induced forces on the plant deceases.

Appendix

In Section 3.1, Eq. (7) can be expanded as:

$$w_c = \hat{a} + O(k_p a_{rms})\hat{a}^2 + h.o.t. \tag{A1}$$

where *h.o.t.* stands for higher order terms, $\hat{a}$ being a first order term while w_c, $O(k_p a_{rms})$ are second order terms. Eq. (A1) can be inverted and $\hat{a}$ expressed in terms of w_c, so that:

$$\hat{a} = w_c - O(k_p a_{rms})\left(w_c - O(k_p a_{rms})\hat{a}^2\right)^2 \tag{A2}$$

which is developed as:

$$\hat{a} = w_c - O(k_p a_{rms})w_c + h.o.t. \tag{A3}$$

Similarly, Eq. (8) can be written as:

$$\hat{u}_c = \hat{a}\frac{\cosh k_p(z+h)}{\cosh k_p h} + O(k_p a_{rms})\hat{a}^2 + h.o.t. \tag{A4}$$

In this expression of $\hat{u}_c$, the first term is a first order term while the second one is of second order. By introducing Eq. (A3) in Eq. (A4) and neglecting the *h.o.t.*, $\hat{u}_c$ is expressed as:

$$\hat{u}_c = w_c\frac{\cosh k_p(z+h)}{\cosh k_p h} + O(k_p a_{rms})w_c\left[w_c - \frac{\cosh k_p(z+h)}{\cosh k_p h}\right] - 2O(k_p a_{rms})^2 w_c^2 + O(k_p a_{rms})^3 w_c^2 \tag{A5}$$

In this second expression of $\hat{u}_c$, the first term is now of second order while the following ones are of higher orders. Since this study is focussing on second order effect, included in the first term, Eq. (A5) can be simplified as:

$$\widehat{u}_c = w_c \frac{\cosh k_p(z+h)}{\cosh k_p h} + h.o.t. \quad \text{(A6)}$$

which corresponds to Eq. (11) by neglecting the higher order terms.

References

Aberle, J., Järvelä, J., 2013. Flow resistance of emergent rigid and flexible floodplain vegetation. J. Hydraulic Res. 51, 33–45.

Aberle, J., Järvelä, J., 2015. Hydrodynamics of vegetated channels. In: Rowinski, P., Radecki-Pawlik, A. (Eds.), Rivers – Physical, Fluvial and Environmental Processes. Springer International Publishing, Berlin, pp. 519–541.

Albayrak, I., Nikora, V., Miler, O., O'Hare, M., 2013. Flow–plant interactions at leaf, stem and shoot scales: drag, turbulence, and biomechanics. Aquat. Sci. 1–26.

Anderson, M.E., Smith, J.M., 2014. Wave attenuation by flexible, idealized salt marsh vegetation. Coast. Eng. 83, 82–92.

Asano, T., Deguchi, H., Kobayashi, N., 1993. Interaction between water waves and vegetation, in: Anon (Ed.). Publ by ASCE, Venice, Italy, pp. 2710–2723.

Asano, T., Tsutsui, S., Sakai, T., 1988. Wave Damping Characteristics Due to Seaweed, 35th Coastal Engineering Conference. JSCE, Japan, pp. 138–142 (in Japanese).

Bradley, K., Houser, C., 2009. Relative velocity of seagrass blades: Implications for wave attenuation in low-energy environments. J. Geophys. Res. Earth Surf. 114, F01004.

Dalrymple, R.A., Kirby, J.T., Hwang, P.A., 1984. Wave diffraction due to areas of energy dissipation. J. Waterw. Port Coast. Ocean Eng. 110, 67–79.

de Langre, E., Gutierrez, A., Cossé, J., 2012. On the scaling of drag reduction by reconfiguration in plants. Comptes Rendus Mécanique 340, 35–40.

Dean, R.G., Dalrymple, R.G.D.R.A., 1991. Water Wave Mechanics for Engineers & Scientists. World Scientific.

Dubi, A., Torum, A., 1995. Wave Damping by Kelp Vegetation. ASCE, Kobe, Jpn, pp. 142–156.

Feagin, R.A., Irish, J.L., Möller, I., Williams, A.M., Colón-Rivera, R.J., Mousavi, M.E., 2011. Short communication: engineering properties of wetland plants with application to wave attenuation. Coast. Eng. 58, 251–255.

Forristall, G.Z., 2000. Wave Crest distributions: observations and second-order theory. J. Phys. Oceanogr. 30, 1931–1943.

Gaylord, B., Blanchette, C.A., Denny, M.W., 1994. Mechanical consequences of size in wave-swept algae. Ecol. Monogr. 64, 287–313.

Gosselin, F.P., De Langre, E., 2011. Drag reduction by reconfiguration of a poroelastic system. J. Fluids Struct. 27, 1111–1123.

Henry, P.-Y., Myrhaug, D., 2013. Wave-induced drag force on vegetation under shoaling random waves. Coast. Eng. 78, 13–20.

Hu, Z., Suzuki, T., Zitman, T., Uittewaal, W., Stive, M., 2014. Laboratory study on wave dissipation by vegetation in combined current–wave flow. Coast. Eng. 88, 131–142.

Hudspeth, R.T., Sulisz, W., 1991. Stokes drift in two-dimensional wave flumes. J. Fluid Mech. 230, 209–229.

Jadhav, R.S., Chen, Q., Smith, J.M., 2013. Spectral distribution of wave energy dissipation by salt marsh vegetation. Coast. Eng. 77, 99–107.

Kobayashi, N., Raichle, A.W., Asano, T., 1993. Wave attenuation by vegetation. J. Waterw. Port Coast. Ocean Eng. - ASCE 119, 30–48.

Koftis, T., Prinos, P., Stratigaki, V., 2013. Wave damping over artificial Posidonia oceanica meadow: a large-scale experimental study. Coast. Eng. 73, 71–83.

Li, R.M., Shen, H.W., 1973. Effect of tall vegetations on flow and sediment. J. Hydraul. Div. Proc. ASCE 99.

Lindner, K., 1982. Der Strömungswiderstand von Pflanzen-beständen. SPE-8584-PA. Mitteilungen Leichtweiss-Institut für Wasser-bau, No. 75. TU Braunschweig.

Lowe, R.J., Falter, J.L., Koseff, J.R., Monismith, S.G., Atkinson, M.J., 2007. Spectral wave flow attenuation within submerged canopies: Implications for wave energy dissipation. J. Geophys. Res. Oceans 112 n/a-n/a.

Massel, S.R., Furukawa, K., Brinkman, R.M., 1999. Surface wave propagation in mangrove forests. Fluid Dyn. Res. 24, 219–249.

Maza, M., Lara, J.L., Losada, I.J., 2013. A coupled model of submerged vegetation under oscillatory flow using Navier–Stokes equations. Coast. Eng. 80, 16–34.

Mendez, F.J., Losada, I.J., 2004. An empirical model to estimate the propagation of random breaking and nonbreaking waves over vegetation fields. Coast. Eng. 51, 103–118.

Méndez, F.J., Losada, I.J., Losada, M.A., 1999. Hydrodynamics induced by wind waves in a vegetation field. J. Geophys. Res. 104, 18383–18396.

Miller, L.A., Santhanakrishnan, A., Jones, S., Hamlet, C., Mertens, K., Zhu, L., 2012. Reconfiguration and the reduction of vortex-induced vibrations in broad leaves. J. Exp. Biol. 215, 2716–2727.

Myrhaug, D., Holmedal, L.E., 2011. Drag force on a vegetation field due to long-crested and short-crested nonlinear random waves. Coast. Eng. 58, 562–566.

Myrhaug, D., Holmedal, L.E., Ong, M.C., 2009. Nonlinear random wave-induced drag force on a vegetation field. Coast. Eng. 56, 371–376.

Möller, I., Kudella, M., Rupprecht, F., Spencer, T., Paul, M., van Wesenbeeck, B.K., Wolters, G., Jensen, K., Bouma, T.J., Miranda-Lange, M., Schimmels, S., 2014. Wave attenuation over coastal salt marshes under storm surge conditions. Nat. Geosci. 7, 727–731.

Nepf, H.M., 2011. 2.13-Flow over and through Biota. In: Wolanski, E., McLusky, D. (Eds.), Treatise on Estuarine and Coastal Science. Academic Press, Waltham, pp. 267–288.

Nepf, H.M., 2012. Flow and transport in regions with aquatic vegetation. Annu. Rev. Fluid Mech. 44, 123–142.

Nikora, V., 2010. Hydrodynamics of aquatic ecosystems: an interface between ecology, biomechanics and environmental fluid mechanics. River Res. Appl. 26, 367–384.

Nikora, V., Cameron, S., Albayrak, I., Miler, O., Nikora, N., Siniscalchi, F., Stewart, M., Hare, M.O., 2012. Flow-biota Interactions in Aquatic Systems. Environ Fluid Mech. CRC Press, pp. 217–235.

Ozeren, Y., Wren, D., Wu, W., 2014. Experimental investigation of wave attenuation through model and live vegetation. J. Waterw. Port Coast. Ocean Eng. 140, 04014019.

Paul, M., Amos, C.L., 2011. Spatial and seasonal variation in wave attenuation over Zostera noltii. J. Geophys. Res. C Oceans 116.

Sánchez-González, J.F., Sánchez-Rojas, V., Memos, C.D., 2011. Wave attenuation due to Posidonia oceanica meadows. J. Hydraulic Res. 49, 503–514.

Siniscalchi, F., Nikora, V.I., Aberle, J., 2012. Plant patch hydrodynamics in streams: mean flow, turbulence, and drag forces. Water Resour. Res. 48, W01513.

Stratigaki, V., Manca, E., Prinos, P., Losada, I.J., Lara, J.L., Sclavo, M., Amos, C.L., Cáceres, I., Sánchez-Arcilla, A., 2011. Large-scale experiments on wave propagation over Posidonia oceanica. J. Hydraulic Res. 49, 31–43.

Suzuki, T., Zijlema, M., Burger, B., Meijer, M.C., Narayan, S., 2012. Wave dissipation by vegetation with layer schematization in SWAN. Coast. Eng. 59, 64–71.

Vogel, S., 1984. Drag and flexibility in sessile organisms. Integr. Comp. Biol. 24, 37–44.

Västilä, K., Järvelä, J., 2014. Modeling the flow resistance of woody vegetation using physically based properties of the foliage and stem. Water Resour. Res. 50, 229–245.

Whittaker, P., Wilson, C., Aberle, J., Rauch, H.P., Xavier, P., 2013. A drag force model to incorporate the reconfiguration of full-scale riparian trees under hydrodynamic loading. J. Hydraulic Res. 51, 569–580.

Whittaker, P., Wilson, C.A.M.E., Aberle, J., 2015. An improved Cauchy number approach for predicting the drag and reconfiguration of flexible vegetation. Adv. Water Resour. 83, 28–35.

Zeller, R.B., Weitzman, J.S., Abbett, M.E., Zarama, F.J., Fringer, O.B., Koseff, J.R., 2014. Improved parameterization of seagrass blade dynamics and wave attenuation based on numerical and laboratory experiments. Limnol. Oceanogr. 59, 251–266.

PAPER III

Paul, M., **Henry, P.Y.T.** and Thomas, R.E., [**2014**]. Geometrical and mechanical properties of four species of northern European brown macroalgae. *Coastal Engineering*, 84: 73-80.

Coastal Engineering 84 (2014) 73–80

Contents lists available at ScienceDirect

Coastal Engineering

journal homepage: www.elsevier.com/locate/coastaleng

Short communication

Geometrical and mechanical properties of four species of northern European brown macroalgae

M. Paul [a,*], P.-Y.T. Henry [b], R.E. Thomas [c]

[a] Leibniz Universität Hannover, Forschungszentrum Küste, Merkurstr. 11, 30419 Hannover, Germany
[b] Department of Marine Technology, Norwegian University of Science and Technology, Otto Nielsens vei 10, NO-7491 Trondheim, Norway
[c] Department of Geography, Environment and Earth Sciences, University of Hull, Cottingham Road, Hull HU6 7RX, UK

ARTICLE INFO

Article history:
Received 23 May 2013
Received in revised form 4 October 2013
Accepted 14 November 2013
Available online 10 December 2013

Keywords:
Brown macroalgae
Bending modulus
Flexural rigidity
Buoyancy

ABSTRACT

Aquatic vegetation interacts with the flow by posing an obstruction and in return experiences drag and is reconfigured by acting forces. It is suggested that plant buoyancy and stiffness affect these bio-physical interactions and hence should be considered when including vegetation in physical and numerical hydrodynamic models. However, data on these parameters is either lacking for many species or existing information is insufficient to model flexible aquatic vegetation correctly. Previous studies have focused on plant stems, but did not take plant foliage into account. The present study extends the existing knowledge base by providing data for four northern European brown macroalgae and also provides a comparison between the mechanical properties of stem and blade tissue for these species. Specimens of *Alaria esculenta*, *Laminaria digitata*, *Fucus serratus* and *Fucus vesiculosus* were collected from a small tidal inlet in Norway. Other than *F. serratus*, the macroalgae were positively buoyant and all stems showed bending moduli in agreement with previous studies with respect to their order of magnitude. Only *L. digitata* exhibited a significant difference between bending moduli for stems and blades and also between the tip and the base of the blades. However, there were differences in flexural rigidities (product of bending modulus and second moment of cross-sectional area) of both stems and blades and the tip and the base of blades of all but *F. serratus*. This highlights the important influence of cross-sectional area and cross-sectional shape on stiffness.

1. Introduction

It has been recognised that coastal vegetation enhances wave attenuation (Augustin et al., 2009; Méndez and Losada, 2004; Möller et al., 1999; Paul et al., 2012) and that there may be great potential in using vegetation for coastal protection purposes (Feagin et al., 2010; Feagin et al., 2011). Aquatic vegetation reduces fluid velocities by imposing a blockage, causing drag (Bal et al., 2011; Miler et al., 2012), generating turbulence and enhancing roughness (Ghisalberti and Nepf, 2002; Nepf and Ghisalberti, 2008). In return, hydrodynamic forcing leads to plant reconfiguration which can cause leaf shading and impact upon photosynthesis (Bal et al., 2011). These bio-physical interactions are partly governed by geometrical plant properties such as stem and shoot dimensions and density (i.e. number of plants per unit area) (Boller and Carrington, 2006; Bouma et al., 2010; Bradley and Houser, 2009; Fonseca and Koehl, 2006; Möller et al., 1999; Newell and Koch, 2004; Paul and Amos, 2011). Additionally, mechanical parameters, in particular buoyancy and stiffness, strongly influence the drag imposed on vegetation (Nepf and Koch, 1999) and play a significant role in wave attenuation (Bouma et al., 2005; Denny and Gaylord, 2002; Paul et al., 2012; Stewart, 2006).

Advances have been made to numerically simulate the interaction of vegetation with hydrodynamics (Dijkstra and Uittenbogaard, 2010; Luhar and Nepf, 2011), but validation has only been undertaken using surrogate plants. To date, the ability of physical models of plants to mimic real vegetation has mainly been determined by visual observation (Folkard, 2005; Manca, 2010; Paul et al., 2012). However, a more quantitative approach is desirable to increase transferability of results between the field and numerical and laboratory models. A recent study of *Laminaria digitata* based on the data presented here shows that knowledge of mechanical plant properties can aid the production of more realistic surrogates (Paul and Henry, 2013). The effect of the developed surrogates on hydrodynamics was compared with real vegetation under field conditions at the field site used during this study and yielded very good agreement for mean velocity and turbulence profiles adjacent to plant locations (unpublished data). Moreover, detailed knowledge of mechanical plant properties may improve the performance of numerical models that simulate the interaction between vegetation and hydrodynamics through improved parameterisation (Dijkstra and Uittenbogaard, 2010; Méndez and Losada, 2004).

* Corresponding author. Tel.: +49 511 7629233.
E-mail addresses: paul@fzk-nth.de (M. Paul), pierre-yves.henry@ntnu.no (P.-Y.T. Henry), R.Thomas@hull.ac.uk (R.E. Thomas).

0378-3839/$ – see front matter © 2013 Elsevier B.V. All rights reserved.
http://dx.doi.org/10.1016/j.coastaleng.2013.11.007

However, mechanical parameters are not commonly established during field monitoring of aquatic vegetation and hence data is lacking to adequately consider bio-physical processes in physical and numerical models.

A number of past studies have presented data for mechanical properties, especially Young's bending modulus, with most data being available for riparian vegetation (e.g. Freeman et al., 2000; Ostendorp, 1995). Recently, engineering properties of the salt marsh plant *Spartina alterniflora* were evaluated, which yielded a bending modulus of 1.41 ± 0.71 GPa for healthy, fully developed stems (Feagin et al., 2011). This value is similar to bending moduli obtained for the seagrasses *Zostera marina* (0.4–2.4 GPa) (Luhar and Nepf, 2011) and *Posidonia oceanica* (0.47 ± 0.06 GPa) (Folkard, 2005). Other aquatic species that have been investigated to date yielded lower values, indicating that they are more flexible. Miler et al. (2012), for instance, analysed four fresh water species and observed bending moduli of 12.5–90 MPa, with one species being too fragile for testing. Several other studies have addressed macroalgae (Dubi, 1995; Harder et al., 2006; Koehl, 1979; Stewart, 2004), yielding values between 3.5 MPa (*Durvillaea antarctica*) and 109.4 MPa (*Laminaria hyperborea*). It should, however, be noted that all previous studies focused on plant stems only and did not evaluate the mechanical properties of leaves or blades.

The present study adds to the existing datasets by presenting geometrical and mechanical properties of four species of brown macroalgae from a field site in Norway. Moreover, and to our knowledge, for the first time, data for blade sections are also presented. Together with the data for stems of the same specimens, this identifies differences between plant parts that may be of importance for future modelling activities.

2. Methods

2.1. Site

The study site is a small tidal inlet located at the entrance of Trondheimsfjord, Sør-Trøndelag, Norway (Fig. 1a). The inlet is approximately triangular in planform, with its mouth to the northwest. The deepest parts of the inlet are to the centre and northeast, where the depth is between 25 and 30 m. A delta, formed of coarse sand and broken shells, has been deposited in the northwest corner of the inlet (Fig. 1b). This delta is fed by a channel which connects the inlet to the fjord. The channel is 15 m wide and up to 4 m deep at the bridge that marks the seaward margin of the inlet (Fig. 1b). The bed of the outlet channel is formed of gravel and cobbles. The outlet channel is pinned to the northern edge of the delta and thus the depth of water over the delta shallows from west to east and from north to south. For much of the delta, the average water depth above the flat sandy bed is 0.5 m.

The site is well sheltered from waves and the speed of the current in the study area is entirely dependent upon tidal forcing. In the sampling area, the tidal range varies between 0.3 m during neap and 1 m during spring tides; tides are semi-diurnal, strongly asymmetric and flood-dominated. During the sampling period (May 2012) maximum velocities of 0.4 m s^{-1} during flood tides and 0.15 m s^{-1} during ebb tides were observed in the sampling area. Flow velocities increase towards the mouth of the inlet and can reach up to 6 m s^{-1}. The catchment area of the inlet is negligible (1.9 km^2). Therefore the salinity in the inlet is close to the values found in the fjord (31 ± 4 ppm), and varies depending on the thermal and tidal conditions. A more detailed site description can be found in Thomas et al. (2013), who evaluated the effect of macroalgae presence on the mean and turbulent flow fields at the location.

2.2. Species

Biodiversity in the study area is remarkably high, with many species of algae, molluscs, crustaceans and fish observed in a very small area. Different species of algae cover much of the study area in spring and summer. Most specimens are brown algae, but green algae have also been observed. In this study, samples of four different species of brown macroalgae were collected along the southern shoreline of the outlet channel (Fig. 1b). The species under investigation are *Alaria esculenta*, *L. digitata*, *Fucus vesiculosus* and *Fucus serratus*. All four species colonise hard substrate along the eastern and western shores of the North Atlantic with the *Fucus* species extending south as far as the Azores and Canary Islands. At the study site, rocks, pebbles and mussel shells, both dead and alive, provided the substrate to which plants attach with their holdfast.

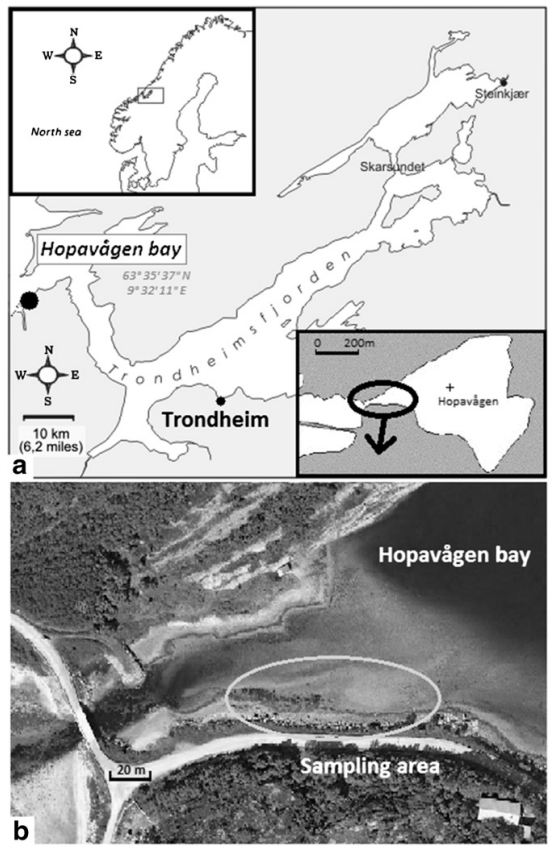

Fig. 1. a) Location of the tidal inlet (Hopavågen bay; 63°35′37″N, 9°32′11″E); b) aerial view of the sampling area (www.norgeskart.no).

A. esculenta (Fig. 2a) colonises the lower intertidal and the upper subtidal zone along rocky shores of the North Atlantic (Dring, 1982). It grows a single stipe from a holdfast that continues as a tapering midrib through the whole blade. In sheltered conditions, *A. esculenta* produces a long stipe and wide lamina base while both stipe and base tend to be shorter under exposed conditions (Widdowson, 1971). The wavy blade is brown in colour, and is very thin, flexible and delicate. Blades typically grow to 0.3–1.5 m in length and may be torn by waves. However, they can reach up to 4 m in length in locations with strong currents and low wave action. Below the base of the blade, flat sporophylls that carry the reproductive organs branch off the stipe (Guiry, 1997).

At its lower depth boundary, *A. esculenta* overlaps with *L. digitata* (Fig. 2b). *L. digitata* also consists of a holdfast, a single stipe and a large (up to 2 m length) oval blade. However, in contrast to *A. esculenta*, the blade lacks a midrib, and is thicker and less flexible than that of *A. esculenta* (Lobban and Harrison, 1997). The substrate conditions in

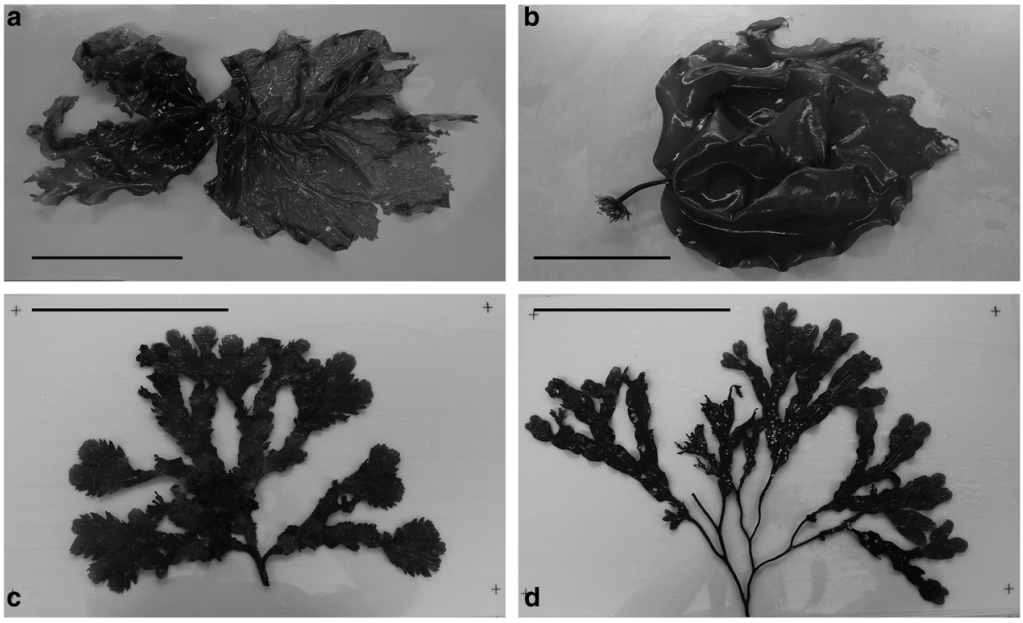

Fig. 2. Example images of brown algae found in the study area. a) *Alaria esculenta*, b) *Laminaria digitata*, c) *Fucus serratus*, and d) *Fucus vesiculosus*. The bar in each image represents a length of 0.20 m.

the study area do not allow *L. digitata* specimens to grow close to one another, as pebbles and mussels that act as support are spaced widely apart. Thus, competition for light is low, which may be one reason why specimens in the study area produce only a short stipe that supports a large, smooth, brown blade.

F. serratus (Fig. 2c) is a much smaller species of the lower eulittoral and the upper sublittoral along sheltered and semi-exposed shores. Its blades are olive-green, dichotomously branched and grow to lengths of 0.3–0.6 m. The flattened blades have serrated edges and a midrib (Lüning, 1990) that extends from short dark stalks which originate from a common holdfast. *F. serratus* is prone to colonisation by briozoa, which was the case for many specimens in the study area.

F. vesiculosus (Fig. 2d) can be found landward of *F. serratus*. *F. vesiculosus* has dark green fronds with smooth edges. It can be easily identified by almost spherical air bladders in the upper part of the blades that provide buoyancy (Lüning, 1990). However, air bladders may be reduced or absent in wave exposed locations. Blades develop from a branching stem that continues as a midrib through the dichotomously branched fronds. *F. vesiculosus* is a common host for the tube worm *Spirorbis spirorbis*, which was observed to colonise the majority of *F. vesiculosus* specimens at the study site.

2.3. Measurements

Plants were collected from the study area (Fig. 1b) between 21st and 31st May 2012. They were removed by hand, including the object their respective holdfast was attached to, and transferred to the laboratory. There, they were immersed in salt water collected from the sampling location and stored at 4 °C. The number of specimens per species was limited by availability and a sample size larger than 10 was hence only achieved for *L. digitata* (Table 1). Each specimen was tested within 48 h of harvesting and all plant parts were kept under a damp cloth between tests.

Prior to processing, the holdfast was removed from the plant and is consequently not included in the values for plant mass and mass density ρ. To obtain the mass of each plant, all excess water was removed from the surface of the specimen with a paper towel and then the plant was weighed on a balance with a precision of ± 0.1 g. To evaluate mass density (mass/volume) and hence buoyancy, the total volume of a plant was determined by measuring its displacement in unfiltered fresh water at room temperature (20 °C).

Stem dimensions were measured with a calliper gauge to the nearest 0.05 mm. To record the extent of stem tapering, measurements were taken at the base, centre and tip of the stem. The projected surface area was computed from digital photographs. To enable this, the plants were laid flat onto a white background and pressed down with a transparent Perspex sheet. Photographs were then taken from directly above from a height of approximately 1.5 m and were rectified in MATLAB® using markers with known x, y coordinates on the white background. The images were then split into the individual RGB colour channels, where the blue channel yielded the strongest contrast between the plant and the background. Pixels with a blue value <50 were defined as part of the plant and the number of pixels in combination with the set pixel size of 1 mm^2 gave the projected plant area.

To investigate whether differences in internal and external shapes and structures between stem and blade lead to differences in flexural rigidity and bending modulus, bending tests were performed on stems and parts cut from the base and tip of the blade. Stems were left at full length and blade parts were cut to a length of 180 mm. For the blades of *A. esculenta* and *L. digitata*, blade parts were trimmed to a width of 40 mm while the parts of *Fucus sp.* were kept untrimmed. Each sample was clamped horizontally between two metal plates on either side with a span s of 43 mm for the stems and 155 mm for blade parts. The short span for stem samples was chosen to minimise the effect tapering might have on the bending behaviour. A metal bar (15 mm wide) attached to a force meter (FMI-250A5 from Alluris, Freiburg, Germany, resolution 0.001 N, precision $\pm 0.05\%$) was lowered manually onto the centre of the test section using a lever (Fig. 3). The bar spanned the width of the sample and the vertical deflection h was recorded, together with the required force P. Tests were terminated when applied forces exceeded the maximum measurable load of the force metre (5 N) or the sample ripped. The latter was only observed for *A. esculenta* blades.

Table 1
Mean values (±1 standard deviation) for physical and mechanical parameters of four brown macroalgae.

	Wet weight [g]	Mass density [kg m^{-3}]	Stem width [cm]	Stem length [cm]	Projected area [cm^2]	Flexural rigidity [$\times 10^{-4}$ Nm^2]	Young's bending or tangent modulus [MPa]	Sample size n
A. esculenta	146.9 ± 51.7	861.7 ± 143.2	0.58 ± 0.09	9.5 ± 1.4	1985.7 ± 409.2			
Stem						24.57 ± 6.16	16.12 ± 4.08	5
Blade base						13.95 ± 7.89	3059.32 ± 4629.88	5
Blade tip						2.31 ± 0.88	15520.09 ± 12880.45	4
L. digitata	203.7 ± 90.7	1001.5 ± 102.7	0.78 ± 0.14	9.3 ± 1.9	2145.5 ± 504.1			
Stem						28.88 ± 7.06	28.67 ± 13.22	20
Blade base						54.15 ± 27.58	3073.55 ± 1627.08	21
Blade tip						51.96 ± 30.35	13355.75 ± 8385.60	20
F. serratus	119.6 ± 98.5	1485.6 ± 692.4	0.76 ± 0.22	11.3 ± 1.3	772.1 ± 563.6			
Stem						19.54 ± 8.89	10.68 ± 4.15	2
Blade base						39.09 ± 17.78	4321.46 ± 1845.88	5
Blade tip						30.19 ± 15.16	3879.68 ± 1806.66	4
F. vesiculosus	257.8	839.7	0.23 ± 0.03	11.6 ± 3.9	253.4 ± 54.2			
Stem						4.21 ± 2.54	353.21 ± 232.06	5
Blade base						220.92 ± 155.86	123987.34 ± 91968.72	5
Blade tip						78.83 ± 67.59	70226.44 ± 77641.58	5

Strain rate variations caused by the manual operation of the test stand may introduce uncertainty into measured material properties, although previous studies have shown that algal tissues are reasonably insensitive to strain rate variations (Gaylord et al., 2001). Furthermore, brown algae tissue may be viscoelastic and which may lead to creeping under applied loads (Dunn and Dabney, 1996). However, creeping was considered negligible in this case, as each loading lasted less than 5 s.

From a mechanical perspective, half the sample (from a fixed end to the centre) can be considered a cantilever that is fixed at one end and exposed to a point load at the other, where the load in this case is $\frac{P}{2}$. For deflections less than 10% of the cantilever length, shear and tensile stresses can be neglected and the force–deflection curve can be used to calculate flexural rigidity according to beam theory (Niklas, 1992):

$$J = \frac{\left(\frac{s}{2}\right)^3 P}{6h}. \quad 1$$

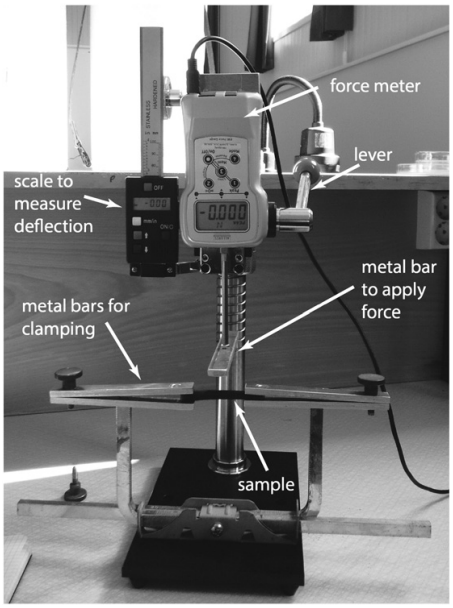

Fig. 3. Three point bending test apparatus.

For linear force–deflection curves, the bending modulus E is defined as the ratio of flexural rigidity to the area second moment of inertia I at the point of application of the force (Miler et al., 2012):

$$E = \frac{J}{I}. \quad 2$$

The force–deflection curve for stems of *A. esculenta*, *L. digitata* and *F. serratus* was linear (Fig. 4) and its slope for a deflection up to 10% of cantilever length yielded the ratio P/h. However, the force–deflection curve for the stem of *F. vesiculosus* and all blade samples was best described by a power relationship, indicating nonlinear elasticity. Each best fit curve was used to compute P/h for a deflection of 10% cantilever length. For nonlinear elastic materials, $\Delta P/\Delta h$ gives the instantaneous ratio for a given deflection and allows calculation of the tangent modulus E_t equivalent to Eq. (2). However, $\Delta P/\Delta h$ increases with increasing stress levels and hence results in different E_t depending on the location in the force–deflection curve. To enable comparison between bending and tangent modulus for the different materials in this study, a deflection of 10% cantilever length was used to compute P/h in all cases.

The area second moment of inertia I is a geometric quantity that accounts for the size and shape of a sample, and therefore differed for samples with differing cross-sectional shapes. Visual observation identified *F. vesiculosus* stems as filled circular, *A. esculenta* and *F. serratus* stems as elliptic and all blades as rectangular (subscripts *cf*, *e*, and *r*, respectively). *L. digitata* stems, however, consist of a relatively stiff wall with a soft pith in the centre. It is assumed that the pith does not contribute significantly to the stability of the stem, and that any strength and stiffness can be attributed solely to the wall (cf. Dunn and Dabney, 1996). Thus, in cross-section, *L. digitata* stems were identified as hollow circular (subscript *ch*):

$$I_{cf} = \frac{\pi d^4}{64} \quad 3a$$

$$I_e = \frac{\pi\left(\alpha^3\gamma\right)}{64} \quad 3b$$

$$I_r = \frac{bt^3}{12} \quad 3c$$

$$I_{ch} = \frac{\pi\left(d_{out}^4 - d_{in}^4\right)}{64} \quad 3d$$

where d = diameter (outer and inner, respectively), α = semi-major axis, γ = semi-minor axis, b = strip width and t = blade thickness.

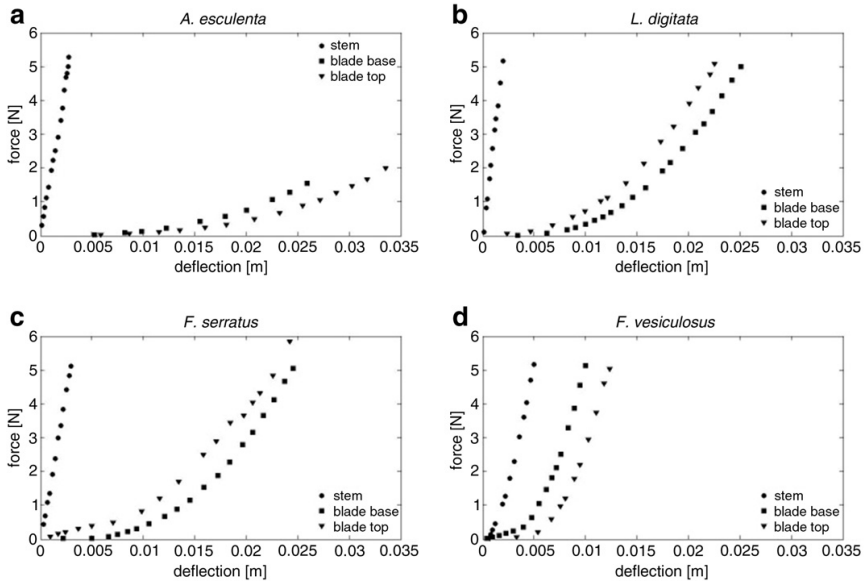

Fig. 4. Examples of force–deflection curves for a) *A. esculenta*, b) *L. digitata*, c) *F. serratus*, and d) *F. vesiculosus*. Curve shapes are representative for all specimens in this study.

3. Results and discussion

Measurements of plant dimensions reflect the general differences in size between the four species (Table 1). *A. esculenta* and *L. digitata* have similar stem lengths and are comparable in projected area while both *Fucus* species are smaller in area but grow, on average, longer stems. These similarities do not hold, however, for mass density and resulting buoyancy. As expected, *F. vesiculosus* is positively buoyant ($\rho = 839.7$ kg m^{-3}), due to the air bladders near the blade tips. The data show that *A. esculenta* yields a similar mass density ($\rho = 861.7$ kg m^{-3}) without visible air inclusions in the tissue. *L. digitata* is almost neutrally buoyant ($\rho = 1001.5$ kg m^{-3}), while *F. serratus* is significantly denser than sea water ($\rho = 1485.6$ kg m^{-3}).

Flexural rigidity varies from 2.31×10^{-4} N m^2 (*A. esculenta* blade top) to 2.21×10^{-2} N m^2 (*F. vesiculosus* blade base) and hence is within an order of magnitude of the flexural rigidity of the tropical brown algae *Turbinaria ornata* (1.45-4.51 $\times 10^{-3}$ N m^2, Stewart, 2004) and the fresh water plants *Glyceria fluitans* (6.78×10^{-4} N m^2), *Ranunculus penicillatus* (2.2×10^{-5} N m^2) and *Myriophyllum alterniflorum* (2.5×10^{-5} N m^2) (Miler et al., 2012). There is fairly large variability in the data for flexural rigidity of all four species (Fig. 5), which may be attributed to internal (e.g. age, vitality) and/or external (e.g. damage, feeding) factors. It should be noted that variability was not reduced by increased sample populations (Table 1) which suggests that these deviations are not measurement artefacts but existing natural variability.

There is a significant difference (ANOVA, $p < 0.05$) between stem and blade values for three of the species; only for *F. serratus* are the values similar ($p > 0.5$). As flexural stiffness determines plant posture and hence drag under hydrodynamic forcing (Bouma et al., 2005), this difference should be accounted for when estimating the effect of vegetation on waves and flow.

Values of the bending modulus E (Table 1) of the stems of *A. esculenta*, *F. serratus* and *L. digitata* fall within the values derived for other aquatic plants (Table 2) while the values for *F. vesiculosus* well exceed the observed range. Harder et al. (2006) derived mean bending moduli for *L. digitata* stems (83.8 ± 84.1 MPa) which are approx. three times higher than the E-values measured for this study (28.7 ± 13.2 MPa). However, the data of Harder et al. (2006) show very high natural variability (expressed by the standard deviation) which suggests that a careful interpretation of the discrepancy is required. The deviation may be caused by differences in the environmental factors to which the respective populations are exposed. The *L. digitata* population studied by Harder et al. (2006) grows in a location with higher wave exposure than the vegetation in our study area and is also likely to be exposed to different abiotic conditions (e.g. salinity, water temperature). These differences in environmental conditions may lead to a difference in mechanical properties. Moreover, a different method was used in the present study than in the study of Harder et al. (2006), which can lead to differences in the results (Bower, 2010). Harder et al. (2006) used a modified four-point-bending test, with loose support of the sample and forces applied to its ends. The current study, however, applied a three-point-bending test following studies on other marine species (e.g. Miler et al., 2012) where the sample was clamped at both sides to prevent slippage. Comparative studies on abiotic materials have shown that bending moduli obtained from four-point-bending tests are generally higher than outcomes from three-point-bending tests for the same specimen (Mujika, 2006). This observation makes it difficult to directly compare values obtained during different studies and highlights the need for a standardised method to derive mechanical properties for plant parts. A three-point-bending test has been used by several authors (Gaylord and Denny, 1997; Miler et al., 2012; Stewart, 2006), but they usually do not mention whether sample ends were fixed or loosely supported which changes the bending behaviour of the sample (Bower, 2010). Additionally, it has been noted in the past that sample preparation can affect the measured mechanical properties (Harder et al., 2006) but it is not yet clear in what way and how big this effect is in comparison to natural variation.

Tangent modulus values for blade parts are several orders of magnitude higher than the bending/tangent modulus for the stems for all four species (Table 1) and exceed previously observed values for flexible aquatic plants (Table 2). However, from the presented data this difference is only significant for *L. digitata* ($p < 0.01$); the difference between blade base and tip values is also significant ($p < 0.01$) for this species, which may be due to the timing of experiments. *L. digitata* grows a

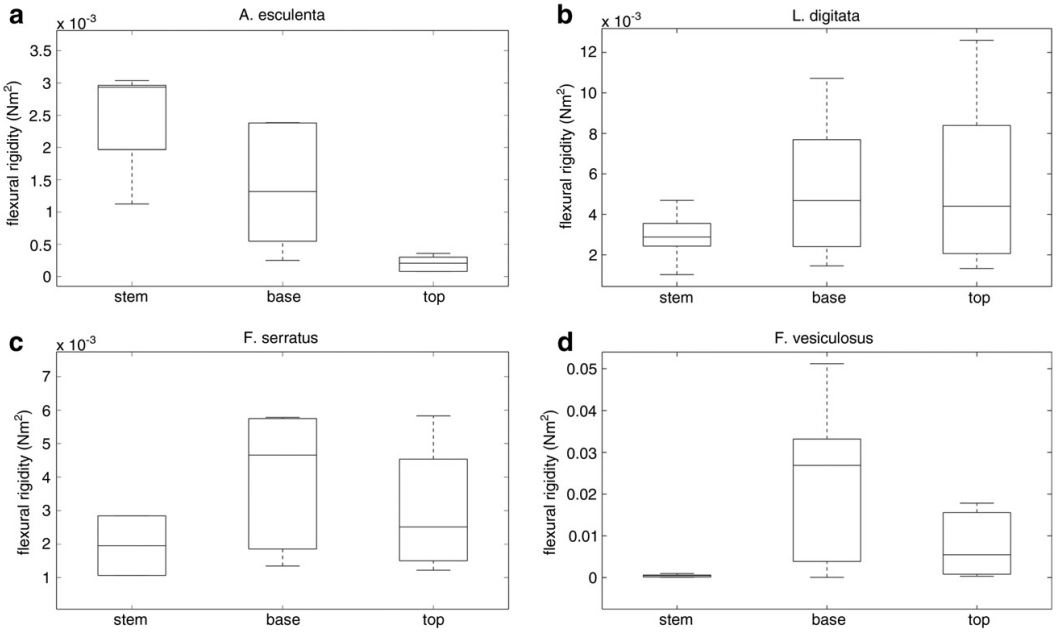

Fig. 5. Median and variability in flexural rigidity for four brown algae. Only *F. serratus* does not show a difference between stem and blade parts statistically significant at the 5% level (ANOVA). a) *A. esculenta* ($F = 11.76$, $p = 0.0015$), b) *L. digitata* ($F = 4.96$, $p = 0.01$), c) *F. serratus* ($F = 0.72$, $p = 0.51$), and d) *F. vesiculosus* ($F = 3.77$, $p = 0.05$).

new blade from the base of the blade and sheds the old blade during late spring every year. Specimens for this study were collected during late May when the blade consisted of tissue grown the previous year followed by newly grown tissue at the base of the same blade. The difference in tangent modulus between base and tip may thus have been caused by the difference in vitality between the old and new blade sections.

The lack of significant differences between stem and blade values, however, is surprising, given the differences of several orders of magnitude between mean bending moduli and flexural rigidities. The general difference in behaviour between stem and blade tissue is also evident in the force–deflection curves derived during the bending tests (Fig. 4). Apart from *F. vesiculosus*, stems exhibited a linear relationship between applied force and deflection within the tested force range (<5 N), while blades exhibited a power relationship, where the change of deflection Δh caused by an increase of force ΔP was greater at large deflections than at small deflections.

Table 2
Young's bending modulus for selected aquatic vegetation (mean ± 1 standard deviation).

	Young's bending modulus [MPa]	Source
Durvillaea antarctica	8.5 ± 1.5	Harder et al. (2006)
Durvillaea antarctica	3.5	Koehl (1979)[a]
Durvillaea willana	12.2 ± 8.0	Harder et al. (2006)
Glyceria fluitans	90 ± 33	Miler et al. (2012)
Laminaria digitata	83.8 ± 84.1	Harder et al. (2006)
Laminaria hyperborea	109.4 ± 54.9	Harder et al. (2006)
Lessonia nigrescens	22.0	Koehl (1979)[a]
Myriophyllum alterniflorum	89 ± 38	Miler et al. (2012)
Nereocystis leutkeana	~50	Denny and Gaylord (2002)
Ranunculus penicillatus	12.5 ± 7.1	Miler et al. (2012)
Turbinaria ornata	29–34	Stewart (2004)

[a] It is not known how this modulus was derived and whether it refers to bending or tension.

The results show that plant blades yield different tangent moduli than plant stems which suggests that plant parts are adapted differently to hydrodynamic forcing. Nikora (2010) identified 'tensile plants' with low flexural rigidity that passively follow the flow and mainly experiencing viscous drag and 'bending plants' which have high flexural rigidity and resist flow, generating downstream vortices and force drag. The presented data suggests that a similar differentiation may be possible within a specimen, particularly for tensile plants where stems may be stiffer than blades, but blade tissue is more tolerant to tension. Two non-dimensional parameters that have been identified as potentially controlling the dominant forms of plant adjustment are the buoyancy number, i.e. the ratio between buoyant and elastic forces (Luhar and Nepf, 2011) and the Cauchy number, i.e. the ratio between inertial and elastic forces (Nikora, 2010). Both these numbers assume uniform values for blade width and thickness as well as flexural rigidity which emphasises the importance of blade length, width, thickness and also the cross-sectional shape (through I). This is supported by the data presented here which show that cross-sectional area and shape of a plant are critical parameters when evaluating a plant's hydrodynamic behaviour and thus care needs to be taken as to which values are used to derive the area second moment of inertia I for Eq. (2). Neither stems nor blades are necessarily uniform in cross section along a plant. For the blades of *F. serratus* (0.8 mm) and *F. vesiculosus* (0.5 mm) no change in blade thickness was observed with position along the blade, but both *A. esculenta* and *L. digitata* tapered towards the blade tip (Table 3). *L. digitata* blades reduce in thickness by 39% and *A. esculenta* blades reduce in thickness by 82% from their base to their tip. The circular stems of *L. digitata* tapered by 30%, while the elliptic stems of *F. serratus* widened from the holdfast to the base of the blade by 64%. For *A. esculenta*, on the other hand, the cross-sectional area increased in the middle of the stem. This shape may be caused by the onset of sporophylls in the mid-section of the stem, which may require extra support. Due to these cross-sectional variations along the stems, a single value may not be adequate to describe the stem structure,

Table 3
Stem and blade tapering of three brown algae (mean ± 1 standard deviation).

		Base	Middle	Top
Alaria esculenta				
Mean stem cross section	[mm^2]	27.96	36.22	15.41
Stem width	[mm]	5.77 ± 0.72	5.86 ± 0.75	4.03 ± 0.94
Stem thickness	[mm]	6.17 ± 0.91	7.87 ± 1.10	4.87 ± 0.86
Blade thickness	[mm]	1.11 ± 0.50	0.46 ± 0.25	0.20 ± 0.05
Laminaria digitata				
Mean stem cross section	[mm^2]	67.49	44.77	32.98
Stem diameter	[mm]	9.27 ± 1.93	7.55 ± 1.63	6.48 ± 0.74
Blade thickness	[mm]	0.82 ± 0.13	0.64 ± 0.08	0.49 ± 0.05
Fucus serratus				
Mean stem cross section	[mm^2]	32.26	39.49	49.52
Stem width	[mm]	7.93 ± 0.38	8.48 ± 0.08	13.0 ± 1.3
Stem thickness	[mm]	5.18 ± 1.48	5.93 ± 0.33	4.85 ± 0.15
Blade thickness	[mm]		0.80 ± 0.12	

especially as it is not clear which stem dimensions can be considered representative (Feagin et al., 2011).

4. Conclusions

The data presented here provides some mechanical properties of four brown macroalgae species from the North Atlantic. The samples for this study were all taken from the same current-dominated environment habitat that enables inter- and intra-species comparison under identical environmental conditions. Specimens of the species under investigation varied in size and shape and the geometrical and mechanical properties of the components of individuals (i.e., stems and blades) also varied. This emphasises the difficulty of describing plant dimensions with single values for e.g. stem diameter or blade thickness. However, values agree with previous findings for brown macroalgae and other aquatic species and therefore contribute to the description of aquatic vegetation for engineering purposes.

Variability between and within species was also observed for buoyancy and stiffness, both key parameters controlling the response of a plant to hydrodynamic forcing. This variability may be caused by environmental factors, age, vitality or other yet unknown factors. During this study, it was not possible to establish whether the buoyancy of plant tissue was consistent within the plants, with the exception of *F. vesiculosus* where the presence of air bladders indicated a non-uniform buoyancy distribution. However, it is suggested that the vertical distribution of flexural rigidity and buoyancy affects the posture and reconfiguration of a plant under hydrodynamic forcing (Feagin et al., 2011). Therefore, a numerical or physical plant representation with uniformly distributed bending modulus and buoyancy may lead to inaccurate results, especially with respect to plant motion. Incorporating non-uniform distributions of these parameters within numerical and physical models of flexible vegetation may thus improve model performance and enhance understanding of the interaction of vegetation with waves and flow.

List of symbols

b	strip width
d_{in}	inner diameter
d_{out}	outer diameter
E	Young's bending modulus
E_t	tangent modulus
F	F-value (ANOVA)
h	vertical deflection
I	second moment of inertia
J	flexural rigidity
p	statistical significance (ANOVA)
P	bending force
s	span of sample
t	blade thickness
α	semi-major axis of ellipse
γ	semi-minor axis of ellipse
ρ	mass density
ρ_w	mass density of water

subscripts

cf	filled circular
ch	hollow circular
e	elliptic
r	rectangular

Acknowledgements

The work described in this publication was supported by the European Community's 7th Framework Programme through the grant to the budget of the Integrated Infrastructure Initiative HYDRALAB-IV, Contract no. 261520. The authors thank the members of the PISCES project for assistance during field work. Discussions with Jussi Evertsen (NTNU) and comments from two anonymous reviewers helped to improve the manuscript.

References

Augustin, L.N., Irish, J.L., Lynett, P., 2009. Laboratory and numerical studies of wave damping by emergent and near-emergent wetland vegetation. Coast. Eng. 56, 332–340.
Bal, K.D., Bouma, T.J., Buis, K., Struyf, E., Schoelynck, J., Backx, H., Meire, P., 2011. Trade-off between drag reduction and light interception of macrophytes: comparing five aquatic plants with contrasting morphology. Funct. Ecol. 25 (6), 1197–1205. http://dx.doi.org/10.1111/j.1365-2435.2011.01909.x.
Boller, M.L., Carrington, E., 2006. The hydrodynamic effects of shape and size change during reconfiguration of a flexible macroalga. J. Exp. Biol. 209 (10), 1894–1903. http://dx.doi.org/10.1242/jeb.02225.
Bouma, T.J., de Vries, M.B., Low, E., Peralta, G., Tánczos, I.C., van de Koppel, J., Herman, P.M.J., 2005. Trade-offs related to ecosystem engineering: a case study on stiffness of emerging macrophytes. Ecology 86 (8), 2187–2199.
Bouma, T.J., de Vries, M.B., Herman, P.M.J., 2010. Comparing ecosystem engineering efficiency of 2 plant species with contrasting growth strategies. Ecology 91 (9), 2696–2704.
Bower, A.F., 2010. Applied Mechanics of Solids, XXV. CRC Press, Boca Raton 794.
Bradley, K., Houser, C., 2009. Relative velocity of seagrass blades: implications for wave attenuation in low-energy environments. J. Geophys. Res. 114 (F01004), 1–13. http://dx.doi.org/10.1029/2007JF000951.
Denny, M.W., Gaylord, B., 2002. The mechanics of wave-swept algae. J. Exp. Biol. 205 (10), 1355–1362.
Dijkstra, J.T., Uittenbogaard, R.E., 2010. Modeling the interaction between flow and highly flexible aquatic vegetation. Water Resour. Res. 46, W12547. http://dx.doi.org/10.1029/2010WR009246.
Dring, M., 1982. The Biology of Marine Plants. Edward Arnold, London.
Dubi, A., 1995. Wave damping by kelp vegetation. 24. Coastal Engineering Conference. Am. Soc. of Civil Eng, New York, pp. 142–156.
Dunn, H., Dabney, S.M., 1996. Modulus of elasticity and moment of inertia of grass hedge stems. Trans. ASAE 39 (3), 947–952.
Feagin, R.A., Mukherjee, N., Shanker, K., Baird, A.H., Cinner, J., Kerr, A.M., Koedam, N., Sridhar, A., Arthur, R., Jayatissa, L.P., Lo Seen, D., Menon, M., Rodriguez, S., Shamsuddoha, M., Dahdouh-Guebas, F., 2010. Shelter from the storm? Use and misuse of coastal vegetation bioshields for managing natural disasters. Conserv. Lett. 3 (1), 1–11. http://dx.doi.org/10.1111/j.1755-263X.2009.00087.x.
Feagin, R.A., Irish, J.L., Möller, I., Williams, A.M., Colón-Rivera, R.J., Mousavi, M.E., 2011. Short communication: engineering properties of wetland plants with application to wave attenuation. Coast. Eng. 58 (3), 251–255. http://dx.doi.org/10.1016/j.coastaleng.2010.10.003.
Folkard, A.M., 2005. Hydrodynamics of model *Posidonia oceanica* patches in shallow water. Limnol. Oceanogr. 50 (5), 1592–1600.
Fonseca, M.S., Koehl, M.A.R., 2006. Flow in seagrass canopies: the influence of patch width. Estuar. Coast. Shelf Sci. 67, 1–9.
Freeman, G.E., Rahmeyer, W.J., Copeland, R.R., 2000. Determination of Resistance Due to Shrubs and Woody Vegetation, Vicksburg (64 pp.).
Gaylord, B., Denny, M.W., 1997. Flow and flexibility: I. Effects of size, shape and stiffness in determining wave forces on the stipitate kelps *Eisenia arborea* and *Pterygophora californica*. J. Exp. Biol. 200, 3141–3164.
Gaylord, B., Hale, B.B., Denny, M.W., 2001. Consequences of transient fluid forces for compliant benthic organisms. J. Exp. Biol. 204, 1347–1360.

Ghisalberti, M., Nepf, H.M., 2002. Mixing layers and coherent structures in vegetated aquatic flows. J. Geophys. Res. Oceans 107 (C2).
Guiry, M., 1997. Research and Development of a Sustainable Irish Seaweed Industry. Royal Dublin Society, Dublin.
Harder, D., Hurd, C., Speck, T., 2006. Comparison of mechanical properties of four large, wave-exposed seaweeds. Am. J. Bot. 93 (10), 1426–1432.
Koehl, M.A.R., 1979. Stiffness or extensibility of intertidal algae: a comparative study of modes of withstanding wave action. J. Biomech. 12, 634.
Lobban, C., Harrison, P., 1997. Seaweed Ecology and Physiology. Cambridge University Press, Cambridge.
Luhar, M., Nepf, H.M., 2011. Flow-induced reconfiguration of buoyant and flexible aquatic vegetation. Limnol. Oceanogr. 56 (6), 2003–2017. http://dx.doi.org/10.4319/lo.2011.56.6.2003.
Lüning, K., 1990. Seaweeds. Their Environment, Biogeography and Ecophysiology.John Wiley & sons, New York.
Manca, E., 2010. Effects of *Posidonia oceanica* Seagrass on Nearshore Waves and Wave-induced Flows. University of Southampton, Southampton (PhD thesis).
Méndez, F.J., Losada, I.J., 2004. An empirical model to estimate the propagation of random breaking and nonbreaking waves over vegetation fields. Coast. Eng. 51 (2), 103–118. http://dx.doi.org/10.1016/j.coastaleng.2003.11.003.
Miler, O., Albayrak, I., Nikora, V., O'Hare, M., 2012. Biomechanical properties of aquatic plants and their effects on plant–flow interactions in streams and rivers. Aquat. Sci. 74 (1), 31–44. http://dx.doi.org/10.1007/s00027-011-0188-5.
Möller, I., Spencer, T., French, J.R., Leggett, D.J., Dixon, M., 1999. Wave transformation over salt marshes: a field and numerical modelling study from North Norfolk, England. Estuar. Coast. Shelf Sci. 49, 411–426.
Mujika, F., 2006. On the difference between flexural moduli obtained by three-point and four-point bending tests. Polym. Test. 25 (2), 214–220. http://dx.doi.org/10.1016/j.polymertesting.2005.10.006.
Nepf, H.M., Ghisalberti, M., 2008. Flow and transport in channels with submerged vegetation. Acta Geophys. 56 (3), 753–777. http://dx.doi.org/10.2478/s11600-008-0017-y.
Nepf, H.M., Koch, E.W., 1999. Vertical secondary flows in submersed plant-like arrays. Limnol. Oceanogr. 44, 172–1080.
Newell, R.I.E., Koch, E.W., 2004. Modeling seagrass density and distribution in response to changes in turbidity stemming from bivalve filtration and seagrass sediment stabilization. Estuaries 27, 793–806.
Niklas, K., 1992. Plant Biomechanics. University of Chicago Press, Chicago (607 pp.).
Nikora, V.I., 2010. Hydrodynamics of aquatic ecosystems: an interface between ecology, biomechanics and environmental fluid mechanics. River Res. Appl. 26 (4), 367–384. http://dx.doi.org/10.1002/rra.1291.
Ostendorp, W., 1995. Estimation of mechanical resistance of lakeside Phragmites stands. Aquat. Bot. 51 (1/2), 87–101.
Paul, M., Amos, C.L., 2011. Spatial and seasonal variation in wave attenuation over *Zostera noltii*. J. Geophys. Res. 116, C08019. http://dx.doi.org/10.1029/2010JC006797.
Paul, M., Henry, P.-Y.T., 2013. Evaluation of the use of surrogate *Laminaria digitata* in eco-hydraulic laboratory experiments. 35th IAHR World Congress. The Wise Find Pleasure in Water. 35th IAHR World Congress, Chengdu, China. 8–13 September.
Paul, M., Bouma, T.J., Amos, C.L., 2012. Wave attenuation by submerged vegetation: combining the effect of organism traits and tidal current. Mar. Ecol. Prog. Ser. 444, 31–41. http://dx.doi.org/10.3354/meps09489.
Stewart, H.L., 2004. Hydrodynamic consequences of maintaining an upright posture by different magnitudes of stiffness and buoyancy in the tropical alga *Turbinaria ornata*. J. Mar. Syst. 49 (1–4), 157–167. http://dx.doi.org/10.1016/j.jmarsys.2003.05.007.
Stewart, H.L., 2006. Hydrodynamic consequences of flexural stiffness and buoyancy for seaweeds: a study using physical models. J. Exp. Biol. 209 (11), 2170–2181. http://dx.doi.org/10.1242/jeb.02254.
Thomas, R.E., McLelland, S., Frostick, L., 2013. The impact of macroalgae on mean and turbulent flow fields. 35th IAHR World Congress. The Wise Find Pleasure in Water. 35th IAHR World Congress, Chengdu, China. 8–13 September.
Widdowson, T., 1971. A taxonimic revision of the genus Alaria Greville. Syesis 4, 11–49.

PAPER IV

Paul, M, **Henry, P-Y T.** [**2014**], Evaluation of the Use of Surrogate Laminaria digitata in eco-hydraulic Laboratory Experiments, *Journal of Hydrodynamics*, Ser. B, 26(3), 374–383.

ELSEVIER

Available online at www.sciencedirect.com
ScienceDirect
Journal of Hydrodynamics
2014,26(3):374-383
DOI: 10.1016/S1001-6058(14)60042-1

www.sciencedirect.com/
science/journal/l0016058

Evaluation of the use of surrogate *Laminaria digitata* in eco-hydraulic laboratory experiments*

PAUL Maike
Forschungszentrum Küste, Leibniz Universität Hannover, Hannover, Germany, E-mail: paul@fzk-nth.de
HENRY Pierre-Yves T.
Department of Marine Technology, Norwegian University of Science and Technology, Trondheim, Norway

(Received March 27, 2014, Revised May 11, 2014)

Abstract: Inert surrogates can avoid husbandry and adaptation problems of live vegetation in laboratories. Surrogates are generally used for experiments on vegetation-hydrodynamics interactions, but it is unclear how well they replicate field conditions. Here, surrogates for the brown macroalgae *Laminaria digitata* were developed to reproduce its hydraulic roughness. Plant shape, stiffness and buoyancy of *L. digitata* were evaluated and compared to the properties of inert materials. Different surrogate materials and shapes were exposed to unidirectional flow. It is concluded that buoyancy is an important factor in low flow conditions and a basic shape might be sufficient to model complex shaped plants resulting in the same streamlined shape.

Key words: bending modulus, buoyancy, hydraulic forcing, *Laminaria digitata*, plant surrogate

Introduction

The interaction between hydrodynamics and vegetation is of ecological interest, and also concerns questions regarding coastal protection and river management. Coastal vegetation attenuates waves and mitigates storm flood effects[1] and can potentially be used for coastal protection measures[2,3]. Riparian vegetation can stabilize river banks[4] and submerged plants and plant parts can reduce flow rates[5,6], resulting in increased sedimentation rates[7] and potentially causing flow blockage and hence increase the risk of flooding. In order to predict these effects and their variability as well as assessing associated risks, it is important to understand the processes involved. One important tool for gaining insight into bio-physical interactions is the use of physical models, but such experiments face major challenges when using live vegetation in the laboratory. Requirements with respect to plant health, vitality and adaptation to different and changing environmental conditions limit the use of vegetation in hydraulic laboratories.

As an alternative, abiotic surrogates have been used to investigate how individual plant properties affect flow[8] and wave motion[9] or a combination of the two[10]. Bouma et al.[9] used materials with varying stiffness and identical shape to investigate how plants with different growth strategies performed under identical hydrodynamic forcing. Other studies used surrogates that resembled certain plant species in size, shape and stiffness[10,11]. However, bending behaviour was only compared visually between real plants and surrogates. It is not known whether such an optical similarity also reflects a hydraulic comparability and hence it is uncertain whether gained results can be transferred to real vegetation in the natural environment.

The aim of this study is therefore to evaluate how well abiotic surrogates can reproduce the hydraulic roughness of live vegetation and to investigate to what extend simplifications are possible while still yielding significant and transferrable results. The experiments are part of the eco-hydraulic work package (PISCES) of the HYDRALAB IV project which compares results from physical experiments to those obtained in the field. Vegetation, substrate and hydraulic conditions have been monitored at a field site and will be repro-

* **Biography:** Maike Paul (1978-), Female, Ph. D., Researcher

duced in the laboratory as closely as possible. Consequently, hydrodynamic conditions in the close vicinity of plants in the field and laboratory will be measured using identical instruments (see Ref.[12]). The dominant species at the field site is the brown macroalgae *Laminaria digitata* which was chosen as an example species for the present study.

1. Material and methods

1.1 *Plant species*

The brown macroalgae *Laminaria digitata* will be modelled. This species was chosen as it dominates the region that is used for other field studies within the PISCES project. *L. digitata* colonises the upper subtidal along rocky shores of the temperate zone. It consists of a holdfast, a single stipe and a large oval blade that can grow up to 2 m in length. The blade does not have a midrib and has a smooth glossy surface which is dark brown in colour and tapers slightly towards the tip where it can be ripped due to exposure to wave action[13].

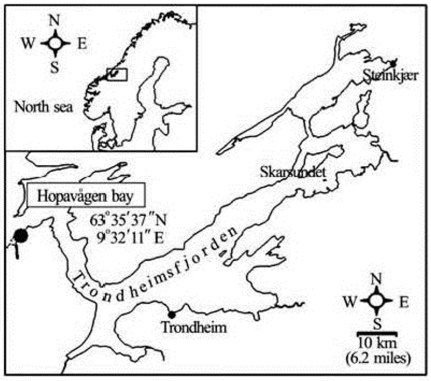

Fig.1(a) Location of Hopavågen bay (63°35′37″N, 9°32′11″E)

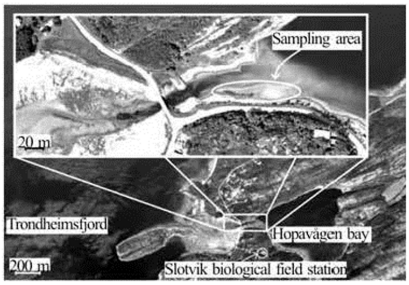

Fig.1(b) Aerial view of the sampling area (www.norgeskart.no)

Specimens for this study were collected in the Hopavågen Bay, Sør-Trøndelag, Norway (Fig.1). The bay is connected to the Trondheim Fjord by a small inlet, which shelters it from waves and limits tidal variation. The tidal curve is strongly asymmetric and flood dominated, tidal elevation varies from 0.3 m during neap and up to 1 m during spring tides. The substrate is mainly comprized of sand, but is interspersed with gravel, cobbles and mussel shells which provide support for *L. digitata*. A more detailed description of the sampling location was given in Ref.[12].

1.2 *Measurement of plant and material properties*

At the site, 20 specimens of *L. digitata* were collected and analysed for their morphological and physical properties in the laboratory within 48 h of collection. During this time period, the macroalgae were stored in salt water from the bay at 4°C and samples were kept under a damp cloth between tests.

Prior to analysis, the holdfasts were removed and were hence not part of this study. The thickness of stems and blades were measured with a calliper gauge to the nearest 5×10^{-5} m. The surface area of the blades was obtained from digital photographs. Photographs were taken vertically from approx. 1.5 m height on a white background. Markers on the background were used to rectify the images in MATLAB®. From the RGB colour channels, the blue channel provided the strongest contrast between plant and background. Plant size was evaluated by defining pixels with a blue value < 50 as part of the plant and computing the projected plant area from the number of pixels and the set pixel size of 10^{-6} m^2.

Each specimen was dried with a paper towel to remove excess water from the surface and was then weighed with a precision of ± 0.0001 kg. Mass density (mass/volume) and hence buoyancy was determined by measuring the plant's displacement in unfiltered fresh water at 20°C.

In order to quantify the stiffness of plants, a three-point-bending test was performed for stems and parts of the blade cut from the base and the tip respectively. Stems were used in one piece while blade sections were cut to strips of 0.18 m length and 0.04 m width. Samples were clamped horizontally between metal plates, the distance between plates was 0.043 m for stems and 0.155 m for blade sections. Consequently, a metal bar of 0.015 m width was lowered manually onto the centre of the sample. The bar was attached to a force meter (FMI-250A5 from Alluris, resolution 0.001 N, precision $\pm 0.05\%$). The required force to bend the sample was recorded in conjunction with the resulting deflection (resolution 10^{-5} m). Tests were terminated when applied forces exceeded the maximum measurable load of the force meter (5 N). Manual operation of the test apparatus may have caused strain rate variations and hence may have introduced uncertainty into the measured material properties.

Moreover, the tissue may creep under applied loads due to viscoelasticity[14]. Both sources of error were considered negligible in this case as algal tissues are considered reasonable insensitive to strain rate variations[15] and each loading lasted less than 5 s.

The force deflection curve was used to derive flexural rigidity J according to beam theory for a cantilever with one fixed end[16]

$$J = \frac{\left(\frac{s}{z}\right)^3 P}{6h} \tag{1}$$

where s is the distance between clamped ends of the sample, P the applied force and h the resulting vertical deflection. For deflections $\leq 10\%$ of the cantilever length, a best fit for P/h and consequently J was computed after[16] and the bending/tangent modulus E was derived. In this case, E is defined as the ratio between flexural rigidity and the area second moment of inertia I at the point of application of the force:

$$E = \frac{J}{I} \tag{2}$$

The latter is a geometric quantity that differs for samples with different cross-sectional shapes as it accounts for the size and shape of a sample. *L. digitata* stems have a relatively stiff wall and a soft pith in the centre. Strength and stiffness are solely attributed to the wall and it is assumed that the pith does not contribute to the stem's stability[14]. The cross-section for *L. digitata* stems is therefore approximated as a hollow circular shape (I_s), while the blade sections are considered to be rectangular in cross-section (I_b):

$$I_s = \frac{\pi(d_o^4 - d_i^4)}{64} \tag{3}$$

$$I_b = \frac{bt^s}{12} \tag{4}$$

with d is the diameter (outer and inner respectively), b is the sample width and t is the blade thickness.

The same method of analysis was applied to several inert materials in order to find materials with properties comparable to *L. digitata* stems and blades with the aim to produce adequate surrogates. Plastic tubing of 0.09 m length was investigated as possible material for stem models as they are hollow cylinders. For blade models, various materials were tested that were all cut to 0.18 m×0.04 m. For each material, three samples were tested.

1.3 *Surrogate development*

Surrogates were developed from the chosen materials. The stems for all surrogates were produced from the same material with the length of 0.1 m, while three different materials (moosipren, artificial leather, geotextile) were used to mimic the blade of *L. digitata*. To compare material performance, the surrogates all had the same elliptic shape with a surface area of a = 0.13 m^2. Additionally, different shaped surrogates with identical surface area $(a = 0.38\ \text{m}^2)$ were produced from one of the chosen materials (artificial leather) to assess the impact of shape complexity on hydrodynamics. These surrogates approximate the natural shape of a *L. digitata* blade to a closer (hand shape), intermediate (ellipse) or lesser (rectangle) degree.

1.4 *Laboratory experiments*

The surrogates were exposed to unidirectional flow under controlled laboratory conditions to evaluate their effect on velocity and turbulence levels. Experiments were conducted in a 20 m long flume with a cross-sectional area of approx. 1 m×1 m at Franzius-Institute in Hannover, Germany. It is equipped with a pumping system that allows discharges of up to 200 l/s and a weir at the end to regulate water depth. Water depth was set to the maximum to provide full submergence of the surrogates and enable sufficient depth to collect velocity profiles that also cover the area above the surrogate. For the chosen flow velocities (0.1 m/s and 0.2 m/s) these were > 0.4 m above the test section. The set velocities cover the typical velocity range encountered *L. digitata* in the Hopavågen Bay.

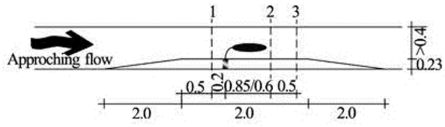

Fig.2 Experimental setup. dashed lines indicate ADV positions. dimensions (m)

The surrogates were deployed 10 m downstream of the inlet on an elevated test section of 2 m length (Fig.2). Profiles of the velocity components (u, v and w in the downstream, cross-stream and vertical direction, respectively) were recorded with an acoustic Doppler velocimiters (ADV, Sontek) placed 0.2 m in front of the surrogate, 0.15 m and 0.65 m behind the surrogate to monitor the size of a turbulent wake cau-

Table 1 Properties of *L. digitata* parts and selected abiotic materials (± standard deviation). Mass density is given for dry/wet material

	Thickness (10^{-3} m)	Mass density (kg/m^3)	Bending/tangent modulus (MPa)	Flexural rigidity (10^{-4} Nm^2)
L. digitata stem	7.8±1.4	1001.5±102.7	28.67±13.22	28.88±7.06
Fluor elastomer	8.0	435.0	17.61±0.53	30.01±0.90
L. digitata blade base	0.8	1001.5±102.7	3073.55±1627.08	54.15±27.58
L. digitata blade tip	0.5	1001.5±102.7	13355.75±8385.60	51.96±30.35
Moosipren	1.0	186.1 / 280.6	10613.55±1475.34	44.22±6.15
Artificial leather, PVC	1.3	568.1 / 938.0	14430.73±9367.02	60.13±39.03
Geotextile, PP	0.8	258.1 / 1093.8	3316.58±1357.88	110.55±45.26

sed by the surrogates. As the size of the surrogates varied, the two latter positions were not constant with respect to the flume setup but changed, depending on the experimental run. Velocity profiles consisted of 10 measurement points each, with a vertical spacing of 0.02 m, starting 0.04 m above the floor due to the limitations of the ADVs. Each measurement was taken at 100 Hz and lasted 4 min. Additionally, measurements were performed without surrogates, but with the test section in place for reference.

From the ADV records time averaged velocities ($\overline{u}$, $\overline{v}$ and $\overline{w}$) and their fluctuations (u', v' and w') were computed at each sampling location and turbulent kinetic energy (TKE, Jm^{-3}) was calculated with ρ being the density of water

$$\mathrm{TKE} = 0.5\rho(u'^2 + v'^2 + w'^2) \quad (5)$$

Previous studies on the effect of vegetation on flow fields and turbulence have used the vegetation Reynolds number Re_v to describe the vegetation-flow interaction non-dimensionally[17-19]. Re_v requires a length scale specific for the vegetation and for simple, strip like vegetation (e.g., seagrass) the width of the plant can be used. For complex shaped vegetation and surrogates, however, it is debatable which length scale is adequate to enable comparison between specimens. It was therefore refrained from using Re_v in this study.

2. Results and discussion

2.1 *Property comparison*

The *L. digitata* specimens tested during this study (Table 1) had a mean weight of 0.2037±0.0907 kg and a mass density of 1001.5±102.7 kg/m^3 which makes them almost neutrally buoyant. The plants had a projected area of 0.21±0.05 m^2 and were hence relatively small for this species. In comparison to other populations, *L. digitata* in Hopavågen produced short stems (0.093±0.019 m) which may have been caused by the habitat's substrate conditions. Pebbles and shells, to which holdfasts can attach, are spaced widely apart within the Hopavågen Bay and *L. digitata* specimens cannot grow close to one another. Consequently, specimens do not have to compete for light availability and it is sufficient to produce a short stipe.

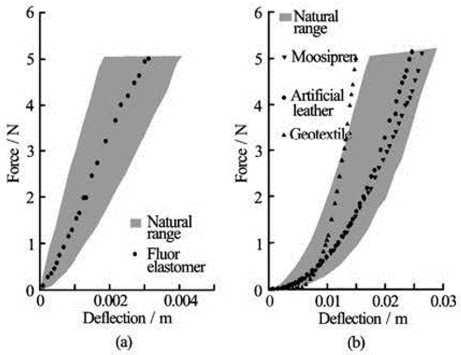

Fig.3 Force deflection curves for *L. digitata* and curves for selected materials

The bending moduli for stems (28.67±13.22 MPa) are approx. one third of bending moduli derived for an *L. digitata* population (83.8±84.1 MPa) on the island of Helgoland, Germany[20]. The high standard deviation in Harder's[20] data indicates a high natural variability and hence a careful interpretation of the differences to the present study is

Table 2 Time and space averaged velocities and TKE (± standard deviation) for all profiles and velocity settings

	$\overline{u}$ (m/s)	$\overline{v}$ (m/s)	$\overline{w}$ (m/s)	TKE (J/m^3)
ADV 1	0.097 ± 0.018	-0.005 ± 0.006	0.005 ± 0.003	1.2 ± 2.7
	0.189 ± 0.039	-0.009 ± 0.006	0.006 ± 0.004	1.4 ± 3.6
ADV 2	0.010 ± 0.004	0.001 ± 0.006	0.001 ± 0.001	1.5 ± 1.6
	0.200 ± 0.005	0.004 ± 0.006	-0.002 ± 0.002	0.8 ± 0.4
ADV 3	0.102 ± 0.002	0.005 ± 0.002	-0.004 ± 0.004	0.7 ± 0.7
	0.197 ± 0.004	0.012 ± 0.005	$-0.011 + 0.007$	0.6 ± 0.2

required. The two populations are likely to be exposed to different biotic and abiotic conditions (e.g., salinity, water temperature, nutrient availability) and the Helgoland population will also experience higher wave exposure than the specimens in the Hopavågen Bay. It is assumed that such differences in environmental conditions can lead to differences in mechanical plant properties. Moreover, the testing methods applied in the two studies differed and in conjunction with possibly different environmental conditions during analysis may have led to the different values obtained for plants of the same species[16,21].

Classic 3-point bending tests usually require a ratio equal or lower than 16 between sample length and thickness[21]. This condition could not be met for the tests on *L. digitata* blades and therefore E has been named "bending modulus" for the stems and "tangent modulus" for the blades[16]. Comparison of bending/tangent moduli for stems and blades (Table 1) showed a distinct difference between plant parts and the difference between blade base ($3\,073.55 \pm 1\,627.08$ MPa) and tip ($13\,355.75 \pm 8\,385.6$ MPa) was statistically significant ($p < 0.01$), highlighting the inhomogeneity of blade tissue. The disparity between stems and blades suggests a difference in bending behaviour which also reflects in the force deflection curves (see Fig.3). Within the force range applied during this study (< 5 N) stems showed a linear relationship between force and deflection while blade sections resulted in a J-shaped curve with different slopes in the upper and lower parts of the relationship. These variations may be generated by the use of the same method for two different types of sample (stiff stems and very flexible blades). Therefore, direct comparison between bending moduli for stems and tangent moduli for blades should be avoided, particularly when attempting to compare absolute values to results obtained with other methods. However, qualitative comparison between stiff materials and stems or flexible materials and blades remains possible in order to determine a surrogate material with a similar flexibility.

A total of eight different tubes and 15 sheet like abiotic materials were tested to evaluate their comparability to *L. digitata* stems and blades, respectively. A comprehensive list can be found in the appendix and the materials considered most suitable for surrogate development are listed in Table 1.

2.2 *Results of laboratory experiments*

In the control runs, velocity profiles were logarithmic and values averaged over the profiles indicated that the downstream flow dominated and both cross-stream and vertical velocities were negligible (Table 2).

The three materials showed very different posture when exposed to the flow which can be attributed to their mass density. Moosipren is highly buoyant (wet mass density of 280.6 kg/m^3) and remained upright in still water conditions, even penetrating the water surface. The slow flow scenario was not sufficient to overcome this buoyancy and the surrogate only bent and streamlined at the high flow velocity. The geotextile had a similar dry mass density (258.1 kg/m^3) but had open pores. Consequently, it soaked with water resulting in a wet mass density (1 093.8 kg/m^3) higher than water, it hovered close to the ground under both flow conditions. The artificial leather (wet mass density of 938.0 kg/m^3) remained floating at the surface in still water conditions and the tips of the large hand shaped surrogate remained at the surface during low flow. But at a flow of 0.2 m/s all of the artificial leather surrogates streamlined at approx. 0.05 m-0.15 m above the ground.

Apart from the moosipren in low flow, the surrogates moved very little due to the lack of turbulence in the approaching water (Table 2). Only the upright posture of moosipren in a free stream flow velocity of 0.1 m/s caused an undulating motion that moved the surrogate beyond the vertical against the approaching flow for short periods of time.

Velocity profiles were affected by the presence of surrogates, irrespective of their material and posture. This included the profiles 0.2 m in front of them

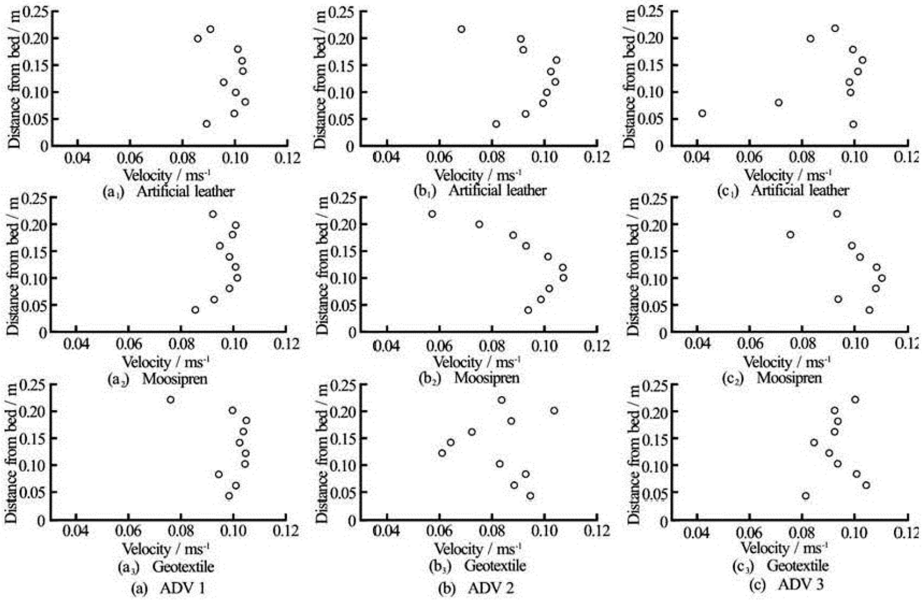

Fig.4 Velocity profiles $(\overline{u})$ for elliptic surrogates $(a = 0.13\ \mathrm{m}^2)$ of different materials under identical hydrodynamic forcing

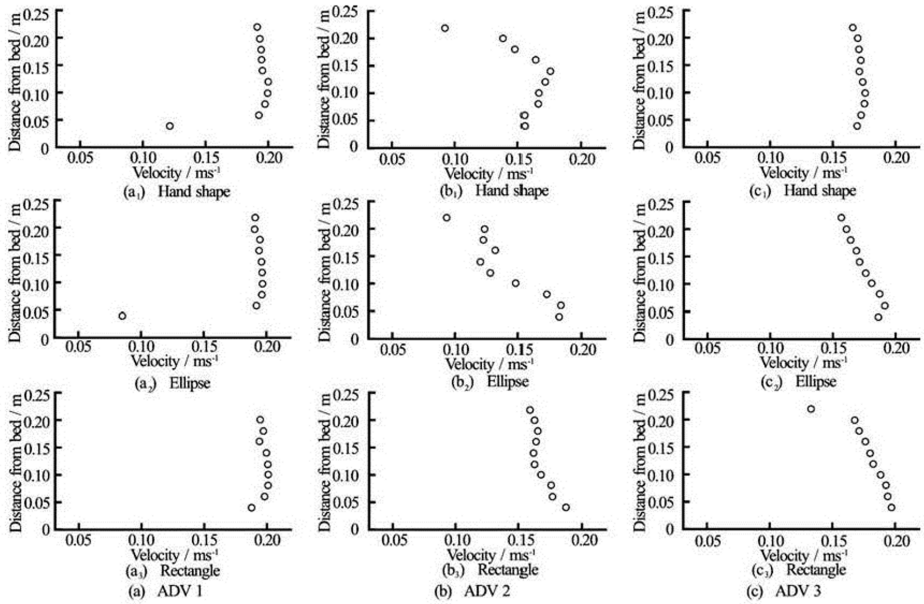

Fig.5 TKE for elliptic surrogates $(a = 0.13\ \mathrm{m}^2)$ of different materials under identical hydrodynamic forcing, corresponding to velocity profiles in Fig.4

(ADV 1). At this position, the velocity profile was still roughly logarithmic (see Fig.4) but the values of $\overline{u}$ were more scattered than in the profiles of the control runs. This upstream effect of flexible structures agrees

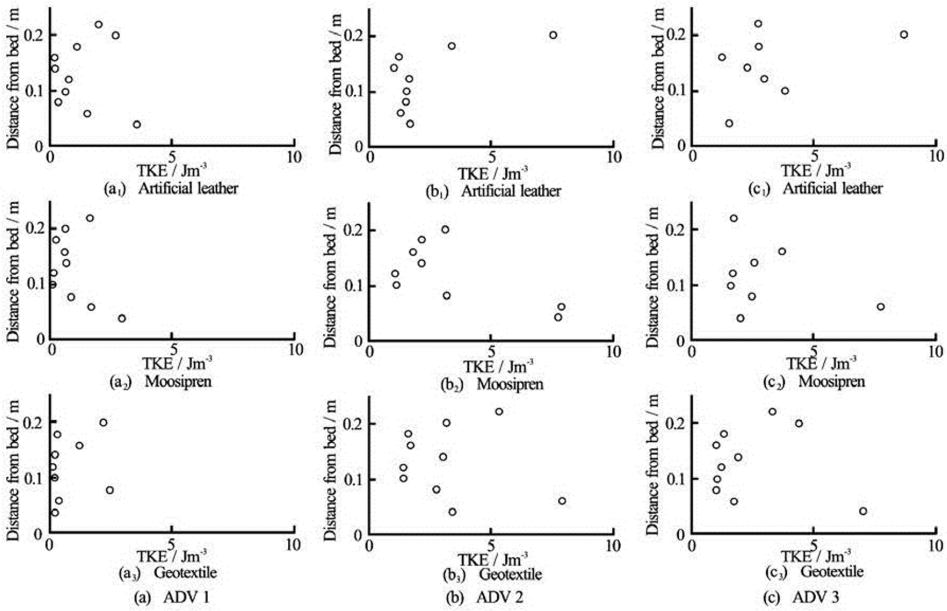

Fig.6 Velocity profiles $(\overline{u})$ for artificial leather surrogates $(a = 0.38\ \mathrm{m}^2)$ of different shapes under identical hydrodynamic forcing

with observations made during measurements in a vegetated stream, where the effect of a *Ranunculus penicillatus* patch could be observed in the velocity profiles 0.5 m upstream[22] although the flow diversion during the present study was not so pronounced. This could be explained with the different values of the ratio between stream/flume width and size of the vegetation. In the field study, *Ranunculus penicillatus* occupied a large part of the stream's cross-section, leading to a blockage high enough to cause water head loss[22], while in the present study no water head loss could be observed due to the small ratio of flume cross-section to frontal area of a single surrogate.

Directly behind the surrogates (ADV 2), the artificial leather and moosipren surrogates yielded similar velocity profiles despite the difference in posture. They showed a peak in the centre of the profile and reduced velocities just above the bed and above the surrogate (see Fig.4). The geotextile, on the contrary, produced a scattered $\overline{u}$ profile without a clear trend. At the last position 0.5 m further downstream (ADV 3), the effect of surrogate presence reduced again to a scattered profile similar to ADV 1 and no difference between materials or posture was observed. Especially the profile similarity for moosipren and artificial leather was unexpected, given their difference in posture at low flow. However, the observed differences reflect in the caused turbulence at ADV 2. Moosipren obstructed the flow mainly in the upper part $(z > 0.1\ \mathrm{m})$ of the profile where the blade was positioned, while the artificial leather surrogate bent and hence obstructed the flow in the lower part of the profile $(z < 0.15\ \mathrm{m})$. These areas of obstruction correspond to lower TKE while turbulence is increased in unobstructed profile regions for both surrogates (Fig.5). This trend still persists 0.5 m further downstream (ADV 3), but is not as pronounced anymore.

Under high flow, the moosipren surrogate also deflected and blade posture changed from buoyancy to stiffness dominated[23]. The obtained posture was similar to the one of the artificial leather, while the geotextile remained closer to the bed. This behaviour reflects the observations made during bending tests, where the force-deflection curves for moosipren and artificial leather were not significantly different while the geotextile yielded a different curve (Fig.3(b)).

Tests with the different shaped surrogates yielded a decrease in $\overline{u}$ in the upper part of the profile at ADV 1, although the intensity of decrease varied with shape (see Fig.6). The effect continued further downstream (ADV 3) for the rectangle and ellipse, resulting in the same almost linear profile, while the profile for the hand shaped surrogate returned back to the profile shape in front of the surrogate. All three shapes led to increased TKE in the upper part of the profile, but the

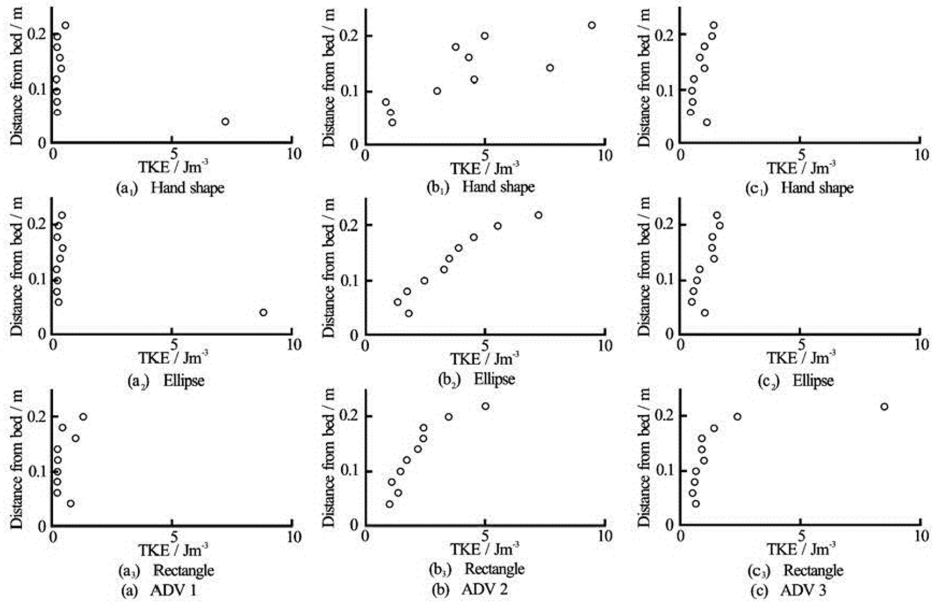

Fig.7 TKE for artificial leather surrogates ($a = 0.38\ \mathrm{m}^2$) of different shapes under identical hydrodynamic forcing, corresponding to velocity profiles in Fig.6

profile for the hand shaped surrogate was more scattered than the other two (Fig.7). This increased scatter may be due to the higher overall length of the hand shaped surrogate. Hence the tip of the surrogate was closer to the profile than for the other two surrogates and turbulence levels may fluctuate more closer to the surrogate. At ADV 3, however, no difference in turbulence could be observed between the three shapes. In addition to the shape and biomechanic properties, other parameters such as the blade surface roughness can affect vegetation-flow interactions and may need to be considered in designing surrogates. However, Albayrak et al.[24]found that leaf surface roughness does not affect the flow field at spatial scales considered in this study and this aspect was therefore not addressed here. Nevertheless, it should be part of future work to improve plant modelling, particularly for numerical applications.

All surrogates curled to the shape of a funnel under hydrodynamic forcing. The diameter of the funnel increased with increasing buoyancy for the three surrogate materials, but was independent of shape. This curling may be an artefact of the flume, where wall effects may have caused lateral forces that lead to a curling response of the surrogates, although no significant lateral velocities existed in the obtained velocity profiles that may have indicated such an effect. No such curling has been observed for natural *L. digitata* specimen in the field (Paul, pers. obs.) but have been reported for fresh water macrophytes in laboratory settings (E. Penning, pers. com.). Hence, further tests with natural plants and surrogates under identical conditions are required to evaluate this behaviour.

3. Conclusions

This preliminary study confirms the observations that flexible structures streamline under hydrodynamic forcing depending on their buoyancy and stiffness[23] and in return affect velocities and turbulence levels downstream as well as upstream of the structure.

Identically shaped surrogates of different materials lead to differences in velocity and turbulence profiles directly behind the surrogates. Velocity profiles are more scattered with increased flexural rigidity while turbulence profiles depend on the posture of the surrogates in the water column with higher turbulence levels in the regions that are not directly obstructed by the surrogates. However, further 0.5 m downstream, no significant differences in profiles between the different materials could be observed.

For the different shaped surrogates, the differences in velocity and turbulence are reduced with in-

creasing flow velocity, which may be due to the overall similar posture of the surrogates after streamlining. The present study therefore suggests that a simple shaped surrogate may be an adequate substitute for real complex shaped plants, given it assumes the same posture when streamlining. However, detailed research is necessary to evaluate whether the observed curling represents natural behaviour under the given hydrodynamic forcing.

Acknowledgements

The authors thank the members of the PISCES project for their assistance during field work. The work described in this publication was supported by the European Community's 7th Framework Programme through the grant to the budget of the Integrated Infrastructure Initiative HYDRALAB-IV, Contract No. 261520.

References

[1] KOCH E. W., BARBIER E. B. and SILLIMAN B. R. et al. Non-linearity in ecosystem services: Temporal and spatial variability in coastal protection[J]. **Frontiers in Ecology and the Environment,** 2009, 7(1): 29-37.

[2] FEAGIN R. A., MUKHERJEE N. and SHANKER K. et al. Shelter from the storm? Use and misuse of coastal vegetation bioshields for managing natural disasters[J]. **Conservation Letters,** 2010, 3(1): 1-11.

[3] FEAGIN R. A., IRISH J. L. and MÖLLER I. et al. Short communication: Engineering properties of wetland plants with application to wave attenuation[J]. **Coastal Engineering,** 2011, 58(3): 251-255.

[4] THOMAS R. E., POLLEN-BANKHEAD N. Modeling root-reinforcement with a fiber-bundle model and Monte Carlo simulation[J]. **Ecological Engineering,** 2001, 36(1): 47-61.

[5] BAL K. D., BOUMA T. J. and BUIS K. et al. Trade-off between drag reduction and light interception of macrophytes: Comparing five aquatic plants with contrasting morphology[J]. **Functional Ecology,** 2011, 25(6): 1197-1205.

[6] MILER O., ALBAYRAK I. and NIKORA V. I. et al. Biomechanical properties of aquatic plants and their effects on plant–flow interactions in streams and rivers[J]. **Aquatic Science,** 2012, 74(1): 31-44.

[7] BOS A. R., BOUMA T. J. and De KORT G. L. J., et al. Ecosystem engineering by annual intertidal seagrass beds: Sediment accretion and modification[J]. **Estuarine, Coastal and Shelf Science,** 2007, 74(1-2): 344-348.

[8] GHISALBERTI M., NEPF H. M. Mixing layers and coherent structures in vegetated aquatic flows[J]. **Journal of Geophysical Research: Oceans,** 2002, 107(C2): 3-1-3-11.

[9] BOUMA T. J., De VRIES M. B. and LOW E. et al. Trade-offs related to ecosystem engineering: A case study on stiffness of emerging macrophytes[J]. **Ecology,** 2005, 86(8): 2187-2199.

[10] PAUL M., BOUMA T. J. and AMOS C. L. Wave attenuation by submerged vegetation: Combining the effect of organism traits and tidal current[J]. **Marine Ecology Progress Series,** 2012, 444: 31-41.

[11] STRATIGAKI V., MANCA E. and PRINOS P. et al. Large-scale experiments on wave propagation over Posidonia oceanica[J]. **Journal of Hydraulic Research,** 2011, 49(Supp1.): 31-43.

[12] THOMAS R. E., Mclelland S. J. and FROSTICK L. E. The impact of macroalgae on mean and turbulent flow fields[C]. **Proceedings of the 35th IAHR World Congress: The Wise Find Pleasure in Water.** Chengdu, China, 2013.

[13] LOBBAN C., HARRISON P. **Seaweed ecology and physiology**[M]. Cambridge, UK: Cambridge University Press, 1997.

[14] DUNN H., DABNEY S. M. Modulus of elasticity and moment of inertia of grass hedge stems[J]. **Transactions of the ASAE,** 1996, 39(3): 947-952.

[15] GAYLORD B., HALE B. B. and DENNY M. W. Consequences of transient fluid forces for compliant benthic organisms[J]. **Journal of Experimental Biology,** 2001, 204: 1347-1360.

[16] PAUL M., HENRY P. T. and THOMAS R. E. Variation of mechanical properties for four northern European brown macroalgae[J]. **Coastal Engineering,** 2014, 84: 73-80.

[17] PAUL M., AMOS C. L. Spatial and seasonal variation in wave attenuation over Zostera noltii[J]. **Journal of Geophysical Research: Oceans,** 2011, 116(C8): C08019.

[18] BRADLEY K., HOUSER C. Relative velocity of seagrass blades: Implications for wave attenuation in low-energy environments[J]. **Journal of Geophysical Research: Earth Surface,** 2009, 114(F1): 1-13.

[19] MÉNDEZ F. J., LOSADA I. J. and LOSADA M. A. Hydrodynamics induced by wind waves in a vegetation field[J]. **Journal of Geophysical Research: Oceans**, 1999, 104(C8): 18383-18396.

[20] HARDER D., HURD C. and SPECK T. Comparison of mechanical properties of four large, wave-exposed seaweeds[J]. **American Journal of Botany,** 2006, 93(10): 1426-1432.

[21] BOWER A. F. **Applied mechanics of solids**[M]. Boca Raton, USA: CRC Press, 2010.

[22] PAUL M., THOMAS R. E. and KEEVIL G. M. Concurrent field measurements of turbulent velocities, plant reconfiguration and drag forces on Ranunculus penicillatus[C]. **10th International Conference on Fluvial Sedimentology.** Leeds, UK, 2013.

[23] LUHAR M., NEPF H. M. Flow-induced reconfiguration of buoyant and flexible aquatic vegetation[J]. **Limnology and Oceanography,** 2011, 56(6): 2003-2017.

[24] ALBAYRAK I., NIKORA V. I. and MILER O. et al. Flow-plant interactions at a leaf scale: Effects of leaf shape, serration, roughness and flexural rigidity[J]. **Aquatic Science,** 2012, 74(2): 267-286.

Appendix

Table A1 Properties of tested abiotic sheet materials as possible blade surrogates. All samples were 0.04 m wide and 0.18 m long, mass and density were only evaluated for one sample each

	Thickness (10^{-3} m)	Dry mass (10^{-3} kg)	Dry density (kg/m^3)	Wet mass (kg)	Wet density (kg/m^3)	Flexural rigidity (10^{-4} Nm^2)	Tangent modulus (MPa)
PVC	0.5	3.88	1077.78	3.95	1097.22	1263.95 ± 20.27	303348.59 ± 4865.64
PVC foil	0.2	1.04	719.910	1.09	756.940	376.54 ± 99.59	1412039.10 ± 373475.23
PVC mesh	0.5	0.76	212.040	1.23	341.670	469.41 ± 92.87	112658.59 ± 22287.90
Rubber gloves	0.5	2.63	729.630	3.04	844.440	37.79 ± 8.17	9069.34 ± 1959.85
Bubble wrap	0.2	0.40	280.090	2.03	1409.72	139.23 ± 13.01	522106.68 ± 48794.84
Geotextile	0.8	1.49	258.100	6.30	1093.75	110.55 ± 45.26	3316.58 ± 1357.88
Artificial leather	1.3	6.16	568.120	8.78	938.030	60.13 ± 39.03	14430.73 ± 9367.02
Crafting foil	0.1	0.84	1166.67	0.89	1236.11	160.09 ± 21.84	4802777.57 ± 655151.87
Moosipren I	1.0	0.67	186.110	1.01	280.560	44.22 ± 6.15	10613.55 ± 1475.34
Moosipren II	2.0	1.35	90.9600	1.55	104.410	116.48 ± 7.98	436.82 ± 29.91
Lamp foil	0.5	3.52	977.780	3.56	988.890	527.80 ± 225.61	126670.87 ± 54147.38
Cloth	0.5	0.82	227.780	9.96	2766.67	94.54 ± 9.35	22690.09 ± 2242.82
Carbofol 406	0.5	6.02	1003.33	6.14	1023.33	564.68 ± 117.84	135524.13 ± 28282.63
PP mesh	0.1	1.00	1388.89	1.45	2013.89	198.52	5955741.44

Table A2 Properties of tested abiotic tube materials as possible stem surrogates. All samples were 0.09 m long

	Outer diameter (10^{-3} m)	Inner diameter (10^{-3} m)	Mass (10^{-3} kg)	Density (kg/m^3)	Flexural rigidity (10^{-4} Nm^2)	Bending modulus (MPa)
Rubber	8.00	5.0	5.32	482.45	17.120 ± 0.640	10.050 ± 0.380
Silicone	8.00	5.0	2.98	270.25	11.510 ± 0.510	6.7600 ± 0.300
PVC	8.00	5.0	3.14	284.76	22.000 ± 1.470	12.910 ± 0.860
PVC mesh inforced	12.0	6.0	9.50	311.21	55.890 ± 15.50	5.8600 ± 1.620
Tygon	8.00	4.8	3.40	293.29	12.990 ± 0.070	7.4200 ± 0.040
Tygon R 100	8.00	4.8	3.12	269.12	6.9400 ± 0.020	3.9700 ± 0.010
Fluor elastomer	8.00	5.0	4.80	434.99	30.010 ± 0.900	17.610 ± 0.530
Teflon	7.00	5.0	3.84	565.88	115.37 ± 18.09	132.34 ± 20.75

PAPER V

Henry, P.-Y.T., [**2014**]. Bending properties of a macroalga: Adaptation of peirce's cantilever test for in situ measurements of laminaria digitata (laminariaceae). *American Journal of Botany*, 101(6): 1050-1055.

American Journal of Botany
Celebrating 100 years 1914–2014

American Journal of Botany 101(6): 1050–1055. 2014.

BRIEF COMMUNICATION

Bending properties of a macroalga: Adaptation of Peirce's cantilever test for in situ measurements of *Laminaria digitata* (Laminariaceae)[1]

Pierre-Yves T. Henry[2]

Department of Marine Technology, Norwegian University of Science and Technology, NO-7491 Trondheim, Norway

- *Premise of the study:* The mechanical properties of a plant are key variables governing the interaction between the plant and its environment. Thus, measuring variables such as the flexural rigidity (bending) of a plant element is necessary to understand and predict the plant–flow interaction. However, plant elements such as macrophyte blades can be relatively thin and flexible, thus difficult to characterize. Different adaptations of the classical 3-point bending tests can also affect the interpretation of the flexural rigidity of an element. A simple, robust, method is newly applied to a biomaterial and validated here as an alternative to measure flexural rigidity of thin, flexible plant elements.
- *Methods:* Based on a bending test procedure developed for the textile industry, an apparatus for in-situ measurements was developed and compared with other normalized methods, then used in a field test on the blade of a marine macroalga (*Laminaria digitata*) to assess its suitability to measure the bending modulus of a biomaterial.
- *Key results:* Results of the presented method on selected surrogate materials agree with a normalized cantilever method (ISO 9073-7:1998) and 3-point bending test (ISO 178:2010). Values determined for the bending moduli for blades of *L. digitaria* were in the typical range for algal material. The range of validity of the method is discussed.
- *Conclusion:* By validating this method with existing norms, this study suggests a better approach to measure bending properties of different biomaterials in the field compared with more traditional bending tests and opens new possibilities.

Key words: bending test; bending modulus; biomaterial; biomechanics; flexural rigidity; *Laminaria digitata*; Laminariaceae; macroalga.

Plant biomechanics is a complex science where the traditional approaches of mechanics and structural engineering meet the complexity and the diversity of biological systems. When plants live in dynamic fluid environments, the biomechanical properties of the plant become the key variables to understand behavior, adaptations, and the impacts of the plant on its environment (Gaylord and Denny, 1997; Koehl, 1999; Bouma et al., 2005; Niklas et al., 2006; Demes et al., 2011; Miler et al., 2012; Nepf, 2012; Nikora et al., 2012). Adopting an engineering approach allows the description of the plant behavior in terms of nondimensional numbers, based on the ratios of the different forces acting in the plant–flow system (Nikora, 2010; Luhar and Nepf, 2011; de Langre et al., 2012). Because the flexural rigidity (or stiffness) of a plant represents the ability of the plant to stand in the flow, it is the most critical variable determining the mechanical response of the plant as well as its hydrodynamic performances. This fact has been highlighted by almost 30 yr of research on plants such as seaweeds (Biedka et al., 1987; Johnson and Koehl, 1994; Gaylord and Denny, 1997; Koehl, 1999; Hale, 2001; Stewart, 2004; Harder et al., 2006; Stewart, 2006; Boller and Carrington, 2007; Martone and Denny, 2008; Demes et al., 2011; Miler et al., 2012).

The flexural rigidity given as $G = E_b I$ can be decomposed into the second moment of inertia of the plant's cross section I, and the (elastic) bending modulus E_b. The latter is a characteristic of the plant's material and is the result of the integration of the biomechanical properties of the plant at a smaller scale. For this reason, these mechanical variables present a high variability according to species, scale, and environment, and many of these aspects are still to be explored, especially on aquatic plants. For this reason, Nikora (2010) remarked on the high priority of collecting such data to improve the understanding of the plant–flow interaction in different contexts, as well as to develop solid mathematical and physical modeling works. However, researchers have been using various techniques with advanced laboratory set-ups to test plant mechanics, limiting measurements in the field and preventing most researchers from measuring flexural stiffnesses and comparing values across studies. In addition, Paul and Henry (2014) and Paul et al. (2014) recently pointed out that traditional testing methods (such as a 3-point bending test) may only give qualitative estimates of the bending properties of a plant because the testing procedures used may not be valid for thin flexible materials, meaning that the high flexibility of a biomaterial (as macroalgal blades) is a limitation to the correct implementation of such tests.

To simplify the collection of some important mechanical data of different plant parts, this paper presents a method validated with standard techniques to collect flexural rigidity values

[1] Manuscript received 8 April 2014; revision accepted 14 April 2014.

The author thanks Prof. Dag Myrhaug for his support during this work in partial fulfillment of his PhD requirements and Dr. Maike Paul for valuable discussions. Helpful comments were also received from the editors and reviewers on the first version of this paper.

[2] E-mail: pierre-yves.henry@ntnu.no

doi:10.3732/ajb.1400163

of thin blade-type biomaterials. This method finds its origins in the textile industry (Peirce, 1930) and can easily and inexpensively be adapted by any researcher who wishes to collect mechanical data in a manner that will be easily understood and implemented by others. One characteristic of this method is to leave little room for error during the implementation. The measurements can also be carried out directly in the field, allowing tests on intact plants. An example of the implementation of this method is given with flexural rigidity measurements on *Laminaria digitata* (Hudson) J.V.F. Lamouroux (Lamouroux, 1813), a marine macroalga of the order Laminariales (Phaeophyceae), widely represented on the shores of the North Atlantic.

Peirce's cantilever test—This method describes the bending properties of flexible materials, such as fabrics, and has been presented the first time by Peirce (1930). In this work, the bending behavior of a thin beam (strip) was derived for large deflections on the basic principles of the bending theory. Assuming a linear elastic behavior of the material, the integration of the bending stresses over the strip's cross section characterizes the deflection of the strip through the relation:

$$1/r = M/G, \tag{1}$$

where r is the radius of curvature of the deflected beam, M is the bending moment at a given section, and G is the bending rigidity or flexural rigidity of the beam. The curvature κ is given as $\kappa = 1/r$, so the bending moment M can be expressed as:

$$M = G\kappa. \tag{2}$$

Considering a point P at a distance s from the hanging edge of the strip, φ is the angle between the tangent in P and the horizontal plane (see Fig. 1), the curvature κ is $\mathrm{d}\varphi/\mathrm{d}s$ and the bending moment $-G\cdot\mathrm{d}\varphi/\mathrm{d}s$. For an infinitesimal change in the distance Δs, the variation of the bending moment $\Delta(-G\cdot\mathrm{d}\varphi/\mathrm{d}s)$ is equal to the change of the overhanging weight, $ws\cdot\cos\varphi\cdot\Delta s$, where w is the weight per unit area of the strip (Peirce, 1930). Thus, the flexural rigidity G is related to the deflection characteristics (s and φ) through the nonlinear second order differential equation along the strip:

$$\mathrm{d}^2\varphi/\mathrm{d}s = ws\cdot\cos\varphi/G. \tag{3}$$

This problem has been analyzed numerically by Szablewski and Kobza (2003), but at the time when this problem was derived, only an approximation of the exact solution could be proposed.

Peirce (1930) described a simple test for characterizing the flexural rigidity of strips. Based on a cantilever test (a strip fixed on one edge and bending under its own weight), the sample is first slowly moved forward until the tip of the specimen touches a plane at an angle of $\theta = 43°$ with the horizontal plane. The projection of the length of the sample on the horizontal plane, known as the cantilever length l (see Fig. 1), is then measured. Peirce introduced the notion of bending length C defined as:

$$C = l\cdot f(\theta), \tag{4}$$

where the function $f(\theta)$ is expressed in the formula:

$$f(\theta) = 0.5\left[\frac{\cos(\theta/2)}{\tan\theta}\right]^{1/3}. \tag{5}$$

The flexural rigidity J (per unit width) of the sample is then related to these quantities by the relation $J = C^3w$, where w is the weight per unit area of the strip (in N/m^2). This finally gives the relationship between the length of the overhanging strip l, the angle that it bends to θ and the flexural rigidity per unit width J, also known as Peirce's formula:

$$J = wl^3\left[\frac{\cos(\theta/2)}{8\tan\theta}\right]. \tag{6}$$

The bending modulus of the sample is then deduced from:

$$E_b = Jb/I = \frac{12wl^3}{t^3}\left[\frac{\cos(\theta/2)}{8\tan\theta}\right], \tag{7}$$

where I is the second moment area of the sample considering a rectangular cross section, given by $I = bt^3/12$, where b is the width and t the thickness of the sample (Young et al., 2011).

Peirce (1930) designed this test with $\theta = 43°$ for practical purposes as $\cos(43/2)/\tan(43) \approx 1$. However, this relation is valid for different values of θ, and angles of $\theta = 41.5°$ and $\theta = 45°$ can also be used. Szablewski and Kobza (2003) conducted a sensitivity analysis of Peirce's formula and found that a test conducted with an angle of $\theta = 53°$ gives the best accuracy for the definition of the flexural rigidity. Although the variation of this accuracy is relatively small for angles between 40° and 50°, they recommended staying at least in this range ($\theta > 40°$) to reduce the uncertainties introduced during the measurements.

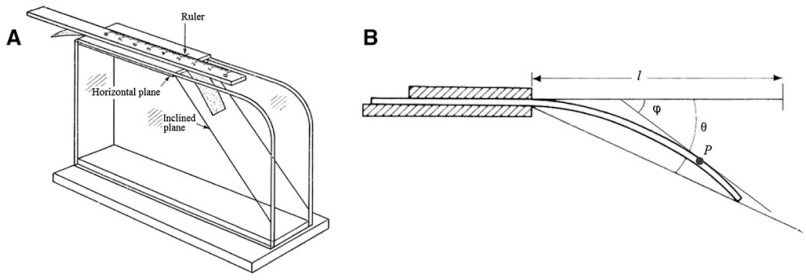

Fig. 1. (A) Peirce's testing apparatus and (B) two-dimensional parameterization of the problem. Figure adapted from Booth (1969).

MATERIALS AND METHODS

***In-situ implementation on* L. digitata—**Based on the physics described in the introduction, it is possible to define an experimental protocol to measure the bending properties of a plant strip in situ. The flexural rigidity G and the flexural rigidity per unit width J (respectively in Nm^2 and Nm, both deduced from Eq. 5) are quantities depending on the geometry of the strip tested (width and thickness). Therefore, the equation of interest is Eq. 6, which defines the bending modulus E_b (in Pa or N/m^2), a unique characteristic of the biomaterial tested. The bending modulus can be obtained by assuming the tests done on a homogeneous material. Although commonly used (Niklas, 1992; Harder et al., 2006), this assumption is relatively crude when applied to biomaterials. Therefore, this modulus is to be considered as an estimation of the more complex mechanical properties of the plant material (Nikora, 2010).

For calculating the bending modulus for a given strip, the dimensions and properties of the strip (its length L, width b, thickness t, and weight w) have to be measured (in S. I. units with two significant digits). In this study, rectangular strips 20 cm × 2.5 cm were cut longitudinally from the middle of one of the blades of the plant. As soon as the samples were cut, thickness was measured, the sample weighed, and cantilever tests were realized. To do the cantilever test and measure the cantilever length l of the hanging strip, an apparatus made of a horizontal plane and a plane inclined at a known angle θ was set up by bending an aluminum plate at an angle θ of 45°, as this is the easiest angle to implement in a workshop (Fig. 2). As mentioned, this angle is in agreement with the conclusions of the sensitivity analysis conducted by Szablewski and Kobza (2003). Since gravity is playing a role in the test, it is important to set up the apparatus on a horizontal plane, which can be done by clamping it onto a table in a laboratory or any other horizontal structure in the field. Once these conditions are met, the strip is laid on the horizontal plane with the extreme edge coinciding with the sharp angle of the apparatus. The upper support consists of a ruler with zero placed at the tested edge of the strip. Then, the sample is slowly moved forward until the tip of the specimen touches the inclined plane. During this phase, care should be taken that the strip does not slide away from the ruler or undulate. In that case, the projection of the length of the hanging sample on the horizontal plane is the same as the length between the tip of the ruler and the sharp angle of the apparatus (Fig. 1A, B). When the sample touches the inclined plane, this length is the cantilever length l, and can be read directly on the ruler at the sharp angle (Figs. 1, 2). Recent standardizations of Peirce's method suggest repeating measurements four times, i.e. on both ends of both sides of the strip, to improve accuracy (i.e., ISO 9073-7:1998 [ISO, 1998]). We followed this recommendation to calculate the mean value, standard deviation (SD), and a coefficient of variation for each measure (CV, in percentage, CV = 100·SD/Mean).

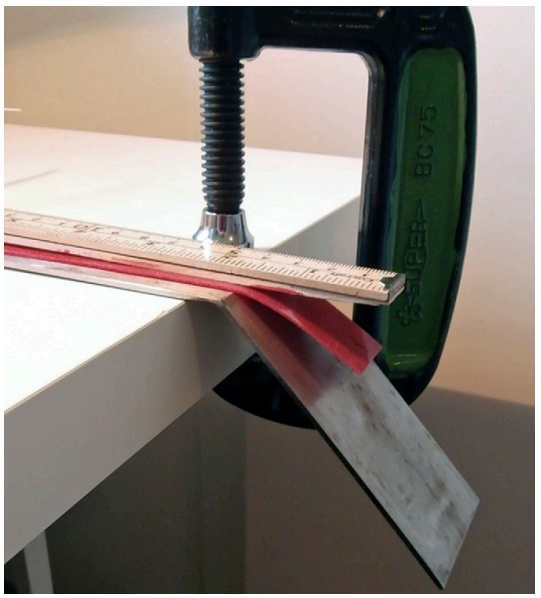

Fig. 2. Picture of the cantilever test device applied to one of the artificial materials (Sample 1).

This procedure was applied to *Laminaria digitata* (order Laminariales, class Phaeophyceae) collected in the surrounding of Trondheim in Norway (N 63 26.8522, E 10 19.7306). This species is widely represented on the sheltered or moderately exposed shores of the North Atlantic, typically located in the upper sublittoral zone (Lüning, 1990). Ongoing research on different aspects of physical modeling of algae in hydraulic experiments led to the choice of this species (Paul and Henry, 2014; Paul et al., 2014). Biomechanics of *L. digitata* has also been studied by Harder et al. (2006), thus providing results for direct comparison. To provide a first set of results for this species and give an indication of the repeatability in time of the test on the same sample, the bending modulus of one sample from each of five plants was monitored for 30 min after the blades were cut (samples numbered from 5 to 9). The testing protocol described above takes approximately 30 s, each blade was tested directly after being cut, then every 3–4 min for 30 min. Between the tests, the samples were stored in (cold) seawater taken directly from the fjord.

***Validation of the technique*—**To assess the accuracy of the method for determining a biomaterial's bending modulus and promoting the comparison of these moduli across studies, we compared international standardized techniques. Two different standards were chosen: the ISO 178:2010 standard (ISO, 2010), representing the classic mechanical test (3-point bending test) which inspired Harder et al. (2006) and Paul et al. (2014) to measure flexural rigidities of *L. digitata* stipes, and the ISO 9073-7:1998 standard (ISO, 1998), standardization of Peirce's (1930) method for industrial textile tests. In comparison to Peirce's method developed previously, a 3-point bending test consists of laying the stripe of material on two supports (two points) and applying a force in the center of the sample at a third point. The force applied is recorded and plotted against the amount of displacement of the center point, allowing the bending modulus to be calculated (refer to the standard ISO 178:2010 [ISO, 2010] for further information). The main constraint of this standard is that the tested length of the strip (the distance between the two support points) can be a maximum of 16 times the thickness of the sample. For reference material testing, samples were chosen among artificial materials (in contrast to biomaterials that are instable, thus highly dependent on time and environmental factors). The ISO 178:2010 testing was done by SINTEF Materials and Chemistry in Oslo (Norway), and the ISO 9073-7:1998 was done by Swerea IVF in Mölndal (Sweden). Because of the long distance between the testing sites, the blades of *L. digitata* could not be incorporated into this comparison because the stability of the blades during the standardized tests could not be guaranteed. Furthermore, due to the thickness constraint mentioned, Paul and Henry (2014) recognized that a 3-point bending technique may not be valid when determining the bending modulus of the blades of *L. digitata*. Consequently, materials slightly less flexible than the algal blades had to be chosen to allow a comparison between the two standardized tests. The final artificial materials were a thin silicone of the same apparent flexibility and thickness as the blades of *L. digitata* (sample 1), the thin geotextile presented in Paul and Henry (2014) (sample 2), a coated geotextile (sample 3), and a thick silicone (sample 4). All the artificial samples were tested according to the ISO 9073-7:1998 standard and the present method adapted for in-situ measurements. Only samples 3 and 4 could be tested according to the ISO 178:2010 standard; the other two were too flexible to follow the same treatment. Finally, to assess the repeatability of the measure done with the field apparatus and the impact of the experimenter's judgment on the results of the tests, 10 people tested the four artificial samples using the protocol defined earlier. Thus, for each sample, means and standard deviations from the 10 tests were compared with a single measurement.

RESULTS

Table 1 presents the mean values of the cantilever lengths measured, as well as the bending moduli and the densities deduced from the measurements for the four testing procedures. When applicable, the standard deviations of the cantilever length measured and the calculated bending moduli are shown. Since the ISO 178:2010 standard (3-point bending test) calculates the bending modulus directly from the force deflection curves, only this last parameter is given. To analyze the standard

TABLE 1. Summary of the determination of cantilever length (l), the bending modulus (B_b), and density (ρ) for the four artificial samples via the two standardized methods and the field method.

			Standard tests						Tests with field apparatus					
			ISO 178:2010			ISO 903-7:1998			1 person			10 people		
Sample	Variable	Unit	Means	SD	CV %	Means	SD	CV %	Means	SD	CV %	Means	SD	CV %
1	l	cm				5.90	0.18	3.00	5.00	0.25	5.03	4.98	0.47	9.51
	E_b	MPa	—	—		4.40	0.41	9.27	3.31	0.79	23.8	3.32	0.93	28.0
	ρ	kg/m^3	—	—		1157.65	—		1268.29	—		1268.29	—	
2	l	m				7.80	0.55	7.00	7.63	0.36	4.71	7.58	0.38	5.05
	E_b	MPa	—	—		2.87	0.65	22.5	1.97	0.27	13.5	1.94	0.30	15.5
	ρ	kg/m^3	—	—		188.57	—		140.00	—		140.00	—	
3	l	m				11.00	0.33	3.00	11.18	0.33	2.99	10.81	0.37	3.41
	E_b	MPa	95.08	6.39	6.72	51.19	4.75	9.27	57.91	5.79	10.0	52.40	5.40	10.3
	ρ	kg/m^3	—	—		1188.57	—		1449.28	—		1449.28	—	
4	l	m				8.80	0.09	1.00	8.10	0.10	1.23	8.34	0.49	5.92
	E_b	MPa	9.42	0.90	9.60	8.59	0.26	3.03	7.98	0.34	4.27	8.79	1.52	17.3
	ρ	kg/m^3	—	—		1182.79	—		1460.87	—		1460.87	—	

Notes: Dimensions (L, b, t) in meters of sample 1, thin silicone (2.05×10^{-1}, 2.50×10^{-2}, 8.50×10^{-4}); sample 2, thin geotextile (2.00×10^{-1}, 2.50×10^{-2}, 7.00×10^{-4}); sample 3, coated geotextile (2.05×10^{-1}, 2.50×10^{-2}, 6.90×10^{-4}); sample 4, thick silicone (2.05×10^{-1}, 2.50×10^{-2}, 1.15×10^{-3}). Coefficient of variation CV was calculated as CV = 100·SD/mean. A dash (—) indicates that no measurement was done.

deviations (SDs) in the context of their means, the coefficients of variation CV (as percentage of the mean) are calculated as CV = 100·SD/mean. Density calculations (based on mass and size measurements) are reported and can be further used to choose a surrogate material for the blades of *L. digitata* (Paul and Henry, 2014). Because samples 1 and 2 were too thin and flexible, they could not be tested using the ISO 178:2010 standard, confirming that the 3-point bending test is not applicable to thin, flexible materials. Thus, only samples 3 and 4 could be tested according to both standardized methods, allowing a direct comparison of the two types of tests (3-point bending and Peirce's tests). The mean bending moduli for sample 4 is comparable with the two standardized tests (columns 1 and 4), and the standard deviations are relatively low. However, for sample 3, the bending modulus obtained with the ISO 178:2010 standard (3-point test) is almost double the bending modulus obtained with the ISO 9073-7:1998 standard (Peirce test). The associated standard deviations are both relatively low (CV < 10%) indicating small variations of the result for both measures. This point is discussed further in the next section.

In general, the results from the ISO 9073-7:1998 standard (standardized Peirce test) and the results from the tests with the field apparatus compare very well with similar mean values and standard deviations of the four samples (columns 4 to 9). Note that the coefficients of variations CV are in the range of 10–20% for samples 1, 2, and 3, compared with sample 4 with CV = 3.03% and CV = 4.27 for the two tests. Finally, when 10 people did the same test on the same materials, the mean values remained similar, but the standard deviation increased slightly; CV ranked between 10 and 28% for the four samples (columns 10 to 12). As mentioned previously, the statistics for the ISO 9073-7:1998 test and a single field test (columns 4 to 9) were based on four measurements, while the statistics for 10 tests with the field apparatus (columns 10 to 12) were based on $10 \times 4 = 40$ measures. The statistics for the ISO 178:2010 test (columns 1 to 3) were based on five measurements.

Figure 3 presents the temporal variation in the bending moduli from single tests with the field apparatus of the five samples of the algal blades (samples 5 to 9). It can be seen that for samples 6 to 9, there is no clear change in the mean bending modulus for each sample over time, and all the values are between 0.4 and 1.3 MPa. However, sample 5 clearly shows a temporal decrease of its bending modulus, starting around 3.5 MPa when the blade is cut and finishing in the same range as the other samples (0.85 MPa). In parallel, the change in the standard deviation does not appear to be time dependent, but after 15 min it is on average higher (SD ≈ 0.5, CV > 50%) for sample 5 and sample 8.

DISCUSSION

***Validation of the technique*—**First, the results presented highlight the fact that bending of thin, flexible materials cannot be tested with a 3-point bending technique (ISO 178:2010), but a Peirce test (ISO 9073-7:1998 and adapted field test) is suitable for thin materials with a low bending modulus (sample 2; 1–2 MPa). Both methods agreed reasonably well for determining

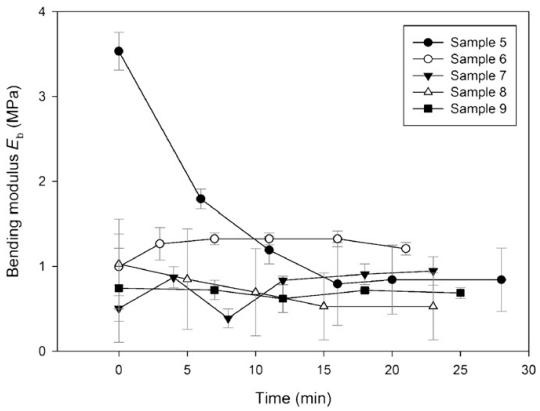

Fig. 3. Bending modulus over time of blades of *Laminaria digitata*, determined using the Peirce method adapted for the field. The time origin refers to the time when samples were cut. The standard deviation for the four measurements at each time point is indicated by light-gray error bars.

the bending modulus of the sample 3, indicating that the flexural rigidity of the sample is in the range of validity of both methods ($E_b \approx 10$ MPa, $t \approx 0.7$mm). Sample 3 seems to have a higher bending modulus than the other samples (around 100 MPa with ISO 178:2010; 50 MPa with ISO 9073-7:1998), which means that this strip is stiffer than the other strip tested. The methods disagreed on the value of the modulus of this stiffer strip, but the standard deviations of the value for the modulus of both strips are relatively low (CV < 10%), indicating that both measurements are trustable. Since only two materials could be tested with the two standardized methods, it is difficult to draw any conclusion, and further tests with different material should be done. However, in a Peirce-type test (ISO 9073-7:1998), the deflection of the strip depends on a balance between the weight of the strip and its stiffness. Therefore, this type of test is not adapted to stiffer material, while 3-point bending tests are valid for these materials. Thus, the most probable reason for the factor of two difference obtained from the two methods is that sample 3 is already too stiff for the bending modulus to be measured properly with the ISO 9073-7:1998 standard. Therefore, this study suggests that the 3-point bending test (ISO 178:2010) is applicable for strips stiffer than sample 4 (from Eq. 5, $J = 2.66 \times 10^{-2}$ Nm), while a Peirce-type test (ISO 9073-7:1998) is applicable for strips less stiff than sample 3 (from Eq. 5, $J = 5.23 \times 10^{-2}$ Nm). Based on the tests on *L. digitata*, flexural rigidity per unit width (J) was around 2 to 3×10^{-2} Nm, confirming the better suitability of the Peirce-type of test.

The comparison of the results between the standardized Peirce test (ISO 9073-7:1998) and the adapted field method shows that the use of a simplified field apparatus does not lessen the quality of the results (similar means and standard deviations). In addition, the mean values of the bending moduli of the four samples were similar whether one test was done with the field apparatus or 10 people did the test on the same apparatus. Thus, the bending moduli can be collected by several persons, and results can be compared across studies. The fact that the standard deviation of the moduli increases between 1 test and 10 tests is due to the increase of the population size to calculate the statistics (4 measures for one test, 40 measures for 10 tests). The increase of the standard deviation is more important for sample 4 (corresponding to an increase of CV from 4.27 to 17.3%). However, the final value lies within the range of the other samples, suggesting a more precise measurement for the single test on sample 4 than the others (with low SD).

As mentioned, no direct test on *L. digitata* blade was possible with the two standardized methods, but a good correlation between the results from the field apparatus and the standardized methods could be obtained for different type of materials: homogeneous (samples 1 and 4), inhomogeneous (samples 2 and 3), with different surface roughnesses of the strips, and different stiffnesses. By covering a wider range of different materials, it is reasonable to assume that the Peirce-type test with the field apparatus is valid for strip-like biomaterials, such as the blades of *L. digitata*.

***Bending moduli collection for blades of* L. digitata—**To the author's knowledge, Fig. 3 documents the first values of bending moduli collected for blades of *L. digitata*. Without focusing on temporal changes, all the mean values are in the range 0.4–3.5 MPa, which is one to two orders of magnitude smaller than the bending moduli found by Harder et al. (2006) for stipes of *L. digitata* (mean = 83.8 MPa, SD = 84.1 MPa). No study that compared the bending moduli of an algal stipe with the blade could be found, but our values lie in the average range for algal material, typically 1–100 MPa (Denny and Gaylord, 2002). In addition, the standard deviations obtained from the plant strips (samples 5 to 9) tend to be much greater than for the artificial materials (samples 1 to 4). For the artificial materials, the CVs were in the range of 5–30%, but CVs for the blades were sometimes over 50% (variations indicated by the error bars in Fig. 3). The reason for that is the "impurity" of the blade's material. This biomaterial is strongly inhomogeneous and anisotropic (Harder et al., 2006). In addition, the blades of *L. digitata* sometimes had a small curvature, and small epibionts (for example, bryozoans) may be present at the surface of the blade. Because these factors influence the bending of the strip under its own weight, it will equally influence the determination of the bending modulus of the strip, resulting in a larger standard deviation of the measurements. However, the bending modulus of a biomaterial is an idealized parameter, which does not reflect the reality of the mechanics of the different tissues of the plant part (Nikora, 2010). Therefore, the mean bending modulus should be considered as an estimation of the more complex bending properties of the plant's material, while the standard deviation of the modulus characterizing the variation of the measure gives an indication of the level of impurity/complexity of the material. These reasons also help explain why Harder et al. (2006) found a CV around 100% while determining the bending modulus of the stipes of some *L. digitata* (mean = 83.8 MPa, SD = 84.1 MPa).

In general, it is not clear to which extent cutting a plant strip for a mechanical test can affect its mechanical properties. This procedure is even more critical for the thin blades of macroalgae (fragile material), and the potential effects on the blade's mechanics is one of the reasons for carrying out time-dependent tests after the blades were cut. During the testing of the blades, the strips released a viscous liquid of unknown composition. After monitoring each strip for approximately 30 min (Fig. 3), it was observed that except for sample 5, their bending moduli were not affected. However, the bending modulus of sample 5 clearly decreased, suggesting a deterioration in the quality of the material over time. To the author's knowledge, this phenomenon is not documented and thus calls for further investigation. The fact that the blade strip can show signs of deterioration highlights the importance of testing the plant as close as possible to its environment, a requirement achievable with this alternative technique. However, other parts of macroalgae may prove to be more resistant to deterioriation; for example, in mechanical tests on stipes of *L. digitata* in the laboratory, there was little deterioration (Harder et al., 2006).

Conclusion—The method developed is suited for collecting data in the field and is valid for strip-like flexible materials. This simple and low cost method can be implemented by any researcher and lead to a good estimation of the bending modulus of a biomaterial. Cross comparisons between studies will be easier when a standard protocol is used. In case of biomaterials with a more complex structure (for example, undulating blades), other techniques in the same study by Peirce (1930, see the heart-loop method) can be validated as in the present study.

LITERATURE CITED

BIEDKA, R. F., J. M. GOSLINE, AND R. E. DE WREEDE. 1987. Biomechanical analysis of wave-induced mortality in the marine alga *Pterygophora californica*. *Marine Ecology Progress Series* 36: 163–170.

BOLLER, M. L., AND E. CARRINGTON. 2007. Interspecific comparison of hydrodynamic performance and structural properties among intertidal macroalgae. *Journal of Experimental Biology* 210: 1874–1884.

BOOTH, J. E. 1969. Principles of textile testing: An introduction to physical methods of testing textile fibres, yarns, and fabrics, 3rd ed. Chemical Publishing, New York, New York, USA.

BOUMA, T. J., M. B. DE VRIES, E. LOW, G. PERALTA, I. C. TÁNCZOS, J. VAN DE KOPPEL, AND P. M. J. HERMAN. 2005. Trade-offs related to ecosystem engineering: A case study on stiffness of emerging macrophytes. *Ecology* 86: 2187–2199.

DE LANGRE, E., A. GUTIERREZ, AND J. COSSÉ. 2012. On the scaling of drag reduction by reconfiguration in plants. *Comptes Rendus. Mécanique* 340: 35–40.

DEMES, K. W., E. CARRINGTON, J. GOSLINE, AND P. T. MARTONE. 2011. Variation in anatomical and material properties explains differences in hydrodynamic performances of foliose red macroalgae (Rhodophyta). *Journal of Phycology* 47: 1360–1367.

DENNY, M., AND B. GAYLORD. 2002. The mechanics of wave-swept algae. *Journal of Experimental Biology* 205: 1355–1362.

GAYLORD, B., AND M. DENNY. 1997. Flow and flexibility. I. Effects of size, shape and stiffness in determining wave forces on the stipitate kelps *Eisenia arborea* and *Pterygophora californica*. *Journal of Experimental Biology* 200: 3141–3164.

HALE, B. 2001. Macroalgal materials: Foiling fracture and fatigue from fluid forces. Ph.D. dissertation, Stanford University, Stanford, California, USA.

HARDER, D. L., C. L. HURD, AND T. SPECK. 2006. Comparison of mechanical properties of four large, wave-exposed seaweeds. *American Journal of Botany* 93: 1426–1432.

ISO [INTERNATIONAL ORGANIZATION FOR STANDARDIZATION]. 1998. ISO 9073-7:1998, Textiles. Test methods for nonwovens. Part 7: Determination of bending length. http://www.iso.org, ISO, Geneva, Switzerland.

ISO. 2010. ISO178:2010, Plastics. Determination of flexural properties. www.iso.org, ISO, Geneva, Switzerland.

JOHNSON, A., AND M. KOEHL. 1994. Maintenance of dynamic strain similarity and environmental stress factor in different flow habitats: Thallus allometry and material properties of a giant kelp. *Journal of Experimental Biology* 195: 381–410.

KOEHL, M. A. 1999. Ecological biomechanics of benthic organisms: Life history, mechanical design and temporal patterns of mechanical stress. *Journal of Experimental Biology* 202: 3469–3476.

LAMOUROUX, J. V. F. 1813. Essai sur les genres de la famille des thalassiophytes non articulées. *Annales du Muséum d'Histoire Naturelle, Paris* 20: 21–47, 115–139, 267–293, pls. 7–13.

LUHAR, M., AND H. M. NEPF. 2011. Flow-induced reconfiguration of buoyant and flexible aquatic vegetation. *Limnology and Oceanography* 56: 2003–2017.

LÜNING, K. 1990. Seaweeds: Their environment, biogeography, and ecophysiology. Wiley & Sons, New York, New York, USA.

MARTONE, P. T., AND M. W. DENNY. 2008. To break a coralline: Mechanical constraints on the size and survival of a wave-swept seaweed. *Journal of Experimental Biology* 211: 3433–3441.

MILER, O., I. ALBAYRAK, V. NIKORA, AND M. O'HARE. 2012. Biomechanical properties of aquatic plants and their effects on plant–flow interactions in streams and rivers. *Aquatic Sciences* 74: 31–44.

NEPF, H. M. 2012. Flow and transport in regions with aquatic vegetation. *Annual Review of Fluid Mechanics* 44: 123–142.

NIKLAS, K. J. 1992. Plant biomechanics: An engineering approach to plant form and function. University of Chicago Press, Chicago, Illinois, USA.

NIKLAS, K. J., H.-C. SPATZ, AND J. VINCENT. 2006. Plant biomechanics: An overview and prospectus. *American Journal of Botany* 93: 1369–1378.

NIKORA, V. 2010. Hydrodynamics of aquatic ecosystems: An interface between ecology, biomechanics and environmental fluid mechanics. *River Research and Applications* 26: 367–384.

NIKORA, V., S. CAMERON, I. ALBAYRAK, O. MILER, N. NIKORA, F. SINISCALCHI, M. STEWART, AND M. O. HARE. 2012. Flow–biota interactions in aquatic systems: Scales, mechanisms and challenges. *In* W. Rodi and M. Uhlmann [eds.], Environmental fluid mechanics, 217–235. CRC Press, Boca Raton, Florida, USA.

PAUL, M., AND P. Y. T. HENRY. 2014. Evaluation of the use of surrogate *Laminaria digitata* in eco-hydraulic laboratory experiments. *Journal of Hydrodynamics*: in press.

PAUL, M., P. Y. T. HENRY, AND R. E. THOMAS. 2014. Geometrical and mechanical properties of four species of northern European brown macroalgae. *Coastal Engineering* 84: 73–80.

PEIRCE, F. T. 1930. The "handle" of cloth as a measurable quantity. *Journal of the Textile Institute Transactions* 21: T377–T416.

STEWART, H. L. 2004. Hydrodynamic consequences of maintaining an upright posture by different magnitudes of stiffness and buoyancy in the tropical alga *Turbinaria ornata*. *Journal of Marine Systems* 49: 157–167.

STEWART, H. L. 2006. Ontogenetic changes in buoyancy, breaking strength, extensibility, and reproductive investment in a drifting macroalga *Turbinaria ornata* (Phaeophyta). *Journal of Phycology* 42: 43–50.

SZABLEWSKI, P., AND W. KOBZA. 2003. Numerical analysis of Peirce's cantilever test for the bending rigidity of textiles. *Fibres and Textiles in Eastern Europe* 11: 54–57.

YOUNG, W., R. BUDYNAS, AND A. SADEGH. 2011. Roark's formulas for stress and strain, 8th ed. McGraw-Hill Education, New York, New York, USA.

PAPER VI

Henry, P.-Y.T., Nedrebø, E. L., Myrhaug, D., [**2016**]. Visualisation of the effect of different types of marine growth on cylinders' wake structure in low Re steady flows. *Ocean Engineering*, In Press (Uncorrected proof).

Ocean Engineering 115 (2016) 182–188

Contents lists available at ScienceDirect

Ocean Engineering

journal homepage: www.elsevier.com/locate/oceaneng

Short Communication

Visualisation of the effect of different types of marine growth on cylinders' wake structure in low *Re* steady flows

Pierre-Yves Henry*, Eirik Leikvoll Nedrebø, Dag Myrhaug

Department of Marine Technology, Norwegian University of Science and Technology, No. 7491 Trondheim, Norway

ARTICLE INFO

Article history:
Received 3 July 2015
Accepted 7 February 2016
Available online 22 February 2016

Keywords:
Visualisation
Marine growth
Wake structure
Circular cylinders
Low Reynolds number
Steady flow

ABSTRACT

Marine growth is a large technical, economic and environmental problem for almost all activities at sea. Circular cylinders being widely used in different types of offshore structures, this study focuses on the effects of different types of marine growth on cylinders' wake structure for low *Re* steady flows ($2.16 \times 10^3 < Re < 1.94 \times 10^4$). Qualitative results from wake visualisations and simple drag force measurements confirmed that soft and hard roughnesses have completely different effects on the cylinder hydrodynamics for the transitional subcritical regime, as soft fouling act as a passive flow separation control. This study highlights the changes on the cylinder hydrodynamics induced by a developing fouling community, going from small hard roughnesses to fully developed soft fouling.

1. Introduction

When a structure is submerged in the ocean, marine micro-organisms concentrate from the beginning at the water/hard body interfaces, initiating the settlement of a more complex fouling community on the structure (Cooksey and Wigglesworth-Cooksey, 1995; Jonsson et al., 2004; Kerckhof et al., 2010; Railkin, 2003). In return, these fouling communities cause the flow around the structure to be altered as compared to without fouling, which in general affect its performances (Heaf, 1979). As a consequence, marine fouling is a large technical, economic and environmental problem for almost all activities at sea, receiving an early interest from oil and gas industries (Houghton, 1978), naval industries (Woods Hole Oceanographic Institution, 1952), and more recently aquaculture (Fitridge et al., 2012) and marine renewable energy industries (Gill, 2005; Langhamer et al., 2009). The consequences of marine fouling range from issues such as higher fuel costs and emissions from ships, to lower the fatigue life for offshore structures or physical blockage of important systems, and by concealing cracks and corrosion on a structure (Edyvean et al., 1988). Thus, characterising the hydrodynamics of marine growth is crucial to understand its effects when designing, installing and operating offshore structures (El-Reedy, 2014; Engel and Ray, 1985; Iberahin and Wolfram, 1996). The extent of the problem can be reduced by using anti-fouling paint or by regularly inspecting and removing the marine fouling, but this can be both expensive and environmentally unfriendly. Especially the use of toxic anti-fouling paints has caused great harm to the environment over the years (Karlsson et al., 2010; Katranitsas et al., 2003). Gradually, such paints have been banned from the market, and this has made surface coating more challenging and costly for the maritime industry (Banerjee et al., 2011). However, innovative non-toxic physico-chemical antifouling strategies (Magin et al., 2010) and antifouling solutions inspired from biological processes (enzyme-based coatings, see Olsen et al. (2007)) are being developed with success, offering future solutions to the fouling issue.

Marine growth varies in time and space. The fouling process starting at a molecular level, micro-communities (bacteria, microalgae, fungi) and then macro-communities (macroalgae, invertebrates) later develop at the surface of the structure, sometime hosting a more complex ecosystem (Langhamer, 2009). Once fully grown, the fouling community may also vary depending on the changing hydrodynamic conditions and seasonal variations. In general, the composition of the community will depend on the average temperature, turbidity, depth (Iberahin and Wolfram, 1996), distance from the coast, and type of seabed; thus making marine growth a site-specific process. Finally, the species composing the fouling community mostly depend on larval and spore dispersion, thus relying on turbulent diffusion processes in the wake of the structure (Langhamer, 2009).

From an engineering point of view, marine growth has an impact on the hydrodynamic properties of a structure by increasing its projected area and the surface roughness (increasing the drag and inertia coefficients), and this modifies the properties of the structure by increasing its mass, which in return decreases

* Corresponding author.
E-mail address: pierre-yves.henry@ntnu.no (P.-Y. Henry).

http://dx.doi.org/10.1016/j.oceaneng.2016.02.023
0029-8018/

its natural frequency (Shi et al., 2012). Circular cylinders are widely used as structural members in different types of offshore structures, and therefore their hydrodynamics has been thoroughly studied and well documented (Sumer and Fredsøe, 1997; Williamson, 1996; Zdravkovich, 1997). Investigations on the effects of surface irregularities on the surface of circular cylinders in steady currents began in the 1930s, when Fage and Warsap (1930) measured the drag on circular cylinders with different sand paper coverings. Later, Achenbach and Heinecke (1981) conducted similar experiments investigating the vortex shedding. These types of experiments often focus on hard marine growth, such as models of mussel colonisation, but fewer studies consider soft growth due to the difficulty to link artificial yarn properties to biomechanical properties of soft organisms (Baarholm and Skaugset, 2008). However, there is an increasing interest of the aerodynamic science community as poroelastic systems offer an efficient passive flow control solution (Favier et al., 2009; Gosselin and de Langre, 2011).

In order to identify and understand the hydrodynamics of the different types of marine growth, this study highlights the main effects of hard and soft marine fouling on the wake structure behind a cylinder using visualisation techniques, and characterises the variations induced on the bulk forces in low *Re* number steady flows ($2.16\times10^3 < Re < 1.94\times10^4$). This experimental study provides qualitative information on the flow regime changes on a single cylinder that occurs at different stages of the fouling process.

2. Material and methods

2.1. Experimental set-up

Experiments were conducted in the circulating water tunnel (CWT) at the Department of Marine Technology at the Norwegian University of Science and Technology (NTNU). The test section is 2.50 m long, 0.61 m wide and 0.54 m deep; while the flume has a total length of 9.10 m. The incoming free-stream turbulence intensity is 1% of the mean speed. The set-up consisted of a stiff frame made of Rexroth tubes fixed to the top of the CWT, on which a force sensor was mounted (PW4MC3 single point load cell from HBM GmbH). The cylinder was stiffly attached to the sensor via a connection especially designed for this purpose, and the other end remained free, 4 cm above the bottom of the flume (Fig. 1). As the main focus of these pilot tests was on the fouling effect on of the mean drag forces, a single load cell was aligned to measure the streamwise forces. At lower velocities, oscillating forces from vortex shedding were too small to be registered with this set-up. At higher velocities vortex induced vibrations occurred, and the standard deviation of the drag force measurement time series suddenly increased (from $\sigma < 0.1$ N to $\sigma > 1.5$ N). As the cylinder was only clamped in its upper part, these vibrations led to a visible movement of the cylinder. In order to make sure that this process did not bias the observations made, the standard deviation criterion has been used to discard measurements where vortex induced vibrations where too large to be assumed neglectable regarding the cylinders' hydrodynamics. The load cell was connected to a computer via an *A*/*D* converter where the drag time series were saved. The bulk drag force *F* was then taken as the time average of each force time series (3 min at 100 Hz). Velocities are given in terms of the bulk velocities U_{bulk}, deduced by dividing the discharge of the pumps by the wet cross section of the flume. Bulk drag coefficients C_D were defined for each run as $C_D = F/0.5\,\rho\,LD\,U_{\text{bulk}}^2$, where ρ is the density of water (rounded to 1000 kg/m^3), *D* the diameter of the smooth cylinder, and *L* is the length of the cylinder in water. Drag forces and drag coefficients are reported for each of the conditions tested in Fig. 2, and discussed in Section 3.

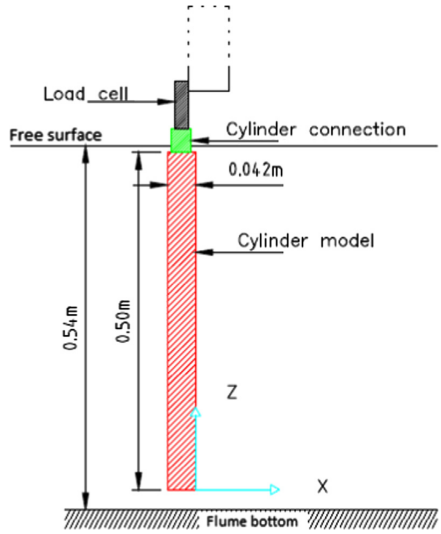

Fig. 1. Test set-up as seen from the side of the tank. Water flowing in the positive *x* direction.

2.2. Visualisation technique

Flow visualizations were carried out by inserting fluorescent dye just upstream of the cylinder and using UV light to reveal the colours. The dye was inserted at mid-length of the cylinder to minimize boundary effects (free end and free surface). Video records were taken with a Canon EOS 5D, having a frame resolution of 1920×1080 at 23 fps. Single frames were extracted to document the wake structure. The vortex shedding frequency *f* was estimated as half the number of vortex structures advected downstream divided by the duration of the video record. The Strouhal number is then calculated as $St = \frac{fD}{U_{\text{bulk}}}$. Visualisations of the different wake developments are reported in Figs. 3–5 for the different cylinder tested.

2.3. Experimental conditions

Five steel cylinder models with the same dimensions (0.5 m long, $D = 42$ mm) were used in the experiments; one smooth cylinder for reference, and four cylinders covered with different types of artificial roughness. The cylinders are henceforth referred to as cylinders 1–5, where cylinder 1 is the smooth reference cylinder, cylinders 2–4 are the hard roughened cylinders, and cylinder 5 is coated with an artificial fur made out of synthetic fibres (42% modacrylic, 42% polyacrylic, 16% polyester), with the fibres having an approximately equal length of 34 mm (Table 1). Drag force measurements were carried out for 3 min for each of the 10 different flow speeds (from 0.058 m/s to 0.526 m/s), the Reynolds number varying from 2.16×10^3 to 1.94×10^4 ($Re = U_{\text{bulk}}D/\nu$, where $\nu = 1\times10^{-6}$ m^2/s is the kinematic viscosity of the fluid). The repeatability of these tests has been checked, and the flow visualisations were realised at a flow speed of 0.21 m/s only ($Re = 7.73\times10^3$).

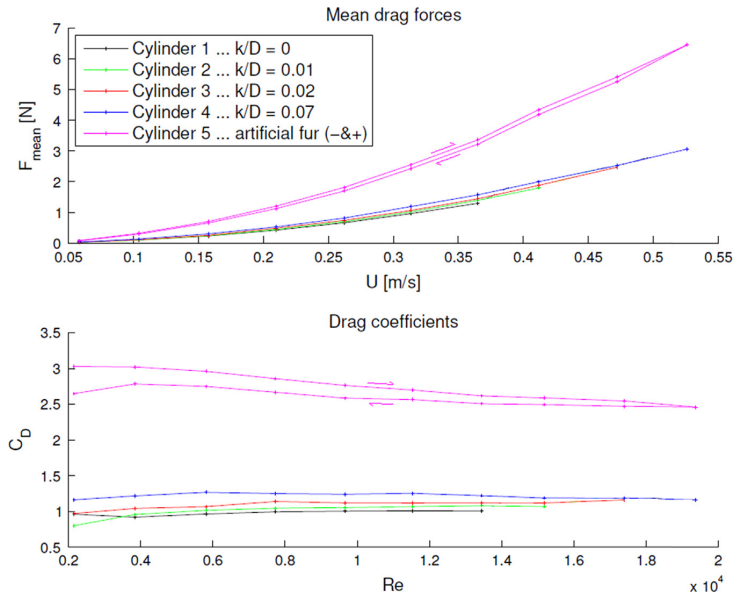

Fig. 2. Mean drag forces and drag coefficients for each cylinder.

3. Results and discussion

Even though *St* and C_D-coefficients are derived from these observations, the results of this study remain qualitative as the facilities and the set-up used does not allow for precise measurements of cylinders' hydrodynamics.

3.1. Smooth cylinder

With *Re* in the range $2.16\times10^3-1.94\times10^4$ for all these observations, the vortex shedding regime can be qualified as a shear-layer transition regime for the smooth cylinder, i.e. as part of the sub-critical regime (Williamson, 1996). As can be seen in Fig. 3 for the cylinder 1, this regime is characterised by a two-dimensional laminar-like vortex shedding mode together with fine-scale two- and three-dimensional vortex structures developing from the shear layer Kevin–Helmholtz instabilities at the sides of the cylinder (Williamson, 1996). The video records suggest the presence of a small recirculation region behind the cylinder at $Re=7.73\times10^3$, with a formation length of about one to two cylinder diameter (see Fig. 3), which is in agreement with previous investigations (Norberg, 1998; Unal and Rockwell, 1988; Zhou et al., 2015). For this condition, *St* for the smooth cylinder is estimated to about 0.19 (Table 1), which is typical of the vortex-shedding process at this *Re* (Sumer and Fredsøe, 1997; Unal and Rockwell, 1988). The value of the bulk C_D-coefficient derived from these tests for the range $2.16\times10^3<Re<1.94\times10^4$ is $C_D=0.9$, which is slightly lower than the value expected for this range (around 1.1, see Schlichting and Gersten (2000) or Sumer and Fredsøe (1997)). This discrepancy is expected to come from the experimental set-up used (free end at the lower part of the cylinder, bulk velocity and force measurements). However, the value of C_D tends to confirm that these tests are in the shear-layer transition regime (Williamson, 1996), or sub-critical regime (Sumer and Fredsøe, 1997).

3.2. Hard roughness

One of the assumption of this study is to represent marine hard fouling (such as barnacles and mussels) by an equivalent sand roughness. Although this practice has been reported as acceptable (Miller, 1976), and is still commonly used (Baarholm and Skaugset, 2008), the roughness characteristics between sand grains and barnacle/mussel colonies are obviously different, potentially affecting the boundary layer at the surface of the cylinder. In addition, Theophanatos (1988) pointed out that the parameter *k/D* might not be the best roughness parameter to characterise hard marine fouling as other parameters, such as roughness skewness, distribution, or coverage have been shown to have a greater influence on cylinders' hydrodynamics. Ameryoun (2015) recently reviewed these challenges and introduced a stochastic approach to describe the roughness of hard marine fouling in time and space. However, as the aim of this study is to provide qualitative information on the evolution of the cylinder hydrodynamics during the development of a fouling community (from small hard roughnesses to fully developed soft fouling), the representation of hard marine growth by surfaces with sand roughness can be considered as an appropriate approximation of hard marine roughness.

Although an increasing roughness at the cylinder's surface lowers the critical Reynolds number at which the drag crisis occurs (sudden decrease of the drag coefficient due to the transition from laminar to turbulent boundary layer, see Achenbach and Heinecke (1981)), the range of conditions tested appears to remain below this critical *Re* as the bulk C_D-coefficients derived for each test remains relatively constant over the *Re*-range tested (Fig. 2). From Table1 and Fig. 2 it can be seen that C_D increases from 0.9 to 1.24 as *k/D* increases from 0 to 0.07. This confirms that for a transitional subcritical regime, hard marine growth increases the drag coefficient, and thus the drag forces. These results are in agreement with the conclusions of Zhou et al. (2015). In addition, Table 1 highlights the fact that the shedding frequency and the *St*-number decrease as the roughness increases; i.e. at $Re=7.73\times10^3$ *f* decreases from 0.93 Hz to 0.63 Hz, and *St* decreases from 0.19 to

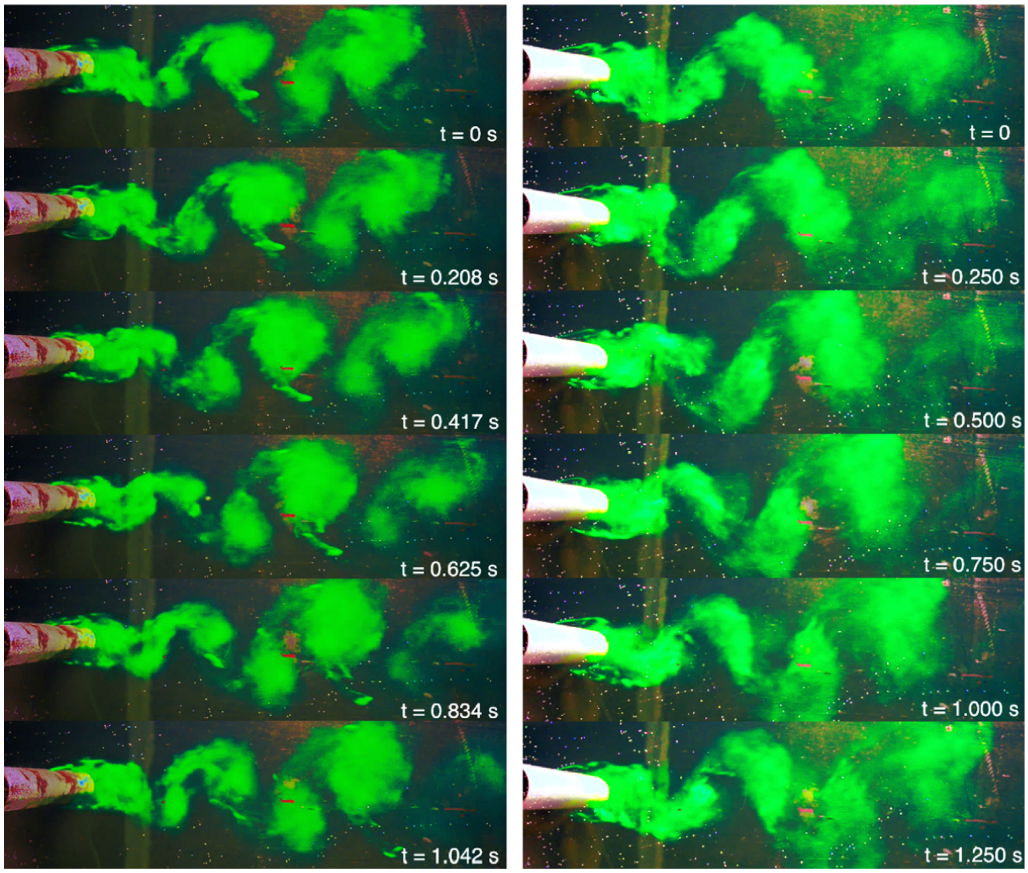

Fig. 3. Time series of flow visualisation at $Re=7.73\times10^3$ for cylinders 1 (left, smooth) and 2 (right, $k/D=0.01$).

0.13 as k/D increases from 0 to 0.07 (Adachi, 1997). For this experimental set-up, this phenomenon delays the appearance of Vortex Induced Vibrations (VIV), which is confirmed by the fact that vibrations of the cylinder were not detected for $k/D=0.07$ for the Re-range tested, while VIV were detected for the smooth cylinder ($k/D=0$) for $Re>1.4\times10^4$. Note that the effect of the roughness on these parameters may be influenced by the type and the shape of the roughness elements (Achenbach and Heinecke, 1981).

Figs. 3 and 4 indicate that the morphology of the vortex street at $Re=7.73\times10^3$ is very similar for the three roughened cylinders (cylinders 2–4) compared to the smooth case. However, in addition to the change of shedding frequency, it can be seen that the width of the vortex street increases for the roughnesses $k/D=0.01$ (Fig. 3, right) and $k/D=0.02$ (Fig. 4, left) compared to the smooth case (Fig. 3, left), while for the rough case ($k/D=0.07$, Fig. 4 right) it decreases compared to the lower roughnesses. Regarding the wake structure in the vicinity of the cylinder, Zhou et al. (2015) found that for subcritical Re, the formation length of the recirculation region behind the cylinder is expected to decrease with increasing roughness for $Re<1.2\times10^4$. However, this result as well as the position of the flow separation on the cylinder wall cannot be observed from the present video records as the area covered (10D to 11D downstream) is too large to see the details of the cylinder and of the recirculation zone.

3.3. Soft/flexible fouling

The soft fouling modelled here by the artificial fur has a different impact on the flow compared to a hard sand roughness as the interface between the cylinder and the fluid is now a poroelastic system, as described by Gosselin and de Langre (2011) and Favier et al. (2009). Because each single element of the fur adapts and bends to counteract the near-wall separated flow, the fur dampens the initiation of the larger scale vortices and elongates the recirculation region behind the cylinder (Favier et al., 2009). From Fig. 5 it can be seen that the formation length is about 6–7 cylinder diameters, compared to 1–2 diameters for the smooth case. The Kevin–Helmoltz instabilities generated on the sides of the cylinder are more visible and propagate along the elongated recirculation region behind the cylinder. The vortex shedding generated by these instabilities is characterised by a much lower shedding frequency compared to the smooth case ($f=0.44$ Hz, Table1), giving $St=0.09$. In addition to stabilise and modify the shedding process in the wake of the cylinder, the fur increases dramatically the drag forces on the cylinder, leading to a C_D in the range 2.5–3 (Fig. 2), confirming the findings of Favier et al. (2009). However this result is to be linked to the fur high density, which acts as a thick porous media. For some lower yarn densities, one might expect a drag reduction, as small sparse “hairy” surface can reduce the shear stress generated at the surface of the cylinder

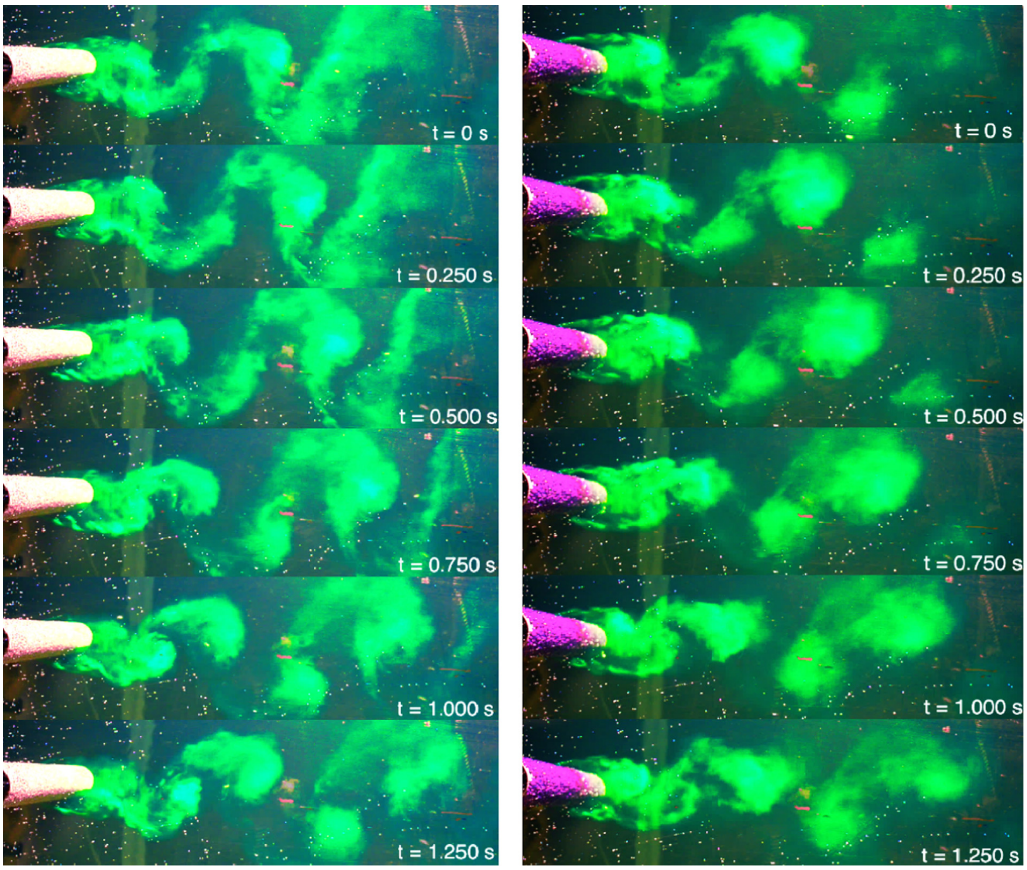

Fig. 4. Time series of flow visualisation at $Re=7.73\times10^3$ for Cylinders 3 (left, $k/D=0.02$) and 4 (right, $k/D=0.07$).

Table 1
Main characteristics of the modelled artificial marine growth, vortex shedding frequency, Strouhal number and drag force coefficient for the five cylinders.

Cylinder no. Coating description	1 Smooth surface	2 Fine grained sand	3 Medium grained sand	4 Coarse sand	5 Artificial fur
Mean grain size (μm)	0	427.5	900	3000	–
Relative roughness k/D	0	0.01	0.02	0.07	–
Mean yarn length (mm)	–	–	–	–	34
Mean yarn diameter (mm)	–	–	–	–	0.02
Yarn density (per cm^2)	–	–	–	–	~400
f (Hz) at $Re=7.73\times10^3$	0.93	0.77	0.73	0.63	0.44
St at $Re=7.73\times10^3$	0.19	0.15	0.15	0.13	0.09
C_D for $2\times10^3<Re<2\times10^4$	0.9	1.06	1.12	1.24	2.7[a]

[a] Varying from 2.5 to 3 due to different yarn alignments in the flow.

compared to the smooth cylinder case (see e.g. the review from Bechert et al. (1997)). Note that in Fig. 2, the force–velocity curves for Cylinder 5 have been obtained by first increasing the flow rate (upper curve), and then decreasing it (lower curve). This hysteresis reveals the dependence of the yarn position to the previous flow condition. Due to yarn-to-yarn interactions, extra forces are required to align the yarns in the flow direction as the flow increases, while when the flow decreases, the yarns are already aligned providing a more streamlined surface.

Soft marine fouling can be very diverse with algae going from a couple of centimetres to the largest kelp species, and including more diverse forms as biofilms or sea anemones (Ameryoun, 2015). Thus the fur used in these experiments is a simplified representation of the structure of such biological assemblages. In natural conditions, one might expect these assemblages of soft marine fouling to be less dense (more porous), more flexible and with a greater spatial heterogeneity compared to the dense artificial fur tested in this study. This simplification gives, however, a good example of the potential impact of soft marine fouling on cylinders' hydrodynamics.

4. Concluding remarks

The current visualisation study confirmed that soft and hard roughnesses have completely different effects on the cylinder hydrodynamics. In the subcritical regime, hard roughness enhances slightly the drag forces on the cylinder; reduces the shedding frequency; and increases the vortex street width for small roughnesses, while it decreases again for the largest roughness. On the other hand, soft fouling interacts strongly with the vortex

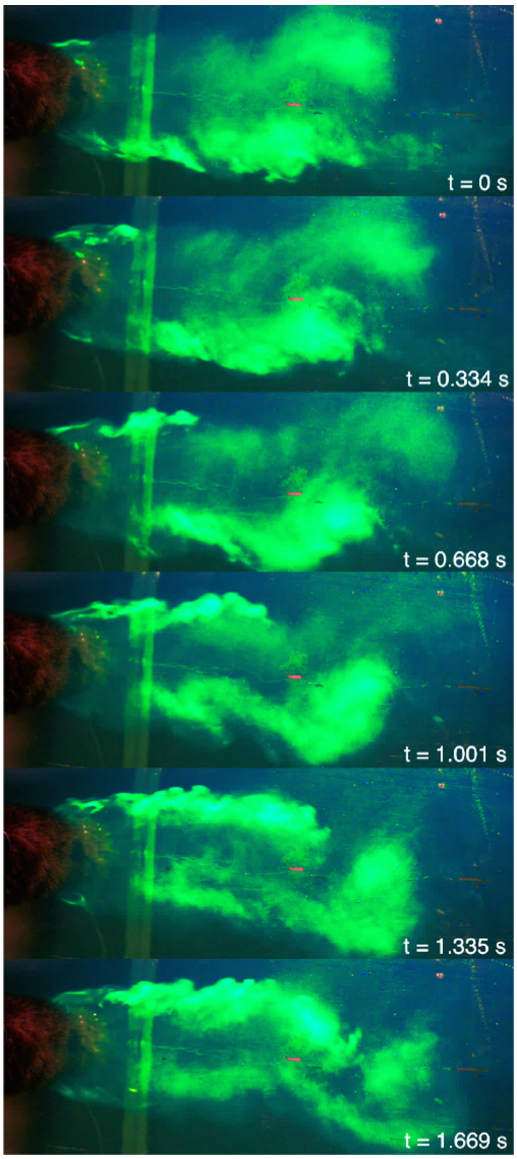

Fig. 5. Time series of flow visualisation at $Re = 7.73 \times 10^3$ for cylinder 5 (artificial fur).

shedding processes by stabilising the cylinder wake. As a result, the length of the recirculation region behind the cylinder increases about 5 times, and the shedding frequency is reduced significantly. This is of major importance for both industrial and ecological considerations. By stabilising the wake, soft marine fouling modifies the conditions of occurrence of VIV, and is recognized as a passive separation control solution in different aerodynamic applications (Favier et al., 2009). Furthermore, by creating an extended recirculation zone behind the cylinder, soft marine fouling increases the mixing processes in the vicinity of the cylinder, which is the key to successful reproduction and spore dispersion for many marine (benthic) species, and shelter pelagic species (Langhamer, 2009). In terms of impacts of the marine fouling on the cylinder hydrodynamics, this study highlights the changes involved with a developing fouling community, going from small hard roughnesses to fully developed soft fouling.

References

Achenbach, E., Heinecke, E., 1981. On vortex shedding from smooth and rough cylinders in the range of Reynolds numbers 6×10^3 to 5×10^6. J. Fluid Mech. 109, 239–251.

Adachi, T., 1997. Effects of surface roughness on the universal strouhal number over the wide Reynolds number range. J. Wind Eng. Ind. Aerodyn. 69–71 (0), 399–412.

Ameryoun, H., 2015. Probabilistic Modeling of Wave Actions on Jacket Type Offshore Wind Turbines in Presence of Marine Growth. 267. University of Nantes, Nantes (France).

Baarholm, R., Skaugset, K., 2008. Modelling and characterization of artificial marine growth. In: Proceedings of the ASME 2008 27th International Conference on Offshore Mechanics and Arctic Engineering, pp. 863–870.

Banerjee, I., Pangule, R.C., Kane, R.S., 2011. Antifouling coatings: recent developments in the design of surfaces that prevent fouling by proteins, bacteria, and marine organisms. Adv. Mater. 23 (6), 690–718.

Bechert, D., Bruse, M., Hage, W., Meyer, R., 1997. Biological surfaces and their technological application-laboratory and flight experiments on drag reduction and separation control In: Proceedings of the 28th Fluid Dynamics Conference. Fluid Dynamics and Co-located Conferences. American Institute of Aeronautics and Astronautics.

Cooksey, K.E., Wigglesworth-Cooksey, B., 1995. Adhesion of bacteria and diatoms to surfaces in the sea: a review. Aquat. Microb. Ecol. 09 (1), 87–96.

Edyvean, R.G.J., Thomas, C.J., Brook, R., 1988. The effect of marine fouling on fatigue and corrosion-fatigue of offshore structures. In: Houghton, D.R., Smith, R.N., Eggins, H.O.W. (Eds.), Biodeterioration, vol. 7. Springer, Netherlands, pp. 385–390.

El-Reedy, M., 2014. Marine Structural Dessign Calculations. Butterworth-Heinemann, Oxford, p. 456.

Engel, R., Ray, J., 1985. Bio-shield: an anti-fouling system for offshore platforms that works! In: Proceedings of the Oceans'85—Ocean Engineering and the Environment, pp. 62–70.

Fage, A., Warsap, J.H., 1930. The effects of turbulence and surface roughness on the drag of a circular cylinder. H. M. Station. Off.

Favier, J., Dauptain, A., Basso, D., Bottaro, A., 2009. Passive separation control using a self-adaptive hairy coating. J. Fluid Mech. 627, 451–483.

Fitridge, I., Dempster, T., Guenther, J., de Nys, R., 2012. The impact and control of biofouling in marine aquaculture: a review. Biofouling 28 (7), 649–669.

Gill, A.B., 2005. Offshore renewable energy: ecological implications of generating electricity in the coastal zone. J. Appl. Ecol. 42 (4), 605–615.

Gosselin, F.P., de Langre, E., 2011. Drag reduction by reconfiguration of a poroelastic system. J. Fluids Struct. 27 (7), 1111–1123.

Heaf, N.J., 1979. The effect of marine growth on the performance of fixed offshore platforms in the north sea. In: Proceedings of the Offshore Technology Conference.

Houghton, D.R., 1978. Marine fouling and offshore structures. Ocean Manag. 4 (2–4), 347–352.

Iberahin, J., Wolfram, J., 1996. Effects of marine growth and hydrodynamic loading on offshore structures. J. Mek. 1 (1), 77–96.

Jonsson, P.R., Berntsson, K.M., Larsson, A.I., 2004. Linking larval supply to recruitment: flow-mediated control of initial adhesion of barnacle larvae. Ecology 85 (10), 2850–2859.

Karlsson, J., Ytreberg, E., Eklund, B., 2010. Toxicity of anti-fouling paints for use on ships and leisure boats to non-target organisms representing three trophic levels. Environ. Pollut. (Barking, Essex: 1987) 158 (3), 681–687.

Katranitsas, A., Castritsi-Catharios, J., Persoone, G., 2003. The effects of a copper-based antifouling paint on mortality and enzymatic activity of a non-target marine organism. Mar. Pollut. Bull. 46 (11), 1491–1494.

Kerckhof, F., Rumes, B., Jacques, T., Degraer, S., Norro, A., 2010. Early development of the subtidal marine biofouling on a concrete offshore windmill foundation on the thornton bank (southern north sea): first monitoring results. Int. J. Soc. Underw. Technol. 29 (3), 137–149.

Langhamer, O., 2009. Wave Energy Conversion and the Marine Environment: Colonization Patterns and Habitat Dynamics. Uppsala University, Acta Universitatis Upsaliensis, Uppsala, p. 50 pp.

Langhamer, O., Wilhelmsson, D., Engström, J., 2009. Artificial reef effect and fouling impacts on offshore wave power foundations and buoys – a pilot study. Estuar. Coast. Shelf Sci. 82 (3), 426–432.

Magin, C.M., Cooper, S.P., Brennan, A.B., 2010. Non-toxic antifouling strategies. Mater. Today 13 (4), 36–44.

Miller, B.L., 1976. The hydrodynamic drag of roughened circular cylinders, The Royal Institution of Naval Architects, Spring Meeting. National Maritime Institute, Feltham, pp. 55–70.

Norberg, C., 1998. Ldv-measurements in the near wake of a circular cylinder. Advances in Understanding of Bluff Body Wakes and Vortex-Induced Vibration, Washington D.C.

Olsen, S.M., Pedersen, L.T., Laursen, M.H., Kiil, S., Dam-Johansen, K., 2007. Enzyme-based antifouling coatings: a review. Biofouling 23 (5), 369–383.

Railkin, A.I., 2003. Marine Biofouling: Colonization Processes and Defenses. CRC Press. Taylor & Francis, Boca Raton, FL, USA.
Schlichting, H., Gersten, K., 2000. Boundary-Layer Theory. XXIII. Springer-Verlag, Berlin, Heidelberg, p. 800.
Shi, W., et al., 2012. Study on the marine growth effect on the dynamic response of offshore wind turbines. Int. J. Precis. Eng. Manuf. 13 (7), 1167–1176.
Sumer, B.M., Fredsøe, J., 1997. Hydrodynamics Around Cylindrical Structures. World Scientific, Singapore.
Theophanatos, A., 1988. Marine growth and the hydrodynamic loading of offshore structures. Strathclyde University, Glasgow (United Kingdom), p. 274.
Unal, M.F., Rockwell, D., 1988. On vortex formation from a cylinder. Part 1. The initial instability. J. Fluid Mech. 190, 491–512.
Williamson, C.H.K., 1996. Vortex dynamics in the cylinder wake. Annu. Rev. Fluid Mech. 28 (1), 477–539.
Woods Hole Oceanographic Institution, 1952. Marine Fouling and its Prevention, United States Naval Institute, United States. Navy Department Bureau of Ships.
Zdravkovich, M.M., 1997. Flow Around Circular Cylinders: A Comprehensive Guide Through Flow Phenomena, Experiments, Applications, Mathematical Models, and Computer Simulations. Oxford University Press, Oxford, New York.
Zhou, B., Wang, X., Gho, W.M., Tan, S.K., 2015. Force and flow characteristics of a circular cylinder with uniform surface roughness at subcritical Reynolds numbers. Appl. Ocean Res. 49 (0), 20–26.

PAPER VII

Detert, M., Weitbrecht, V., Aberle, J., Rowinski, P., **Henry, P.Y.** [**2015]**. 6.5 Auxiliary hydrodynamic variables, in "Experimental hydraulics: Methods, Instrumentation, Data processing & Management" by Muste et al. *IAHR Monograph* under publication process, Taylor & Francis.

Is not included due to copyright

APPENDIX I

Thomas, R.E. Johnson, M., Frostick, L., Parsons, D., Bouma, T.J., Dijkstra, J., Eiff, O., Gobert, S., **Henry, P.Y. T.**, Kemp, P., McLelland, S., Moulin, F.Y., Myrhaug, D., Neyts, A., Paul, M., Penning, E., Puijalon, S., Rice, S., Stanica, A., Tagliapietra, D., Tal, M., Tørum, A., Vousdoukas, M., [**2014**]. Physical modelling of water, fauna and flora: Knowledge gaps, avenues for future research and infrastructural needs. *Journal of Hydraulic Research*, 52(3): 311-325.

Is not included due to copyright

APPENDIX II

Thomas, R.E., McLelland, S., **Henry, P.Y.,** Paul, M., Eiff, O., Evertsen, A.J., Aberle, J., Teacă, A. [**2015**]. Not all Laminaria digitata are the same! Phenotypic plasticity and the selection of appropriate surrogate macroalgae for ecohydraulic experimentation. *EGU General Assembly*; 2015 Vienna.

Geophysical Research Abstracts
Vol. 17, EGU2015-13349-1, 2015
EGU General Assembly 2015

Not all Laminaria digitata are the same! Phenotypic plasticity and the selection of appropriate surrogate macroalgae for ecohydraulic experimentation

Robert E. Thomas (1), Stuart J. McLelland (2), Pierre-Yves T. Henry (3), Maike Paul (4), Olivier Eiff (5), Antti-Jussi O. Evertsen (3), Jochen Aberle (3), and Adrian Teacă (6)

(1) Earth & Environment, University of Leeds, Leeds, United Kingdom (r.e.thomas02@members.leeds.ac.uk), (2) Geography, Environment and Earth Sciences, University of Hull, Hull, United Kingdom, (3) Faculty of Engineering Science and Technology, Norwegian University of Science and Technology (NTNU), Trondheim, Norway, (4) Leibniz Universität Hannover, Forschungszentrum Küste, Hannover, Germany, (5) Institut de Mecanique des Fluides, UMR CNRS/INP-UPS 5502, Toulouse, France, (6) GeoEcoMar, Dimitrie Onciul Nr.23-25, Bucureşti, Romania

Whilst early physical modelling and theoretical studies of the interactions between vegetation and flowing water employed rigid structures such as wooden dowels, recent studies have progressed to flexible surrogate plants. However, even appropriately-scaled flexible surrogates fail to capture the variability in thallus morphology, flexibility and strength, both within and between individuals, and frontal or planform area over space and time. Furthermore, although there have been a number of field studies, measurements of hydraulic variables have generally been limited to time-averaged at-a-point measurements that aim to approximate the depth-mean velocity. This is problematic because in spatially heterogeneous flows, point measurements are dependent upon the sampling location. Herein, we describe research carried out by the participants in the PISCES work package of the HYDRALAB IV project that sought to address these limitations and assess the level of complexity needed to adequately reproduce the hydrodynamics of the natural system in physical models.

We selected an 11 m long $\times$ 6 m wide region of a tidal inlet, the Hopavågen Bay, Sør-Trøndelag, Norway, that contained 19 Laminaria digitata thalli and 101 other macroalgae thalli. Two L. digitata specimens $\sim$0.50 m apart were selected for detailed study and a 2 m long $\times$ 8 m wide frame was oriented around them by enforcing zero cross-stream discharge at its upstream edge. We then quantified: 1. the mean and turbulent flow field of the undisturbed condition (Case A); 2. the positions, geometrical and biomechanical properties of the macroalgae; and 3. the mean and turbulent flow field after the macroalgae were completely removed (Case B). Later, Case A was replicated in the same location ($\pm$0.025 m) before the 19 L. digitata thalli were replaced with 19 "optimized" surrogates (Case C). These three cases were then repeated in the Total Environment Simulator at the University of Hull, UK. Live macroalgae thalli could not be transported from Norway to the UK, so we used the same species of live macroalgae harvested from a wave-dominated coast in the UK. These algae exhibited longer, narrower and more flexible blades. The same surrogate plants were used in both the field and flume experiments. In all cases, a profiling ADV was used to collect 45 velocity profiles composed of up to seven 35 mm-high profiles collected for 240 s at 100 Hz, at a streamwise spacing of 0.25 m and cross-stream spacing of 0.20 m.

The results show that the live macroalgae in the flume simulation exerted less influence on the flow field than the live macroalgae at the field site. In contrast, the "optimized" surrogate macroalgae behaved similarly to the live algae at the field site and yielded similar mean and turbulent velocity fields as our prototype live macroalgae. This emphasizes both the importance of phenotypic plasticity and the importance of selecting surrogates that adequately represent the mean characteristics of the species of interest.

APPENDIX III

Henry, P.Y., Aberle, J., Dijkstra, J., Myrhaug, D., [**2016**]. An integrated, multi-sensing approach to describe the dynamic relations between turbulence, fluid-forces, and reconfiguration of a submerged plant model in steady flows. *EGU General Assembly*; 2016 Vienna.

Geophysical Research Abstracts
Vol. 18, EGU2016-7544, 2016
EGU General Assembly 2016

An integrated, multi-sensing approach to describe the dynamic relations between turbulence, fluid-forces, and reconfiguration of a submerged plant model in steady flows.

Pierre-Yves Henry (1), Jochen Aberle (2), Jasper Dijkstra (3), and Dag Myrhaug (1)

(1) Dept. of Marine Technology, Norwegian University of Science and Technology (NTNU), Trondheim, Norway (pierre-yves.henry@ntnu.no), (2) Dept. of Hydraulic and Environmental Engineering, Norwegian University of Science and Technology (NTNU), Trondheim, Norway, (3) Deltares, Rotterdamseweg 185, Delft, The Netherlands

Aquatic vegetation plays a vital role in ecohydrological systems regulating many physical, chemical, and biological processes across a wide range of spatial and temporal scales. As a consequence, plant-flow interactions are of particular interest to a wide range of disciplines. While early studies of the interactions between vegetation and flowing water employed simplified and non-flexible structures such as rigid cylinders, recent studies have included flexible plants to identify the main characteristics of the hydrodynamics of vegetated flows. However, the description of plant reconfiguration has often been based on a static approach, i.e. considering the plant's deformation under a static load and neglecting turbulent fluctuations. Correlations between drag fluctuations, plant movements, and upstream turbulence were recently established showing that shear layer turbulence at the surface of the different plant elements (such as blades or stems) can contribute significantly to the dynamic behaviour of the plant. However, the relations between plant movement and force fluctuations might change under varying flow velocities, and although this point is crucial for mixing processes and plant dislodgement by fatigue, these aspects of fluid-structure interactions applied to aquatic vegetation remain largely unexplored.

Using an innovative combination of sensing techniques in one set of experiments, this study investigates the relations between turbulence, fluctuating fluid forces and movements of a flexible cylindrical plant surrogate. A silicone-based flexible cylinder was attached at the bottom of a 1m wide flume in fully-developed uniform flow. The lower 22 cm of the plant surrogate were made of plain flexible silicone, while the higher 13cm included a casted rigid sensor, measuring accelerations at the tip of the surrogate. Forces were sampled at high frequencies at the surrogate's base by a 6-degrees-of-freedom force/torque sensor measuring down to the gram-force. Point measurements of turbulence were realized by two ADVs which were located upstream and downstream of the surrogate. Detailed motions of the surrogate were recorded by two cameras above and next to the flume. Image processing allowed for the characterization of the mean deformation and the different modes of horizontal and vertical 'vibration' of the surrogate.

The experimental results were compared to numerical simulations obtained from an updated version of the Dynveg code developed by Deltares. The results showed a clear correlation between the cylinder's movements and the (drag) force fluctuations. Due to the swaying motion of the surrogate, the turbulence spectrum is significantly affected when the flow passes the plant model. The succession of several motion modes are observed as the velocity increases, affecting the dominant frequencies in the drag force spectrum and the overall drag. These preliminary results emphasise the importance of the dynamics of the plant flow interactions, and provide an example of the use of new methodologies to provide deeper insights into the physics of complex flows.

APPENDIX IV

Statements form co-authors

NTNU

Encl. to application for assessment of PhD thesis

STATEMENT FROM CO-AUTHOR

(cf. section 10.1 in the PhD regulations)

Pierre-Yves Henry applies to have the following thesis assessed:

Parametrisation of aquatic vegetation in hydraulic and coastal research: The importance of plant biomechanics in the hydrodynamics of vegetated flows

The statement is to describe the work process and the sharing of work and approve that the article may be used in the thesis.

Jochen Aberle:

Statement from co-author on article: Henry, P.Y., D. Myrhaug, and J. Aberle (2015).

Drag forces on aquatic plants in nonlinear random waves plus current.
Estuarine, Coastal and Shelf Science, 165, 10-24.

PYH was responsible for the critical review of the drag coefficient formulation, the implementation of the analytical model in Matlab, data analysis, interpretation and writing of the manuscript. The derivation of the model was realized by PYH and DM. JA and DM contributed to the data analysis, interpretation and during the finalization of the paper. This article may be used in the thesis.

Trondheim, 12/12/2016
Place, date

.....
Signature co-author

Statement from co-author on article: Detert, M., Weitbrecht, V., Aberle, J., Rowinski, P., Henry, P.Y (-).

6.5 Auxiliary hydrodynamic variables, in "Experimental hydraulics: Methods, Instrumentation, Data Processing & Management" edited by Muste, M. et al.
IAHR Monograph under edition/publication process, Taylor & Francis.

Based on the presentation by Henry at al. given at the 10th International Symposium on Ecohydraulics, PYH has been the main contributor on the subchapter on drag forces. PYH also contributed to general review of the other parts of the Chapter 6.5. This chapter may be used in the thesis.

Trondheim, 12/12/2016
Place, date

.....
Signature co-author

.....
J. Aberle, on behalf of the editorial team

Dag Myrhaug:

Statement from co-author on article: Henry, P.-Y. and Myrhaug, D., (2013).

Wave-induced drag force on vegetation under shoaling random waves.
Coastal Engineering, 78(0): 13-20.

PYH was responsible for the implementation of the analytical model in Matlab, data analysis, interpretation and writing of the manuscript. The derivation of the model was realized by PYH and DM. DM contributed to the data analysis, interpretation and finalization of the paper. This article may be used in the thesis.

NTNU, 11.02.2016
Place, date

Dag Myrhaug
Signature co-author

Statement from co-author on article: Henry, P.Y., D. Myrhaug, and J. Aberle (2015).

Drag forces on aquatic plants in nonlinear random waves plus current.
Estuarine, Coastal and Shelf Science, 165, 10-24.

PYH was responsible for the critical review of the drag coefficient formulation, the implementation of the analytical model in Matlab, data analysis, interpretation and writing of the manuscript. The derivation of the model was realized by PYH and DM. JA and DM contributed to the data analysis, interpretation and finalization of the paper. This article may be used in the thesis.

NTNU, 11.02.2016
Place, date

Dag Myrhaug
Signature co-author

Statement from co-author on article: Henry, P.-Y.T., Leikvoll, E., Myrhaug, D. (2016).

Visualisation of the effect of different types of marine growth on cylinders' wake structure in low Re steady flows.
Ocean Engineering, Accepted for publication on the 07.02.2016.

This work is a result of the MSc thesis written by EL. PYH initiated the idea of the project and co-supervised the work of EL together with DM. The experimental work was carried by EL under the guidance of PYH. The review of the topic and writing of the paper was done by PYH with contributions from DM. This article may be used in the thesis.

NTNU, 11.02.2016
Place, date

Dag Myrhaug
Signature co-author

Eirik Leikvoll Nedrebø:

Statement from co-author on article: Henry, P.-Y.T., Leikvoll, E., Myrhaug, D. (2016).

Visualisation of the effect of different types of marine growth on cylinders' wake structure in low Re steady flows.
Ocean Engineering, Accepted for publication on the 07.02.2016.

This work is a result of the MSc thesis written by EL. PYH initiated the idea of the project and co-supervised the work of EL together with DM. The experimental work was carried by EL under the guidance of PYH. The review of the topic and writing of the paper was done by PYH with contributions from DM. This article may be used in the thesis.

Stavanger, 11.02.2016 ..... Eirik L. Nedrebø .....
Place, date Signature co-author

Maike Paul:

Statement from co-author on article: Paul, M., Henry, P.Y. and Thomas, R.E., (2014).

Geometrical and mechanical properties of four species of northern European brown macroalgae
Coastal Engineering, 84: 73-80.

MP organized the field data collection & analysis and was responsible for writing the manuscript. PYH and RET were involved in the algae collection and data analysis. PYH interpreted the data with MP, with contributions from RET. The paper was finalised by MP and PYH. This article may be used in the thesis.

Perth, 16.2.16 .....
Place, date Signature co-author

Statement from co-author on article: Paul, M., Henry, P.Y. , (2014).

Evaluation of the Use of Surrogate Laminaria digitata in eco-hydraulic Laboratory Experiments
Journal of Hydrodynamics, Ser. B, 26(3), 374--383.

MP led the surrogate development, the flume tests and was responsible for writing the manuscript. PYH was involved in the data analysis, discussions and interpretation. Finalization of the paper was carried out by PYH and MP. This article may be used in the thesis.

Perth, 16.2.16 .....
Place, date Signature co-author

Rob Thomas:

Statement from co-author on article: Paul, M., Henry, P.Y. and Thomas, R.E., (2014).

Geometrical and mechanical properties of four species of northern European brown macroalgae Coastal Engineering, 84: 73-80.

MP organized the field data collection & analysis and was responsible for writing the first draft of the manuscript. PYH and RET were involved in the algae collection and data analysis. PYH interpreted the data with MP, with contributions from RET. The paper was edited by RET and finalised by MP and PYH. This article may be used in the thesis.

Leeds, 17/02/2016

.....

Place, date

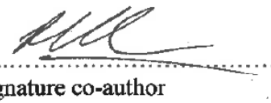

.....

Signature co-author

Previous PhD theses published at the Departement of Marine Technology
(earlier: Faculty of Marine Technology)
NORWEGIAN UNIVERSITY OF SCIENCE AND TECHNOLOGY

Report No.	Author	Title
	Kavlie, Dag	Optimization of Plane Elastic Grillages, 1967
	Hansen, Hans R.	Man-Machine Communication and Data-Storage Methods in Ship Structural Design, 1971
	Gisvold, Kaare M.	A Method for non-linear mixed -integer programming and its Application to Design Problems, 1971
	Lund, Sverre	Tanker Frame Optimalization by means of SUMT-Transformation and Behaviour Models, 1971
	Vinje, Tor	On Vibration of Spherical Shells Interacting with Fluid, 1972
	Lorentz, Jan D.	Tank Arrangement for Crude Oil Carriers in Accordance with the new Anti-Pollution Regulations, 1975
	Carlsen, Carl A.	Computer-Aided Design of Tanker Structures, 1975
	Larsen, Carl M.	Static and Dynamic Analysis of Offshore Pipelines during Installation, 1976
UR-79-01	Brigt Hatlestad, MK	The finite element method used in a fatigue evaluation of fixed offshore platforms. (Dr.Ing. Thesis)
UR-79-02	Erik Pettersen, MK	Analysis and design of cellular structures. (Dr.Ing. Thesis)
UR-79-03	Sverre Valsgård, MK	Finite difference and finite element methods applied to nonlinear analysis of plated structures. (Dr.Ing. Thesis)
UR-79-04	Nils T. Nordsve, MK	Finite element collapse analysis of structural members considering imperfections and stresses due to fabrication. (Dr.Ing. Thesis)
UR-79-05	Ivar J. Fylling, MK	Analysis of towline forces in ocean towing systems. (Dr.Ing. Thesis)
UR-80-06	Nils Sandsmark, MM	Analysis of Stationary and Transient Heat Conduction by the Use of the Finite Element Method. (Dr.Ing. Thesis)
UR-80-09	Sverre Haver, MK	Analysis of uncertainties related to the stochastic modeling of ocean waves. (Dr.Ing. Thesis)
UR-81-15	Odland, Jonas	On the Strength of welded Ring stiffened cylindrical Shells primarily subjected to axial Compression
UR-82-17	Engesvik, Knut	Analysis of Uncertainties in the fatigue Capacity of

		Welded Joints
UR-82-18	Rye, Henrik	Ocean wave groups
UR-83-30	Eide, Oddvar Inge	On Cumulative Fatigue Damage in Steel Welded Joints
UR-83-33	Mo, Olav	Stochastic Time Domain Analysis of Slender Offshore Structures
UR-83-34	Amdahl, Jørgen	Energy absorption in Ship-platform impacts
UR-84-37	Mørch, Morten	Motions and mooring forces of semi submersibles as determined by full-scale measurements and theoretical analysis
UR-84-38	Soares, C. Guedes	Probabilistic models for load effects in ship structures
UR-84-39	Aarsnes, Jan V.	Current forces on ships
UR-84-40	Czujko, Jerzy	Collapse Analysis of Plates subjected to Biaxial Compression and Lateral Load
UR-85-46	Alf G. Engseth, MK	Finite element collapse analysis of tubular steel offshore structures. (Dr.Ing. Thesis)
UR-86-47	Dengody Sheshappa, MP	A Computer Design Model for Optimizing Fishing Vessel Designs Based on Techno-Economic Analysis. (Dr.Ing. Thesis)
UR-86-48	Vidar Aanesland, MH	A Theoretical and Numerical Study of Ship Wave Resistance. (Dr.Ing. Thesis)
UR-86-49	Heinz-Joachim Wessel, MK	Fracture Mechanics Analysis of Crack Growth in Plate Girders. (Dr.Ing. Thesis)
UR-86-50	Jon Taby, MK	Ultimate and Post-ultimate Strength of Dented Tubular Members. (Dr.Ing. Thesis)
UR-86-51	Walter Lian, MH	A Numerical Study of Two-Dimensional Separated Flow Past Bluff Bodies at Moderate KC-Numbers. (Dr.Ing. Thesis)
UR-86-52	Bjørn Sortland, MH	Force Measurements in Oscillating Flow on Ship Sections and Circular Cylinders in a U-Tube Water Tank. (Dr.Ing. Thesis)
UR-86-53	Kurt Strand, MM	A System Dynamic Approach to One-dimensional Fluid Flow. (Dr.Ing. Thesis)
UR-86-54	Arne Edvin Løken, MH	Three Dimensional Second Order Hydrodynamic Effects on Ocean Structures in Waves. (Dr.Ing. Thesis)
UR-86-55	Sigurd Falch, MH	A Numerical Study of Slamming of Two-Dimensional Bodies. (Dr.Ing. Thesis)
UR-87-56	Arne Braathen, MH	Application of a Vortex Tracking Method to the Prediction of Roll Damping of a Two-Dimension Floating Body. (Dr.Ing. Thesis)

UR-87-57	Bernt Leira, MK	Gaussian Vector Processes for Reliability Analysis involving Wave-Induced Load Effects. (Dr.Ing. Thesis)
UR-87-58	Magnus Småvik, MM	Thermal Load and Process Characteristics in a Two-Stroke Diesel Engine with Thermal Barriers (in Norwegian). (Dr.Ing. Thesis)
MTA-88-59	Bernt Arild Bremdal, MP	An Investigation of Marine Installation Processes – A Knowledge - Based Planning Approach. (Dr.Ing. Thesis)
MTA-88-60	Xu Jun, MK	Non-linear Dynamic Analysis of Space-framed Offshore Structures. (Dr.Ing. Thesis)
MTA-89-61	Gang Miao, MH	Hydrodynamic Forces and Dynamic Responses of Circular Cylinders in Wave Zones. (Dr.Ing. Thesis)
MTA-89-62	Martin Greenhow, MH	Linear and Non-Linear Studies of Waves and Floating Bodies. Part I and Part II. (Dr.Techn. Thesis)
MTA-89-63	Chang Li, MH	Force Coefficients of Spheres and Cubes in Oscillatory Flow with and without Current. (Dr.Ing. Thesis
MTA-89-64	Hu Ying, MP	A Study of Marketing and Design in Development of Marine Transport Systems. (Dr.Ing. Thesis)
MTA-89-65	Arild Jæger, MH	Seakeeping, Dynamic Stability and Performance of a Wedge Shaped Planing Hull. (Dr.Ing. Thesis)
MTA-89-66	Chan Siu Hung, MM	The dynamic characteristics of tilting-pad bearings
MTA-89-67	Kim Wikstrøm, MP	Analysis av projekteringen for ett offshore projekt. (Licenciat-avhandling)
MTA-89-68	Jiao Guoyang, MK	Reliability Analysis of Crack Growth under Random Loading, considering Model Updating. (Dr.Ing. Thesis)
MTA-89-69	Arnt Olufsen, MK	Uncertainty and Reliability Analysis of Fixed Offshore Structures. (Dr.Ing. Thesis)
MTA-89-70	Wu Yu-Lin, MR	System Reliability Analyses of Offshore Structures using improved Truss and Beam Models. (Dr.Ing. Thesis)
MTA-90-71	Jan Roger Hoff, MH	Three-dimensional Green function of a vessel with forward speed in waves. (Dr.Ing. Thesis)
MTA-90-72	Rong Zhao, MH	Slow-Drift Motions of a Moored Two-Dimensional Body in Irregular Waves. (Dr.Ing. Thesis)
MTA-90-73	Atle Minsaas, MP	Economical Risk Analysis. (Dr.Ing. Thesis)
MTA-90-74	Knut-Aril Farnes, MK	Long-term Statistics of Response in Non-linear Marine Structures. (Dr.Ing. Thesis)
MTA-90-75	Torbjørn Sotberg, MK	Application of Reliability Methods for Safety Assessment of Submarine Pipelines. (Dr.Ing.

		Thesis)
MTA-90-76	Zeuthen, Steffen, MP	SEAMAID. A computational model of the design process in a constraint-based logic programming environment. An example from the offshore domain. (Dr.Ing. Thesis)
MTA-91-77	Haagensen, Sven, MM	Fuel Dependant Cyclic Variability in a Spark Ignition Engine - An Optical Approach. (Dr.Ing. Thesis)
MTA-91-78	Løland, Geir, MH	Current forces on and flow through fish farms. (Dr.Ing. Thesis)
MTA-91-79	Hoen, Christopher, MK	System Identification of Structures Excited by Stochastic Load Processes. (Dr.Ing. Thesis)
MTA-91-80	Haugen, Stein, MK	Probabilistic Evaluation of Frequency of Collision between Ships and Offshore Platforms. (Dr.Ing. Thesis)
MTA-91-81	Sødahl, Nils, MK	Methods for Design and Analysis of Flexible Risers. (Dr.Ing. Thesis)
MTA-91-82	Ormberg, Harald, MK	Non-linear Response Analysis of Floating Fish Farm Systems. (Dr.Ing. Thesis)
MTA-91-83	Marley, Mark J., MK	Time Variant Reliability under Fatigue Degradation. (Dr.Ing. Thesis)
MTA-91-84	Krokstad, Jørgen R., MH	Second-order Loads in Multidirectional Seas. (Dr.Ing. Thesis)
MTA-91-85	Molteberg, Gunnar A., MM	The Application of System Identification Techniques to Performance Monitoring of Four Stroke Turbocharged Diesel Engines. (Dr.Ing. Thesis)
MTA-92-86	Mørch, Hans Jørgen Bjelke, MH	Aspects of Hydrofoil Design: with Emphasis on Hydrofoil Interaction in Calm Water. (Dr.Ing. Thesis)
MTA-92-87	Chan Siu Hung, MM	Nonlinear Analysis of Rotordynamic Instabilities in Highspeed Turbomachinery. (Dr.Ing. Thesis)
MTA-92-88	Bessason, Bjarni, MK	Assessment of Earthquake Loading and Response of Seismically Isolated Bridges. (Dr.Ing. Thesis)
MTA-92-89	Langli, Geir, MP	Improving Operational Safety through exploitation of Design Knowledge - an investigation of offshore platform safety. (Dr.Ing. Thesis)
MTA-92-90	Sævik, Svein, MK	On Stresses and Fatigue in Flexible Pipes. (Dr.Ing. Thesis)
MTA-92-91	Ask, Tor Ø., MM	Ignition and Flame Growth in Lean Gas-Air Mixtures. An Experimental Study with a Schlieren System. (Dr.Ing. Thesis)
MTA-86-92	Hessen, Gunnar, MK	Fracture Mechanics Analysis of Stiffened Tubular Members. (Dr.Ing. Thesis)

MTA-93-93	Steinebach, Christian, MM	Knowledge Based Systems for Diagnosis of Rotating Machinery. (Dr.Ing. Thesis)
MTA-93-94	Dalane, Jan Inge, MK	System Reliability in Design and Maintenance of Fixed Offshore Structures. (Dr.Ing. Thesis)
MTA-93-95	Steen, Sverre, MH	Cobblestone Effect on SES. (Dr.Ing. Thesis)
MTA-93-96	Karunakaran, Daniel, MK	Nonlinear Dynamic Response and Reliability Analysis of Drag-dominated Offshore Platforms. (Dr.Ing. Thesis)
MTA-93-97	Hagen, Arnulf, MP	The Framework of a Design Process Language. (Dr.Ing. Thesis)
MTA-93-98	Nordrik, Rune, MM	Investigation of Spark Ignition and Autoignition in Methane and Air Using Computational Fluid Dynamics and Chemical Reaction Kinetics. A Numerical Study of Ignition Processes in Internal Combustion Engines. (Dr.Ing. Thesis)
MTA-94-99	Passano, Elizabeth, MK	Efficient Analysis of Nonlinear Slender Marine Structures. (Dr.Ing. Thesis)
MTA-94-100	Kvålsvold, Jan, MH	Hydroelastic Modelling of Wetdeck Slamming on Multihull Vessels. (Dr.Ing. Thesis)
MTA-94-102	Bech, Sidsel M., MK	Experimental and Numerical Determination of Stiffness and Strength of GRP/PVC Sandwich Structures. (Dr.Ing. Thesis)
MTA-95-103	Paulsen, Hallvard, MM	A Study of Transient Jet and Spray using a Schlieren Method and Digital Image Processing. (Dr.Ing. Thesis)
MTA-95-104	Hovde, Geir Olav, MK	Fatigue and Overload Reliability of Offshore Structural Systems, Considering the Effect of Inspection and Repair. (Dr.Ing. Thesis)
MTA-95-105	Wang, Xiaozhi, MK	Reliability Analysis of Production Ships with Emphasis on Load Combination and Ultimate Strength. (Dr.Ing. Thesis)
MTA-95-106	Ulstein, Tore, MH	Nonlinear Effects of a Flexible Stern Seal Bag on Cobblestone Oscillations of an SES. (Dr.Ing. Thesis)
MTA-95-107	Solaas, Frøydis, MH	Analytical and Numerical Studies of Sloshing in Tanks. (Dr.Ing. Thesis)
MTA-95-108	Hellan, Øyvind, MK	Nonlinear Pushover and Cyclic Analyses in Ultimate Limit State Design and Reassessment of Tubular Steel Offshore Structures. (Dr.Ing. Thesis)
MTA-95-109	Hermundstad, Ole A., MK	Theoretical and Experimental Hydroelastic Analysis of High Speed Vessels. (Dr.Ing. Thesis)
MTA-96-110	Bratland, Anne K., MH	Wave-Current Interaction Effects on Large-Volume Bodies in Water of Finite Depth. (Dr.Ing. Thesis)
MTA-96-111	Herfjord, Kjell, MH	A Study of Two-dimensional Separated Flow by a Combination of the Finite Element Method and

		Navier-Stokes Equations. (Dr.Ing. Thesis)
MTA-96-112	Æsøy, Vilmar, MM	Hot Surface Assisted Compression Ignition in a Direct Injection Natural Gas Engine. (Dr.Ing. Thesis)
MTA-96-113	Eknes, Monika L., MK	Escalation Scenarios Initiated by Gas Explosions on Offshore Installations. (Dr.Ing. Thesis)
MTA-96-114	Erikstad, Stein O., MP	A Decision Support Model for Preliminary Ship Design. (Dr.Ing. Thesis)
MTA-96-115	Pedersen, Egil, MH	A Nautical Study of Towed Marine Seismic Streamer Cable Configurations. (Dr.Ing. Thesis)
MTA-97-116	Moksnes, Paul O., MM	Modelling Two-Phase Thermo-Fluid Systems Using Bond Graphs. (Dr.Ing. Thesis)
MTA-97-117	Halse, Karl H., MK	On Vortex Shedding and Prediction of Vortex-Induced Vibrations of Circular Cylinders. (Dr.Ing. Thesis)
MTA-97-118	Igland, Ragnar T., MK	Reliability Analysis of Pipelines during Laying, considering Ultimate Strength under Combined Loads. (Dr.Ing. Thesis)
MTA-97-119	Pedersen, Hans-P., MP	Levendefiskteknologi for fiskefartøy. (Dr.Ing. Thesis)
MTA-98-120	Vikestad, Kyrre, MK	Multi-Frequency Response of a Cylinder Subjected to Vortex Shedding and Support Motions. (Dr.Ing. Thesis)
MTA-98-121	Azadi, Mohammad R. E., MK	Analysis of Static and Dynamic Pile-Soil-Jacket Behaviour. (Dr.Ing. Thesis)
MTA-98-122	Ulltang, Terje, MP	A Communication Model for Product Information. (Dr.Ing. Thesis)
MTA-98-123	Torbergsen, Erik, MM	Impeller/Diffuser Interaction Forces in Centrifugal Pumps. (Dr.Ing. Thesis)
MTA-98-124	Hansen, Edmond, MH	A Discrete Element Model to Study Marginal Ice Zone Dynamics and the Behaviour of Vessels Moored in Broken Ice. (Dr.Ing. Thesis)
MTA-98-125	Videiro, Paulo M., MK	Reliability Based Design of Marine Structures. (Dr.Ing. Thesis)
MTA-99-126	Mainçon, Philippe, MK	Fatigue Reliability of Long Welds Application to Titanium Risers. (Dr.Ing. Thesis)
MTA-99-127	Haugen, Elin M., MH	Hydroelastic Analysis of Slamming on Stiffened Plates with Application to Catamaran Wetdecks. (Dr.Ing. Thesis)
MTA-99-128	Langhelle, Nina K., MK	Experimental Validation and Calibration of Nonlinear Finite Element Models for Use in Design of Aluminium Structures Exposed to Fire. (Dr.Ing. Thesis)
MTA-99-	Berstad, Are J., MK	Calculation of Fatigue Damage in Ship Structures.

129		(Dr.Ing. Thesis)
MTA-99-130	Andersen, Trond M., MM	Short Term Maintenance Planning. (Dr.Ing. Thesis)
MTA-99-131	Tveiten, Bård Wathne, MK	Fatigue Assessment of Welded Aluminium Ship Details. (Dr.Ing. Thesis)
MTA-99-132	Søreide, Fredrik, MP	Applications of underwater technology in deep water archaeology. Principles and practice. (Dr.Ing. Thesis)
MTA-99-133	Tønnessen, Rune, MH	A Finite Element Method Applied to Unsteady Viscous Flow Around 2D Blunt Bodies With Sharp Corners. (Dr.Ing. Thesis)
MTA-99-134	Elvekrok, Dag R., MP	Engineering Integration in Field Development Projects in the Norwegian Oil and Gas Industry. The Supplier Management of Norne. (Dr.Ing. Thesis)
MTA-99-135	Fagerholt, Kjetil, MP	Optimeringsbaserte Metoder for Ruteplanlegging innen skipsfart. (Dr.Ing. Thesis)
MTA-99-136	Bysveen, Marie, MM	Visualization in Two Directions on a Dynamic Combustion Rig for Studies of Fuel Quality. (Dr.Ing. Thesis)
MTA-2000-137	Storteig, Eskild, MM	Dynamic characteristics and leakage performance of liquid annular seals in centrifugal pumps. (Dr.Ing. Thesis)
MTA-2000-138	Sagli, Gro, MK	Model uncertainty and simplified estimates of long term extremes of hull girder loads in ships. (Dr.Ing. Thesis)
MTA-2000-139	Tronstad, Harald, MK	Nonlinear analysis and design of cable net structures like fishing gear based on the finite element method. (Dr.Ing. Thesis)
MTA-2000-140	Kroneberg, André, MP	Innovation in shipping by using scenarios. (Dr.Ing. Thesis)
MTA-2000-141	Haslum, Herbjørn Alf, MH	Simplified methods applied to nonlinear motion of spar platforms. (Dr.Ing. Thesis)
MTA-2001-142	Samdal, Ole Johan, MM	Modelling of Degradation Mechanisms and Stressor Interaction on Static Mechanical Equipment Residual Lifetime. (Dr.Ing. Thesis)
MTA-2001-143	Baarholm, Rolf Jarle, MH	Theoretical and experimental studies of wave impact underneath decks of offshore platforms. (Dr.Ing. Thesis)
MTA-2001-144	Wang, Lihua, MK	Probabilistic Analysis of Nonlinear Wave-induced Loads on Ships. (Dr.Ing. Thesis)
MTA-2001-145	Kristensen, Odd H. Holt, MK	Ultimate Capacity of Aluminium Plates under Multiple Loads, Considering HAZ Properties. (Dr.Ing. Thesis)
MTA-2001-146	Greco, Marilena, MH	A Two-Dimensional Study of Green-Water

		Loading. (Dr.Ing. Thesis)
MTA-2001-147	Heggelund, Svein E., MK	Calculation of Global Design Loads and Load Effects in Large High Speed Catamarans. (Dr.Ing. Thesis)
MTA-2001-148	Babalola, Olusegun T., MK	Fatigue Strength of Titanium Risers – Defect Sensitivity. (Dr.Ing. Thesis)
MTA-2001-149	Mohammed, Abuu K., MK	Nonlinear Shell Finite Elements for Ultimate Strength and Collapse Analysis of Ship Structures. (Dr.Ing. Thesis)
MTA-2002-150	Holmedal, Lars E., MH	Wave-current interactions in the vicinity of the sea bed. (Dr.Ing. Thesis)
MTA-2002-151	Rognebakke, Olav F., MH	Sloshing in rectangular tanks and interaction with ship motions. (Dr.Ing. Thesis)
MTA-2002-152	Lader, Pål Furset, MH	Geometry and Kinematics of Breaking Waves. (Dr.Ing. Thesis)
MTA-2002-153	Yang, Qinzheng, MH	Wash and wave resistance of ships in finite water depth. (Dr.Ing. Thesis)
MTA-2002-154	Melhus, Øyvin, MM	Utilization of VOC in Diesel Engines. Ignition and combustion of VOC released by crude oil tankers. (Dr.Ing. Thesis)
MTA-2002-155	Ronæss, Marit, MH	Wave Induced Motions of Two Ships Advancing on Parallel Course. (Dr.Ing. Thesis)
MTA-2002-156	Økland, Ole D., MK	Numerical and experimental investigation of whipping in twin hull vessels exposed to severe wet deck slamming. (Dr.Ing. Thesis)
MTA-2002-157	Ge, Chunhua, MK	Global Hydroelastic Response of Catamarans due to Wet Deck Slamming. (Dr.Ing. Thesis)
MTA-2002-158	Byklum, Eirik, MK	Nonlinear Shell Finite Elements for Ultimate Strength and Collapse Analysis of Ship Structures. (Dr.Ing. Thesis)
IMT-2003-1	Chen, Haibo, MK	Probabilistic Evaluation of FPSO-Tanker Collision in Tandem Offloading Operation. (Dr.Ing. Thesis)
IMT-2003-2	Skaugset, Kjetil Bjørn, MK	On the Suppression of Vortex Induced Vibrations of Circular Cylinders by Radial Water Jets. (Dr.Ing. Thesis)
IMT-2003-3	Chezhian, Muthu	Three-Dimensional Analysis of Slamming. (Dr.Ing. Thesis)
IMT-2003-4	Buhaug, Øyvind	Deposit Formation on Cylinder Liner Surfaces in Medium Speed Engines. (Dr.Ing. Thesis)
IMT-2003-5	Tregde, Vidar	Aspects of Ship Design: Optimization of Aft Hull with Inverse Geometry Design. (Dr.Ing. Thesis)
IMT-	Wist, Hanne Therese	Statistical Properties of Successive Ocean Wave

2003-6		Parameters. (Dr.Ing. Thesis)
IMT-2004-7	Ransau, Samuel	Numerical Methods for Flows with Evolving Interfaces. (Dr.Ing. Thesis)
IMT-2004-8	Soma, Torkel	Blue-Chip or Sub-Standard. A data interrogation approach of identity safety characteristics of shipping organization. (Dr.Ing. Thesis)
IMT-2004-9	Ersdal, Svein	An experimental study of hydrodynamic forces on cylinders and cables in near axial flow. (Dr.Ing. Thesis)
IMT-2005-10	Brodtkorb, Per Andreas	The Probability of Occurrence of Dangerous Wave Situations at Sea. (Dr.Ing. Thesis)
IMT-2005-11	Yttervik, Rune	Ocean current variability in relation to offshore engineering. (Dr.Ing. Thesis)
IMT-2005-12	Fredheim, Arne	Current Forces on Net-Structures. (Dr.Ing. Thesis)
IMT-2005-13	Heggernes, Kjetil	Flow around marine structures. (Dr.Ing. Thesis
IMT-2005-14	Fouques, Sebastien	Lagrangian Modelling of Ocean Surface Waves and Synthetic Aperture Radar Wave Measurements. (Dr.Ing. Thesis)
IMT-2006-15	Holm, Håvard	Numerical calculation of viscous free surface flow around marine structures. (Dr.Ing. Thesis)
IMT-2006-16	Bjørheim, Lars G.	Failure Assessment of Long Through Thickness Fatigue Cracks in Ship Hulls. (Dr.Ing. Thesis)
IMT-2006-17	Hansson, Lisbeth	Safety Management for Prevention of Occupational Accidents. (Dr.Ing. Thesis)
IMT-2006-18	Zhu, Xinying	Application of the CIP Method to Strongly Nonlinear Wave-Body Interaction Problems. (Dr.Ing. Thesis)
IMT-2006-19	Reite, Karl Johan	Modelling and Control of Trawl Systems. (Dr.Ing. Thesis)
IMT-2006-20	Smogeli, Øyvind Notland	Control of Marine Propellers. From Normal to Extreme Conditions. (Dr.Ing. Thesis)
IMT-2007-21	Storhaug, Gaute	Experimental Investigation of Wave Induced Vibrations and Their Effect on the Fatigue Loading of Ships. (Dr.Ing. Thesis)
IMT-2007-22	Sun, Hui	A Boundary Element Method Applied to Strongly Nonlinear Wave-Body Interaction Problems. (PhD Thesis, CeSOS)
IMT-2007-23	Rustad, Anne Marthine	Modelling and Control of Top Tensioned Risers. (PhD Thesis, CeSOS)
IMT-2007-24	Johansen, Vegar	Modelling flexible slender system for real-time simulations and control applications
IMT-2007-25	Wroldsen, Anders Sunde	Modelling and control of tensegrity structures.

		(PhD Thesis, CeSOS)
IMT-2007-26	Aronsen, Kristoffer Høye	An experimental investigation of in-line and combined inline and cross flow vortex induced vibrations. (Dr. avhandling, IMT)
IMT-2007-27	Gao, Zhen	Stochastic Response Analysis of Mooring Systems with Emphasis on Frequency-domain Analysis of Fatigue due to Wide-band Response Processes (PhD Thesis, CeSOS)
IMT-2007-28	Thorstensen, Tom Anders	Lifetime Profit Modelling of Ageing Systems Utilizing Information about Technical Condition. (Dr.ing. thesis, IMT)
IMT-2008-29	Refsnes, Jon Erling Gorset	Nonlinear Model-Based Control of Slender Body AUVs (PhD Thesis, IMT)
IMT-2008-30	Berntsen, Per Ivar B.	Structural Reliability Based Position Mooring. (PhD-Thesis, IMT)
IMT-2008-31	Ye, Naiquan	Fatigue Assessment of Aluminium Welded Box-stiffener Joints in Ships (Dr.ing. thesis, IMT)
IMT-2008-32	Radan, Damir	Integrated Control of Marine Electrical Power Systems. (PhD-Thesis, IMT)
IMT-2008-33	Thomassen, Paul	Methods for Dynamic Response Analysis and Fatigue Life Estimation of Floating Fish Cages. (Dr.ing. thesis, IMT)
IMT-2008-34	Pákozdi, Csaba	A Smoothed Particle Hydrodynamics Study of Two-dimensional Nonlinear Sloshing in Rectangular Tanks. (Dr.ing.thesis, IMT/ CeSOS)
IMT-2007-35	Grytøyr, Guttorm	A Higher-Order Boundary Element Method and Applications to Marine Hydrodynamics. (Dr.ing.thesis, IMT)
IMT-2008-36	Drummen, Ingo	Experimental and Numerical Investigation of Nonlinear Wave-Induced Load Effects in Containerships considering Hydroelasticity. (PhD thesis, CeSOS)
IMT-2008-37	Skejic, Renato	Maneuvering and Seakeeping of a Singel Ship and of Two Ships in Interaction. (PhD-Thesis, CeSOS)
IMT-2008-38	Harlem, Alf	An Age-Based Replacement Model for Repairable Systems with Attention to High-Speed Marine Diesel Engines. (PhD-Thesis, IMT)
IMT-2008-39	Alsos, Hagbart S.	Ship Grounding. Analysis of Ductile Fracture, Bottom Damage and Hull Girder Response. (PhD-thesis, IMT)
IMT-2008-40	Graczyk, Mateusz	Experimental Investigation of Sloshing Loading and Load Effects in Membrane LNG Tanks Subjected to Random Excitation. (PhD-thesis, CeSOS)
IMT-2008-41	Taghipour, Reza	Efficient Prediction of Dynamic Response for Flexible amd Multi-body Marine Structures. (PhD-

		thesis, CeSOS)
IMT-2008-42	Ruth, Eivind	Propulsion control and thrust allocation on marine vessels. (PhD thesis, CeSOS)
IMT-2008-43	Nystad, Bent Helge	Technical Condition Indexes and Remaining Useful Life of Aggregated Systems. PhD thesis, IMT
IMT-2008-44	Soni, Prashant Kumar	Hydrodynamic Coefficients for Vortex Induced Vibrations of Flexible Beams, PhD thesis, CeSOS
IMT-2009-45	Amlashi, Hadi K.K.	Ultimate Strength and Reliability-based Design of Ship Hulls with Emphasis on Combined Global and Local Loads. PhD Thesis, IMT
IMT-2009-46	Pedersen, Tom Arne	Bond Graph Modelling of Marine Power Systems. PhD Thesis, IMT
IMT-2009-47	Kristiansen, Trygve	Two-Dimensional Numerical and Experimental Studies of Piston-Mode Resonance. PhD-Thesis, CeSOS
IMT-2009-48	Ong, Muk Chen	Applications of a Standard High Reynolds Number Model and a Stochastic Scour Prediction Model for Marine Structures. PhD-thesis, IMT
IMT-2009-49	Hong, Lin	Simplified Analysis and Design of Ships subjected to Collision and Grounding. PhD-thesis, IMT
IMT-2009-50	Koushan, Kamran	Vortex Induced Vibrations of Free Span Pipelines, PhD thesis, IMT
IMT-2009-51	Korsvik, Jarl Eirik	Heuristic Methods for Ship Routing and Scheduling. PhD-thesis, IMT
IMT-2009-52	Lee, Jihoon	Experimental Investigation and Numerical in Analyzing the Ocean Current Displacement of Longlines. Ph.d.-Thesis, IMT.
IMT-2009-53	Vestbøstad, Tone Gran	A Numerical Study of Wave-in-Deck Impact usin a Two-Dimensional Constrained Interpolation Profile Method, Ph.d.thesis, CeSOS.
IMT-2009-54	Bruun, Kristine	Bond Graph Modelling of Fuel Cells for Marine Power Plants. Ph.d.-thesis, IMT
IMT 2009-55	Holstad, Anders	Numerical Investigation of Turbulence in a Sekwed Three-Dimensional Channel Flow, Ph.d.-thesis, IMT.
IMT 2009-56	Ayala-Uraga, Efren	Reliability-Based Assessment of Deteriorating Ship-shaped Offshore Structures, Ph.d.-thesis, IMT
IMT 2009-57	Kong, Xiangjun	A Numerical Study of a Damaged Ship in Beam Sea Waves. Ph.d.-thesis, IMT/CeSOS.
IMT 2010-58	Kristiansen, David	Wave Induced Effects on Floaters of Aquaculture Plants, Ph.d.-thesis, CeSOS.

IMT 2010-59	Ludvigsen, Martin	An ROV-Toolbox for Optical and Acoustic Scientific Seabed Investigation. Ph.d.-thesis IMT.
IMT 2010-60	Hals, Jørgen	Modelling and Phase Control of Wave-Energy Converters. Ph.d.thesis, CeSOS.
IMT 2010- 61	Shu, Zhi	Uncertainty Assessment of Wave Loads and Ultimate Strength of Tankers and Bulk Carriers in a Reliability Framework. Ph.d. Thesis, IMT/ CeSOS
IMT 2010-62	Shao, Yanlin	Numerical Potential-Flow Studies on Weakly-Nonlinear Wave-Body Interactions with/without Small Forward Speed, Ph.d.thesis,CeSOS.
IMT 2010-63	Califano, Andrea	Dynamic Loads on Marine Propellers due to Intermittent Ventilation. Ph.d.thesis, IMT.
IMT 2010-64	El Khoury, George	Numerical Simulations of Massively Separated Turbulent Flows, Ph.d.-thesis, IMT
IMT 2010-65	Seim, Knut Sponheim	Mixing Process in Dense Overflows with Emphasis on the Faroe Bank Channel Overflow. Ph.d.thesis, IMT
IMT 2010-66	Jia, Huirong	Structural Analysis of Intect and Damaged Ships in a Collission Risk Analysis Perspective. Ph.d.thesis CeSoS.
IMT 2010-67	Jiao, Linlin	Wave-Induced Effects on a Pontoon-type Very Large Floating Structures (VLFS). Ph.D.-thesis, CeSOS.
IMT 2010-68	Abrahamsen, Bjørn Christian	Sloshing Induced Tank Roof with Entrapped Air Pocket. Ph.d.thesis, CeSOS.
IMT 2011-69	Karimirad, Madjid	Stochastic Dynamic Response Analysis of Spar-Type Wind Turbines with Catenary or Taut Mooring Systems. Ph.d.-thesis, CeSOS.
IMT - 2011-70	Erlend Meland	Condition Monitoring of Safety Critical Valves. Ph.d.-thesis, IMT.
IMT – 2011-71	Yang, Limin	Stochastic Dynamic System Analysis of Wave Energy Converter with Hydraulic Power Take-Off, with Particular Reference to Wear Damage Analysis, Ph.d. Thesis, CeSOS.
IMT – 2011-72	Visscher, Jan	Application of Particla Image Velocimetry on Turbulent Marine Flows, Ph.d.Thesis, IMT.
IMT – 2011-73	Su, Biao	Numerical Predictions of Global and Local Ice Loads on Ships. Ph.d.Thesis, CeSOS.
IMT – 2011-74	Liu, Zhenhui	Analytical and Numerical Analysis of Iceberg Collision with Ship Structures. Ph.d.Thesis, IMT.
IMT – 2011-75	Aarsæther, Karl Gunnar	Modeling and Analysis of Ship Traffic by Observation and Numerical Simulation. Ph.d.Thesis, IMT.

Imt – 2011-76	Wu, Jie	Hydrodynamic Force Identification from Stochastic Vortex Induced Vibration Experiments with Slender Beams. Ph.d.Thesis, IMT.
Imt – 2011-77	Amini, Hamid	Azimuth Propulsors in Off-design Conditions. Ph.d.Thesis, IMT.
IMT – 2011-78	Nguyen, Tan-Hoi	Toward a System of Real-Time Prediction and Monitoring of Bottom Damage Conditions During Ship Grounding. Ph.d.thesis, IMT.
IMT- 2011-79	Tavakoli, Mohammad T.	Assessment of Oil Spill in Ship Collision and Grounding, Ph.d.thesis, IMT.
IMT- 2011-80	Guo, Bingjie	Numerical and Experimental Investigation of Added Resistance in Waves. Ph.d.Thesis, IMT.
IMT- 2011-81	Chen, Qiaofeng	Ultimate Strength of Aluminium Panels, considering HAZ Effects, IMT
IMT- 2012-82	Kota, Ravikiran S.	Wave Loads on Decks of Offshore Structures in Random Seas, CeSOS.
IMT- 2012-83	Sten, Ronny	Dynamic Simulation of Deep Water Drilling Risers with Heave Compensating System, IMT.
IMT- 2012-84	Berle, Øyvind	Risk and resilience in global maritime supply chains, IMT.
IMT- 2012-85	Fang, Shaoji	Fault Tolerant Position Mooring Control Based on Structural Reliability, CeSOS.
IMT- 2012-86	You, Jikun	Numerical studies on wave forces and moored ship motions in intermediate and shallow water, CeSOS.
IMT- 2012-87	Xiang ,Xu	Maneuvering of two interacting ships in waves, CeSOS
IMT- 2012-88	Dong, Wenbin	Time-domain fatigue response and reliability analysis of offshore wind turbines with emphasis on welded tubular joints and gear components, CeSOS
IMT- 2012-89	Zhu, Suji	Investigation of Wave-Induced Nonlinear Load Effects in Open Ships considering Hull Girder Vibrations in Bending and Torsion, CeSOS
IMT- 2012-90	Zhou, Li	Numerical and Experimental Investigation of Station-keeping in Level Ice, CeSOS
IMT- 2012-91	Ushakov, Sergey	Particulate matter emission characteristics from diesel enignes operating on conventional and alternative marine fuels, IMT
IMT- 2013-1	Yin, Decao	Experimental and Numerical Analysis of Combined In-line and Cross-flow Vortex Induced Vibrations, CeSOS

IMT-2013-2	Kurniawan, Adi	Modelling and geometry optimisation of wave energy converters, CeSOS
IMT-2013-3	Al Ryati, Nabil	Technical condition indexes doe auxiliary marine diesel engines, IMT
IMT-2013-4	Firoozkoohi, Reza	Experimental, numerical and analytical investigation of the effect of screens on sloshing, CeSOS
IMT-2013-5	Ommani, Babak	Potential-Flow Predictions of a Semi-Displacement Vessel Including Applications to Calm Water Broaching, CeSOS
IMT-2013-6	Xing, Yihan	Modelling and analysis of the gearbox in a floating spar-type wind turbine, CeSOS
IMT-7-2013	Balland, Océane	Optimization models for reducing air emissions from ships, IMT
IMT-8-2013	Yang, Dan	Transitional wake flow behind an inclined flat plate-----Computation and analysis, IMT
IMT-9-2013	Abdillah, Suyuthi	Prediction of Extreme Loads and Fatigue Damage for a Ship Hull due to Ice Action, IMT
IMT-10-2013	Ramìrez, Pedro Agustìn Pèrez	Ageing management and life extension of technical systems- Concepts and methods applied to oil and gas facilities, IMT
IMT-11-2013	Chuang, Zhenju	Experimental and Numerical Investigation of Speed Loss due to Seakeeping and Maneuvering. IMT
IMT-12-2013	Etemaddar, Mahmoud	Load and Response Analysis of Wind Turbines under Atmospheric Icing and Controller System Faults with Emphasis on Spar Type Floating Wind Turbines, IMT
IMT-13-2013	Lindstad, Haakon	Strategies and measures for reducing maritime CO2 emissons, IMT
IMT-14-2013	Haris, Sabril	Damage interaction analysis of ship collisions, IMT
IMT-15-2013	Shainee, Mohamed	Conceptual Design, Numerical and Experimental Investigation of a SPM Cage Concept for Offshore Mariculture, IMT
IMT-16-2013	Gansel, Lars	Flow past porous cylinders and effects of biofouling and fish behavior on the flow in and around Atlantic salmon net cages, IMT
IMT-17-2013	Gaspar, Henrique	Handling Aspects of Complexity in Conceptual Ship Design, IMT
IMT-18-2013	Thys, Maxime	Theoretical and Experimental Investigation of a Free Running Fishing Vessel at Small Frequency of Encounter, CeSOS
IMT-19-2013	Aglen, Ida	VIV in Free Spanning Pipelines, CeSOS

IMT-1-2014	Song, An	Theoretical and experimental studies of wave diffraction and radiation loads on a horizontally submerged perforated plate, CeSOS
IMT-2-2014	Rogne, Øyvind Ygre	Numerical and Experimental Investigation of a Hinged 5-body Wave Energy Converter, CeSOS
IMT-3-2014	Dai, Lijuan	Safe and efficient operation and maintenance of offshore wind farms ,IMT
IMT-4-2014	Bachynski, Erin Elizabeth	Design and Dynamic Analysis of Tension Leg Platform Wind Turbines, CeSOS
IMT-5-2014	Wang, Jingbo	Water Entry of Freefall Wedged – Wedge motions and Cavity Dynamics, CeSOS
IMT-6-2014	Kim, Ekaterina	Experimental and numerical studies related to the coupled behavior of ice mass and steel structures during accidental collisions, IMT
IMT-7-2014	Tan, Xiang	Numerical investigation of ship's continuous- mode icebreaking in leverl ice, CeSOS
IMT-8-2014	Muliawan, Made Jaya	Design and Analysis of Combined Floating Wave and Wind Power Facilities, with Emphasis on Extreme Load Effects of the Mooring System, CeSOS
IMT-9-2014	Jiang, Zhiyu	Long-term response analysis of wind turbines with an emphasis on fault and shutdown conditions, IMT
IMT-10-2014	Dukan, Fredrik	ROV Motion Control Systems, IMT
IMT-11-2014	Grimsmo, Nils I.	Dynamic simulations of hydraulic cylinder for heave compensation of deep water drilling risers, IMT
IMT-12-2014	Kvittem, Marit I.	Modelling and response analysis for fatigue design of a semisubmersible wind turbine, CeSOS
IMT-13-2014	Akhtar, Juned	The Effects of Human Fatigue on Risk at Sea, IMT
IMT-14-2014	Syahroni, Nur	Fatigue Assessment of Welded Joints Taking into Account Effects of Residual Stress, IMT
IMT-1-2015	Bøckmann, Eirik	Wave Propulsion of ships, IMT
IMT-2-2015	Wang, Kai	Modelling and dynamic analysis of a semi-submersible floating vertical axis wind turbine, CeSOS
IMT-3-2015	Fredriksen, Arnt Gunvald	A numerical and experimental study of a two-dimensional body with moonpool in waves and current, CeSOS
IMT-4-2015	Jose Patricio Gallardo Canabes	Numerical studies of viscous flow around bluff bodies, IMT

IMT-5-2015	Vegard Longva	Formulation and application of finite element techniques for slender marine structures subjected to contact interactions, IMT
IMT-6-2015	Jacobus De Vaal	Aerodynamic modelling of floating wind turbines, CeSOS
IMT-7-2015	Fachri Nasution	Fatigue Performance of Copper Power Conductors, IMT
IMT-8-2015	Oleh I Karpa	Development of bivariate extreme value distributions for applications in marine technology,CeSOS
IMT-9-2015	Daniel de Almeida Fernandes	An output feedback motion control system for ROVs, AMOS
IMT-10-2015	Bo Zhao	Particle Filter for Fault Diagnosis: Application to Dynamic Positioning Vessel and Underwater Robotics, CeSOS
IMT-11-2015	Wenting Zhu	Impact of emission allocation in maritime transportation, IMT
IMT-12-2015	Amir Rasekhi Nejad	Dynamic Analysis and Design of Gearboxes in Offshore Wind Turbines in a Structural Reliability Perspective, CeSOS
IMT-13-2015	Arturo Jesùs Ortega Malca	Dynamic Response of Flexibles Risers due to Unsteady Slug Flow, CeSOS
IMT-14-2015	Dagfinn Husjord	Guidance and decision-support system for safe navigation of ships operating in close proximity, IMT
IMT-15-2015	Anirban Bhattacharyya	Ducted Propellers: Behaviour in Waves and Scale Effects, IMT
IMT-16-2015	Qin Zhang	Image Processing for Ice Parameter Identification in Ice Management, IMT
IMT-1-2016	Vincentius Rumawas	Human Factors in Ship Design and Operation: An Experiential Learning, IMT
IMT-2-2016	Martin Storheim	Structural response in ship-platform and ship-ice collisions, IMT
IMT-3-2016	Mia Abrahamsen Prsic	Numerical Simulations of the Flow around single and Tandem Circular Cylinders Close to a Plane Wall, IMT
IMT-4-2016	Tufan Arslan	Large-eddy simulations of cross-flow around ship sections, IMT